Functional Organization of the CCAN Protein Complex

Inaugural-Dissertation
zur
Erlangung des Doktorgrades
Dr. rer. nat.

der Fakultät für Biologie an der

UNIVERSITÄT DUISBURG-ESSEN

vorgelegt von

Kerstin Klare
aus Recklinghausen

durchgeführt am
MAX PLANCK INSTITUT FÜR MOLEKULARE PHYSIOLOGIE
Abteilung für Mechanistische Zellbiolgie

Februar 2015

Die der vorliegenden Arbeit zugrunde liegenden Experimente wurden am Max Planck Institut fur Molekulare Physiologie in der Abteilung für mechanistische Zellbiologie durchgeführt.

1. Gutachter: Prof. Dr. Andrea Musacchio
2. Gutachter: Prof. Dr. Stefan Westermann

Vorsitzender des Prüfungsausschusses: Prof. Dr. Hemmo Meyer
Tag der mündlichen Prüfung: 09. Juni 2015

Diese Arbeit witme ich Peter, einem liebevollen Freund. Er hat mich all die Jahre in guten sowie schweren Zeiten unterstützt und war mir stets ein treuer Weggefährte. Ich vermisse ihn jeden Tag, aber er wird mir in guter Erinnerung bleiben und in meinem Herzen weiterleben.

UNIVERSITÄT DUISBURG-ESSEN

Abstract

Max Planck Institut für Molekulare Physiologie
Abteilung für Mechanistische Zellbiolgie

Dr. rer. nat.

von Kerstin Klare

Kinetochores, huge proteinaceous scaffolds, assemble on centromeric chromatin and bind spindle microtubules to faithfully separate sister chromatids during mitosis. The centromere - kinetochore interface is build by the constitutive centromere associated network (CCAN). CENP-C, a multi-functional CCAN protein, has been proposed to be one of the key players of kinetochore assembly. Although a lot is known about CENP-C functions, its role in CCAN assembly remains elusive. This study provides insights into organization of CENP-C within the CCAN, both by biochemical and structural approaches using recombinant material, but also within the context of human cells. Our analysis clearly demonstrates that the N-terminal half of CENP-C is the assembly platform of the CCAN by directly recruiting the CENP-H/I/K/M and CENP-N/L complexes. Point mutations within conserved patches on CENP-C specifically destroyed the CENP-C:CENP-H/I/K/M interaction, which was followed by a loss of CENP-N/L and CENP-T/W. CENP-T/W has proven not to directly bind to CENP-C. Taken together, we conclude that CENP-C is the CCAN interaction hub of the kinetochore thereby, directly binding to CENP-H/I/K/M provides a platform for CENP-N/L assembly, whereas CENP-T/W indirectly depends on CENP-C through its interaction with the CENP-H/I/K/M complex.

Contents

Abstract iii

List of Figures viii

List of Tables xi

Abbreviations xii

1 Introduction 1
- 1.1 Miracle of life . . . 1
- 1.2 Cell Cycle . . . 2
- 1.3 Mitotic spindle . . . 4
- 1.4 Kinetochore organization & function . . . 7
  - 1.4.1 Centromeric chromatin organization . . . 8
  - 1.4.2 CENP-A nucleosome features . . . 10
  - 1.4.3 CENP-A nucleosome replenishment . . . 11
  - 1.4.4 The outer kinetochore . . . 13
  - 1.4.5 The spindle assembly checkpoint (SAC) . . . 17
- 1.5 CCAN organization & function . . . 20
  - 1.5.1 CENP-C . . . 22
  - 1.5.2 CENP-N and CENP-L . . . 24
  - 1.5.3 CENP-H, CENP-I, CENP-K, CENP-M . . . 25
  - 1.5.4 CENP-T, CENP-W, CENP-S, CENP-X . . . 26
  - 1.5.5 CENP-O, CENP-P, CENP-Q, CENP-U, CENP-R . . . 28
- 1.6 Objectives . . . 29

2 Results 31
- 2.1 CENP-C construct design . . . 31
- 2.2 Establishment of recombinant CENP-C production . . . 33
- 2.3 Production of CCAN subcomplexes . . . 39
- 2.4 CENP-C^{2-545} binding to CENP-H/K complex in solution . . . 41
- 2.5 CENP-C^{1-544}His binding to CENP-H/K complex in solution . . . 43
- 2.6 Limited proteolysis on CENP-C^{2-545}/H/K . . . 44

2.7 Cross-linking and mass spectrometry of CENP-C$^{2-545}$/CENP-H/K . 46
2.8 CENP-C minimal binding region for CENP-H/K on solid surface . 48
2.9 CENP-C/H/K minimal binding interface dissection 49
2.10 CENP-C minimal binding region for CENP-H/K in solution 51
2.11 CENP-H/K:CENP-C interaction affinity 54
2.12 CENP-C binding to CENP-H/I/K/M complex on a solid surface . . 58
2.13 CENP-C binding to CENP-H/I/K/M complex in solution 58
2.14 Proteolytic digestion of CENP-C$^{2-545}$/H/I/K/M complex 60
2.15 Roles of CENP-H and CENP-K N-termini in CENP-C binding . . . 61
2.16 Roles of CENP-I$^{57-281}$ and CENP-M in the CENP-C:CENP-H/I/K/M interaction 62
2.17 CENP-C$^{1-544}$His binding to CENP-N/L in solution 64
2.18 CENP-C binding to CENP-N/L on a solid surface 65
2.19 Cross-linking coupled with mass spectrometry of CENP-C$^{1-544}$His / CENP-H/I/K/M / CENP-N/L / CENP-A^{nucleosome} complex . . . 67
2.20 Multiple sequence alignment reveals conserved patches on CENP-C$^{189-400}$ 69
2.21 CENP-C W317A binding to CENP-H/K, -H/I/K/M and -N/L . . . 70
2.22 CENP-C L265A/F266A/L267A binding to CENP-H/K, -H/I/K/M and -N/L 73
2.23 CENP-C$^{2-545}$E302A/F303A or I305A/D306A binding to CENP-H/K and -N/L 77
2.24 CENP-C L207A/F209A binding to CENP-H/K, -H/I/K/M and -N/L 79
2.25 CENP-C4A is a separation of function mutant *in vitro* 82
2.26 *In vivo* role of CENP-C in CCAN assembly 85
2.26.1 Establishment of doxycycline inducible mCherry-CCAN cell lines 86
2.26.2 Depletion of CENP-C abolishes localization of CCAN proteins to kinetochores 89
2.26.3 Production of CCAN antibodies and generation of GFP-CENP-C cell lines 93
2.26.4 GFP-CENP-C$^{1-544}$ rescue of CENP-H/K localization to kinetochores 98
2.26.5 CENP-H/I/K/M dependency on CENP-C for its kinetochore localization 99
2.26.6 CENP-T/W dependency on CENP-H/I/K/M for its kinetochore localization 101
2.26.7 GFP-CENP-C immunoprecipitation 104

3 Discussion 108
3.1 CENP-C's role in the CCAN assembly hierarchy 108
3.1.1 CENP-C interaction with CENP-H/I/K/M 110
3.1.2 CENP-C interaction with CENP-N/L 113
3.1.3 The stoichiometry of the CENP-C/H/I/K/M/N/L complex 116
3.1.4 CENP-C interaction with CENP-T/W 118

3.1.5 Role of CENP-C in outer kinetochore recruitment 120
3.1.6 The stoichiometry of the kinetochore 123
3.1.7 CENP-A deposition 125
3.1.8 Posttranslational modifications of CENP-C 126

4 Materials and Methods 127
4.1 Instrumentation and software 127
4.2 Chemicals 133
4.3 Enzymes 142
4.4 Kits 143
4.5 Antibodies 143
4.6 Recombinant proteins 145
4.7 Cell lines 147
4.8 Plasmids for bacterial expression 148
4.8.1 CENP-C 148
4.8.2 CENP-T/W 148
4.8.3 CENP-I$^{57-281}$ 149
4.8.4 CENP-N1 – 212 149
4.8.5 CENP-M 149
4.9 Site specific mutagenesis 149
4.10 Protein expression and purification from E. coli 150
4.10.1 (GST-)CENP-C constructs 150
4.10.2 CENP-T/W 151
4.10.3 CENP-I$^{57-281}$ 152
4.10.4 CENP-N$^{1-212}$His 153
4.10.5 CENP-M 154
4.10.6 CENP-A nucleosomes 155
4.11 Protein production with the MultiBac expression system 155
4.12 Plasmids for insect cell expression 156
4.12.1 CENP-C$^{1-544}$-His 156
4.12.2 CENP-C$^{1-400}$-His 156
4.12.3 CENP-C$^{189-400}$ 156
4.12.4 CENP-H/CENP-K-His 157
4.12.5 CENP-H^{29-C}/His-CENP-K^{50-C} 157
4.12.6 CENP-H/I^{57-C}/K/M 157
4.12.7 CENP-N/L 158
4.12.8 Mis12 complex 158
4.13 Virus production and protein expression in insect cells 159
4.13.1 Protein purification from insect cells 160
4.13.2 CENP-C$^{1-544}$-His 160
4.13.3 CENP-H/His-CENP-K 161
4.13.4 CENP-H^{29-C}/His-CENP-K^{50-C} 161
4.13.5 CENP-N/L 162
4.13.6 CENP-H/I^{57-C}/K/M 163

4.13.7 CENP-C$^{1-544}$/H/I^{57-C}/K/L/M/N/CENP-A^{nucleosome} 164
4.13.8 Mis12 complex 165
4.14 GST pulldown assays 165
4.14.1 Preblocking of GSH sepharose beads 166
4.15 Analytical Size exclusion chromatography (SEC) migration shift assays 166
4.16 Limited proteolysis 167
4.17 Cross linking coupled with mass spectrometry 167
4.18 Isothermal Calorimetry (ITC) 168
4.19 Plasmids for mammalian expression 168
4.20 Generation of stable cell lines 168
4.21 Small interfering RNA depletion of CENP-C 169
4.22 Generation of an rabbit anti-CENP-H/K and anti-CENP-C$^{731-849}$ antibody 170
4.23 Immunofluorescence (IF) and image generation 170
4.24 Immunoprecipitation and immunoblotting 171

5 Supplemetary Figures **173**

Bibliography **180**

Acknowledgements **213**

Curriculum Vitae **215**

Declarations **217**

List of Figures

1.1 The eukaryotic cell cycle . . . 3
1.2 Mitotic cell division . . . 5
1.3 Mitotic spindle . . . 6
1.4 General kinetochore organization . . . 8
1.5 Schematic kinetochore organization . . . 9
1.6 CENP-C amino acid composition and functional domains . . . 24

2.1 CENP-C's secondary structure . . . 32
2.2 GST-CENP-C^{2-545} purification . . . 34
2.3 CENP-C^{2-545} purification . . . 35
2.4 CENP-C^{1-544}-His purification from insect cells . . . 36
2.5 CENP-C^{1-544}-His phosphorylations . . . 36
2.6 CENP-$C^{189-400}$ purification . . . 38
2.7 CENP-$C^{189-400}$ purification from insect cells . . . 39
2.8 CENP-N/L purification from insect cells . . . 41
2.9 CENP-C^{2-545} CENP-H/K interaction in SEC . . . 42
2.10 CENP-C^{2-545} CENP-H/K interaction in SEC at high concentrations 43
2.11 CENP-C^{1-544} CENP-H/K interaction in SEC . . . 44
2.12 Limited proteolysis of CENP-C^{2-545}/CENP-H/K complex . . . 45
2.13 CENP-C^{2-545}/CENP-H-K cross-linking and mass spectrometry . . . 47
2.14 GST-CENP-C constructs CENP-H/K pulldown . . . 48
2.15 GST-CENP-$C^{290-400}$ CENP-H/K pulldown . . . 50
2.16 GST-CENP-$C^{189-290}$ CENP-H-K pulldown . . . 50
2.17 CENP-$C^{189-400}$ CENP-H/K interaction in SEC . . . 52
2.18 CENP-$C^{402-544}$ CENP-H/K interaction in SEC . . . 52
2.19 CENP-C^{1-400}His CENP-H/K interaction in SEC . . . 53
2.20 CENP-$C^{189-400}$ CENP-H/K interaction in SEC . . . 53
2.21 CENP-C^{2-545} CENP-H/K interaction in ITC . . . 55
2.22 CENP-$C^{189-400}$ CENP-H/K interaction in ITC . . . 56
2.23 CENP-$C^{290-400}$ CENP-H/K interaction in ITC . . . 57
2.24 GST-CENP-C^{2-545} and GST-CENP-$C^{189-290}$ CENP-H/I/K/M pull-down . . . 59
2.25 CENP-$C^{189-400}$ CENP-H/I/K/M interaction in SEC . . . 59
2.26 Limited proteolysis of CENP-C^{2-545}/CENP-H/I/K/M complex . . . 60
2.27 GST-CENP-$C^{189-400}$ CENP-HΔN CENP-KΔN, CENP-I^{57-281} pull-down . . . 62

2.28 GST-CENP-C$^{2-545}$, CENP-M and CENP-I$^{57-281}$ pulldown 63
2.29 CENP-C$^{1-544}$His CENP-N/L interaction in SEC 64
2.30 GST-CENP-C$^{189-400}$ CENP-N/L pulldown 65
2.31 GST-CENP-C$^{189-290}$ and CENP-C$^{290-400}$ CENP-N/L pulldown . . . 66
2.32 CENP-C$^{2-545}$/CENP-H/I/K/M/N/L/CENP-A^{nucleosome} cross-linking and mass spectrometry 68
2.33 CENP-C$^{189-400}$ multiple sequence alignment (MSA) 69
2.34 GST-CENP-CW317A CENP-H/K pulldown 71
2.35 GST-CENP-CW317A CENP-H/I/K/M pulldown 72
2.36 GST-CENP-C$^{2-545}$3A CENP-H/K pulldown 73
2.37 GST-CENP-C$^{2-545}$4A CENP-H/K pulldown 74
2.38 GST-CENP-C$^{189-290}$3A CENP-H/I/K/M pulldown 75
2.39 GST-CENP-C$^{2-545}$W317A 3A and 4A CENP-H/I/K/M pulldown . 76
2.40 CENP-C$^{2-545}$4A CENP-H/I/K/M interaction in SEC 78
2.41 GST-CENP-C$^{2-545}$4A Mis12c pulldown 82
2.42 CENP-C$^{2-545}$4A Mis12c interaction in SEC 84
2.43 CENP-C RNAi depletion in total cell lysates by RNAi 86
2.44 Generation of mCherry-CCAN cell lines 88
2.45 Quantification of CENP-N, CENP-L, CENP-K CENP-I and CENP-T/W dependency on CENP-C for their kinetochore localization . . 90
2.46 CENP-N, CENP-L and CENP-K dependency on CENP-C 91
2.47 CENP-I and CENP-T/W dependency on CENP-C 92
2.48 Generation of GFP-CENP-C cell lines 94
2.49 CENP-C$^{732-849}$ rabbit polyclonal antibody production 96
2.50 CENP-H/K rabbit polyclonal antibody production 97
2.51 Quantification of CENP-H/K kinetochore localization rescue by GFP-CENP-C$^{1-544}$ 98
2.52 Rescue of CENP-H/K kinetochore localization by GFP-CENP-C$^{1-544}$ 99
2.53 CENP-H/K kinetochore localization rescue by GFP-CENP-C full length wild type and 4A 100
2.54 Quantification of CENP-H/K kinetochore localization rescue by GFP-CENP-C full length wild type and mutants 101
2.55 GST-CENP-C$^{2-545}$ CENP-H/I/K/M CENP-T/W pulldown 102
2.56 CENP-T/W kinetochore localization rescue by GFP-CENP-C full length wild type and 4A 103
2.57 Quantification of CENP-T/W kinetochore localization rescue by GFP-CENP-C full length wild type and mutants 104
2.58 Kinetochore assembly dependency on the CENP-C:CENP-H/I/K/M interaction 105
2.59 GST-CENP-C$^{2-545}$ CENP-H/I/K/M Mis12 complex pulldown . . . 106
2.60 GST-CENP-C$^{189-400}$ CCAN Mis12c pulldown 107

3.1 CENP-C:kinetochore interaction interfaces 108
3.2 CCAN recruitment by direct CENP-C binding 115
3.3 CCAN assembly models 118

3.4 CCAN recruitment hierarchy 119
3.5 MSA of CENP-H/K/I/M binding sites on CENP-C 121
3.6 Updated schematic kinetochore organization 123

5.1 CENP-C$^{189-400}$ binding to CENP-H/K in SEC 173
5.2 CENP-C$^{189-544}$ binding to CENP-H/K in SEC 174
5.3 GST-CENP-C$^{2-545}$W317A CENP-N/L pulldown 174
5.4 GST-CENP-C$^{2-545}$4A CENP-N/L pulldown 175
5.5 GST-CENP-C$^{2-545}$E302/F303 and GST-CENP-C$^{2-545}$I305A/D306A CENP-H/K pulldown 175
5.6 GST-CENP-C$^{2-545}$E302/F303 and GST-CENP-C$^{2-545}$I305/D306 CENP-N/L pulldown 176
5.7 GST-CENP-C$^{189-290}$L207A/F209A CENP-N/L pulldown 176
5.8 GST-CENP-CL207A/F209A CENP-H/K and CENP-H/I/K/M pulldown 177
5.9 GST-CENP-C$^{2-545}$L207A/F209A/E302R/F303S CENP-N/L pulldown 177
5.10 CENP-C$^{2-545}$4A Mis12c interaction in SEC 178
5.11 CENP-C$^{1-544}$-His test expression in Tnao38 cells 179

List of Tables

2.1 Recombinant CENP-C proteins 37
2.2 Recombinant CCAN proteins and complexes 40
2.3 Summary of CENP-C binding to CENP-H/K in solution 54
2.4 Summary of CENP-C binding to CENP-H/K on solid surface . . . 79
2.5 Summary of CENP-C binding to CENP-H/I/K/M on solid surface . 80
2.6 Summary of CENP-C binding to CENP-N/L on solid surface 81
2.7 Summary of CENP-C binding to CENP-H/K and CENP-H/I/K/M in solution 81
2.8 Summary of antibody production against CCAN proteins 95

4.1 Instrumentation 127
4.2 Software 132
4.3 Chemicals & Solutions 133
4.4 Enzymes 142
4.5 Kits 143
4.6 Antibodies 143
4.7 Recombinant CENP-C proteins 145
4.8 Cell lines 147

Abbreviations

AEBSF	4-(2-(**A**mino**E**thyl) **B**enzene**S**ulfonyl **F**luoride
APC	**A**anaphase **P**romoting **C**omplex
ATP	**A**denosin**T**ri**P**hosphate
AUC	**A**nalytical **U**ltra **C**entrifugation
BSA	**B**ovine **S**erum **A**lbumin
BUB1	**B**udding **U**ninhibited by **B**enomyl **1**
BUBR1	**B**ub1 **R**elated
CATD	**C**ENP-**A** **T**argeting **D**omain
CCAN	**C**onstitutive **C**entromere **A**ssociated **N**etwork
CENP	**CEN**tromere **P**rotein
CPC	**C**hromosomal **P**assenger **C**omplex
CREST	**C**alcinosis **R**aynauds syndrome **E**sophageal dysmotility **S**cleroderdactyly **T**elangiectasia
DAPI	4,6-**D**i**A**midin-2-**P**henyl**I**ndoldihydrochlorid
DMEM	**D**ulbecco's **M**odified **E**agle's **M**edium
DMSO	**D**i**M**ethyl **S**ulf**O**xyde
DNA	**D**esoxyribo**N**ucleic **A**cid
eGFP	**e**nhanced **G**reen **F**lourescent **P**rotein
EM	**E**lectron **M**icroscopy
EDTA	**E**thylen**D**iamin**T**etra**A**cetic acid
FBS	**F**etal **B**ovine **S**erum
GSH	**G**lutathion-**S**epharose-**H**igh Performance
GST	**G**lutathion-**S**-**T**ransferase
HJURP	**H**olliday **J**unction **R**ecognition **P**rotein

IF	**I**mmuno**F**luorescence
IPTG	**I**so**p**ropyl-β-D-**T**hio**g**alactopyranosid
ITC	**I**so**T**hermal **C**alorimetry
LB	**L**ennox **B**roth
MAD	**M**itotic **A**rrest **D**eficient
MAPK	**M**itogen **A**ctivated **P**rotein **K**inase
MCC	**M**itotic **C**heckpoint **C**omplex
MCS	**M**ultiple **C**loning **S**ide
MES	2-(N-**M**orpholino)**e**thane**s**ulfonic acid
MSA	**M**ultiple **S**equence **A**lignment
MWM	**M**olecular **W**eight **M**arker
NMR	**N**uclear **M**agnetic **R**esonance
PEST-rich	**P**roline, **G**lutamatic acid, **S**erine, **T**hreonine-rich
PBS	**P**hosphate **B**uffered **S**aline
PFA	**P**ara**F**orm**A**ldehyde
Plk1	**P**olo **L**ike **K**inase **1**
PMSF	**P**henyl**M**ethyl**S**ulfonyl**F**luorid
PP1	**P**rotein **P**hosphatase **1**
PSI-Blast	**P**osition **S**pecific **I**terated-Blast
RNA	**R**ibo**N**ucleic **A**cid
RZZ	**R**OD **Z**WILCH **Z**W10
SAC	**S**pindle **A**ssembly **C**heckpoint
SDS	**S**odium **D**odecyl **S**ulfate
SEC	**S**ize **E**xclusion **C**hromatography
SILAC	**S**table **I**sotope **L**abeling by **A**mino acids in **C**ell culture
Ska complex	**S**pindle- and **K**inetochore **A**ssociated complex
SLIC	**S**equence and **L**igation **I**ndependent **C**loning
TB	**T**errific **B**roth
TCEP	**T**ris(2-**C**arboxy**E**thyl)**P**hospine
TEV-protease	**T**obacco **E**tch **V**irus-protease

Chapter 1

Introduction

1.1 Miracle of life

There is evidence that life on earth emerged at least 3800 million years ago [1]. This is approximately 750 million years after the earth formed, whereas the divergence of animal life started some 3260 million years later [2]. How the roots of life originated and how the first cell came into being can only be speculated, since these events cannot be reproduced experimentally [3]. Nevertheless, from a hypothetical progenitor cell all living organisms emerged, ranging from relatively simple unicellular organisms such as bacteria or yeast to complex multicellular organisms like plants and animals. The driving force that is responsible for the manifoldness of life on earth can be summarized in a complex process called evolution, that is based on events like mutations and selection [4]. Despite an obviously huge diversity of form and function between all cells of different organisms, cells share a common core of molecular features. These features include Adenosin triphosphate (ATP) as an energy source, **d**esoxyribo**n**ucleic **a**cid (DNA) as the carrier of genetic information , **r**ibo**n**ucleic **a**cid (RNA) as the template for protein production and the machinery to transcribe DNA into RNA and translate RNA into proteins that provide structure and function to the cell [2].

Unicellular organisms need to divide in order to reproduce, although this is a very simplified statement. However, a single division is obviously not enough to reproduce multicellular organisms. Here, single cell reproduction is required for the continuation of the germ line of every species and for the production of somatic cells required to build and maintain individuals. On the contrary, cell division

does not occur continuously in all cells of a multicellular being. For instance, differentiated nervous and muscle cells of a human adult do not proliferate anymore and enter a quiescent state that is called G_0 [5]. Furthermore, uncontrolled proliferation in differentiated tissue is frequently not appreciated, since it is a common feature of cancer cells [6–9].
Regardless of whether we are studying a single cell organism or a germ-, or somatic-cell of a multicellular organism, all cells need to fullfill the same requirements in order to reproduce. Dividing cells need to duplicate their genetic material first and than equally distribute it into two identical cells [10], both highly regulated and technically challenging processes for the cell. In the year 1835 the botanist Hugo von Mohl observed the division of a plant cell (*Cladophora glomerata*) for the first time under the microscope [11]. Walther Flemming originally coined the term mitosis for the division of a cell in the early 1880s [12, 13]. The term is used today to summarize the processes in which chromosomes are segregated - as identical sister chromatids - to the dividing daughter cells [14]. Generally speaking, this will be the focus of my thesis.

1.2 Cell Cycle

The term 'cell cycle' summarizes all events cells need to achieve in order to faithfully duplicate and segregate their genetic material [14]. Although the exact details of the cell cycle vary amongst species, certain characteristics remain universal. The cell cycle includes two major functional phases. In S-phase (where S stands for DNA **s**ynthesis) chromosome duplication occurs, after which all chromosomes consist of two exact copies of the genetic material, each forming a sister chromatid. The sister chromatids are linked by cohesin, a ring-like complex of proteins that physically holds the two sisters together until it is cleaved at anaphase onset by the protease separase [15]. Chromosomes are condensed by condensin, a protein complex that helps packing the DNA as tightly as possible before mitosis [16]. Chromosome segregation occurs in M-phase, comprising the division of the nucleus (**m**itosis) and of the cytoplasm (cytokinesis).
Besides duplicating their genomes, cells need to double their mass of proteins and organelles. This occurs in two gap phases between M- and S-phase (G_1) or S- and M-phase (G_2). G_1, S-phase and G_2 belong to the interphase. The whole cell cycle therefore includes the interphase, where cells grow and duplicate their

genetic material and mitosis, where cells divide into two identical offsprings [14] as schematically shown in **Figure** 1.1. The accuracy of this process is crucial for cellular viability as its perturbation leads to aberrations in chromosome number, called aneuploidy, which often result in birth defects and / or cancers [7, 9, 17]. M-phase can be sub-divided into prometa-, meta-, ana-, and telo-phase. In prophase, sister chromatids condense. In the subsequent prometaphase the chromatids become attached to the mitotic spindle, a bipolar array of microtubules (further discussed in **Section** 1.3). At metaphase, mitotic chromosomes are all bioriented and aligned at the spindle equator due to forces of the mitotic spindle. Anaphase is onset by destruction of sister chromatid cohesion, revolving in the pulling of sister chromatids to opposite poles of the spindle. Chromosomes are packaged into separate nuclei at telophase and cytokinesis completes the division of the cell. The mitotic division is schematically shown in **Figure** 1.2.

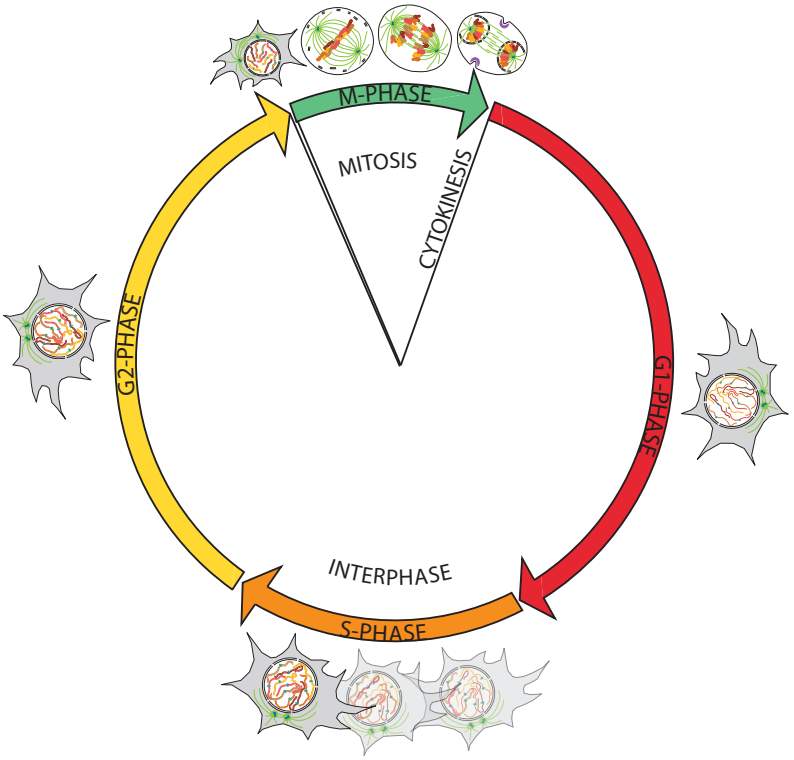

FIGURE 1.1: **The eukaryotic cell cycle**. The cell cycle consists of an interphase, where the cell gains size and replicates its genetic material and a metaphase, where it separates the genetic material into two identical offsprings. Figure modified from [14]

In eukaryotes, cell cycle progression is governed by series of surveillance mechanisms named checkpoints. In simple terms, checkpoints ensure the initiation of the main events of the cell cycle not before earlier events have been completed correctly [18]. The spindle assembly checkpoint (SAC) acts at the metaphase-to-anaphase transition and stimulates sister-chromatid separation after proper attachment of all chromatids to the microtubules in a bipolar fashion (reviewed in [19]).

1.3 Mitotic spindle

In order to align all chromosomes on the metaphase plate and to subsequently partition to the daughter cells, both sister chromatids need to be properly attached to the mitotic spindle [20, 21]. In the 1960s it became evident that the mitotic spindle consists of filaments that run in parallel with the direction of chromosome movement [22, 23]. Tubulin was identified in the same decade [24, 25] as the building block of microtubules [26]. Today it is well established that the filaments of the mitotic spindle consist of long bipolar arrays of microtubule polymers [20], with the minus ends being focused at the two spindle poles and the plus ends radiating outward from the poles of the spindle [14]. Some microtubule plus ends interact with other microtubule plus ends from the opposite pole, thus forming the interpolar microtubules at the spindle midzone [27]. The plus end of other microtubules are bound to large protein structures called kinetochores that are located at specific loci of each sister chromatid named the centromere (discussed in detail in **Section** 1.4.1 and 1.4, respectively). The primary function of kinetochores is to create load-bearing attachments between mitotic chromosomes and microtubules [10]. Therefore, these microtubules are called kinetochore microtubules. They are responsible for pulling sister chromatids to opposite poles of the cell at anaphase [28]. A third set of microtubules, astral microtubules, position the spindle within the cell by radiating outward and contacting the cell cortex. A mitotic spindle is schematically shown in (**Figure** 1.3)

The function of the mitotic spindle depends on rapid turnover of tubulin at the spindle microtubules [29] and the ability of kinetochores to keep attached to growing or disassembling microtubules [30]. Indeed, the half-life of microtubules drops significantly in mitosis, strengthening the importance for a highly dynamic mitotic spindle to function properly [27]. Additionally, the spindles function also relies on numerous microtubule-dependent motor proteins. These proteins belong

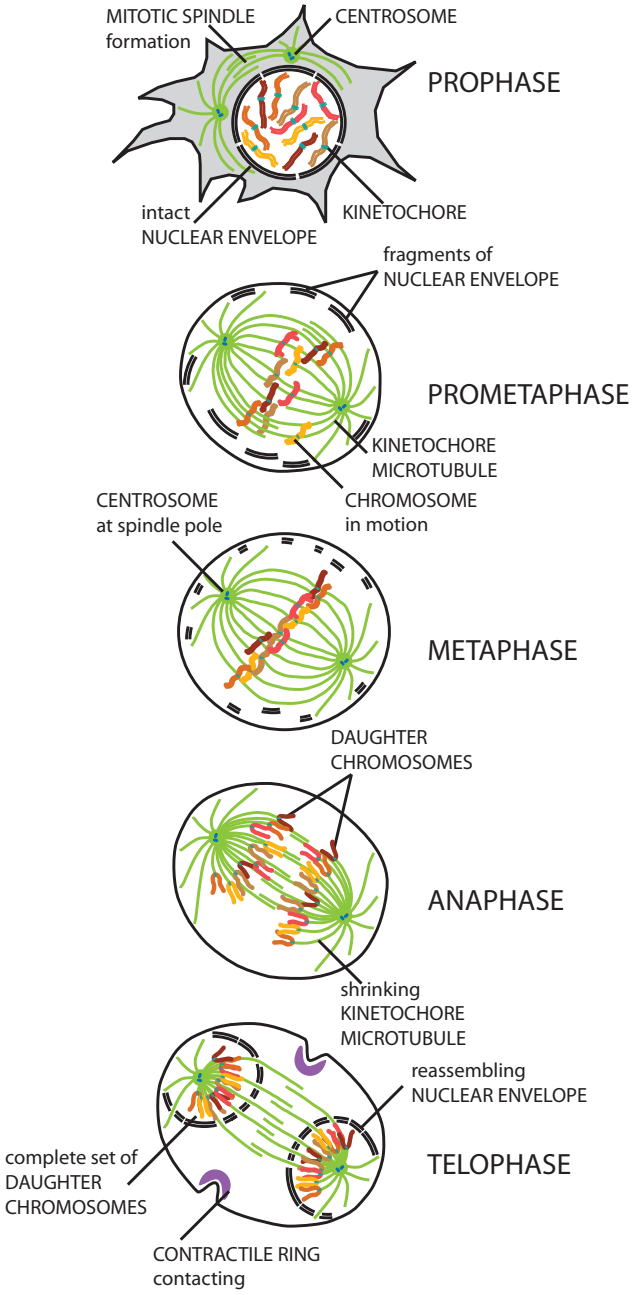

FIGURE 1.2: **Mitotic cell division**. The mitotic division consists of phases that include specific events. In prometaphase the condensed sister chromatids become attached to the mitotic spindle. At metaphase, mitotic chromosomes are all bioriented and aligned at the spindle equator due to forces of the mitotic spindle. Anaphase is onset by destruction of sister chromatid cohesion, revolving in the pulling of sister chromatids to opposite poles of the spindle. Chromosomes are packaged into separate nuclei at telophase. Cytokinesis completes the division of the cell (not shown here). Figure modified from [14].

to either the kinesin-related proteins, which usually move toward the plus end of microtubules [31] or dyneins, which move toward the minus end [32], thus creating forces that push the poles of the mitotic spindle further apart or pull the sister chromatids towards the spindle poles [33]. Only after all chromosomes are properly attached to two opposite poles of the spindle, the cell is released into anaphase. This metaphase to anaphase transition is controlled by the spindle assembly checkpoint that is assembled onto the kinetochores [19], setting the kinetochore at the center of another important function besides creating attachment points for the mitotic spindle.

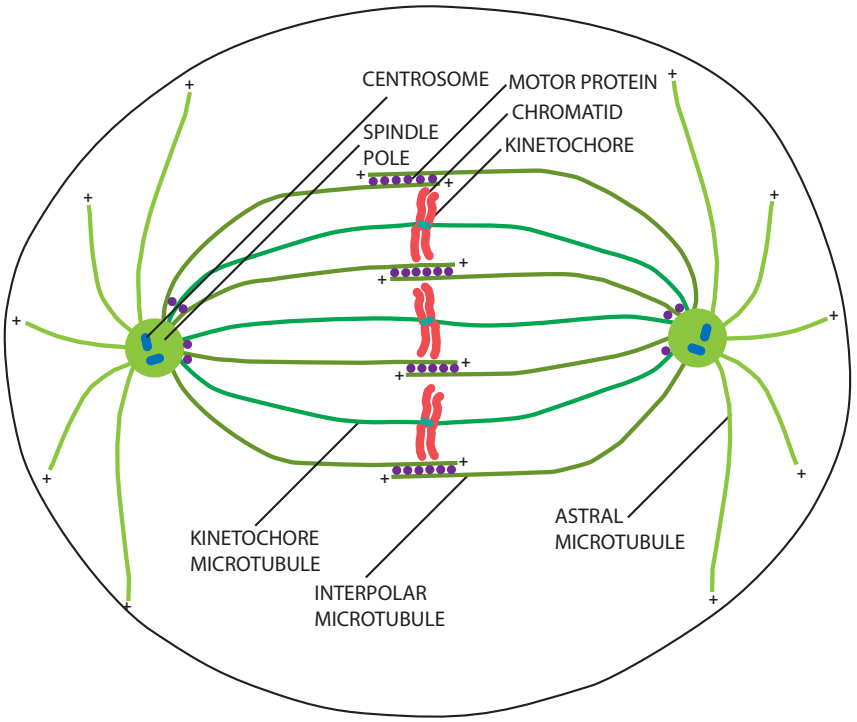

FIGURE 1.3: **Mitotic spindle**. Microtubules of the mitotic spindle radiate outward from two spindle poles and form three different kinds of microtubules. 1. Interpolar microtubules interact with microtubules from the opposite spindle pole. 2. Kinetochore microtubules interact with kinetochores of each sister chromatid. 3. Astral microtubules radiate outward to the cell cortex and help the mitotic spindle to position. Figure modified from [14].

1.4 Kinetochore organization & function

Kinetochores are protein assemblies that bind to several microtubules. The simplest kinetochores only bind a single microtubule and can be found in *Saccharomyces cerevisiae* [34, 35]. Kinetochore subunits are clustered in seven different complexes [34, 35] that are almost all highly conserved from yeast to humans [19, 36, 37]. Conservation of kinetochore components supports the so called repeat subunit model. This model hypothesizes that kinetochores of vertebrates, are assembled from the repetition of the budding yeast microtubule-binding module [38–40]. It remains to be elucidated if this model is true. Not only the subcomplexes are highly conserved from yeast to human, but also major themes in kinetochore organization and function. The position of kinetochore proteins along the inter-kinetochore axis of *S. cerevisiae* [41], *Drosophila melanogaster* [42] and human kinetochores [43] was mapped with nanometer accuracy.
Kinetochores consist of several copies of about 30 core subunits that are able to recruit further regulatory proteins. Electron microscopy (EM) images visualize kinetochores as trilaminar objects [44–46] with electron dense inner and outer kinetochore plates that are separated by an electron lucent middle layer. These layers correspond to different functional units of the kinetochore, which can be summarized in four general modules [10] as schematically shown in **Figure** 1.4 and **Figure** 1.5. The first module is the inner kinetochore that forms a sturdy interface with the centromeric chromatin and corresponds to the electron dense inner plate. It mainly comprises a 16 subunit complex known as the constitutive centromere associated network (CCAN), discussed in detail in **Section** 1.5. The second module is the outer kinetochore, which is built of a 10-subunit protein complex, the KMN network, that comprises the three subunits Knl1-complex, Mis12-complex and Ndc80-complex, further discussed in **Section** 1.4.4. The outer kinetochore contributes to the microtubule binding interface and appears as the electron dense outer plate in an EM image. The third module is responsible for discrimination between correct and incorrect attachments of spindle microtubules to kinetochores [47, 48], preventing the stabilization of improper and selective stabilization of correct attachments [49, 50]. The fourth functional module comprises the spindle assembly checkpoint (SAC), as explained in **Section** 1.4.5. Its components are located to a fibrous corona on the outside of kinetochores. The SAC synchronizes microtubule attachments with the progression of the cell-cycle. SAC components are recruited but also silenced by the outer kinetochore. Anaphase

onset is achieved after the completion of biorientation of all chromosomes through loss of cohesion and degradation of Cyclin B [51]. Besides the SAC components, the outer corona of kinetochores contains microtubule motors, such as CENP-E [52].

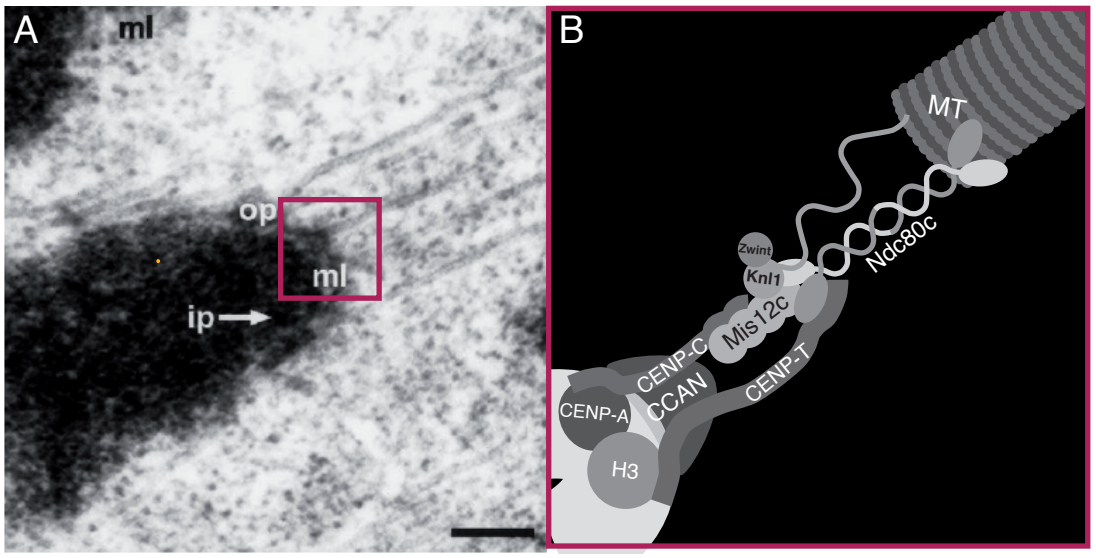

FIGURE 1.4: **General kinetochore organization**. Electron microscope image of a kinetochore bound to microtubules. The electron dense outer plate (op) and inner plate (ip) can be visualized as separated by an electron lucent middle layer (ml) (**A**). EM image taken from [44]. General kinetochore organization includes the binding of CENP-C to the centromere specific nucleosome CENP-A and the interaction of CENP-T with canonical nucleosomes at the centromere. CENP-C and CENP-T have been proposed to make a connection to the outer kinetochore by binding Mis12 and Ndc80 complexes, respectively. For simplicity reasons, the remaining CCAN is only shown as a single object at the basis of the kinetochore and only one microtubule binding unit is represented (**B**).

1.4.1 Centromeric chromatin organization

Kinetochores are built onto centromeres, specific chromosomal *loci* [52–55]. In contrast to the point centromeres of budding yeast that bind a single microtubule [34, 35], human kinetochores are built on regional centromeres [56]. They extend over long arrays of repetitive DNA sequences [52, 56] and are capable of building kinetochores that attach to several microtubules [39, 40, 57]. In theory, if a functional centromere is absent from a chromosome, no kinetochore will form and as a consequence, the chromosome will not segregate in mitosis. On the contrary, the presence of more than one centromere on one chromosome might lead to its

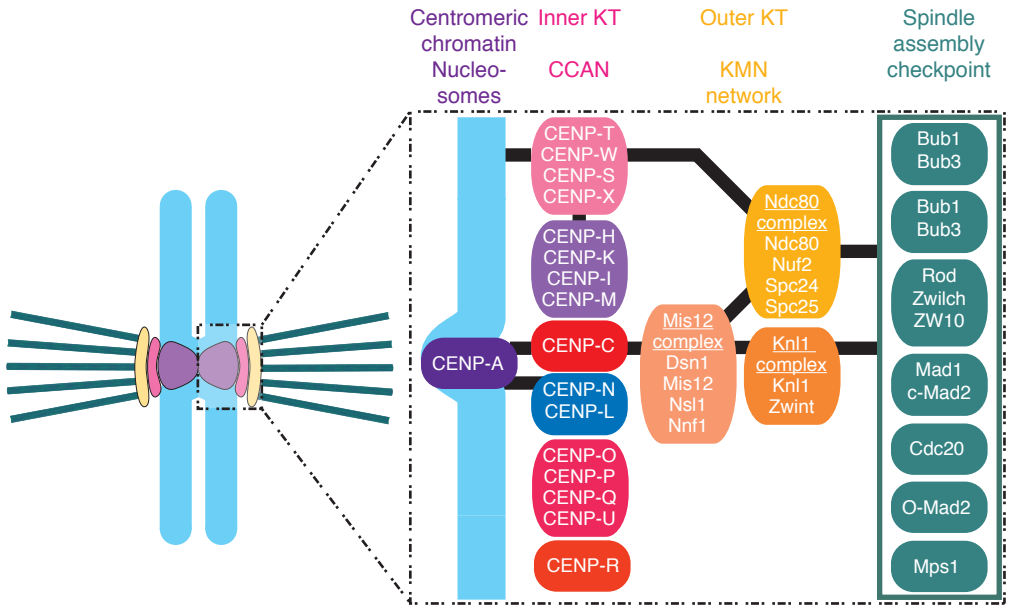

FIGURE 1.5: **Schematic kinetochore organization**. CENP-C directly binds to CENP-A containing nucleosomes and to the outer kinetochore component Mis12 complex. Black lines indicate direct interactions. Proteins that have been shown to recombinantly form subcomplexes are depicted in one box. CENP-N/L has been shown to also directly bind to CENP-A and indicated to interact with CENP-C in yeast. CENP-T/W/S/X complex has been proposed to form a nucleosome like structure at centromeric chromatin. Direct interaction of CENP-T/W/S/X to CENP-H/I/K/M has been demonstrated recently. By binding to Ndc80 complex within the outer kinetochore, CENP-T/W/S/X might provide another axis of kinetochore assembly besides CENP-C. The outer kinetochore is responsible for recruitment, but also silencing of SAC components.

fragmentation by spindle forces. Therefore, centromere specification is a crucial feature of every chromosome.

The DNA of human centromeres consists of thousands of copies of a 171-bp repeat sequence known as α-I satellite DNA. A feature of this α-I satellite DNA is the existence of the so called CENP-B box, which is recognized by the CENP-B protein [58, 59]. This protein is required to establish centromeric chromatin, but is dispensable for its maintenance and suppresses the formation of new centromeres at ectopic sites [60, 61]. The occasional formation of these neo-centromeres on non-centromeric DNA demonstrates that in spite of the unique features of α-I satellite DNA, it is not strictly required for centromere specification [62]. This strongly points towards the existence of an epigenetic mechanism in the establishment and maintenance of centromere identity [56]. Besides histone modifications that are specific for the centromeric region [63, 64], in the recent years it has been established that centromeres are defined by the incorporation of the H3 histone

variant CENP-A [65, 66] into centromeric nucleosomes [67–69]. Point centromeres of budding yeast incorporate a single Cse4p (the CENP-A ortholog) nucleosome per chromosome [70, 71], while the regional centromeres of humans incorporate multiple CENP-A nucleosomes, interspersed with H3 nucleosomes [39]. The observation that CENP-A containing chromatin blocks alternate with H3-containing blocks raises the question of how centromeric chromatin is packed in such a way that would allow several kinetochore units to assemble and microtubules to bind, which can only be speculated so far.

1.4.2 CENP-A nucleosome features

CENP-A was discovered in 1985 by immunoblotting and immunostaining of serum isolated from **C**alcinosis, **R**aynauds syndrome, **E**sophageal dysmotility, **S**clerodactyly and **T**elangiectasia (CREST) syndrome patients [72]. The immunoblots from most patient serum showed three recurrent bands and in tissue culture cells it recognized centromeres. The corresponding proteins were named CENP-A, CENP-B and CENP-C (Centromeric Protein) [73, 74]. A decade later it became evident that CENP-A incorporation into nucleosomes represents a hallmark of centromeres that recruit kinetochore proteins [75]. Additionally, CENP-A was found to be upstream of all other kinetochore proteins during *in vivo* localization studies [76–79]. As a consequence, CENP-A deletion leads to a loss of kinetochores and the frequent occurrence of chromosome segregation defects. Therefore CENP-A deletion is lethal in yeast, mouse, *C. elegans* and chicken cells [79–82].

A comparison of CENP-A to H3 nucleosomes helps to understand how CENP-A specifies centromere identity. Three regions in CENP-A can be found to differ from H3 that include its N-terminus, the CENP-A targeting domain (CATD) and the C-terminus.
The N-terminus is a site of CENP-A specific post-translational modifications [83] and has been shown to be involved in loading of CENP-B to centromeres [84]. In contrast, it is not required for centromere targeting of CENP-A. Interestingly, although the N-terminus shows almost no sequence homology across eukaryotes and differs in size, it shows a conserved feature which is the significant enrichments in arginines in comparison to H3 [85]. The CATD comprises two α-helices within the histone fold domain of CENP-A [86–88]. It has been shown to contain the

determinants crucial for CENP-A centromeric deposition, which will be discussed in more detail in **Section** 1.4.3. CENP-A displays a poorly conserved C-terminus [89], which is hydrophobic in most species.
The two CCAN proteins CENP-N and CENP-C bind directly and specifically to CENP-A nucleosomes [90]. CENP-N binds to the CATD of CENP-A [91]. A recent study has revealed the molecular details of CENP-C:CENP-A interaction by nuclear magnetic resonance (NMR) and crystallography [89]. It demonstrates that CENP-C binds to an acidic patch on the surface of histone H2A and H2B as well as to the hydrophobic C-term of CENP-A [89, 90] with two regions of CENP-C, the central domain and the Mif2 homology domain (schematically depicted in **Figure** 1.6). The central and Mif2 binding sites are conserved in mammals and from yeast to human, respectively. This indicates a conserved mechanism of the CENP-C:CENP-A interaction. Interestingly, CENP-C was implicated to be involved in new CENP-A deposition, which is discussed in the next section.

1.4.3 CENP-A nucleosome replenishment

In human cells, CENP-A nucleosomes are equally partitioned to both centromeres in S-phase [92]. In contrast to canonical nucleosomes, where histone incorporation is linked with DNA replication [93, 94], the time of CENP-A incorporation has been determined to be in telophase and after mitosis in the subsequent G_1 phase [92, 95–97]. This was shown by pulse-chase fluorescent labeling of SNAP-tagged CENP-A in HeLa cells [92]. The exact mechanism for the incorporation of new CENP-A into chromatin is a current field of investigation. Two scenarios can be imagined to happen during DNA replication. Either H3 nucleosomes replace the missing CENP-A nucleosome on each sister chromatid or all CENP-A nucleosomes split into half and form tetramers [98]. Regardless of the reloading mechanism, CENP-A levels at centromeres are half during mitosis, where kinetochores carry out their function.
So far it is known that the CATD of CENP-A is involved in CENP-A replenishment, by recruiting the CENP-A chaperone Holliday junction recognition protein (HJURP) [88, 99, 100]. HJURP is recruited to kinetochores in early G_1, the time of CENP-A replenishment [99]. 72 h after HJURP depletion CENP-A amounts at centromeres are reduced to one third [99]. High-resolution details of a direct interaction between CENP-A and HJURP was revealed in the crystal structure of a fragment of HJURP bound to CENP-A / H4 heterodimer [101]. 26 amino acids

in the N-terminus of HJURP are interacting with the CATD region of CENP-A [102] independent of H2A-H2B [99]. Since the crystal structure of the corresponding budding yeast complex shows substantial similarity, the overall mechanism of CENP-A replenishment seems to be conserved [103]. All these results make a strong indication that HJURP is a CENP-A specific chaperone.

It has been reported that Mis18 complex is also involved in the deposition of CENP-A [95, 104, 105]. Mis18 complex consists of Mis18α, Mis18β and M18BP1/ KNL2 [95, 104–107]. The complex has been demonstrated to play a role in HJURP recruitment to CENP-A nucleosomes [108] and in priming of centromeric DNA, a crucial step of CENP-A replenishment. This might be achieved through acetylation of histone H4 by Mis18 complex. In agreement, Mis18 complex depletion leads to CENP-A level reduction at centromeres, what can be overcome by the inhibition of histone deacetyl transferase, trichostatin A [105]. Therefore, Mis18 complex might provide a status of the centromeric chromatin that allows new CENP-A nucleosome incorporation.

As a possible way to ensure CENP-A deposition only into centromeric chromatin, Mis18 complex is targeted to CENP-C, which is only present at centromeres [109, 110]. Therefore, the whole deposition machinery can only assemble on this specific locus on the DNA. Besides recruiting the Mis18 complex to centromeres, Cenp-C has a yet elusive role in CCAN assembly, which is the focus of this study and will therefore be discussed extensively in the following sections. Besides these two funtions of CENP-C, it acts together with CENP-T in the assembly of the outer kinetochore.

1.4.4 The outer kinetochore

The outer kinetochore consists of the KMN network, which comprises the **K**nl-1, **M**is12 complex and **N**dc80 complex as schematically shown in **Figure** 1.4 and **Figure** 1.5 [111–118], (reviewed in [119]). It starts assembling very rapidly in prophase of the cell cycle [120] and dissociates in telophase [10].
The KMN network fullfills two key functions of active kinetochores. First, it enables the kinetochore to attach to assembling or disassembling microtubules [121–124]. This feature is crucial to align chromatids to the metaphase plate and move them toward the spindle-pole during anaphase. In agreement with the KMN network being the microtubule interaction hub of the kinetochore, kinetochore-microtubule attachments are disrupted in siRNA treated cells for any of the KMN network components [112, 115, 125–133].
As a second feature, the KMN network recruits all SAC components with the possible exception of Aurora B. The outer kinetochore is therefore involved in activation and silencing of SAC components and subsequently in the regulatory machinery of the kinetochore [77, 134–144].

In more detail, the 57-nm-long, 170 kDa Ndc80 complex comprises the two subcomplexes NDC80:NUF2 and SPC24:SPC25 [115, 127, 130, 145]. Ndc80 complex is a crucial component for cell viability, since its functional loss results in kinetochore-microtubule attachment errors and subsequent chromosome mis- or non-segregation [146]. It has been shown to adopt a dumbbell-like structure in which the two heterodimeric subcomplexes occupy the ends of the dumbbell and are separated by a long coiled-coil region [147, 148]. Studies on the structure of Ndc80 complex revealed details of its interaction with microtubules [149, 150]. It serves as the primary binding site for microtubules through a Calponin homology domain and the positively charged N-terminal end of the NUF2:NDC80 dimer [147, 148, 151–155]. Although both NDC80 and NUF2 contain a CH domain, which were both suggested to contribute to microtubule binding [149, 150, 156] it has been shown that NUF2 is not part of the microtubule interaction [151]. The CH domain of NDC80 interacts with the negatively charged C-terminal tails of tubulin monomers (known as E-hooks) [150, 151, 155] with high affinity to straight microtubules and low affinity to curled protofilaments that occur at the end of depolymerizing microtubules. The other heterodimer, SPC24:SPC25 is responsible for its kinetochore recruitment by Mis12 complex, but also CENP-T [157, 158].

The question of how kinetochores keep attached to growing or shrinking microtubules might partly be answered by the nature of the NDC80 interaction with microtubules. Ndc80 complex has been demonstrated to have a relatively low affinity to microtubules [127]. Indeed, in solution NDC80 does not maintain attachment to shrinking microtubules [159]. Nevertheless, in the cell several Ndc80 complexes assemble on each kinetochore [160]. In yeast, 6-8 copies of the KMN network are present per each microtubule attachment site, whereas in *Xenopus leavis* extracts 30 can be found, which was shown by quantitative flourescence microscopy [40, 131, 160]. In vertebrates, multiple fibrillar structures interact with microtubules at each outer kinetochore, as revealed by electron microscopy of the outer kinetochore [46]. Several Ndc80 complexes might therefore act together as a platform that keeps processively associated with depolymerizing microtubules. Indeed, it has been demonstrated that neighboring Ndc80 complexes are held together by the N-terminal tail of NDC80 [127, 151, 155, 161, 162]. Furthermore, when Ndc80 complex is associated with the other KMN network components, the affinity for microtubules is synergistically increased [127]. Besides the microtubule binding feature of Ndc80 complex, other factors might be involved in the ability of kinetochores to keep attached to microtubules. In fungi, a 10-subunit complex known as Dam1, forms a ring-like structure around microtubules [163, 164], which was suggested to embrace and slide down microtubules upon their depolymerization [165]. Indeed, Dam1 complex remains associated with shrinking microtubules *in vitro* [166, 167]. Nevertheless, Dam1 complex only exists in fungi. It has been suggested that the **S**pindle- and **K**inetochore-**A**ssociated (Ska) complex fullfills Dam1 complex function in metazoa [159, 168–172]. Although Ska1 structure [173] and functional mechanism [159] seems to differ from Dam1 complex, it maintains association to shrinking microtubules [172] and it translates this function to the Ndc80 complex *in vitro*, as Dam1 does in fungi [159, 163–167, 172–174].

To prevent stabilization of erroneous attachments, the interaction of Ndc80 complex with tubulin, adjacent Ndc80 complexes, but also with Ska complex is decreased by NDC80 phosphorylation through Aurora B kinase [159, 173–175]. Aurora B is a subunit of the chromosomal passenger complex (CPC), which also contains Incenp, Survivin, and Borealin [176]. Decrease of the affinity between Ndc80 complex and tubulin is achieved through phosphorylation of two separate segments within the N-terminal tail of NDC80 by Aurora B [10, 127, 130]. In agreement with this, *in vivo* activity of Aurora B is crucial for kinetochore microtubule destabilization and microtubule attachment error correction [127, 130, 175, 177, 178].

The importance of NDC80 in this control mechanism is strengthened by the fact that reconstituted NDC80 tracks, stabilizes and rescues the end of depolymerizing microtubules, when dephosphorylated. In contrast, an Aurora B phospomimetic NDC80 mutant is unable to fullfill this function [179]. Additionally, phosphorylation of NDC80 is important for the recruitment and activation of MPS1 at kinetochores, which is essential for the SAC to operate [180–183]. Furthermore, Ndc80 complex is also important for the recruitment of other the SAC proteins: mitotic arrest deficient 1 (MAD1) in complex with MAD2 [137, 139, 184].
Besides Ndc80 complex, another microtubule binding interface seems to exist, since weak kinetochore microtubule attachments can be found in cells depleted for Ndc80 complex [112, 115].
This second microtubule interaction of the outer kinetochore is achieved by the heterodimer KNL1:ZWINT [158]. Members of the KNL1-family are crucial for chromosome segregation and cell viability [112, 185, 186]. The human KNL1 is an elongated 300 kDa presumably unstructured multidomain protein that binds to microtubules on its very N-terminus [127, 187] and Mis12 complex on the other end [158]. Besides microtubule binding, KNL1 is required for kinetochore targeting of several outer-domain proteins of the kinetochore. These proteins include ZWINT, which is constitutively bound to KNL1, CENP-F, the protein phosphatase 1 (PP1), the RZZ complex (**R**OD, **Z**WILCH, **Z**W10) and the mitotic checkpoint proteins budding uninhibited by benomyl 1 (BUB1) and Bub1 related protein 1 (BUBR1) [136, 188]. PP1 binds to the N-terminus of KNL1 and counteracts the Aurora B kinase activity. Besides the already mentioned Ndc80 complex, Aurora B is able to phosphorylate other sites within the KMN network that destabilizes kinetochore microtubule interactions. Therefore, these antagonistic functions of PP1 and Aurora B are involved in regulation of biorientation and chromosome alignment [175, 189–191]. The TPR domains of BUB1 and BUBR1 have been demonstrated to interact with $\sim$ 10-20 amino acids long helical motifs, called KI motifs within the N-terminus of KNL1. These KI motifs have been revealed as crucial for maintenance of SAC activity in human cells, by assembling the mitotic checkpoint complex (MCC; comprising Cdc20, Mad2, BubR1 and Bub3) [135, 192, 193]. In agreement with the major functions of KNL1 being its binding to microtubules and assembling the MCC, depletion of KNL1 in human cells leads to defects in the formation of kinetochore microtubule attachments, chromosome missegregation and displacement of BUB1 and BUBR1 from kinetochores [136, 142, 188].
ZWINT, the 277 amino-acid long constitutive binding partner of KNL1, is also

involved in SAC activation at kinetochores by recruiting the RZZ complex to kinetochores [145, 194–196]. The RZZ complex binds Spindly that enables the assembly of dynein:dynactin motor complexes onto checkpoint proteins such as the MAD1:MAD2 complex [197, 198], which in turn is important for chromosome motility and SAC signaling [199, 200]. ZWINT interaction with RZZ and dynein:dynactin motor proteins is dependent on its phosphorylation by Aurora B kinase.

The third subcomplex of the KMN network, the Mis12 complex, includes the four subunits MIS12, NSL1, NNF1 and DSN1 [115, 127, 130]. Mis12 complex adopts a 22-nm long rod-shaped conformation [158, 201]. Mis12 complex is the only component of the KMN network that does not bind to microtubules *in vitro*. Instead, its major function is to connect the outer kinetochore to the inner kinetochore by directly binding to the CCAN component CENP-C [202]. Depletion of Mis12 complex inhibits the recruitment of multiple proteins to kinetochores [115, 116, 132, 203]. KMN network recruitment is achieved by direct interaction of Mis12 complex with the SPC24 and SPC25 subunits of the Ndc80 complex and the C-terminus of KNL1 [115, 127, 158]. In agreement with this, Mis12 complex has been indicated to be an enhancer of the NDC80 and KNL1 microtubule interactions [127]. Additionally, an interaction of Mis12 complex with the microtubule binding protein Ska has been indicated [174]. Furthermore, Mis12 complex is involved in monitoring the statues of chromosome biorientation by targeting the aforementioned Aurora B kinase to kinetochores. By phosphorylation of Ndc80 complex, KNL1 and Mis12 complex, Aurora B reduces the affinity of the KMN network to microtubules [175], as long as chromosomes are not bioriented. These two functions of Mis12 complex are confirmed by defects in chromosome alignment, biorientation and segregation upon Mis12 complex depletion [132].

Taken together, the KMN network is the interaction hub of kinetochores with microtubules. Control of proper attachment of all chromatids to the mitotic spindle is achieved through attachment-sensitive phosphorylation events within the KMN network. Additionally, the KMN network recruits SAC components that act to prevent anaphase onset in the presence of unattached kinetochores. All these functions are necessary to achieve high fidelity chromosome segregation during mitosis.

1.4.5 The spindle assembly checkpoint (SAC)

In a correctly formed mitotic spindle all kinetochores are bi-oriented, meaning that sister chromatids bind to microtubules from opposite sides of the spindle. During the alignment process attachment errors may occur that include unattached kinetochores, syntelic kinetochores in which both chromatids of one chromosome bind to the same spindle pole, or merotelic kinetochores, where single kinetochores attach to both sites of the spindle. In the mitotic phases prior to anaphase, a protein complex called cohesin holds both sister chromatids together. To proceed into anaphase, this protein complex gets cleaved by the protease separase [204] allowing segregation of the two sister chromatids into two daughter cells. Anaphase onset in the presence of any mistake in spindle attachment would inevitably lead to chromosome segregation errors, which might have catastrophic consequences for the cell, e.g. development of aneuploidies and genetic instability, a common feature of cancer cells [7, 9]. Therefore, it is crucial for the cell to correct all errors of spindle attachment and delay anaphase as long as errors persist before cohesin is irreversibly cleaved.

The SAC is conserved in all eukaryotes and comprises a machinery that delays cell cycle progression to anaphase until all attachment defects are corrected. A set of protein kinases and additional kinetochore associated proteins are key players of this process. Besides the already discussed Aurora B kinase, these include Polo like Kinase 1 (Plk1) [205], the kinases Mps1 [206], mitogen-activated protein kinase (MAPK) and Bub1 [207], the latter being bound to the WD40-βpropeller Bub3 and related to the pseudokinase BubR1 [19]. Furthermore CDK [120, 208] the microtubule motor CENP-E, the proteins Mad1, Mad2, Cdk1-Cyclin B, Nek2, Dynein and dynein-associated proteins [19] and the RZZ complex are involved in this process [19, 209]. Generally speaking, kinases acting in the SAC operate by phosphorylating substrates at the kinetochore. These phosphorylations are involved in promoting kinetochore assembly of further SAC components and preventing incorrect kinetochore microtubule interactions. The two main players of recruitment of downstream SAC components were proposed to be Aurora B and Mps1, but how these kinases promote recruitment of their substrates is not yet clear. Supposedly, both kinases phosphorylate KMN proteins that form a docking site for further SAC components. It has been demonstrated that KNL1 phosphorylation by Mps1 enables Bub1/Bub3 to assemble onto kinetochores [143, 144, 210]. How checkpoint proteins work in detail, has only been partially answered to date.

Likely, the kinases Plk1, Mps1 and Bub1/BubR1 regulate kinetochore-microtubule attachments by influencing Aurora B and PP2A-B56 assembly on kinetochores [211]. Aurora B assembles onto the centromeric chromatin from pro- to metaphase. Phosphorylation of histone H2A by Bub1, H3 by Haspin and Mps1 activity are needed for Aurora B targeting to centromeres [212–215]. Recruitment of PP2A-B56 is mediated by phosphorylation of BubR1 through Plk1 [216, 217]. How Aurora B kinase activity is reinforced in the presence of wrongly attached kinetochores is also a topic of ongoing debate. A current model suggests that the state of attachment influences the access of kinetochore substrates by this kinase. In the absence of biorientation and subsequently low inter-kinetochore tension, Aurora B at the centromeric region is able to reach and phosphorylate its substrates [189]. The distance of Aurora B to its substrates is increased as a consequence of biorientation that leads to high tension within the kinetochore. The question of how stable attachments are created in the first place remains to be elucidated, since the accessibility of Aurora B to its substrates is highest in the beginning of mitosis. After the function of Aurora B and the other kinases is successfully completed, it is critical to remove phosphates from substrates. This is achieved by counteracting phosphatases that localize to kinetochores, such as the PP2A [211, 218] and PP1. PP2A is associated with the B56 regulators that target the holoenzyme to kinetochores during mitosis, via a direct association with the checkpoint component BubR1 [216, 217]. At unattached kinetochores PP2A promotes dephosphorylation of kinetochore substrates, which facilitates kinetochore-microtubule attachments and stabilization of bioriented chromosomes, by keeping phosphorylation levels low in this conformation. It has been shown recently that PP2A counteracts Knl1 phosphorylation by Mps1, and therefore supports silencing of the spindle assembly checkpoint [219].

A second phosphatase, PP1 was proposed to dephosphorylate kinetochore targets of Aurora B [189, 191, 220–224] and possibly also Mps1 [225]. To keep phosphatase activity at a low level at unattached kinetochores, PP1 localization to kinetochores is negatively regulated by Aurora B [189]. Additionally, phophatase-targeting factors help these phosphatases to dephosphorylate their substrates at the right time [189, 216, 226, 227].

How the state of mitotic spindle-kinetochore attachment is sensed in a way that allows anaphase onset only if all kinetochores are bioriented was investigated in the last years. In summary, it has been reported that the checkpoint protein

Mad2 localizes to improperly attached kinetochores, with its kinetochore receptor being Mad1 [228, 229]. Additional SAC components such as Mps1, Bub1, BubR1 and Bub3 are specifically assembling at unattached kinetochores [77, 134–144, 210]. It has been demonstrated through structural work that Mad2 is able to adopt two different conformations, which were named open (O-Mad2) or closed (C-Mad2) [230, 231]. At kinetochores Mad2 is only present as C-Mad2, which is its active form. This C-Mad2 recruits O-Mad2 and promotes its conversion to C-Mad2, which forms the mitotic checkpoint complex (MCC) by binding to Cdc20 and BubR1. MCC prevents Cdc20 [232] from activating the anaphase promoting complex cyclosome (APC/C). The APC/C is an E3 Ubiquitin ligase that degrades proteins which inhibit anaphase initiation e.g. securin, the inhibitory factor of separase [51], and Cyclin B, the activator of CDK1. APC/C is therefore responsible for mitotic progression. As long as the MCC holds Cdc20, the APC/C is not able to operate and therefore initiate anaphase onset. As long as a single kinetochore is not correctly attached to the mitotic spindle, the formation of MCC is promoted and the cell is not released into anaphase. After this last kinetochore got properly attached to the spindle, a set of additional proteins turns off the checkpoint signal. These proteins include e.g. dynein, which removes checkpoint proteins from kinetochores like Mad1 and Mad2 [200, 233–235]. The already mentioned RZZ complex is involved in targeting dynein/dynactin complex to kinetochores. Additionally, RZZ recruits the checkpoint proteins Mad1 and Mad2 to kinetochores [236] and is therefore required for both checkpoint activation and silencing. Additionally, Cdc20 is released from the MCC with help of APC/C dependent ubiquitylation and degradation of BubR1 [237, 238] and p31/Comet introduced sheltering of Mad2 [239, 240]. p31/Comet binds to C-Mad2 at the same binding site where BubR1 would bind within the MCC and therefore promotes MCC disassembly. When Cdc20 is no longer bound to the MCC, the APC/C is activated and degrades securin. Separase is now able to cleave cohesin and the mitotic spindle pulls sister chromatids to opposite sides of the cell.

Taken together, on the one hand the KMN network serves as interaction hub for spindle microtubules and therefore drives chromosome segregation. On the other hand the KMN network is responsible for sensing the status of kinetochore attachments and delaying chromosome segregation until all chromosomes are bioriented by recruiting SAC components.

1.5 CCAN organization & function

The constitutive centromere associated network (CCAN) is a complex of proteins responsible for the recruitment of outer kinetochore components to centromeric DNA and creation of a sturdy interface that sustains spindle forces (summarized in [241]), [78, 157, 242–244]. All members of the CCAN are called CENP (which stands for CENtromere Protein) followed by a letter. CCAN binding to centromeric chromatin is the first step in the kinetochore assembly pathway [245, 246]. Since the CCAN is specifically recruited to CENP-A containing nucleosomes, it restricts kinetochore formation to the centromeric region. Interestingly, some CCAN components have been suggested to be implicated in the replenishment of CENP-A chromatin [96, 110, 247, 248], pointing towards a positive feedback loop for CENP-A incorporation into centromeric DNA. Thus the CCAN is critical to both the recognition and the maintenance of centromeric chromatin.

The CCAN was first described in 2004 by chromatin immunoprecipitation using anti-CENP-A monoclonal antibody and subsequent analysis in mass spectrometry. Although this study did not discriminate generic chromatin binders from centromere binders or provide information about the proximity of the identified proteins to CENP-A, it found about 40 different proteins of known and unknown function, which were called interphase centromere complex (ICEN) [249]. The CCAN was further characterized as a group of CENP-A interacting proteins, localized specifically to the centromere, in the following years by three independent studies in human and chicken cells [76, 250, 251]. These studies identified new CCAN proteins and divided them into different classes, mainly based on their dependencies for localization to kinetochores or their distance from centromeric chromatin. Additionally, although sequence diversity of CCAN components is high, bioinformatic approaches identified CCAN orthologs in yeast, pointing towards a conservation of this protein complex from yeast to humans [252, 253]. Only three CCAN proteins are essential in yeast. Some organisms like *C. elegans* and *D. melanogaster* apparently lost many of their CCAN components except CENP-A and CENP-C, indicating the establishment of a simplified kinetochore version in these organisms, or highly divergent sequences [254]. Despite these differences between species, all organism have in common that the majority of the CCAN proteins are constitutively present at centromeric chromatin throughout the cell cycle [188, 255]. One apparent exception is CENP-N, which has been shown to have varying levels at the centromeric region in different cell cycle phases [255, 256].

Another variable compoenent is CENP-U, which is absent from kinetochores in anaphase [257], and CENP-O, which has apparently reduced levels in metaphase [138].

In vertebrates, the CCAN is built by at least 16 proteins that have been suggested to be organized in subcomplexes that make up a complex network of interactions [76, 250]. The CENP-O/P/Q/U complex is thought to be implicated in microtubule interaction and checkpoint function [241] and to directly bind to CENP-R, a protein of unknown function [78]. CENP-N has been reported to be involved both in CENP-A nucleosomes recognition [91] and formation of a subcomplex with CENP-L in yeast [258, 259]. CENP-C is an elongated protein that binds selectively to CENP-A containing nucleosomes [89, 90] and to the outer kinetochore component Mis12 complex with its N-terminal 71 amino acids [153, 202, 260]. This is one of the two CCAN connections to the outer kinetochore, the other being the direct interaction between the elongated N-terminus of CENP-T and the Ndc80 complex [153, 242, 261, 262]. To underline the importance of these connections in kinetochore assembly, targeting of both CENP-C and CENP-T to ectopic sites on chromosomes leads to assembly of kinetochores, overcoming the requirement for CENP-A [153, 247, 261]. Therefore, a recruitment hierarchy for the whole kinetochore, consisting of two independent pathways made up by CENP-C and CENP-T/W has been proposed. Furthermore, the CENP-T/W forms a complex with CENP-S and CENP-X via their histone fold domains. That quaternary complex has been suggested to create a nucleosome-like structure at centromeres [242] in contrast to the previous observation that CENP-T/W complex selectively binds to H3 containing nucleosomes [246, 263]. Either as an H3 binder, or a nucleosome-like structure, both models assume the CENP-T/W/S/X complex localizes independently to kinetochores. Recently, the complex CENP-H/I/K/M has been introduced as an essential component of CCAN assembly. The CENP-H/I/K/M complex is also a heterotetramer, built around the small pseudo-GTPase CENP-M. CENP-H/I/K/M has been shown to directly bind to the CENP-T/W/S/X complex and siRNA depletion of CENP-H/I/K/M components leads to the loss of CENP-T/W from kinetochores and to chromosome segregation defects [264] (For more information on the CENP-H/I/K/M complex see **Section** 1.5.3). This contrasts the previously indicated independent assembly pathway of CENP-T/W, and as such CENP-C was proposed to be the only pathway for kinetochore assembly. However, proof of a direct interaction of CENP-C with other CCAN components

was not achieved so far, except its interaction with Iml3/Chl4 (CENP-N/L orthologues) [258]. Therefore, fundamental knowledge about the CCAN organization and function is still missing. In particular, the role of CENP-C in CCAN organization and the question whether CENP-C and CENP-T build two independent pathways for kinetochore assembly need to be answered. Additionally, interactions within the CCAN and with other kinetochore components may have as yet eluded us. Therefore, a detailed study of the functional organization of the CCAN protein complex is crucial. This work contributes to a deeper understanding of the CCAN and therefore provides precious information in this flourishing field of investigations.

1.5.1 CENP-C

In 1985, CENP-C was one of the first CCAN components to be identified in serum from CREST syndrome patients [72]. Additionally, CENP-C was the first CCAN protein demonstrated to be a component of the inner kinetochore plate by immunoelectron microscopy [243]. Primarily, CENP-C was identified as crucial kinetochore protein, since preventing it from kinetochore localization through antibody microinjection disturbs kinetochore formation [265]. In agreement, CENP-C depletion mimics the phenotype of CENP-A disruption, including chromosome alignment and kinetochore assembly defects [266–269]. These depletion studies therefore located CENP-C on top of the kinetochore assembly hierarchy. Its loss leads to impaired recruitment of several kinetochore proteins such as CENP-K [270] and CENP-L [271], outer kinetochore components like Mis12c [77, 268, 270] and Ndc80c [77, 268] and SAC proteins including Mad1 [77], Mad2 [77, 268, 270], Bub1 [77] and BubR1 [268]. Underlining its importance, CENP-C is the only CCAN protein that is conserved in all eukaryotes [82, 272–275]. In contrast, most other CCAN components are conserved from yeast to vertebrates, but are absent in *D. melanogaster* and *C. elegans*. Additionally, Mif2 (the *S. cerevisiae* orthologue of CENP-C) is one of only three essential proteins of the inner kinetochore in yeast. It has been demonstrated biochemically that CENP-C copurifies with histones and is a bona fide component of nucleosomes [68, 69]. Furthermore, CENP-C was identified to comprise a DNA binding feature [276–278], which was indicated to be involved in centromere targeting of CENP-C and subsequent kinetochore assembly. Later it has been revealed that CENP-C is involved in centromere specification and kinetochore recruitment by a direct interaction with CENP-A nucleosomes [89, 90].

Additionally, CENP-C has been suggested to be implicated in CENP-A deposition at centromeres [279]. Later on it has been shown that CENP-C parti-cipates in incorporation of new CENP-A nucleosomes into centromeric chromatin via recruitment of the Mis18 complex component Mis18BP1 [109] as further discussed in **Section** 1.4.3. CENP-C is a 943 amino acid protein that is predicted to be highly positively charged and almost completely unstructured as shown in **Figure** 2.1, which might enable it to fulfill its suggested function of connecting the outer kinetochore to centromeric DNA [153, 202, 260]. This and the other aforementioned functions of CENP-C can be mapped to domains of the CENP-C molecule. Although generally speaking the conservation of CENP-C amongst species is rather low, it possesses highly evolutionarily conserved domains implicated in most of its major functions as shown in **Figure** 1.6. Its very N-terminus interacts with the outer kinetochore component Mis12 complex [202], whereas its central region and a more C-terminal CENP-C motif are both involved in targeting CENP-C to centromeres [90, 270, 271, 274, 280]. The determinants of these interactions have been defined in more detail. CENP-Cs N-terminus interacts with Nnf1 and weakly with Nsl1 subunits of the Mis12 complex and targeting of CENP-Cs N-terminal region to a different locus in the cell lead to displacement of KNL1, Ndc80 complex and Mis12 complex from centromeres [260]. CENP-C central domain binds a hydrophobic region in the CENP-A tail and docks onto the acidic patch of histone H2A and H2B. The more broadly conserved CENP-C motif uses the same mechanism for CENP-A nucleosome recognition [89]. Between the Mis12 complex binding and CENP-A central targeting domain, CENP-C exposes a region that is rich in prolines, glutamatic acids, serines and threonines (PEST). This PEST rich domain is of yet unknown function. The very C-terminus of CENP-C, consisting of a cupin domain is responsible for dimerization of the protein [277, 278, 281]. The crystal structure of the Mif2 cupin domain was determined [281], but the physiological function of this dimerization is still elusive. The most important role of CENP-C for the present study is its function in kinetochore localization of other members of the CCAN. This function could yet not be mapped onto the CENP-C protein. CENP-C was indicated to interact with a dimer containing the CENP-H and CENP-K subunits [270], but such interaction was never shown biochemically. Nevertheless, it might be a critical function of CENP-C, since loss of CENP-H or CENP-K in chicken or human cells leads to defects in stable chromosome alignment and aberrant progression from metaphase to anaphase [250]. Therefore, CENP-C might contribute to the formation of a sturdy interface for

the outer kinetochore assembly.

This work will give a greater understanding on how CENP-C functions in kinetochore assembly and how these functions map onto the CENP-C molecule.

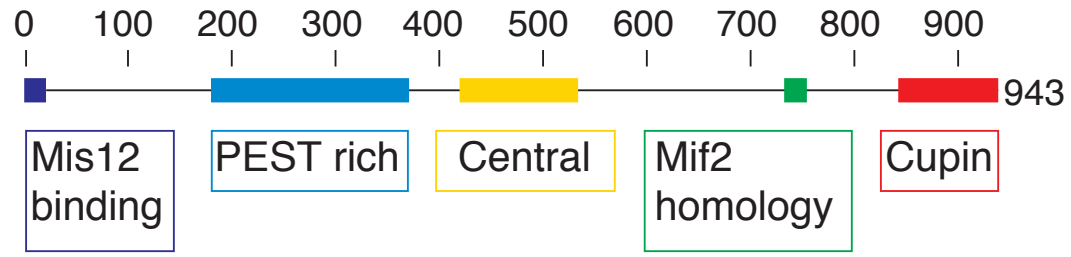

FIGURE 1.6: **CENP-C amino acid composition and functional domains**. The Mis12 complex binding domain is located in the very N-terminus of CENP-C (dark blue) and followed by a proline, glutamatic acid, serine and threonine (PEST) rich region (cyan). CENP-Cs central (yellow) and Mif2 homology domains (green) are both responsible for interaction with CENP-A containing nucleosomes by directly binding to CENP-A and H2A/H2B within the same nucleosome. The cupin domain that is located at the very C-terminus of CENP-C (red) is known to dimerize the protein.

1.5.2 CENP-N and CENP-L

CENP-N and CENP-L were identified in human cells in 2006, where they were suggested to be part of different subcomplexes of the inner kinetochore [76]. Later on, a direct interaction of CENP-L and the C-terminal domain of CENP-N has been identified [91].

Orthologs of both proteins have been identified in fission and budding yeast [252, 261]. A crystal structure of the *S. cerevisiae* orthologs of CENP-N (Chl4) and CENP-L (Iml3) has been published recently [258], confirming their direct interaction. With help of the structure it was demonstrated that Iml3 is able to form homodimers via the interaction of β sheets of each molecule. Interestingly, the Iml3/Chl4 heterodimer relies on the same interface of Iml3, therefore homo- and heterodimer formation is mutually exclusive, but heterodimer formation is favoured due to the larger interaction surface. Furthermore, the Iml3/Chl4 complex binds to the central domain of the CENP-C ortholog Mif2 via the N-terminal domain of Chl4 [258]. This interaction of CENP-N and CENP-C was also identified between the fission yeast orthologs [271].

CENP-N depletion causes chromosome alignment defects through loss of CCAN components, defining CENP-N as critical inner kinetochore protein [76, 91, 255].

Interactions of CENP-N or CENP-L with other CENPs were reported through immunoprecipitation experiments against CENP-H, CENP-K, CENP-I or CENP-M. CENP-N and CENP-L were found to be often associated with these CCAN proteins [76, 250]. Although a direct interaction between the CENP-N/L group and the CENP-H/I/K/M group of proteins has not been identified so far, these findings indicate a close association of these two subcomplexes. In addition, CENP-N was also found to coimmunoprecipitate with CENP-A nucleosomes and CENP-T [90, 91]. Besides CENP-C, CENP-N was reported to directly and specifically bind to CENP-A containing nucleosomes [91]. This binding is independent of the DNA sequence, since binding efficiency was not altered with different DNA wrapped around the histone octamer [91]. With help of several H3-CENP-A chimeric histones, it was observed that CENP-C and CENP-N bind to different structural features on the CENP-A nucleosomes. Therefore, their binding to CENP-A is not competitive [90]. The C-terminal part of CENP-N does not interact with CENP-A containing nucleosomes *in vitro*, but supports its localization *in vivo*, probably through interaction with other CCAN components, possibly CENP-L [91]. In CENP-N depleted cells, CENP-A levels at kinetochores is reduced, pointing towards a role of CENP-N in CENP-A deposition [91, 250].
Thus, while some interesting details about the CENP-N/L subcomplex have been shown to date, their recruitment to kinetochores and interaction with other CCAN components remain insufficiently understood.

1.5.3 CENP-H, CENP-I, CENP-K, CENP-M

CENP-H/I/K has early been proposed to belong to one group of proteins at the inner kinetochore. They all have a known ortholog in *S. cerevisiae* and *S. pombe* [249, 261, 282]. CENP-M, a protein with no known orthologs in yeast [261], has been recently found to form a stable subcomplex with CENP-H/I/K, the CENP-H/I/K/M quaternary complex [264].
The CENP-H, CENP-I, CENP-K and CENP-M proteins were identified separately as constitutive centromere proteins. CENP-H was identified through its colocalization with the already known CENP-A and CENP-C [283, 284]. CENP-I was subsequently defined as a CCAN component, since it colocalizes with CENP-C, CENP-A and CENP-H throughout the cell cycle [282]. CENP-K was initially defined as component more distal from the kinetochore [76]. Later on, CENP-H

and CENP-K were suggested to consist mainly of coiled coils that directly interact in a 1:1 complex [285], thus placing CENP-K in close proximity to CENP-H. Furthermore, CENP-H, CENP-I and CENP-K were found to be closely associated in immunoprecipitation experiments. Additionally, they share similar localization patterns including a dependency on CENP-A and mutual localization dependencies with CENP-N, CENP-L and CENP-M. Therefore, they were defined as CCAN subgroup [76, 91, 250, 255]. CENP-H/K/I, CENP-N/L and CENP-O/P/Q/U/R groups of proteins have been demonstrated to be dependent on, but also influence CENP-M recruitment to kinetochores [76, 250, 251]. CENP-M was first discovered as highly expressed protein in proliferating cells and tumors and therefore termed proliferation-associated nuclear element 1 (PANE1) [286, 287]. Later, CENP-M was characterized in three independent studies as component of the interphase centromere complex, as being in close proximity to CENP-A nucleosomes and as part of the previously defined CENP-H/CENP-I group of proteins [76, 250, 251]. Very recently, CENP-M was characterized as a pseudo-GTPase that is part of the newly identified CENP-H/I/K/M complex, which is a constitutively bound CCAN subcomplex [264]. Before that study, different roles of CENP-C [90, 270] and CENP-T [246] in CENP-H/CENP-I/CENP-K group localization to kinetochores were suggested. Now it became clear that CENP-T/W subcomplex is dependent on CENP-H/I/K/M for its kinetochore recruitment through a direct interaction, whereas the binding platform for the CENP-H/I/K/M is still undiscovered [264]. It was suggested to be localized in the CENP-C protein [264, 268]. How exactly CENP-H/I/K/M is localized to kinetochores is one of the main focuses of this work. Besides CENP-T/W, CENP-H/I/K group of proteins is also required for CENP-O/P/U/U/R group localization to centromeres, but not vica versa [188, 250, 255]. In addition, CENP-H/K/I group contribute to the localization of outer kinetochore components [188, 250, 268, 288].

1.5.4 CENP-T, CENP-W, CENP-S, CENP-X

CENP-T was initially identified as being located in close proximity to CENP-A nucleosomes [76]. Later, CENP-T has been shown to specifically interact with H3, but not CENP-A containing nucleosomes [246]. Super-resolution microcopy indeed placed CENP-T in close proximity to H3 nucleosomes [263]. It has been shown to bind to DNA via a histone fold domain in its C-terminus [248], which is

necessary for centromere localization. Therefore, like CENP-C, CENP-T is able to mediate interaction between the centromeric DNA and the outer kinetochore by binding the outer kinetochore component Ndc80 complex on its N-terminus [153]. CENP-T is predicted as an elongated protein and was suggested to have a flexible structure that stretches upon tension through forces of kinetochore microtubules [289]. Indeed, CENP-T N-terminal construct without the histone fold domain does not localize to chromatin, but induces kinetochore like structures that bind microtubules when artificially localized to ectopic regions on chromosomes [153]. In addition, CENP-T possesses two highly conserved α helices that are functionally relevant, since deletion of this region prevents CENP-T kinetochore localization [242]. CENP-T has also been shown to directly bind to CENP-W [246]. CENP-W is a small protein that is almost entirely comprised of a histone fold domain. The binding of CENP-T and CENP-W to create a heterodimer occurs through their histone folds, which is required for their kinetochore localization in human cells and yeast [242, 261]. Besides CENP-W, CENP-S and CENP-X are small proteins that have been shown to form a complex with CENP-T/W. For all of these proteins orthologs have been identified in fission and budding yeast [261], pointing towards a conservation of their function. CENP-S/X is not required for CENP-T recruitment to kinetochores, as CENP-T assembles onto chromatin in the absence of CENP-S.
CENP-S was initially found in affinity purifications against CENP-M and CENP-U [76]. Subsequently, CENP-X was found as CENP-S binding partner [290]. Both proteins were predicted to have histone fold domains based on sequence comparisons. Recently it has been shown that CENP-S/X interacts with the histone fold domains of CENP-T/W to form a 1:1:1:1 tetrameric complex. The crystal structure of this complex was resolved, which confirmed the predicted histone fold domain of all four components to be the interaction hub of this complex [242]. The protein complex was further shown to interact with DNA and to protect about 100 bp from MNase digestion *in vitro*. This observation let to the conclusion that CENP-T/W/S/X complex forms a nucleosomes like structure at centromeres [242].

Initially, CENP-T/W were placed upstream of CENP-H/I/K and CENP-O/P/Q/U/R group of proteins and parallel to CENP-C for their kinetochore localization by knockout studies in chicken cells [246]. In contrast, CENP-S/X localization to kinetochores was shown to depend not only on CENP-T/W, but also on CENP-H/I/K group [290] and not to depend on CENP-C [246]. A recent study placed also

CENP-T/W downstream of CENP-H/I/K/M in the recruitment hierarchy [264]. In a different study, CENP-T was placed downstream of CENP-C for its kinetochore localization [90], although the interdependency of CENP-C and CENP-T is still a matter of debate. Therefore, a clear picture of how CENP-T/W is recruited and bound to kinetochores is missing. Some more information about this topic is provided in this work.

1.5.5 CENP-O, CENP-P, CENP-Q, CENP-U, CENP-R

CENP-50 was the first protein of this complex being identified as constitutive centromeric component [291]. In a later study CENP-O, CENP-P, CENP-Q and CENP-R were also identified, and CENP-50 renamed CENP-U [76, 250]. Co-expression of CENP-O/P/Q/U in bacteria and subsequent affinity purification and size exclusion chromatography revealed the formation of a stable complex that can bind to CENP-R [78]. In the same study, the complex was revealed to be implicated in recovery from mitotic spindle damage. Depletion of any of the CENP-O/P/Q/U components did not cause lethality in chicken DT40 cells, but they immediately proceeded through the cycle after release from nocodazole. Most of the cells showed mild mitotic defects including slower proliferation and problems in metaphase plate organization. A portion of cells that exhibited extreme mitotic phenotypes died after anaphase, whereas depletion of CENP-R showed a milder effect. CENP-U seems to play a key role in this function, since cells deficient of CENP-U managed to re-align chromosomes after release from nocodazole, but did not progress into anaphase. This indicates that in the absence of CENP-U cells experience irreversible damage caused by nocodazole. Phosphorylation of CENP-U in this process seems to be relevant, since in nocodazole treated cells, it was found hyperphosphorylated by Plk1 [78, 257]. Furthermore, CENP-U has been demonstrated to directly interact with Ndc80 complex and microtubules [292]. These interactions have been shown to be negatively influenced by Aurora B phosphorylation, indicating a contribution to the error correction machinery mediated through Aurora B phosphorylation of CENP-U [292]. Taken together CENP-U plays a role in proper adhesion and delay of anaphase in the case of a damaged spindle [76, 78]. In addition, it has been demonstrated recently that CENP-U depletion in mouse embryonic stem cells or mouse embryos is lethal, indicating a crucial role during embryogenesis [293]. Besides CENP-U, CENP-Q

was reported to interact with microtubules [294].
Probably, CENP-O, CENP-P, CENP-Q and CENP-U function within the quaternary complex, since they are interdependent for their kinetochore localization. Additionally, the CENP-H/K/I group of proteins has been shown to be responsible for recruitment of the CENP-O/P/Q/U/R complex [78, 188, 246, 250] thus placing this complex downstream of most other CCAN components. Only CENP-R, which is of yet unknown function, seems to be located downstream of all components [78, 188, 250, 251, 255]. The binding within the complex was studied in some more details. It is known that the coiled coil of CENP-Q and the leucine zipper of CENP-U are necessary for their interaction and centromere localization [295]. Recently, the crystal structure of *Kluyveromyces lactis* subcomplex of Mcm21 (CENP-O) and Ctf19 (CENP-P) was provided. It reveals that both proteins possess tandem RWD domains that form a Y-shaped structure with an N-terminal flexible extensions [296]. In contrast, CENP-Q, CENP-U an CENP-R consist mainly of coiled coils according to secondary structure prediction, extended by an N-terminal tail only in CENP-U [254].
Except for CENP-R, orthologs for CENP-O,- P, -Q and -U were identified in yeast [252, 255]. The complex in yeast is known as COMA complex, consisting of Ame1, Okp1, Ctf19 and Mcm21. Interestingly, in budding yeast Ame1, Okp1 and Mif2 (CENP-C) are the only three essential CCAN components. This does not seem to strictly correlate with CENP-U/CENP-Q more peripheral function in vertebrates and the mild phenotype of their depletion. A recent study showed that the N-terminus of Ame1 directly interacts with the outer kinetochore component Mtw1 (Mis12). Since the Ame1:Okp1 heterodimer directly associates with Mif2 it was suggested that they act in a cooperative manner to assemble the KMN network onto centromeric chromatin, which might explain their importance in yeast [297].

In summary, CENP-O/P/Q/U is a constitutively associated complex with yet elusive, but not essential function at kinetochores in humans. Also its binding protein CENP-R is of unknown function. In contrast, the COMA complex in yeast is an essential kinetochore component, probably through its critical role in outer kinetochore assembly.

1.6 Objectives

Here, the overall goal is to characterize the interaction of CENP-C with its various binding partners, setting the focus on various members of the inner kinetochore, and especially on the CENP-H/I/K/M and CENP-N/L subcomplexes. On the one hand biochemical approaches using recombinant CENP-C constructs and CCAN subcomplexes will be used, on the other hand cell biological methods in human cells will be exploited. This will shed light on the overall structure and functionality of the inner kinetochore. Especially, it will help us understand CENP-Cs function at kinetochores and the recruitment hierarchy within inner kinetochore components, which is still confusing. Therefore, this work provides very important knowledge about the functionality of one of the biggest and most exiting protein networks within human cells, the kinetochore.

Chapter 2

Results

2.1 CENP-C construct design

To address the role of CENP-C in CCAN assembly, the recombinant expression of the protein was attempted, in order to use it for biochemical interaction studies with other kinetochore components. CENP-C is predicted to be a mostly unfolded protein (see **Figure** 2.1), it has a high theoretical isoelectric point of 9.43 and a strong tendency to bind DNA. In the cell it is associated with a variety of different proteins that might stabilize it. All these characteristics are challenging properties for a protein to be produced recombinantly. Indeed, full length CENP-C purification trials could only produce degradation products of the protein so far. Therefore, CENP-C truncation constructs were designed based on CENP-C domain organization (see **Figure** 1.6), secondary structure prediction (see **Figure** 2.1) and conservation. Generally speaking, the conservation of CENP-C is low with exception of the Mis12c binding site, the CENP-A binding domains, the cupin domain and small patches distributed over the whole protein. Optimal truncation constructs do not disrupt functional domains or secondary structural elements of the protein or cut within highly conserved sequences. The first construct used in this study was designed by Dr. Siva Jeganathan and included CENP-C$^{2-545}$ for bacterial expression. This construct does not disrupt any known functional domains or structured regions of the protein and contains the known Mis12 binding motif (**Figure** 1.6, dark blue), the PEST rich region (**Figure** 1.6, cyan) as well as its central CENP-A interaction domain (**Figure** 1.6, yellow).

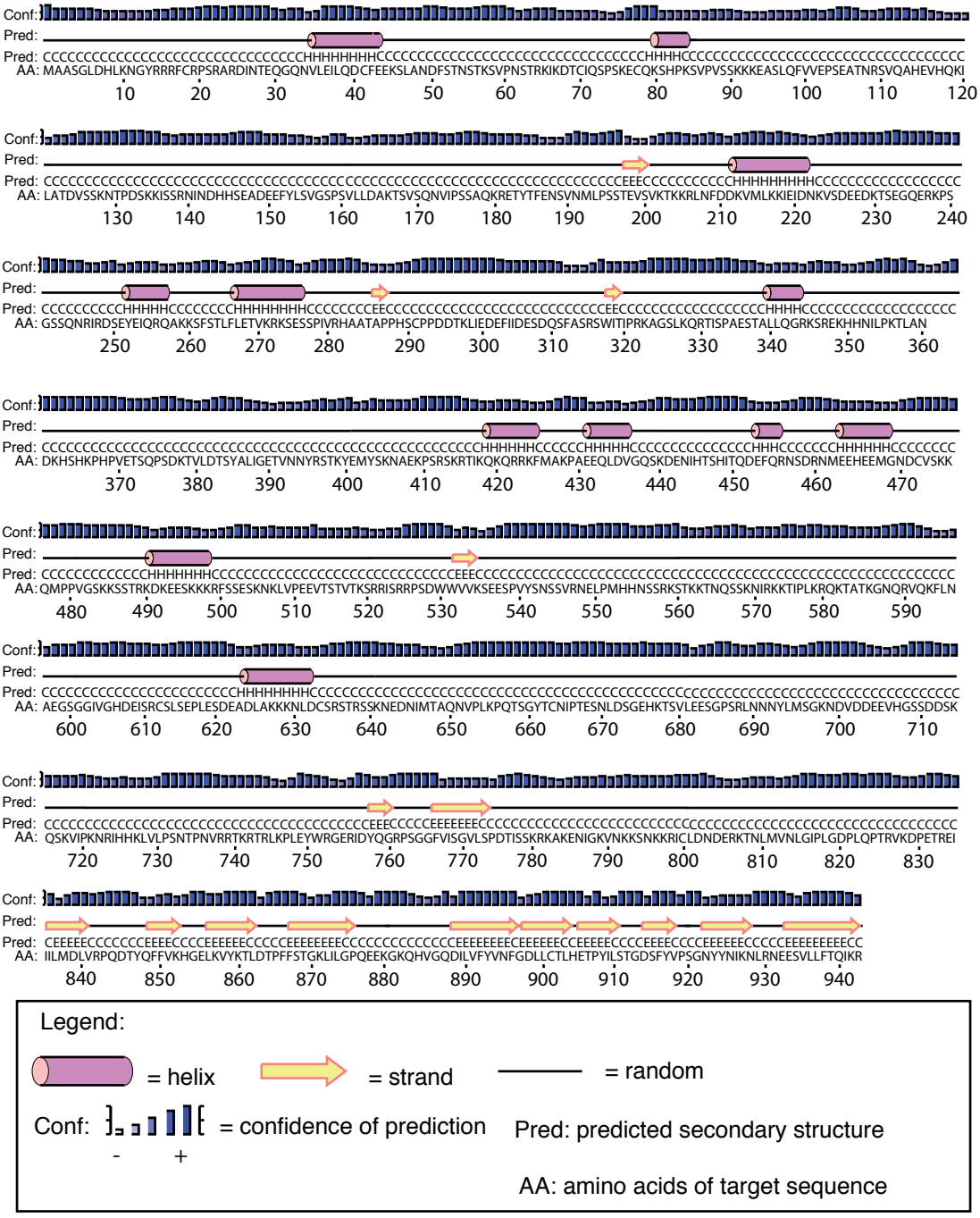

FIGURE 2.1: **CENP-C's secondary structure.** CENP-C secondary structure was predicted with help of PSIPRED v3.3. PSIPRED is an accurate method to predict secondary structures of proteins. It incorporates two feed-forward neural networks that analyse outputs obtained from PSI-BLAST (Position Specific Iterated - BLAST). The secondary structure predicted for CENP-C illustrates that CENP-C is an largely unstructured protein, with exception of some small helices distributed over the whole protein and some β-sheets within its C-terminus, where the cupin domain is located.

2.2 Establishment of recombinant CENP-C production

A protocol for CENP-C$^{2-545}$ purification from bacteria and CENP-C$^{1-544}$His from insect cells was successfully established. Detailed protocols for GST-CENP-C$^{2-545}$ expression and purification with and without tag from bacteria and CENP-C$^{1-544}$His expression and purification from insect cells can be found in **Section** 4.10.1 and 4.13.2. Briefly, GST-CENP-C$^{2-545}$ expressing bacteria or CENP-C$^{1-544}$His producing insect cells were lysed, the cleared lysate was applied to either GSH (reduced Glutathion Sepharose High performance) or nickel beads. After extensive washing of these beads, the protein was either eluted to maintain the GST- or His-tag or cleaved over night with a 3C prescision protease to remove the GST tag and gain an untagged protein. The affinity purified protein was applied to a Heparin column, to get rid of any contaminating DNA and unspecific protein contaminants. For quality control reasons all proteins were loaded on a S200 size exclusion chromatography column. Examples for the final purification step of GST-CENP-C$^{2-545}$, CENP-C$^{2-545}$ and CENP-C$^{1-544}$His can be found in **Figure** 2.2, 2.3 and 2.4.

In order to use that construct for *in vitro* studies in solution and on a solid surface, a purification strategy for untagged and GST (Glutathion-S-Transferase) tagged CENP-C$^{2-545}$ was optimized with yields of 200 μg and 500 μg per liter bacterial expression culture, respectively.

The untagged protein produced a degradation product, visible on a Coomassie stained SDS-PAGE gel as a double band of the protein (see **Figure** 2.3 and 2.9). To increase the yields of the untagged CENP-C$^{2-545}$ and improve its stability, the construct was additionally produced in insect cells with a C-terminal Histidine (His)-tag. The N-terminal methionine of CENP-C was included to allow translation. The resulting construct was CENP-C$^{1-544}$His. The yields were improved to 1 mg per liter of expression culture and the purification resulted in a single band on the Coomassie stained SDS-PAGE gel as seen in **Figure** 2.4.

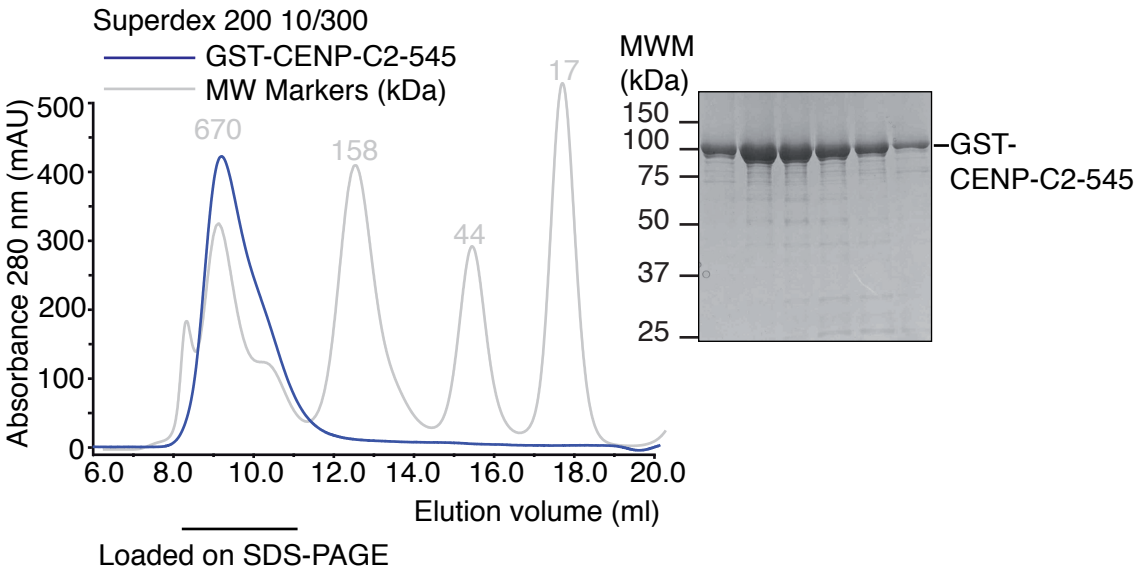

FIGURE 2.2: **GST-CENP-C$^{2-545}$ purification.** CENP-C has been purified from bacteria in three major steps: affinity purification against the GST-tag, a Heparin column, and a size exclusion chromatography. Size exclusion chromatography elution profile of GST-CENP-C$^{2-545}$ ($\sim$ 88 kDa) and Coomassie stained SDS-PAGE gel of the peak fractions are illustrated here. The protein eluted as predicted for a protein of larger Stokes' radius compared to the globular molecular weight markers, consistent with an unfolded structure and a possible dimerization of the protein through its GST tag that has been shown to dimerize [298, 299]. Its relatively small peak is due to a low abundance of aromatic amino acids

A possible explanation for the quality improvement of CENP-C, is the ability of insect cells to perform posttranslational modifications on proteins, such as phosphorylations. To examine if CENP-C$^{1-544}$His is phosphorylated, it was subjected to mass spectrometry analysis, which would unravel the amino acids of CENP-C phosphorylated in insect cells. The sequence coverage of CENP-C in this experiment was 84 %. For control, the protein was also treated with lambda phosphatase and the phosphorylation pattern compared to the untreated sample. A schematic view of CENP-C phosphorylations is shown in **Figure** 2.5.

Indeed, ten phosphorylated amino acids were found in CENP-C$^{1-544}$His. Interestingly, a phosphate at serine 225 was retained in the phosphatase treated sample, suggesting it might be protected in the secondary structure. Bioinformatic analysis of the phosphorylation sites did not indicate any known predicted motif for mitotic kinases. The functional relevance of this phosphorylations therefore needs to be further elucidated.

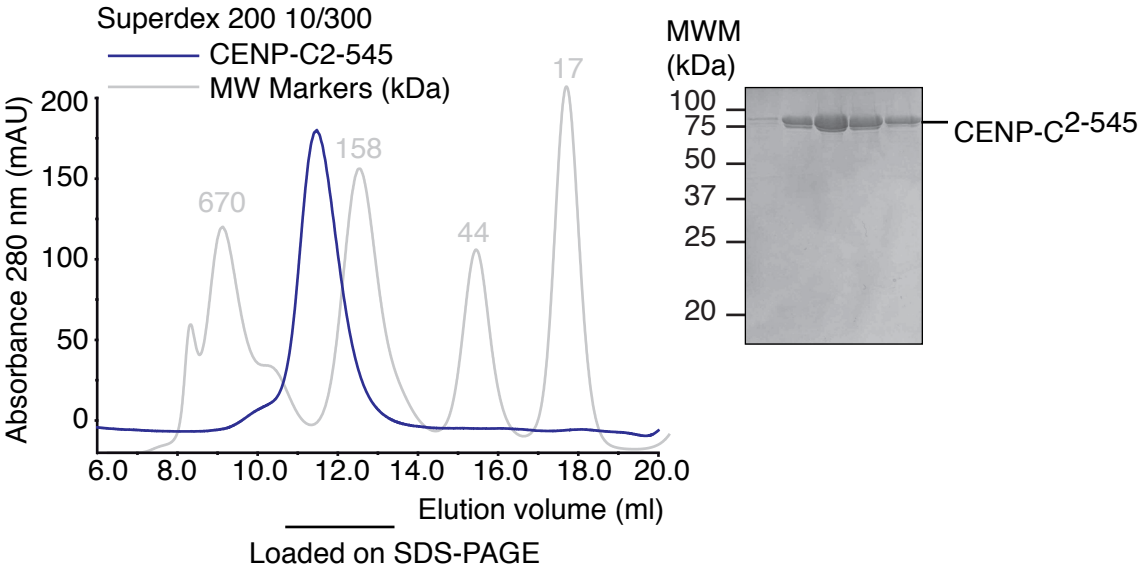

FIGURE 2.3: **CENP-C$^{2-545}$ purification.** CENP-C$^{2-545}$ has been purified from bacteria in three major steps: affinity purification against the GST-tag and cleavage of the tag, a Heparin column and a size exclusion chromatography. Size exclusion chromatography elution profile of CENP-C$^{2-545}$ (∼62 kDa) and Coomassie stained SDS-PAGE gel of the peak fractions are shown here. The protein eluted as predicted for a protein of larger Stokes' radius compared to the globular molecular weight markers, consistent with an unfolded structure, and its relatively small peak is due to a low abundance of aromatic amino acids.

Additionally, the posttranslational modifications of the protein produced from insect cells might induce some folding in the mainly unfolded structure of CENP-C. Indeed, CENP-C$^{1-544}$His runs as a more compact protein compared to CENP-C$^{2-545}$ (compare **Figure** 2.3 and **Figure** 2.4).

During the study of CENP-C interactions with its binding partners, design of additional CENP-C deletion constructs and point mutations became necessary. Amino acids for mutational analysis were chosen on the basis of prior knowledge of this study (see below) and conservation of CENP-C amongst species. A list of all CENP-C constructs and mutants purified and used in this work are summarized in **Table** 2.1. Purification procedures can be found in **Chapter** 4. As an example for a purification of a smaller CENP-C construct, the chromatogram of the final purification step and the Coomassie stained SDS-PAGE gel of CENP-C$^{189-400}$ purified from bacteria can be found in **Figure** 2.6. This construct spans the PEST rich domain of CENP-C, which is of yet unknown function. Therefore, this construct is of particular interest for this study and was also produced in insect cells as depicted in **Figure** 2.7.

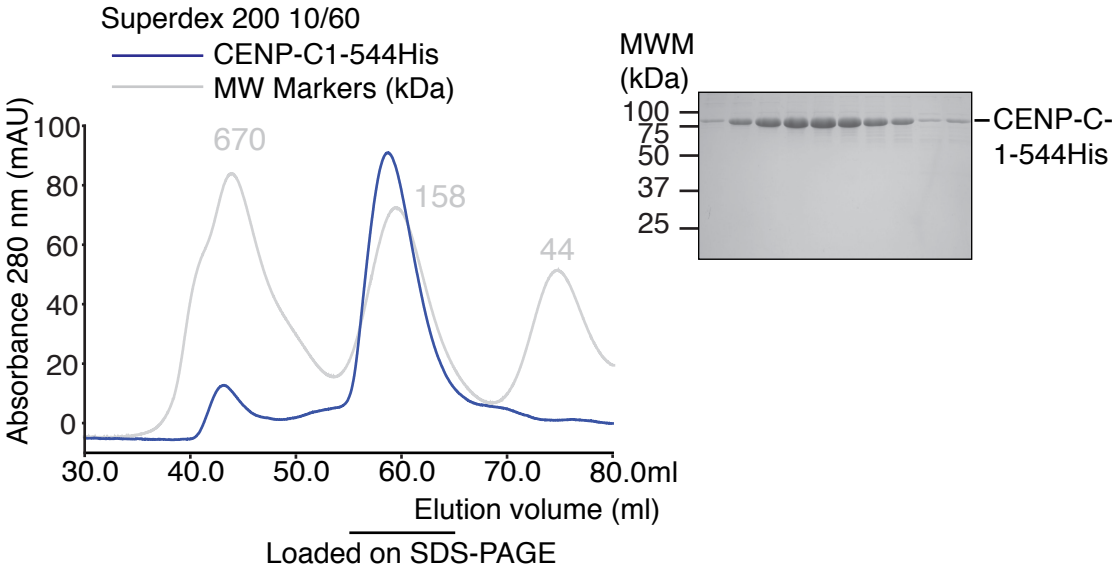

FIGURE 2.4: **CENP-C$^{1-544}$-His purification from insect cells.** Size exclusion chromatography elution profile of CENP-C$^{1-544}$His (∼63 kDa) and Coomassie stained SDS-PAGE gel of the peak fractions are shown here. The protein eluted as predicted for a protein of larger Stokes' radius compared to the globular molecular weight markers, consistent with an unfolded structure, and its relatively small peak is due to a low abundance of aromatic amino acids.

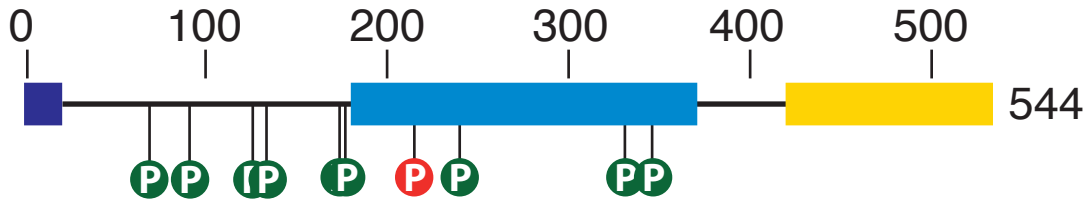

FIGURE 2.5: **CENP-C$^{1-544}$-His phosphorylations.** CENP-C$^{1-544}$His was subjected to mass spectrometry analysis directly after purification from insect cells or after subsequent lambda phosphatase treatment. Phosphorylated amino acids that did not occur in the phosphatase treated sample are depicted as green circles. There was one phosphate that resisted lambda phosphatase treatment, which is depicted here as red circle. The phosphorylated amino acids are serines at positions 73, 96, 127, 176, 177, 225, 240, 333, 345 and a threonine at 130.

TABLE 2.1: Recombinant CENP-C proteins

Protein	**Construct**	**Mutation**
CENP-C	2-545	Wildtype
GST-CENP-C	2-545	Wildtype
GST-CENP-C	2-545	E302A F303A
GST-CENP-C	2-545	E302R F303S
GST-CENP-C	2-545	I305A D306A
GST-CENP-C	2-545	I305A D306A W317A
GST-CENP-C	2-545	L207A F209A
GST-CENP-C	2-545	L207A F209A E302R F303S
CENP-C	2-545	L266A F267A L268A (3A)
GST-CENP-C	2-545	L266A F267A L268A (3A)
CENP-C	2-545	L266A F267A L268A W317A (4A)
GST-CENP-C	2-545	L266A F267A L268A W317A (4A)
CENP-C	2-545	W317A
GST-CENP-C	2-545	W317A
GST-CENP-C	1-71	Wildtype
GST-CENP-C	1-400	Wildtype
CENP-C	402-544	Wildtype
GST-CENP-C	402-544	Wildtype
GST-CENP-C	104-544	Wildtype
CENP-C	189-544	Wildtype
GST-CENP-C	189-544	Wildtype
CENP-C	189-447	Wildtype
GST-CENP-C	189-447	Wildtype
GST-CENP-C	189-420	Wildtype
CENP-C	189-400	Wildtype
GST-CENP-C	189-400	Wildtype
GST-CENP-C	225-400	Wildtype
GST-CENP-C	263-400	Wildtype
GST-CENP-C	290-400	Wildtype
GST-CENP-C	290-400	W317A
GST-CENP-C	189-364	Wildtype

Protein	Construct	Mutation
GST-CENP-C	189-311	Wildtype
GST-CENP-C	189-290	Wildtype
GST-CENP-C	189-290	L207A F209A
GST-CENP-C	189-290	3A
CENP-C	1-400-His	Wildtype
CENP-C	1-544-His	Wildtype

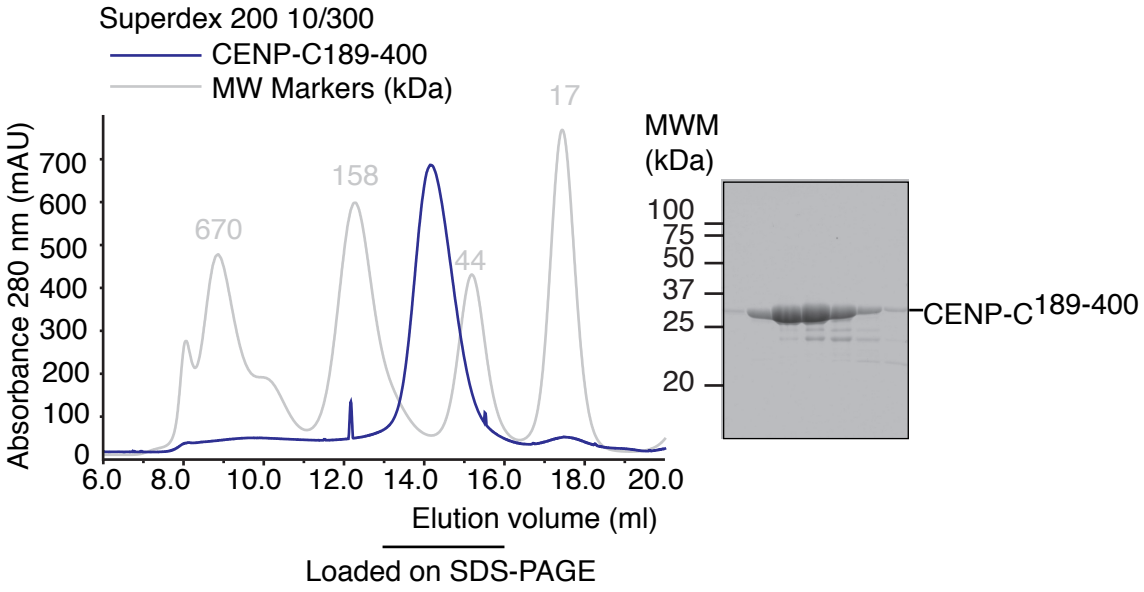

FIGURE 2.6: **CENP-C$^{189-400}$ purification.** Size exclusion chromatography elution profile of CENP-C$^{189-400}$ (∼24 kDa) and Coomassie SDS-PAGE stained gel of the peak fractions are shown here. The protein eluted as predicted for a protein of larger Stokes' radius compared to the globular molecular weight markers, consistent with an unfolded structure.

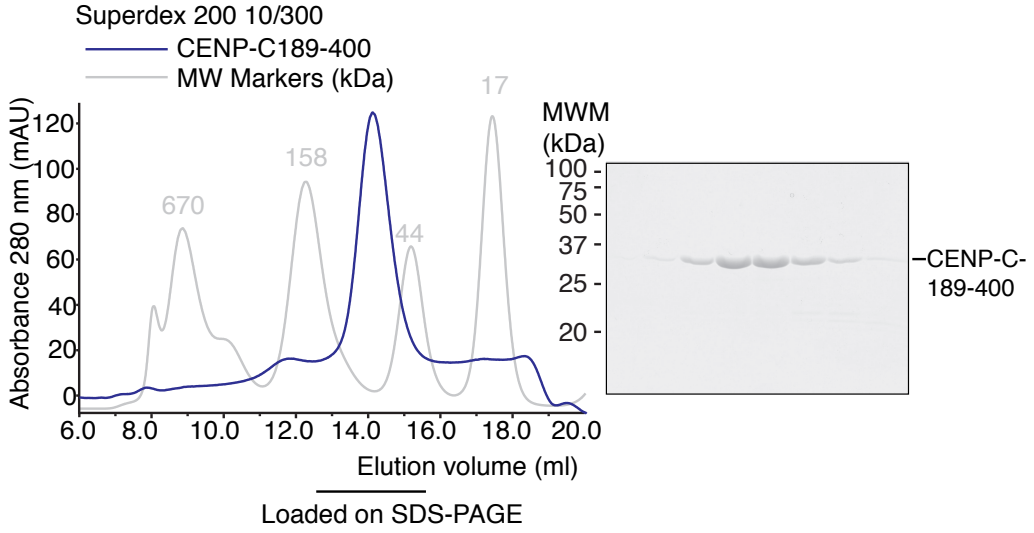

FIGURE 2.7: **CENP-C$^{189-400}$ purification from insect cells**. Size exclusion chromatography elution profile of CENP-C$^{189-400}$ purified from insect cells (~24 kDa) and Coomassie stained SDS-PAGE gel of the peak fractions are shown here. The protein eluted as predicted for a protein of larger Stokes' radius compared to the globular molecular weight markers, consistent with an unfolded structure.

2.3 Production of CCAN subcomplexes

To biochemically investigate whether CCAN proteins bind to CENP-C, a number of human CCAN subcomplexes was produced recombinantly. These subcomplexes were either reported to depend on CENP-C for their kinetochore localization in cells or shown to directly interact with CENP-C in other species. Therefore, they are good candidates to be tested in *in vitro* binding assays.

These subcomplexes include a dimer of CENP-H and CENP-K, expressed and purified from insect cells, with yield of 2 mg per liter of expression culture. Detailed protocols for the CENP-H/K production and purification can be found in **Section** 4.13.3. As final step of the purification, the complex was subjected to a Superdex 200 size exclusion chromatography (SEC) column. The chromatogram from the SEC showed a single peak that eluted as predicted for a protein of larger Stokes' radius compared to the globular molecular weight markers. Since CENP-H/K has previously been determined by static light scattering (SLS) to be a heterodimer (data not shown), this indicates an elongated organization of the CENP-H/K dimer. The Coomassie stained SDS-PAGE gel showed a stoichiometric complex of two proteins with sizes expected for CENP-H and CENP-K. Later during the studies, this dimer was compared with CENP-H/I/K/M complex for a putative

binding to CENP-C. CENP-H/I/K/M purification procedure can be read in **Section** 4.13.6. CENP-H/K and CENP-H/I/K/M complexes are both published in [264].

Furthermore, the full length complex of CENP-N and CENP-L was successfully purified from insect cells and tested for its interaction with CENP-C. For quality control reasons, CENP-N/L was subjected to a Superdex 200 SEC column as last step of its purification. The chromatogram showed a single peak at the expected molecular weight and the Coomassie stained gel showed two bands at the expected sizes for CENP-N and CENP-L (**Figure** 2.8).

During the studies, additional CCAN subcomplexes as well as several truncated complexes and proteins were produced to be able to investigate upcoming scientific questions in further detail. Recombinant proteins and complexes used in this study are summarized in **Table** 2.2. Most CCAN subcomplexes and truncated constructs were designed and produced in collaboration with other group members, including Dr. Federica Basilico, Lucia Massimiliano, Dr. John Weir with kind help of the technical assistance of Doro Vogt, Sabine Wohlgemuth, Nina Ludwigs, Anika Take and Ingrid Hoffmann. Contributions from different group members are further specified in the acknowledgements.

Table 2.2: Recombinant CCAN proteins and complexes

Protein	**Construct**
CENP-H/K	Full length
CENP-H/K	CENP-H^{29-C}, CENP-K^{50-C}
CENP-H/I/K/M	CENP-H/K/M Full length CENP-I^{57-C}
CENP-N/L	Full length
CENP-N	1-212
CENP-M	Full length
CENP-I	57-281
CENP-T/W	Full length
Mis12 complex	Mis12, Nsl1, Nnf1, Dsn1 Full length
CENP-A containing histone octamer	CENP-A, H4, H2A, H2B Full length

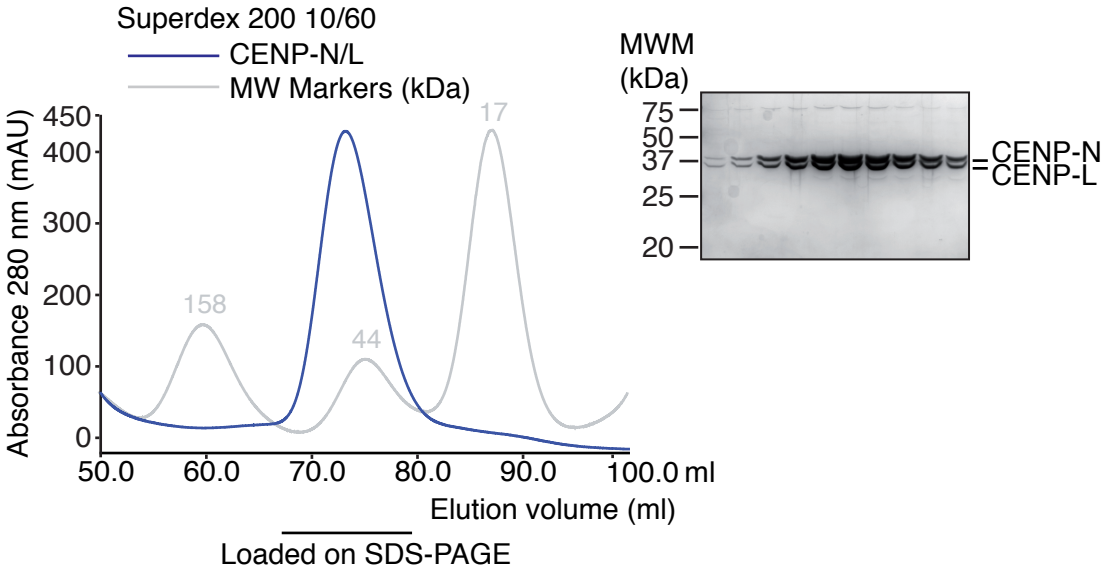

FIGURE 2.8: **CENP-N/L purification from insect cells**. CENP-N/L was purified from insect cells. Purification steps include glutathion affinity chromatography, cleavage of the tag and size exclusion chromatography. Size exclusion chromatography elution profile of CENP-N/L (~79 kDa) and Coomassie stained SDS PAGE gel of the peak fractions are shown here. The protein eluted as expected for its molecular weight, which points towards the formation of a heterodimer.

2.4 CENP-C$^{2-545}$ binding to CENP-H/K complex in solution

The interaction between CENP-C$^{2-545}$ and CENP-H/K has been discovered in analytical SEC experiment. The elution profile of CENP-C and the CENP-H/K dimer shift by one fraction, indicative of complex formation, and also in the Coomassie stained SDS-PAGE gel both proteins show a clear shift to a earlier elution volume. However, the peaks of CENP-C$^{2-545}$ and CENP-H/K do not comigrate, which might be an indication of a low affinity interaction (**Figure** 2.9). When increasing the concentration of CENP-C to 15 μM, co-elution of CENP-C and CENP-H/K is observed, again pointing towards the direction of a low affinity interaction (**Figure** 2.10).

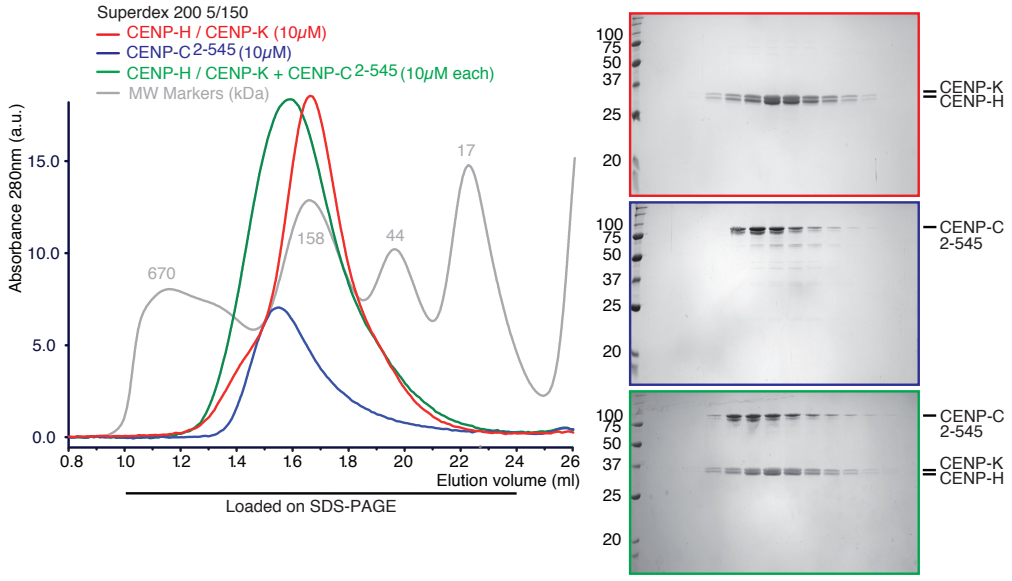

FIGURE 2.9: **CENP-C$^{2-545}$ CENP-H/K interaction in SEC.** Proteins elute from a gelfiltration column depending to their molecular weight and structure. Therefore, analytical SEC can be used to detect direct binding of proteins in solution, since their weight and size changes upon interaction. Here, SEC elution profiles and SDS-PAGE analyses of CENP-H/K complex (red), CENP-C$^{2-545}$ (blue) and their combination (green) is shown. 10 μM of CENP-C$^{2-545}$ and CENP-H/K were mixed in a 1:1 stochiometry, incubated for 1 h at 4°C and run on a Superdex 200 5/150. No major shift of the peak in the chromatogram to an earlier elution volume and only a minor shift of CENP-C and CENP-H/K in the Coomassie stained SDS-PAGE gels indicate a low affinity interaction of CENP-C$^{2-545}$ to CENP-H/K.

It is possible that CENP-C, which was purified from bacterial cells, lacks some posttranslational modification required for the high-affinity binding to CENP-H/K. Therefore, the experiment was repeated with CENP-C purified from insect cells (CENP-C$^{1-544}$His), which is posttranslationally modifiied, as explained above.

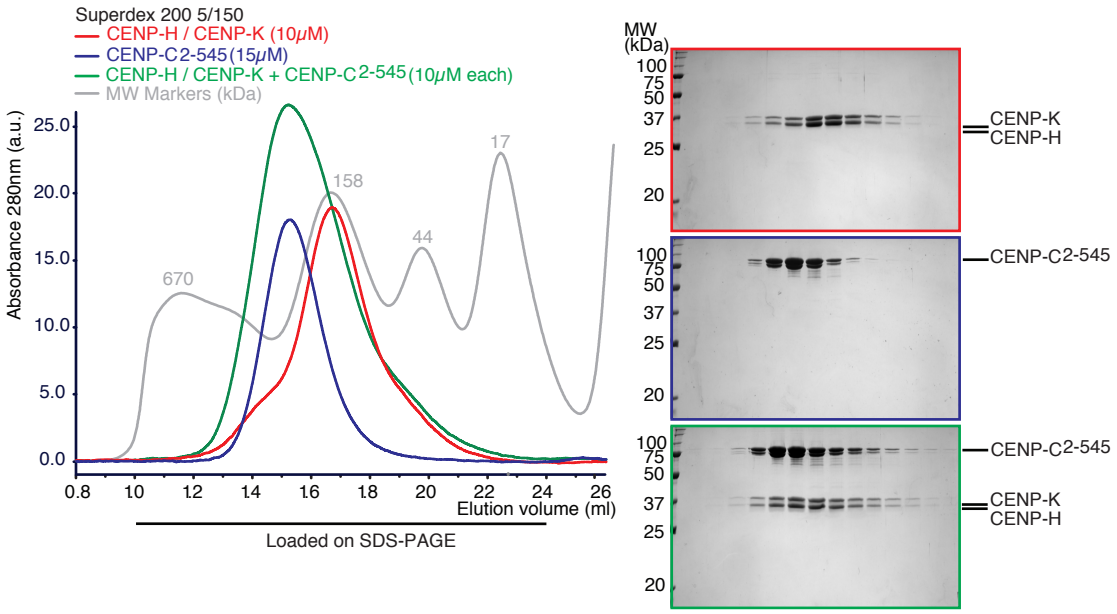

FIGURE 2.10: **CENP-C$^{2-545}$ CENP-H/K interaction in SEC.** SEC elution profiles and SDS-PAGE analyses of CENP-H/K complex (red), CENP-C$^{2-545}$ (blue) and their combination (green) is shown. 10 μM of CENP-H/K were mixed with an excess of CENP-C$^{2-545}$, incubated for 1 h at 4°C and run on a Superdex 200 5/150. The shift of the peak in the chromatogram to an earlier elution volume and the Coomassie stained SDS-PAGE gels show the formation of a ternary complex.

2.5 CENP-C$^{1-544}$His binding to CENP-H/K complex in solution

As CENP-C$^{2-545}$, CENP-C$^{1-544}$His binds to CENP-H/K in analytical size exclusion chromatography (see **Figure** 2.11). CENP-C$^{1-544}$His efficiently bound CENP-H/K already at a concentration of 10 μM. Comparing both experiments, CENP-C$^{1-544}$His/H/K shifts in the chromatogram more clearly compared to CENP-C$^{2-545}$/H/K (see **Figure** 2.9) and the proteins form a stoichiometric complex as seen in the Coomassie stained SDS-PAGE gel. These observations are an indication that posttranslational modifications of CENP-C are important for its interaction with other CCAN components. To get a better idea of which posttranslational modifications play a role and what enzymes are involved, more experiments are required.

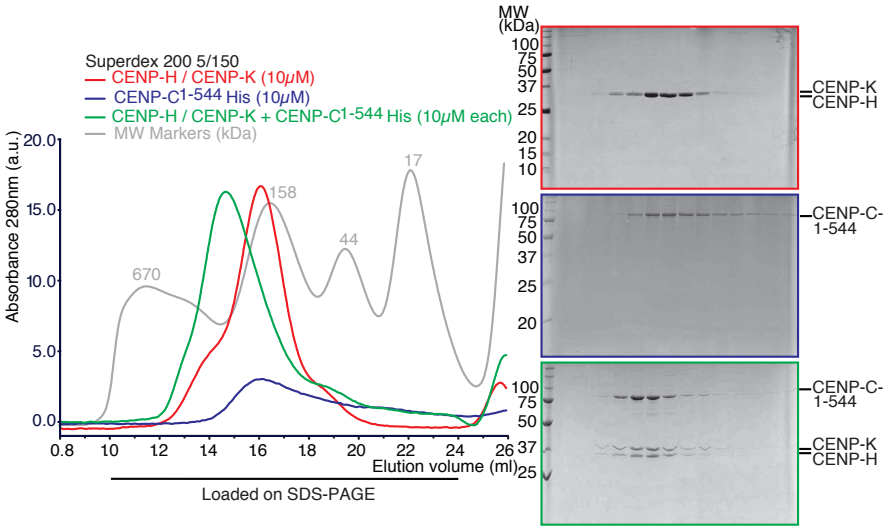

FIGURE 2.11: **CENP-C$^{1-544}$ CENP-H/K interaction in SEC.** SEC elution profiles and SDS-PAGE analyses of CENP-H/K complex (red), CENP-C$^{1-544}$His (blue) and their combination (green) is shown. 10 μM of CENP-C$^{1-544}$His and CENP-H/K were mixed in a 1:1 ratio, incubated for 1 h at 4°C and run on a Superdex 200 5/150. The shift of the peak in the chromatogram to an earlier elution volume and the Coomassie stained SDS-PAGE gels show the formation of an apparently stoichiometric complex.

Next, the molecular details of the CENP-H/K:CENP-C interaction were revealed. To identify the binding interface between CENP-C and CENP-H/K, a limited proteolysis experiment on the separate components as well as on the preformed complex was performed.

2.6 Limited proteolysis on CENP-C$^{2-545}$/H/K

Limited proteolysis is often used to find regions of proteins that are protected from the protease, indicative of a folded region. After proteolytic digestion, the sample is visualized by Coomassie staining of an SDS-PAGE gel. Identity of bands that are potentially interesting are determined by mass spectrometry. Limited proteolysis is usually used to find fragments of proteins or protein complexes that are amenable for X-ray crystallography. Here, it was used in order to understand the organization of the CENP-C$^{2-545}$/H/K complex. The complex was treated in a limited proteolysis experiment to find regions in CENP-C$^{2-545}$ or CENP-H/K protected from the protease when incorporated in the complex compared to CENP-C$^{2-545}$ or CENP-H/K separately. This can give a hint of the spatial

organization of the proteins within the complex, since parts of the proteins that bind to one another might become structured and therefore protected from being digested by proteases. This would result in the appearance of additional bands on a Coomassie stained SDS-PAGE gel in the CENP-C$^{2-545}$:CENP-H/K complex sample (**Figure** 2.12).

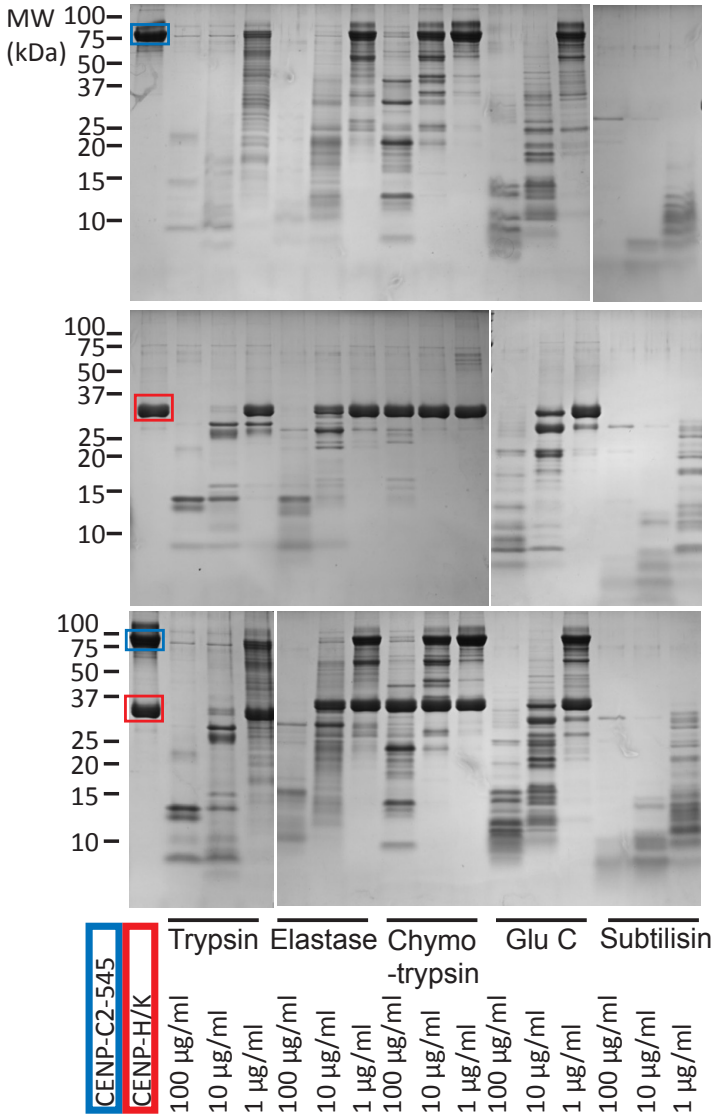

FIGURE 2.12: **Limited proteolysis of CENP-C$^{2-545}$/CENP-H/K complex.** CENP-C$^{2-545}$ and CENP-H/K have been digested with proteases of different specificity in three different concentrations, either separately or in a preformed complex. By comparing the protein pattern in a Coomassie stained SDS-PAGE gel, no additional band appears in the complex sample. This indicates that CENP-C and CENP-H/K interact in such a fashion that does not protect large parts of the proteins.

The limited proteolysis experiment did not show any protection of the proteins within the complex with respect to the separate components. This suggests that CENP-C and CENP-H/K interact in such a fashion that does not protect large parts of the proteins.
Since this did not provide substantial information about the spatial organization of the CENP-C^{2-545} interaction with CENP-H/K, the preformed ternary complex was analyzed in a cross-linking coupled with mass spectrometry experiment (in collaboration with the laboratory of Prof. F. Herzog, Gene Center, Munich).

2.7 Cross-linking and mass spectrometry of CENP-C^{2-545}/CENP-H/K

Cross-linking coupled with mass spectrometry can provide insights into the spatial organization of the CENP-C^{2-545}/CENP-H/K complex. Methodological details can be read in **Section** 4.17.
As depicted in **Figure** 2.13, CENP-H/K sub-complex cross-links with CENP-C in the PEST-rich domain, which is located C-terminal to CENP-C's Mis12 complex interaction site, but N-terminal to its central CENP-A binding domain. Additionally, CENP-H and CENP-K dimer formation seems to occur in the central parts of both proteins, whereas the interaction of the dimer to CENP-C^{2-545} seems to occur more towards the C-termini of CENP-H and CENP-K. CENP-H and CENP-K show a huge variety of intermolecular crosslinks, while there are only very few cross-links between CENP-H/K and CENP-C^{2-545}. All crosslinks between CENP-H/K and CENP-C^{2-545} can be found between the amino acids 200 and 400 of CENP-C^{2-545}. Within this area 4 patches can be found were CENP-H/K interacts with CENP-C that are distributed over the entire CENP-$C^{200-400}$ segment. This suggests that CENP-H/K binding to an elongated surface on CENP-C. This surface includes around 200 amino acids and several patches of CENP-C seem to be involved in the interaction.

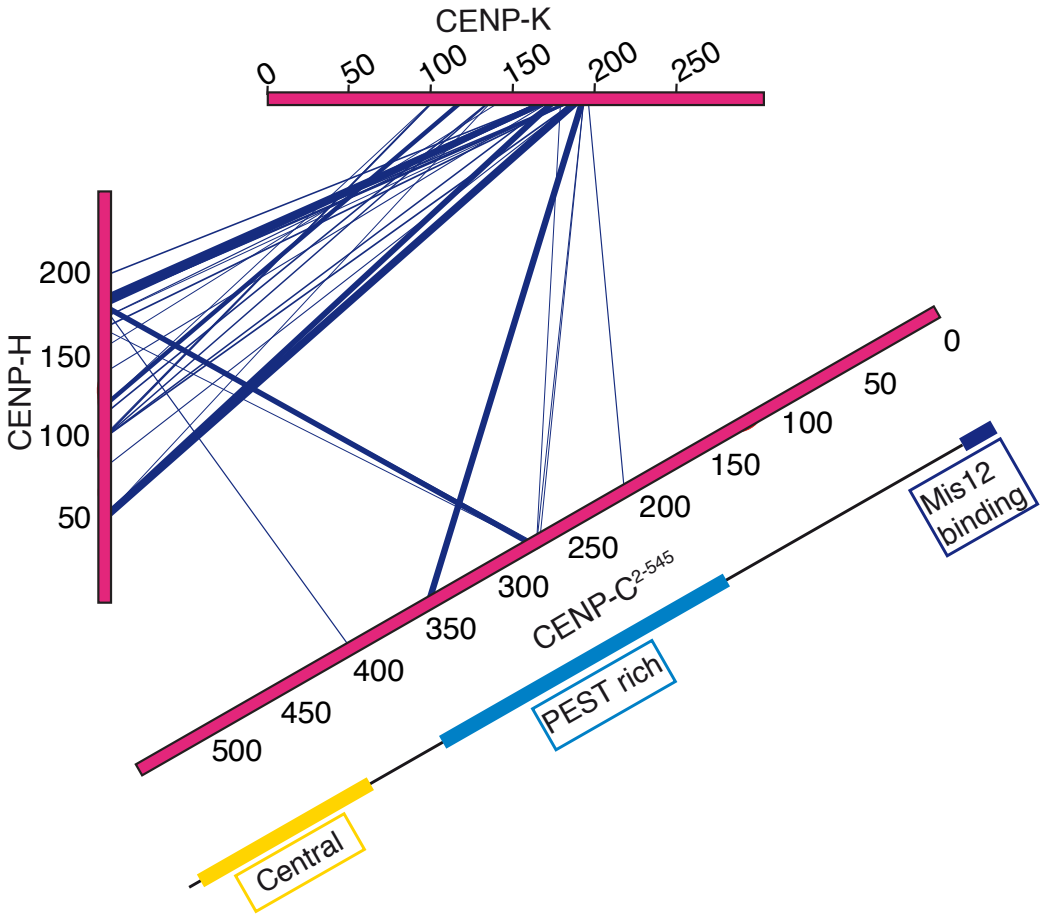

FIGURE 2.13: **CENP-C$^{2-545}$/CENP-H/K cross-linking and mass spectrometry.** Cross-linking of primary amines in lysine pairs by a cross-linker of defined length (7.7 Å) and subsequent mass spectrometry allows insights into the spatial organization of a protein complex. The analysis of the CENP-C$^{2-545}$/H/K ternary complex was performed in collaboration with Dr. Franz Herzogs laboratory at the Ludwig Maximilian University in Munich. Data analysis and figure preparation was done in collaboration with Dr. Ingrid Vetter at the MPI Dortmund. Amino acid numbers are indicated every 50 residues. Cross-links between lysine pairs are represented as lines, whose thickness is proportional to the identification score of the corresponding peptide pair by mass spectrometry. It is apparent that CENP-H and CENP-K display a large number of inter-molecular cross-links, which involve most of their sequence length. Conversely, only few intermolecular cross-links are observed between CENP-C$^{2-545}$ and CENP-H and / or CENP-K. Specifically, they are all restricted to the region of CENP-C between residues 200 - 400.

2.8 CENP-C minimal binding region for CENP-H/K on solid surface

Based on the crosslinking data, new CENP-C constructs were designed to refine the minimal region of CENP-C responsible for its interaction with CENP-H/K. Starting from the CENP-C$^{2-545}$ construct, this was further shortened from its N- and C-terminus up to a minimal construct limited to the CENP-C region that includes all cross-links with CENP-H/K (CENP-C$^{189-400}$) and constitutes the PEST rich domain of CENP-C protein. By using GST-tagged CENP-C constructs in a GST pulldown experiment, we found that shortening the CENP-C$^{2-545}$ from the N- or C-terminus up to construct 189-400 does not negatively influence its binding to CENP-H/K in this assay (**Figure** 2.14 compare lane 5 and lane 10).

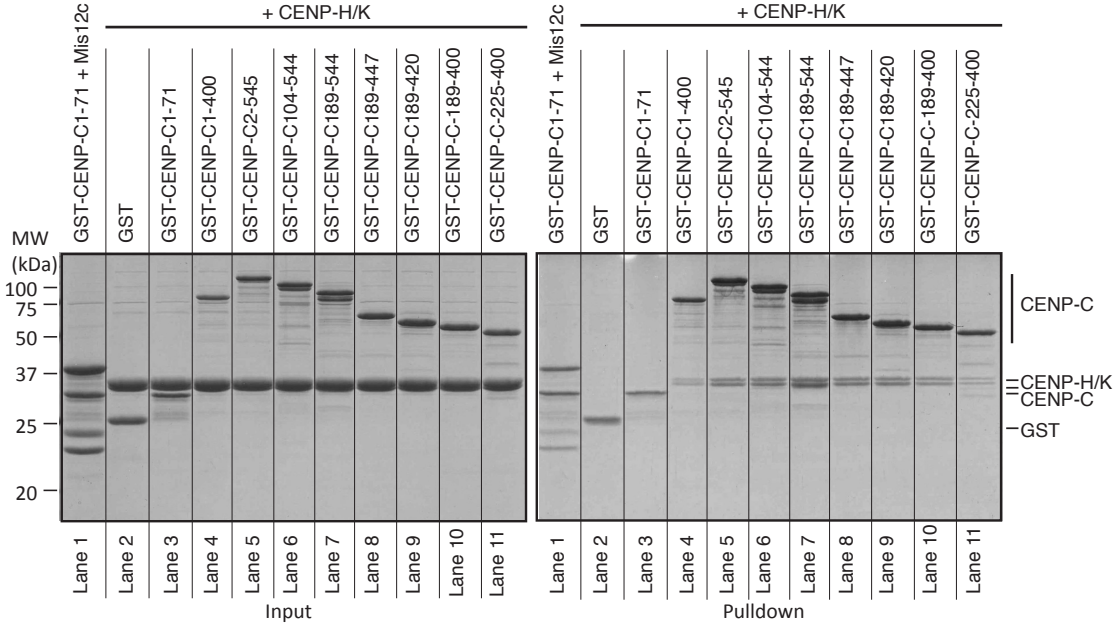

FIGURE 2.14: **GST-CENP-C constructs CENP-H/K pulldown.** GST-pulldowns can be used to observe direct interaction of proteins on a solid surface. The GST tagged protein (bait) is bound onto beads coupled with reduced glutathione. Potential binding partners are added to the reaction (prey). The unbound fraction will be removed in a washing step, while bound proteins will be observed on a Coomassie stained SDS-PAGE gel. Here, different GST-CENP-C constructs have been used as bait (1 μM) and CENP-H/K as prey (3μM) to find the binding region on CENP-C responsible for the CENP-H/K interaction. It has been defined to be in an area around a.a. 189-400 on CENP-C, although additional contribution N- and C-terminal from that region cannot be excluded.

Although in this pulldown experiment the CENP-C minimal construct (around a.a. 189-400) seems to bind an equivalent amount of CENP-H/K compared to CENP-C^{2-545}, additional contacts N- and C-terminal from the minimal region of CENP-C cannot be excluded. In contrast, shortening the N-terminus of CENP-$C^{189-400}$ to CENP-$C^{225-400}$ led to a decrease of CENP-H/K bound in this assay (**Figure** 2.14 compare lane 10 and 11), indicating a drop in binding affinity. This supports the idea that CENP-H/K docks on several binding patches on CENP-C. To further confirm this, a collection of even smaller CENP-C constructs was built and the latter checked for their interaction with CENP-H/K on a solid surface.

2.9 CENP-C/H/K minimal binding interface dissection

Shortening CENP-$C^{189-400}$ construct from the N- or the C-terminus leads to a partial or complete loss of the binding to CENP-H/K. N-terminal truncations of CENP-$C^{189-400}$ are binding a substantially lower amount of CENP-H/K in a GST-pulldown experiment, (**Figure** 2.15 compare lane 2 with lane 3, 4 and 5). However, residual binding is observed for CENP-$C^{290-400}$.

In contrast, C-terminal truncations of CENP-$C^{189-400}$ disrupt the binding to CENP-H/K in a GST-pulldown experiment (**Figure** 2.16 **A**), which was confirmed in a western blot against CENP-K (**Figure** 2.16 **B**). The binding was lost upon shortening CENP-$C^{189-364}$ to CENP-$C^{189-311}$, pointing towards an important interaction site between residues 311 and 364. All GST-CENP-C constructs used in a GST-pulldown against CENP-H/K are summarized in **Table** 2.4.
A GST-pulldown is not a quantitative method, but these findings strongly indicate the presence of an elongated binding interface on CENP-C for CENP-H/K, which goes hand in hand with the mass spectrometry data of the CENP-C^{2-545}/CENP-H/K complex.

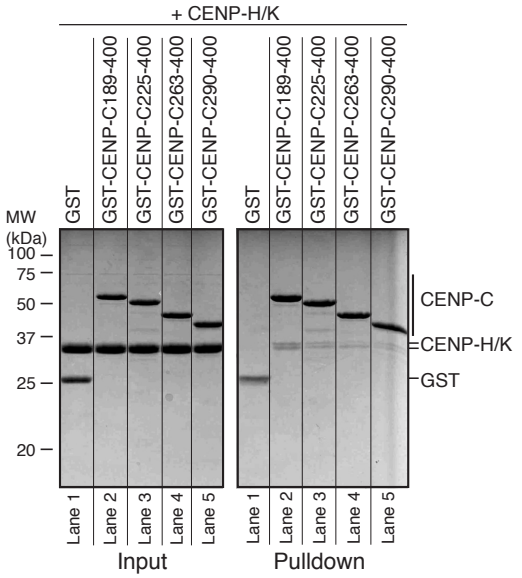

FIGURE 2.15: **GST-CENP-C$^{290-400}$ CENP-H/K pulldown**. GST-CENP-C constructs have been used as bait (1 μM) and CENP-H/K as prey (3 μM) to further refine the minimal binding region on CENP-C responsible for the CENP-H/K interaction. CENP-C$^{290-400}$ is sufficient to pull down CENP-H/K, although the quantity is reduced compared to CENP-C$^{189-400}$.

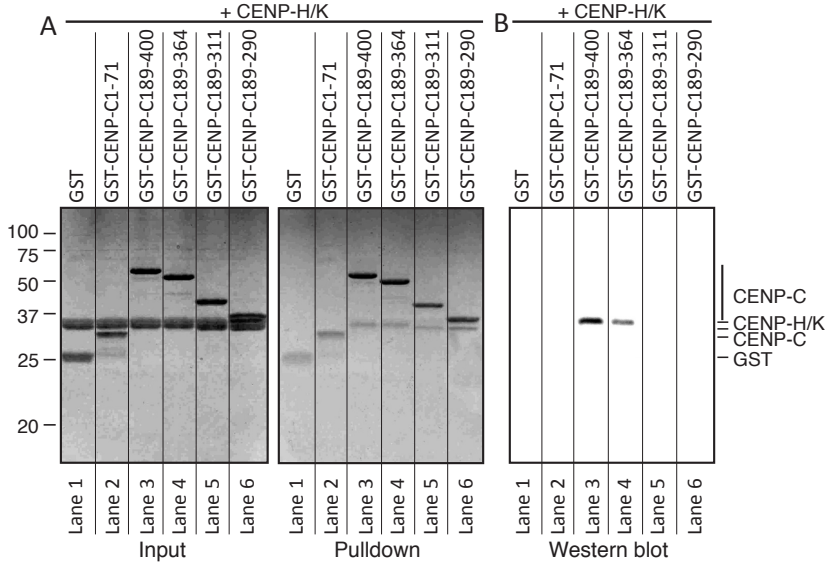

FIGURE 2.16: **GST-CENP-C$^{189-290}$ CENP-H-K pulldown**. GST-CENP-C constructs have been used as bait (1 μM) and CENP-H/K as prey (3 μM) to further refine the minimal binding region on CENP-C responsible for the CENP-H/K interaction. CENP-C$^{189-290}$ is not able to bind CENP-H/K in this pulldown assay (**A**). Western blotting against CENP-K has been performed to confirm the absence of CENP-H/K in the pulldown with GST-CENP-C$^{189-290}$ (**B**).

2.10 CENP-C minimal binding region for CENP-H/K in solution

CENP-C$^{189-400}$ was defined as minimal binding interface of CENP-C for CENP-H/K interaction based on the GST pulldown results. Surprisingly, this construct does not form a complex with CENP-H/K in analytical SEC experiment (**Figure** 2.17). Increasing the concentration of CENP-C to 15 μM did not enhance binding (**Supplementary Figure** 5.1). Since CENP-C$^{2-545}$ binds to CENP-H/K (**Figure** 2.10), contributions from regions N- and/or C-terminal of CENP-C$^{189-400}$ to the interaction were suggested. Additional SEC experiments were performed to elucidate this possibility. CENP-C$^{189-544}$ and CENP-H/K both shift to an earlier elution volume, when run on a SEC, as seen in the Coomassie stained SDS-PAGE gel (**Supplementary Figure** 5.2). This indicates that the binding of CENP-C$^{189-544}$ to CENP-H/K improved through the residues 400-544 of CENP-C, although CENP-C$^{402-544}$ does not bind to CENP-H/K on a SEC or in a GST pulldown experiment on its own (**Figure** 2.18 and 2.27). This points towards a minor contribution from this part of CENP-C to the interaction with CENP-H/K.

In addition, CENP-C$^{1-400}$His was produced in insect cells and tested for its binding to CENP-H/K complex (**Figure** 2.19). Since it was able to form a complex with CENP-H/K, some contribution from residues 1-188 of CENP-C was suggested. Since CENP-C$^{1-544}$His produced from insect cells was shown to bind more efficiently to CENP-H/K, the binding of CENP-C$^{1-400}$His to CENP-H/K could also be a consequence of its production from insect cells rather than contribution from its N-terminal part. Therefore, CENP-C$^{189-400}$ was produced in insect cells and tested for its binding to CENP-H/K (**Figure** 2.20). However, CENP-C$^{189-400}$ did not show complex formation, confirming contribution from residues 1-188 of CENP-C to the interaction with CENP-H/K. All interaction experiments of CENP-C constructs to CENP-H/K are summarized in **Table** 2.3.

Overall we conclude that residues both N- and C-terminal to CENP-C$^{189-400}$ contribute to the binding of CENP-H/K. Therefore, CENP-H/K complex interacts with a extended region within CENP-C$^{2-545}$ with its major interactions within CENP-C$^{189-400}$ and contribution from the regions N- and C-terminal of this construct.

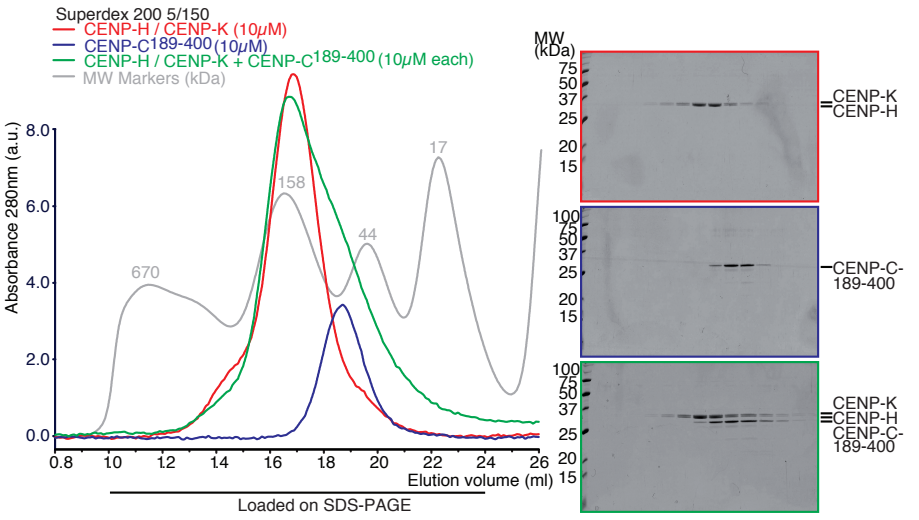

FIGURE 2.17: **CENP-C$^{189-400}$ CENP-H/K interaction in SEC**. SEC elution profiles and SDS-PAGE analyses of CENP-H/K complex (red), CENP-C$^{189-400}$ (blue) and their combination (green) is shown. 10 μM of CENP-C and 10 μM CENP-H/K were mixed, incubated for 1 h at 4°C and run on a Superdex 200 5/150. The consistency of the peaks in the chromatograms and the Coomassie stained SDS-PAGE gel show no complex formation of CENP-C$^{189-400}$ with the CENP-H/K heterodimer, demonstrating contribution from parts N- and C-terminal of CENP-C$^{189-400}$.

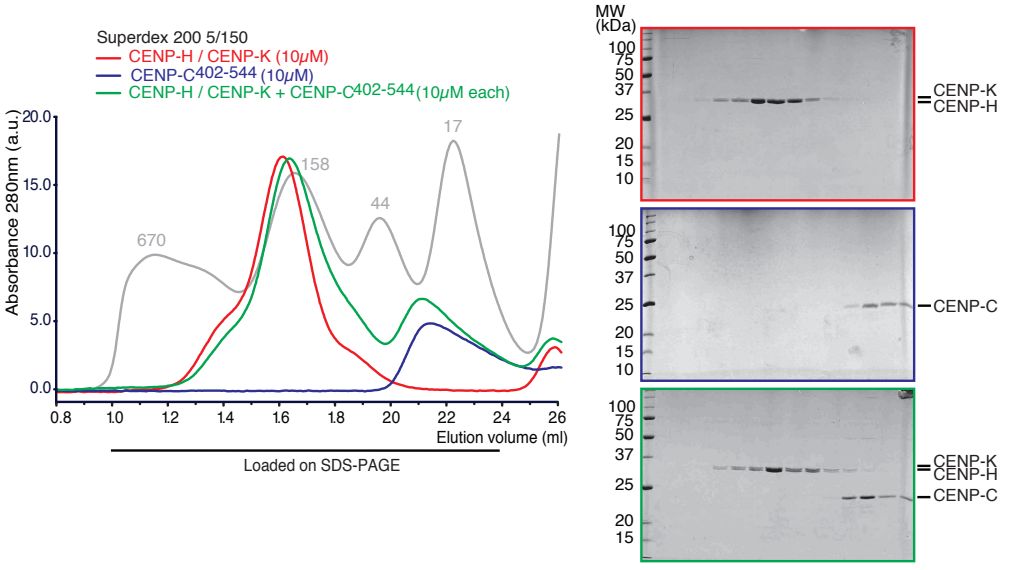

FIGURE 2.18: **CENP-C$^{402-544}$ CENP-H/K interaction in SEC**. SEC elution profiles and SDS-PAGE analyses of CENP-H/K complex (red), CENP-C$^{402-544}$ (blue) and their combination (green). The formation of an ternary complex can not be observed. 10 μM of CENP-C and CENP-H/K were mixed, incubated for 1 h at 4°C and run on a Superdex 200 5/150.

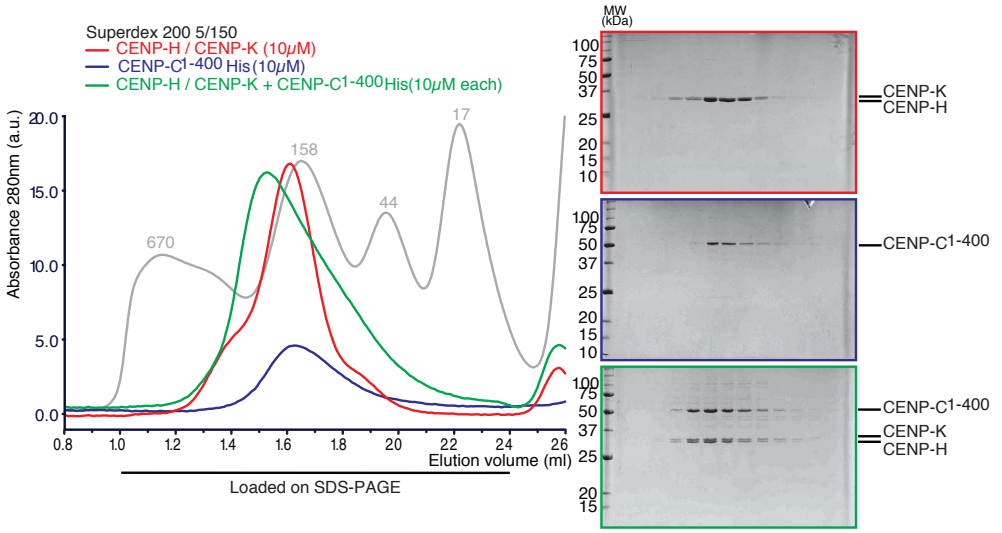

FIGURE 2.19: **CENP-C$^{1-400}$ CENP-H/K interaction in SEC**. SEC elution profiles and SDS-PAGE analyses of CENP-H/K complex (red), CENP-C$^{1-400}$ (blue) and their combination (green). 10 μM of CENP-C and CENP-H/K were mixed, incubated for 1 h at 4°C and run on a Superdex 200 5/150. The shift of the peak in the chromatogram to an earlier elution volume and the Coomassie stained SDS-PAGE gels show the formation of an apparently stoichiometric complex.

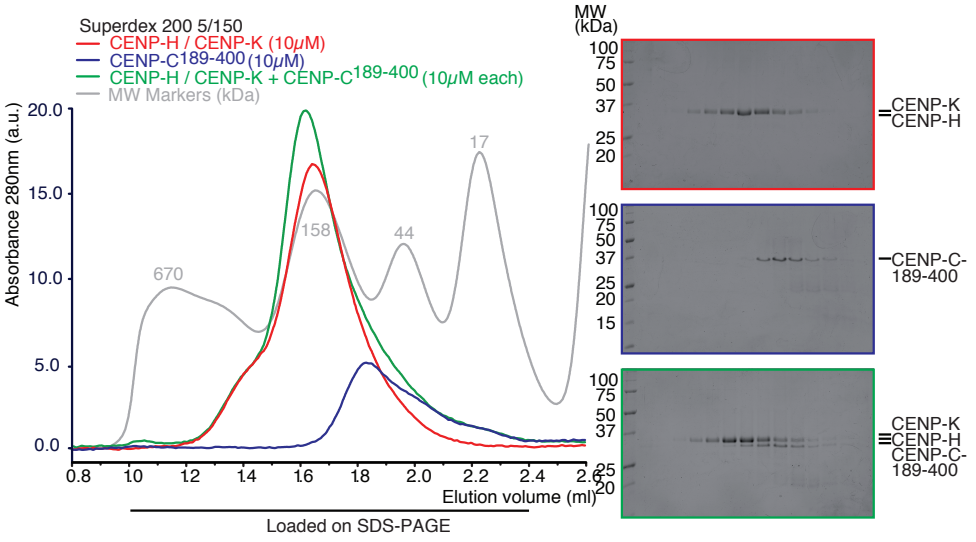

FIGURE 2.20: **CENP-C$^{189-400}$ CENP-H/K interaction in SEC**. SEC elution profiles and SDS-PAGE analyses of CENP-H/K complex (red), CENP-C$^{189-400}$ purified from insect cells (blue) and their combination (green). 10 μM of CENP-C and CENP-H/K were mixed, incubated for 1 h at 4°C and run on a Superdex 200 5/150. The formation of a complex can not be observed in the chromatogram or the Coomassie stained SDS-PAGE gels.

TABLE 2.3: Summary of CENP-C binding to CENP-H/K in solution

CENP-C construct (a.a.)	**CENP-H/K binding**
2-545	Yes
1-400	Yes
189-544	Reduced
189-400	No
402-544	No

2.11 CENP-H/K:CENP-C interaction affinity

To confirm the hypothesis that CENP-$C^{189-400}$ provides the main interaction interface for CENP-H/K we determined the binding affinity of CENP-C^{2-545} and CENP-$C^{189-400}$ for the CENP-H/K complex in an isothermal titration calorimetry (ITC) experiment. In addition, CENP-$C^{189-290}$ and CENP-$C^{290-400}$ affinity for CENP-H/K complex was identified in ITC to confirm a potential contribution from both of these CENP-C parts.
The dissociation constant (Kd) of CENP-C^{2-545} for CENP-H/K was found to be 1.4 μM (Ka = $7.15 \cdot 10^5$ M^{-1}) (**Figure** 2.21), indicative of a rather low affinity interaction, as already indicated in the SEC experiments. The stoichiometry N was 0.65, ΔH = -6344 KJ/mol and ΔS = 5.52 J/K.

The determination of the affinity of CENP-$C^{189-400}$ revealed an only slightly reduced interaction, with Kd = 2.6 μM (**Figure** 2.22) (Ka = $3.88 \cdot 10^5$ M^{-1}). The stoichiometry N was 0.97, ΔH = -3805 KJ/mol and ΔS = 12.8 J/K. However, the fitting of the curve is not as steep as for the CENP-C^{2-545}:CENP-H/K interaction. The ITC data confirm that the main contribution from CENP-C for the CENP-H/K interaction can be found within residues 189-400 and it again points towards the possibility of some minor contribution to the CENP-H/K binding from N- and C-terminal regions of this CENP-C construct.

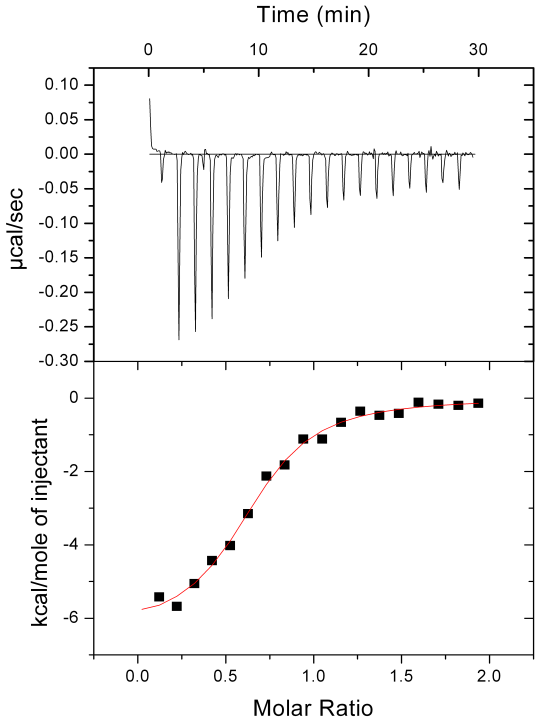

FIGURE 2.21: **CENP-C$^{2-545}$ CENP-H/K interaction in ITC.** ITC is a quantitative biochemical method that allows the investigation of intermolecular interactions. It measures the difference in heat of exo- or endothermic processes that occurs upon stepwise injections of a reagent into a calorimetric cell containing the potential binding partner. Here, the protein-protein interaction of CENP-C$^{2-545}$ and the CENP-H/K dimer was measured in an ITC experiment using 3 μM CENP-C$^{2-545}$ in the calorimetric cell and injections of 2 μl 300 μM CENP-H/K. The Kd of this interaction was determined to be in the low μM range.

CENP-C$^{290-400}$ showed a minor decrease in the binding affinity to CENP-H/K compared to CENP-C$^{189-400}$, being 5 μM (Ka = 1.96$\cdot 10^5$ M^{-1}). The stoichiometry N was 0.72, ΔH = -6827 KJ/mol and ΔS 1.32 J/K. The fit of the curve is similar to CENP-C$^{189-400}$ (**Figure** 2.23). Since also in a GST-pulldown, CENP-C$^{290-400}$ binds less efficiently to CENP-H/K compared to CENP-C$^{189-400}$, some contribution from CENP-C$^{189-290}$ was proposed, although an interaction was not observed in an ITC experiment carried out under the same conditions (data not shown). The ITC result for the CENP-C$^{290-400}$:CENP-H/K interaction indicates that a contribution from CENP-C$^{189-290}$ to the CENP-H/K interaction, is rather low. This would also explain why CENP-C$^{189-290}$ fails to bind CENP-H/K in a GST-pulldown experiment.

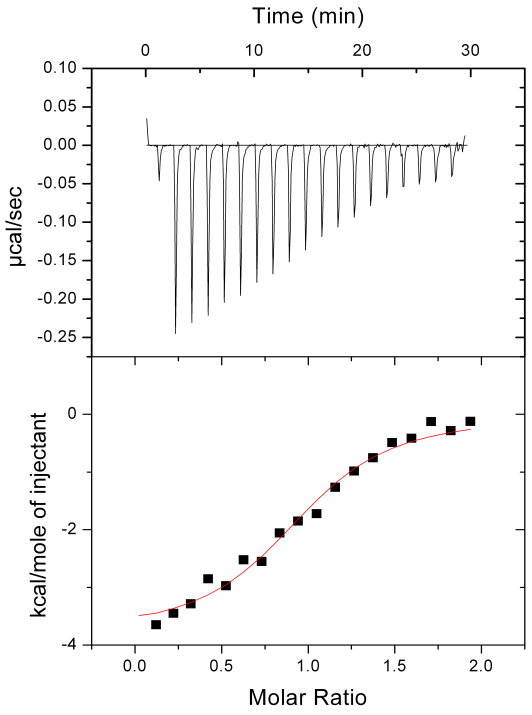

FIGURE 2.22: **CENP-C$^{189-400}$ CENP-H/K interaction in ITC.** The protein-protein interaction of CENP-C$^{189-400}$ and the CENP-H/K dimer was measured in an ITC experiment using 3 μM CENP-C$^{189-400}$ in the calorimetric cell and injections of 2 μl 300 μM CENP-H/K. The Kd of this interaction was determined to be in the low μM range, but slightly higher as for the CENP-C$^{2-545}$:CENP-H/K interaction.

In the binding experiments of CENP-H/K to CENP-C, additional CCAN components might be missing that are necessary for high affinity binding. These proteins could either bind to CENP-C and CENP-H/K and strengthen their interaction or they could induce a structural change in one of these components that improves the binding within the CENP-C/H/K complex. CENP-H/K has been recently shown to form a ternary complex with CENP-I and CENP-M, the CENP-H/I/K/M complex [264]. CENP-I and CENP-M are therefore good candidates for supporting the CENP-C:H/K complex formation.

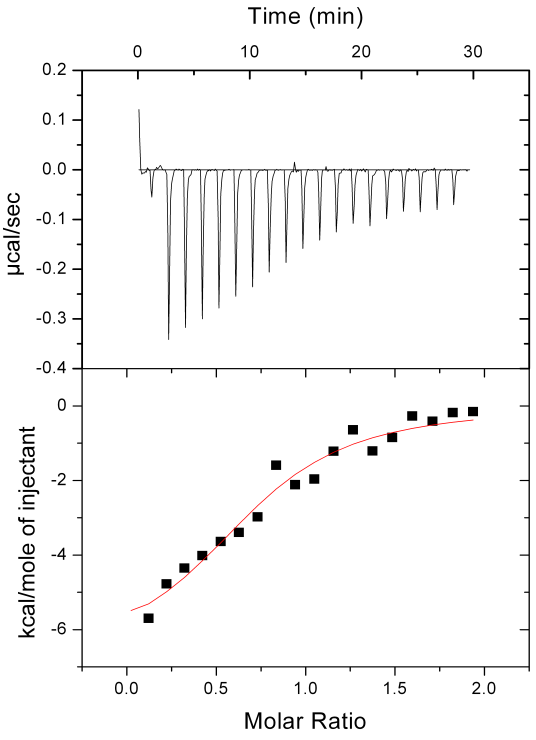

FIGURE 2.23: **CENP-C$^{290-400}$ CENP-H/K interaction in ITC.** The protein-protein interaction of CENP-C$^{290-400}$ and the CENP-H/K dimer was measured in an ITC experiment using 3 μM CENP-C$^{290-400}$ in the calorimetric cell and injections of 2 μl 300 μM CENP-H/K. The Kd of this interaction was determined to be at 5 μM, sligthly higher than for the CENP-C$^{189-400}$:CENP-H/K interaction.

Another possible explanation for the low affinity of the CENP-C:CENP-H/K is that the CENP-C purified from bacteria lacks posttranslational modifications that are needed for efficient interaction with CENP-H/K. As shown above, the equivalent protein purified from insect cells, CENP-C$^{1-544}$His, was indeed phosphorylated and bound to CENP-H/K already at a lower concentration in solution (**Figure** 2.11). Unfortunately, CENP-C$^{1-544}$His could not be used for measuring the affinity to CENP-H/K in an ITC experiment, due to technical problems (data not shown).

2.12 CENP-C binding to CENP-H/I/K/M complex on a solid surface

As described above, the CENP-H/K dimer is part of the CENP-H/I/K/M complex, one of several subcomplexes of the CCAN [264]. Because the affinity of CENP-C to CENP-H/K was found to be rather low (**Section** 2.11), the study was extended to the newly identified tetrameric CENP-H/I/K/M complex.
As an initial experiment, the binding of CENP-H/I/K/M to CENP-C was confirmed in a GST-pulldown as well as in a SEC experiment (**Figure** 2.24 **A** and 2.40 **A**). Unfortunately, determination of the binding affinity of CENP-C to CENP-H/I/K/M was not successful, due to technical problems (data not shown). Therefore, we used an alternative strategy to determine whether CENP-H/K and CENP-H/I/K/M bind CENP-C with different affinity. We asked if CENP-H/I/K/M bound to CENP-C constructs that were not sufficient to bind CENP-H/K using the same assay under the same conditions as for CENP-H/K binding to CENP-C. CENP-$C^{189-290}$ was not sufficient to bind CENP-H/K in a GST pulldown assay (**Figure** 2.16 **A** and **B** lane 6). In contrast, CENP-H/I/K/M complex was able to bind CENP-$C^{189-290}$ (**Figure** 2.24 **B**), indicating a stronger binding of CENP-H/I/K/M to CENP-C compared to CENP-H/K.

2.13 CENP-C binding to CENP-H/I/K/M complex in solution

As shown before, CENP-$C^{189-400}$ is not able to bind CENP-H/K in solution (**Figure** 2.17). Since we hypothesized a stronger interaction of CENP-C to CENP-H/I/K/M, we tested whether CENP-$C^{189-400}$ is sufficient to bind CENP-H/I/K/M in analytical SEC (**Figure** 2.25). Indeed, CENP-H/I/K/M binds this CENP-C construct, indicating that the CENP-H/I/K/M complex has a higher binding affinity for CENP-C.
These observations have two possible explanations. Either CENP-I and CENP-M contribute to the binding by directly interacting with CENP-C themselves or they induce a conformational change within the CENP-H/K complex that enables it to bind more tightly to CENP-C.

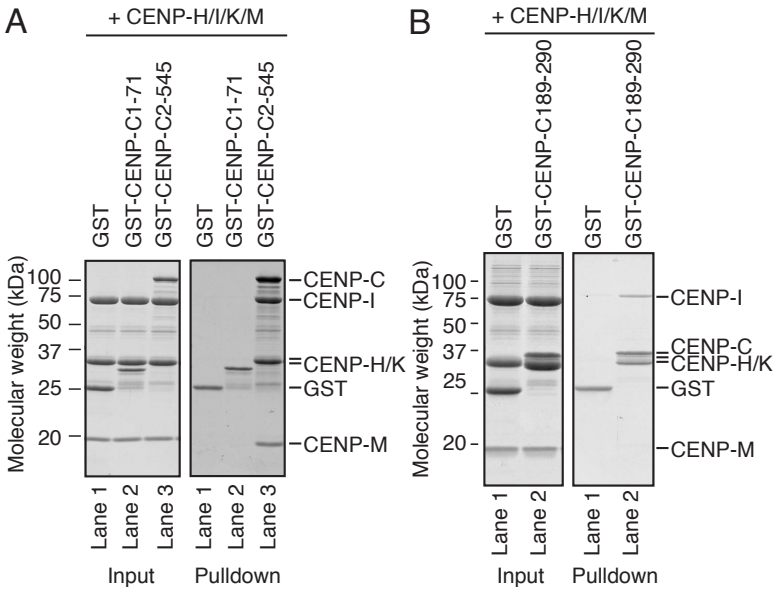

FIGURE 2.24: **GST-CENP-C$^{2-545}$ and GST-CENP-C$^{189-290}$ CENP-H/I/K/M pulldown**. GST-CENP-C$^{2-545}$ or GST-CENP-C$^{189-290}$ have been used as bait (1 μM) and CENP-H/I/K/M as prey (3μM) to find potential differences in CENP-C binding of CENP-H/I/K/M compared to CENP-H/K alone. GST-CENP-C$^{2-545}$ efficiently pulls down CENP-H/I/K/M (**A**). GST-CENP-C$^{189-290}$ that is not sufficient to bind CENP-H/K is able to bind CENP-H/I/K/M in the same assay, indicating a strengthening of the CENP-H/I/K/M interaction to CENP-C (**B**).

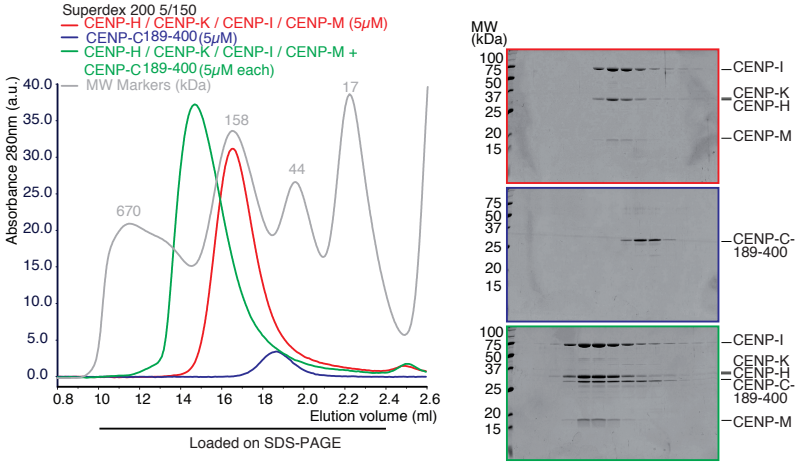

FIGURE 2.25: **CENP-C$^{189-400}$ CENP-H/I/K/M interaction in SEC**. SEC elution profiles and SDS-PAGE analyses of CENP-H/I/K/M complex (red), CENP-C$^{189-400}$ (blue) and their combination (green) is shown. 5 μM of CENP-C and CENP-H/I/K/M were mixed in a 1:1 ratio, incubated for 1 h at 4°C and run on a Superdex 200 5/150. The shift of the peak in the chromatogram to an earlier elution volume and the Coomassie stained SDS-PAGE gels show the formation of an apparently stoichiometric complex.

2.14 Proteolytic digestion of CENP-C$^{2-545}$/H/I/K/M complex

In order to understand the organization of the CENP-C$^{2-545}$/CENP-H/I/K/M complex, it was treated in a limited proteolysis experiment, as described for CENP-C$^{2-545}$/CENP-H/K (see **Section** 2.6). After limited proteolysis the samples were run on an SDS-PAGE gel and proteins observed by Coomassie staining to find regions in either CENP-C$^{2-545}$ or CENP-H/I/K/M that are protected from being digested in the complex compared to CENP-C$^{2-545}$ or CENP-H/I/K/M separately (**Figure** 2.26). Furthermore, this limited proteolysis was compared to the proteolysis of the CENP-C$^{2-545}$/H/K complex (**Figure** 2.12).

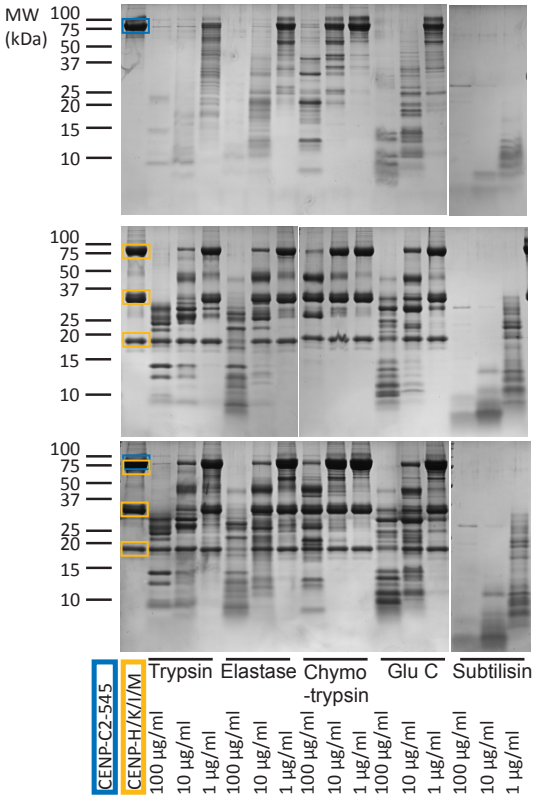

FIGURE 2.26: **Limited proteolysis of CENP-C$^{2-545}$/CENP-H/I/K/M complex.** CENP-C$^{2-545}$ and CENP-H/I/K/M have been digested with proteases of different specificity in three different concentrations, either separately or in a preformed complex. By comparing the protein pattern in a Coomassie stained SDS-PAGE gel, no additional band appears in the complex sample. This indicates that the proteins do not bind in such a manner that cleavage sites may become exposed or protected.

Limited proteolysis of the complex does not show any new protease-protected fragments in the complex, as no additional bands were observed on a Coomassie stained SDS-PAGE gel. This suggests a binding of CENP-H/I/K/M to CENP-C that does not protect large parts of the proteins from proteolytic digest. This is comparable to the result obtained for the CENP-C/H/K proteolytic digest, which did also not show any protection of protein regions upon complex formation. Therefore, a similar binding mode of CENP-H/K and CENP-H/I/K/M is likely.

2.15 Roles of CENP-H and CENP-K N-termini in CENP-C binding

To further understand the roles of the separate components of the CENP-H/I/K/M complex in CENP-C binding, additional experiments were performed on the single components, including CENP-M full length, CENP-H/K heterodimer and CENP-I^{57-281}.

The crosslink experiment suggests no contribution from CENP-H and CENP-K N-termini to the interaction with CENP-C (**Figure** 2.13). To confirm this, a CENP-H/K dimer lacking N-terminal segments of both proteins was designed. CENP-H^{29-C}/CENP-K^{50-C} is still able to form a complex, which can be purified from insect cells. It will be subsequently named CENP-HΔN/KΔN.

Construct design and purification of CENP-HΔN/KΔN can be found in **Section** 4.12.5 and 4.13.4. Their involvement in the interaction with CENP-$C^{189-400}$ was examined in a GST pulldown assay. Indeed, CENP-HΔN/KΔN complex was binding as efficiently as the full length CENP-H/K to GST-CENP-$C^{189-400}$ (**Figure** 2.27 compare lane 3 and lane 6), confirming the idea that the N-terminal segments are not involved in the CENP-C interaction.

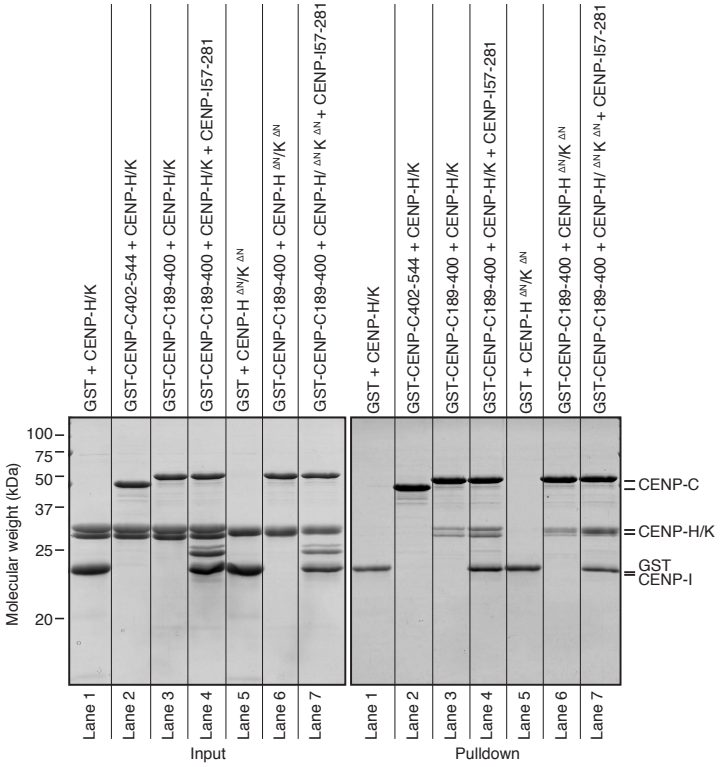

FIGURE 2.27: **GST-CENP-C$^{189-400}$ CENP-HΔN CENP-KΔN, CENP-I$^{57-281}$ pulldown**. GST-CENP-C constructs have been used as bait (1 μM) and CENP-H/K or CENP-HΔN/CENP-KΔN with and without CENP-I$^{57-281}$ as prey (3 μM). CENP-C$^{402-544}$ is not sufficient to bind to CENP-H/K (lane 2). N-termini of CENP-H/K are not required for the interaction with CENP-C$^{189-400}$ (compare lane 3 and 6). CENP-I$^{57-281}$ increases the binding of CENP-H/K and CENP-HΔN/CENP-KΔN to CENP-C (compare lane 3 with 4, lane 6 with 7).

2.16 Roles of CENP-I$^{57-281}$ and CENP-M in the CENP-C:CENP-H/I/K/M interaction

To examine a potential contribution from CENP-I and CENP-M to the binding of CENP-H/I/K/M to CENP-C, we tested whether CENP-I$^{57-281}$ and CENP-M bound to GST-CENP-C$^{2-545}$ in a GST pulldown assay (**Figure** 2.28). In this assay no binding of CENP-I$^{57-281}$ or CENP-M was observed which rules out a strong interaction between CENP-C and these components. Nevertheless, a direct binding can not be completely excluded. It has to be taken into account that only a small part of CENP-I was tested for its binding to CENP-C, since all longer constructs were insoluble when expressed in isolation. Furthermore, binding of CENP-M or CENP-I to CENP-C might only occur within the CENP-H/I/K/M complex through structural rearrangement of CENP-M or CENP-I. Alternatively,

CENP-I or CENP-M could induce a conformational change in CENP-H/K that increases its binding affinity for CENP-C. To test that, the binding of CENP-H/K to CENP-C^{2-545} was examined in the presence or absence of CENP-I^{57-281} in a GST-pulldown assay, since CENP-I^{57-281} was already reported to interact with CENP-H/K [264]. Indeed, CENP-I^{57-281} improved the binding of CENP-H/K to CENP-C in a GST-pulldown, strengthening the idea of CENP-I^{57-281} being involved in the CENP-C:CENP-H/I/K/M interaction by improving the binding of CENP-H/K to CENP-C (**Figure** 2.27 lane 3 and 4). The same was observed with CENP-HΔN CENP-KΔN (**Figure** 2.27 lane 6 and 7), indicating that the N-termini of CENP-H and CENP-K are not important for the binding of CENP-I and the putative conformational change.

Taken together, the CENP-H/I/K/M binding to CENP-C is mainly provided through CENP-H/K, with minor contributions from CENP-I and/or CENP-M, possibly through the induction of a structural change within CENP-H/K. The CENP-H/I/K/M interaction with CENP-C is mediated by several binding patches within residues 189-400 of CENP-C.

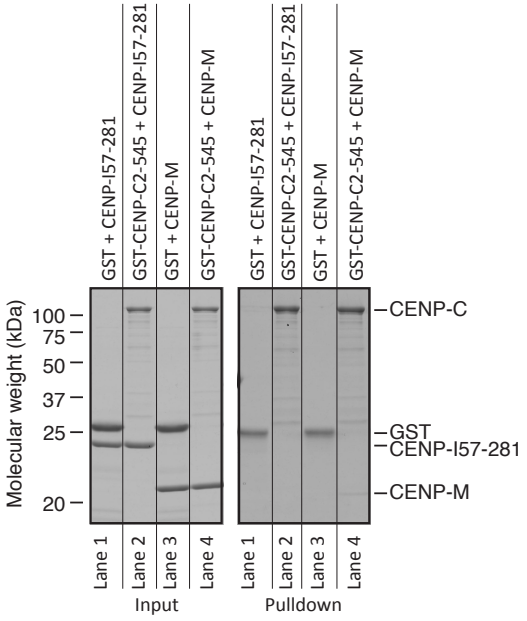

FIGURE 2.28: **GST-CENP-C^{2-545}, CENP-M and CENP-I^{57-281} pulldown**. GST-CENP-C^{2-545} has been used as bait (1 μM) and CENP-I^{57-281} or CENP-M as prey (3 μM) to further examine the role of these proteins in the CENP-H/I/K/M interaction with CENP-C. CENP-C^{2-545} is not able to bind CENP-I^{57-281} or CENP-M in this pulldown assay (lane 2 and 4).

2.17 CENP-C$^{1-544}$His binding to CENP-N/L in solution

To further understand the role of CENP-C within the inner kinetochore, the study was extended to the CENP-N/L complex. This complex has been shown to directly interact with CENP-C in yeast [258]. Therefore, the binding of the human orthologs was tested *in vitro*. In analytical SEC experiment, an interaction of CENP-C$^{1-544}$His and CENP-N/L was observed. Although the peak in the chromatogram of the complex does not show a major shift, the Coomassie stained SDS-PAGE gel shows a clear shift of the elution volume of CENP-N/L even if the latter did not form a stoichiometric complex with CENP-C$^{1-544}$His. This likely indicates a rather weak interaction between these components.

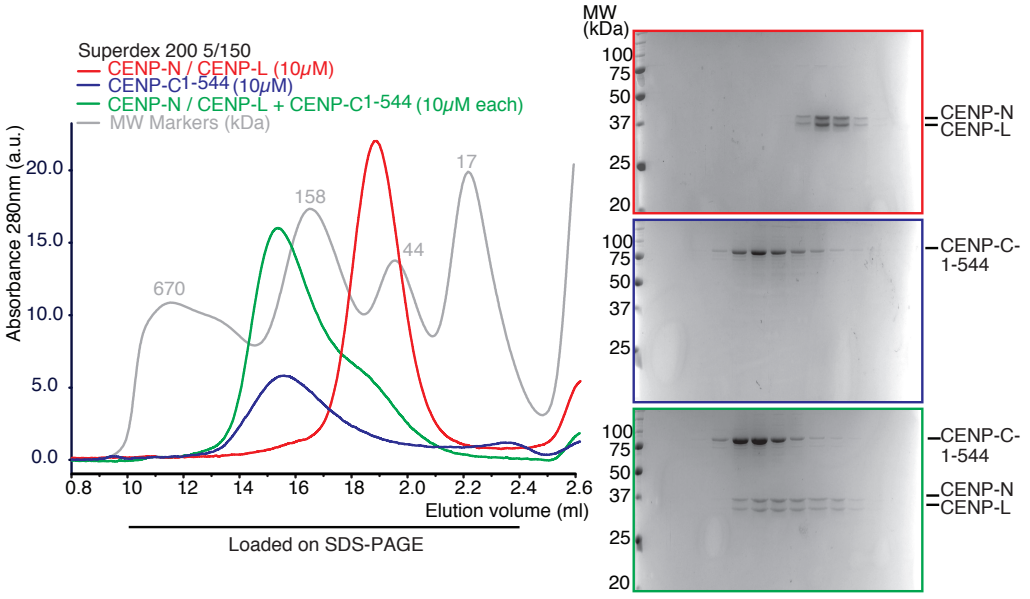

FIGURE 2.29: **CENP-C$^{1-544}$His CENP-N/L interaction in SEC**. SEC elution profiles and SDS-PAGE analyses of CENP-N/CENP-L complex (red), CENP-C$^{1-544}$His (blue) and their combination (green) is shown. 10 μM of CENP-C$^{1-544}$His and CENP-N/L were mixed in a 1:1 ratio, incubated for 1 h at 4°C and run on a Superdex 200 5/150. The shift of the CENP-N/L complex on the Coomassie stained gels SDS-PAGE shows binding to CENP-C that is not strong.

2.18 CENP-C binding to CENP-N/L on a solid surface

Next, the binding of CENP-C to CENP-N/L was investigated in a GST pulldown assay. On solid surface a direct interaction of GST-CENP-C$^{2-545}$ to CENP-N/L was confirmed (**Figure** 2.30 lane 3). To examine if CENP-N/L binds to the same region of CENP-C than CENP-H/I/K/M does, a GST-pulldown experiments with further truncated versions of CENP-C was performed.

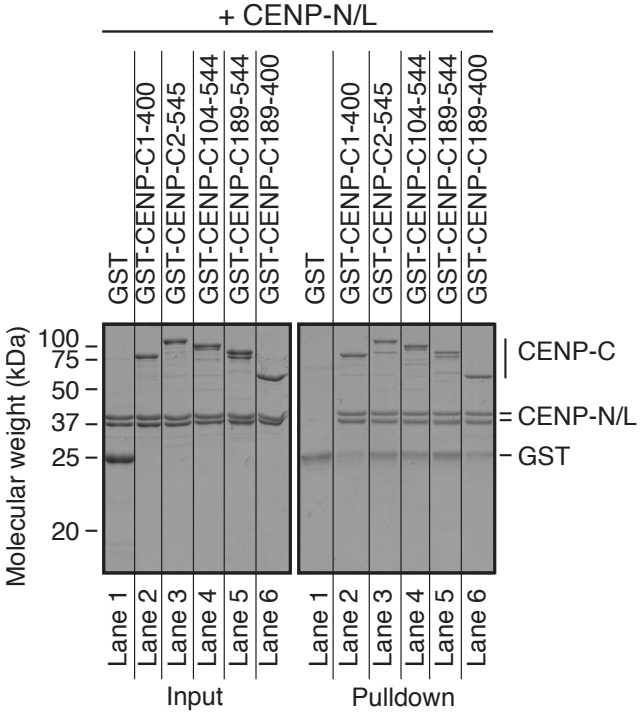

FIGURE 2.30: **GST-CENP-C CENP-N/L pulldown experiment.** Different GST-CENP-C constructs have been used as bait (1 μM) and CENP-N/L as prey (3 μM) to confirm a direct interaction of CENP-C with CENP-N/L and find the binding region on CENP-C responsible for the CENP-N/L interaction. CENP-C$^{2-545}$ directly binds to CENP-N/L in this condition (lane 3). The minimal binding region has been defined to also lie within a.a. 189-400 on CENP-C, although additional contribution N- and C-terminal from that region cannot be excluded. Therefore, CENP-N/L binds to the same region onto CENP-C as CENP-H/I/K/M. The band that arises in the GST-CENP-C$^{2-545}$ CENP-N/L pulldown sample compared to input, probably is GST. CENP-N/L purification includes a step of GST-Prescision treatment and some of this protease might be contaminating the purified sample, therefore leading to a cleavage of GST-CENP-C during the incubation of the bait with the prey.

Truncating CENP-C$^{2-545}$ from the N- and C-terminus to CENP-C$^{189-400}$ did not impair the binding of CENP-N/L to CENP-C (**Figure** 2.30 compare lane 3 and 6). Therefore, CENP-H/I/K/M and CENP-N/L both bind to the PEST rich domain of CENP-C. Again, contribution to the binding from regions N- and C-terminal of CENP-C$^{189-400}$ can not be excluded. To understand if CENP-N/L interacts with multiple sites of CENP-C$^{189-400}$, we truncated CENP-C$^{189-400}$ further and investigated the binding of CENP-N/L.

Interaction of CENP-N/L to both CENP-C$^{189-290}$ and CENP-C$^{290-400}$ was observed (**Figure** 2.31 lane 4 and 5), suggesting that multiple binding patches within CENP-C are responsible for its interaction with CENP-N/L.

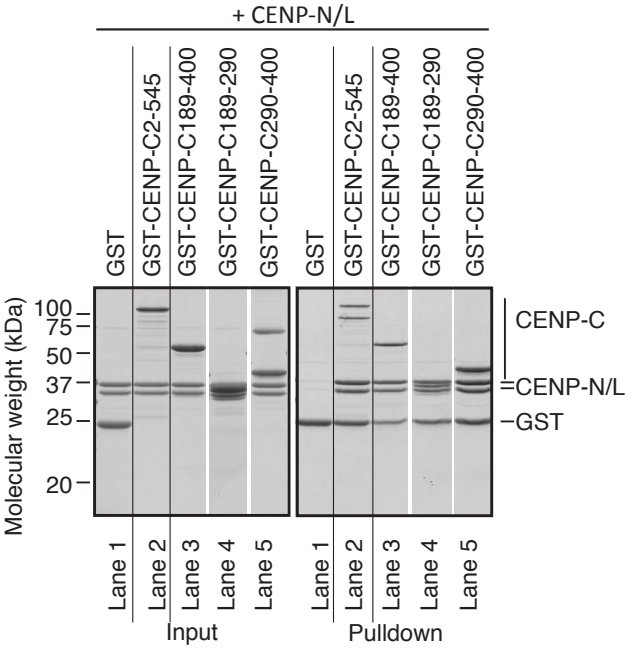

FIGURE 2.31: **GST-CENP-C$^{189-290}$ and CENP-C$^{290-400}$ CENP-N/L pulldown**. Different GST-CENP-C constructs have been used as bait (1 μM) and CENP-N/L as prey (3μM) to further refine the binding interface on CENP-C for CENP-N/L. As for CENP-H/I/K/M, several binding patches on CENP-C seem to be involved in CENP-N/L interaction, as seen in a binding of CENP-N/L to both CENP-C$^{189-290}$ and CENP-C$^{290-400}$.

2.19 Cross-linking coupled with mass spectrometry of CENP-C$^{1-544}$His / CENP-H/I/K/M / CENP-N/L / CENP-A^{nucleosome} complex

To test if CENP-H/I/K/M and CENP-N/L can bind to CENP-C concomitantly, a complex consisting of CENP-C$^{1-544}$His/H/I/K/M/N/L was produced. The successful production of this complex demonstrated the compatibility of CENP-H/I/K/M and CENP-N/L binding to CENP-C (data not shown). The complex is further capable of binding to CENP-A nucleosomes, since a complex consisting of CENP-C$^{1-544}$His/H/I/K/M/N/L bound to CENP-A containing recombinant nucleosomes was produced. This complex was further characterized by cross-linking coupled with mass spectrometry, providing insights into the spatial organization of the complex (in collaboration with Dr.John Weir, Dr.Federica Basilico and Dr.Ingrid Vetter at the MPI Dortmund and the laboratory of Prof.F. Herzog, Gene Center, Munich) (**Figure** 2.32).

Suggesting a successful experiment, most of the expected interactions were found. CENP-N and -L crosslink to each other, all histones crosslink, and CENP-H/I/K/M proteins crosslink to each other. The pattern of crosslinks confirmed that CENP-H/I/K/M and CENP-N/L bind to the same region of CENP-C, but probably interact with CENP-C through different residues, which will be addressed in detail in the following sections. Most of the crosslinks between CENP-C and CENP-H/I/K/M are provided by CENP-H and CENP-K. Interestingly, a connection of CENP-M to CENP-C was also found. Although CENP-I was shown to support the binding of CENP-H/K to CENP-C, no interaction of CENP-I to CENP-C was found in this experiment.

Binding of CENP-N/L to CENP-C is mediated largely by CENP-N, whereas CENP-L does not crosslink to CENP-C. The interactions of CENP-N and CENP-C to CENP-A containing nucleosomes were already described in the literature and were also depicted here. Surprisingly, CENP-I crosslinks with histone H2B, indicating close proximity of the CENP-H/I/K/M complex to the nucleosomes. Additionally, only the N-terminal half of CENP-I is involved in CENP-H/I/K/M complex formation, which raises the question of the role of its C-terminus. Interestingly, CENP-H/I/K/M crosslinks with CENP-N/L. Although we were not able to directly measure the binding affinity of CENP-N/L to CENP-C, the experiments in solution argue for a rather weak binding. An additional interaction

of CENP-N/L to CENP-H/I/K/M and CENP-A might strengthen CENP-N/L binding to the inner kinetochore.

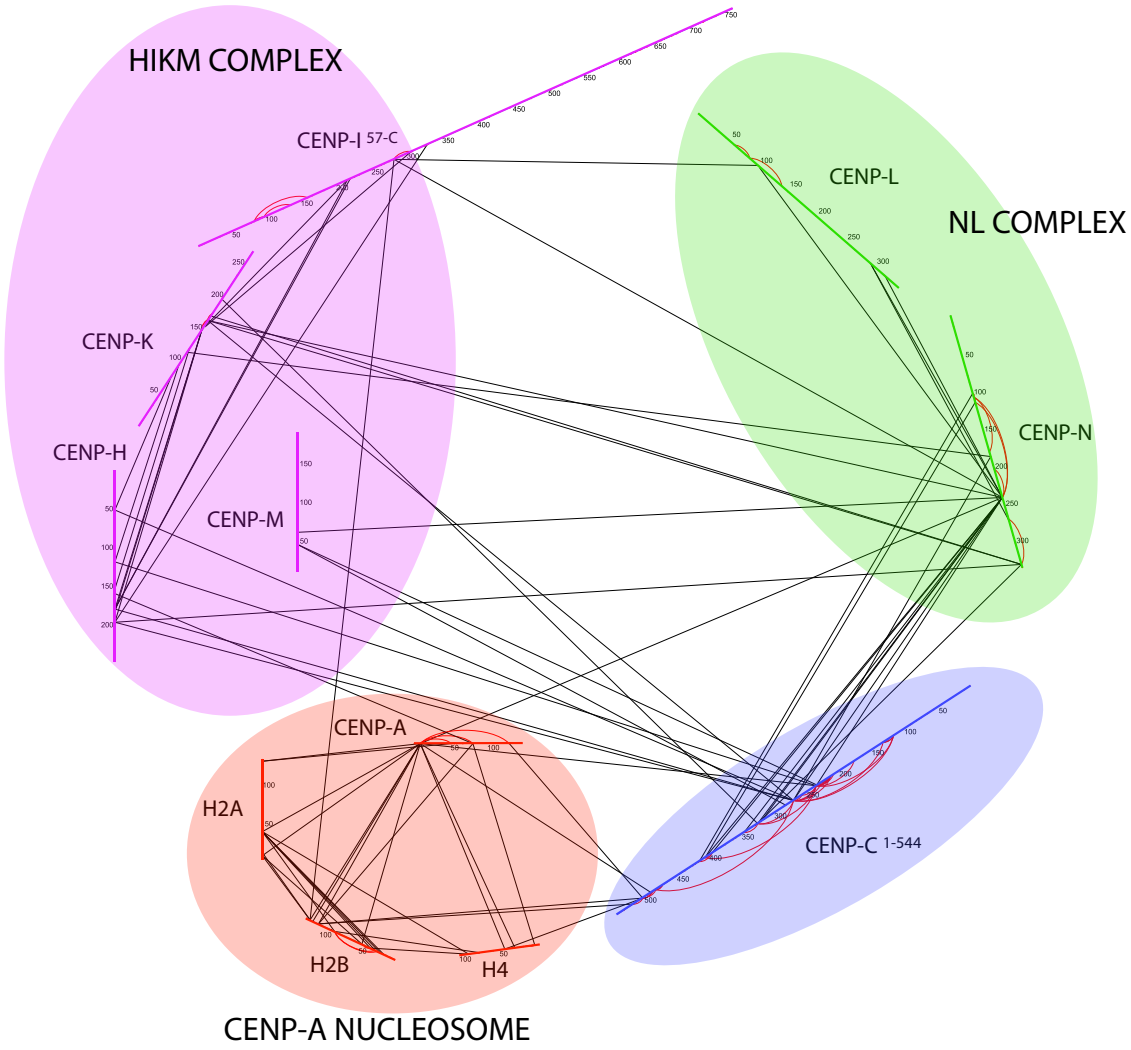

FIGURE 2.32: **CENP-C$^{2-545}$ CENP-H/I/K/M/N/L/CENP-A^{nucleosome} cross-linking and mass spectrometry.** Cross-linking of primary amines in lysine pairs by a cross linker of defined length (7.7 Å) and subsequent mass spectrometry allows insights into the spatial organization of a protein complex. Complex formation was carried out in collaboration with Dr. John Weir and Dr. Federica Basilico. The analysis was performed in collaboration with Dr. Franz Herzogs laboratory at the Ludwig Maximilian University in Munich. Data analysis and figure preparation was done in collaboration with Dr. Ingrid Vetter at the MPI Dortmund. Amino acid numbers are indicated every 50 residues. Cross-links between lysine pairs are represented as lines.

2.20 Multiple sequence alignment reveals conserved patches on CENP-C$^{189-400}$

To further understand the organization of the CENP-H/I/K/M:CENP-C and CENP-N/L:CENP-C interaction, mutations in conserved residues of CENP-C were investigated for their influence on CENP-C's interaction to CENP-H/K, CENP-H/I/K/M or CENP-N/L. To design mutants, a multiple sequence alignment was performed in order to find evolutionary conserved residues within CENP-C$^{189-400}$, the potential minimal interaction site with CENP-H/I/K/M and CENP-N/L (**Figure** 2.33).

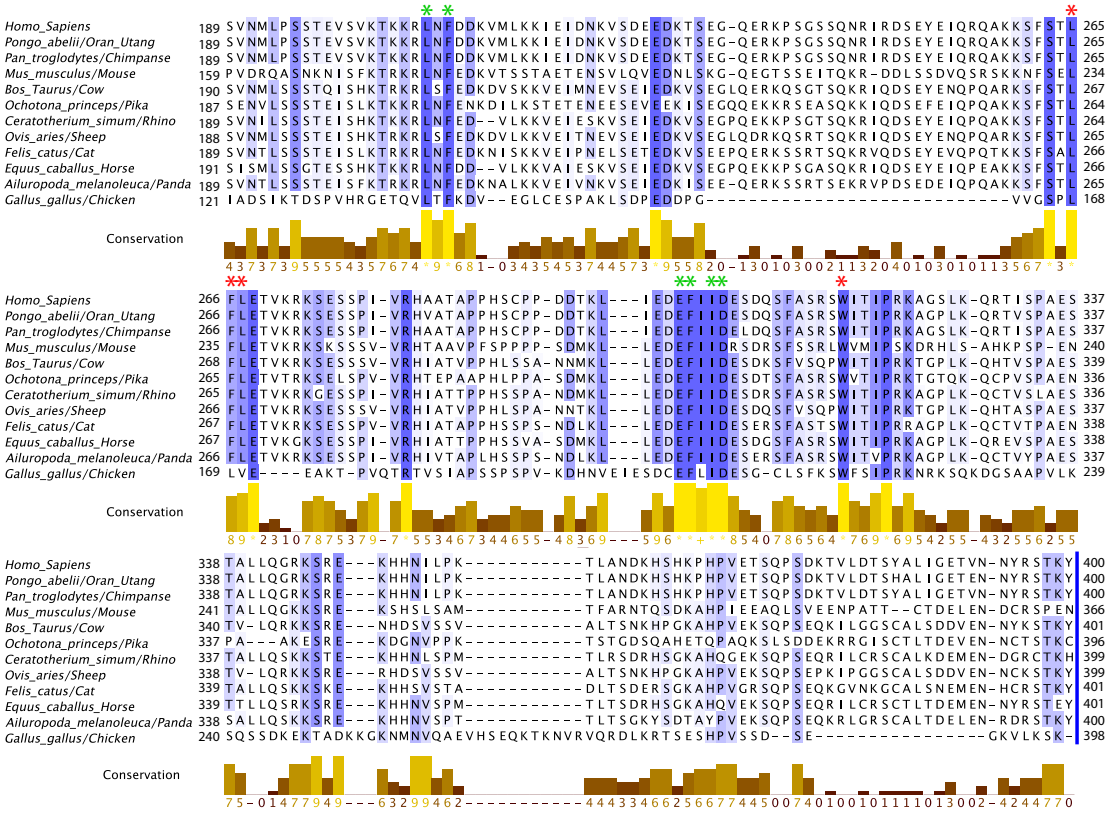

FIGURE 2.33: **CENP-C$^{189-400}$ multiple sequence alignment (MSA)**. A multiple sequence alignment of CENP-C$^{189-400}$ was performed with the software Jalview version 14.0 to find evolutionary conserved amino acids. These can be used for mutagenesis and subsequent determination of the residues involved in CENP-C's interaction with CENP-H/I/K/M or CENP-N/L. Residues mutated and found not to have an effect on CENP-C binding to CENP-H/I/K/M or CENP-N/L are marked with green asterisks. Mutants having an effect on CENP-C:CENP-H/I/K/M are indicated with red asterisks.

Four patches were found to be evolutionary conserved, indicated with asterisks. These sites were used as targets for mutagenesis. Additionally, the cross-link data and the observations from the GST pulldowns were considered to find potentially interesting residues as targets for mutagenesis. Green asterisks indicate residues shown not to have any effect on CENP-H/I/K/M or CENP-N/L binding to CENP-C when mutated, whereas red asterisks were shown to be involved in the interaction of CENP-C to CENP-H/I/K/M. For a summary of all CENP-C residues tested in the binding to CENP-H/K, CENP-H/I/K/M and CENP-N/L see **Tables** 2.4, 2.5 and 2.6.

2.21 CENP-C W317A binding to CENP-H/K, -H/I/K/M and -N/L

Since an extended segment of CENP-C seems to be involved in its interaction with CENP-H/I/K/M and CENP-N/L, finding relevant mutations might be difficult. Initially, the involvement of single amino acids of CENP-C in its interaction with CENP-H/K or CENP-N/L was investigated by mutating these amino acids to alanines in GST-CENP-C^{2-545} and performing pulldown assays. Later, promising mutants were introduced into smaller CENP-C constructs and tested for CENP-H/I/K/M, CENP-H/K and CENP-N/L binding.

In a GST pulldown assay, the binding of CENP-H/K to CENP-C was lost upon shortening CENP-$C^{189-364}$ to CENP-$C^{189-311}$, demonstrating an important interaction site between residues 311 and 364. A conserved tryptophane at position 317 was discovered to be involved in the interaction of CENP-C to CENP-H/K, but not CENP-N/L, as shown by a single point mutation to alanine and subsequent GST-pulldowns. GST-CENP-C^{2-545}W317A was reduced in its capability to bind CENP-H/K (**Figure** 2.34 **A**) lane 3 and 4), again supporting the idea of CENP-H/K binding to several patches on CENP-C. In contrast, binding of CENP-N/L to wild type or mutant GST-CENP-C^{2-545} was found to be unaltered (**Supplementary Figure** 5.3).

To understand if Trp317 is the main interaction site within CENP-C$^{290-400}$, the W317A mutant was introduced in this construct and the GST pulldown was repeated. As seen in **Figure** 2.34 **B** lane 3 and 4, the binding of CENP-H/K to CENP-C$^{290-400}$ was abolished upon mutation of Trp317 to alanine, pointing towards a major contribution from Trp317 to the CENP-H/K binding within that CENP-C region.

In addition, the binding of CENP-H/I/K/M to GST-CENP-C$^{2-545}$W317A and GST-CENP-C$^{290-400}$W317A compared to the wild type constructs was tested. Introducing the W317A mutation into CENP-C$^{2-545}$ did not apparently decrease the amount of bound CENP-H/I/K/M in a GST pulldown assay (**Figure** 2.35 lane 3 and 4). In the CENP-C$^{290-400}$ construct the W317A mutant abolished the binding completely as seen for the CENP-H/K in a GST pulldown assay (**Figure** 2.35 lane 5 and 6), confirming that within CENP-C$^{290-400}$ region, Trp317 is the binding residue necessary for the CENP-H/K and CENP-H/I/K/M interaction.

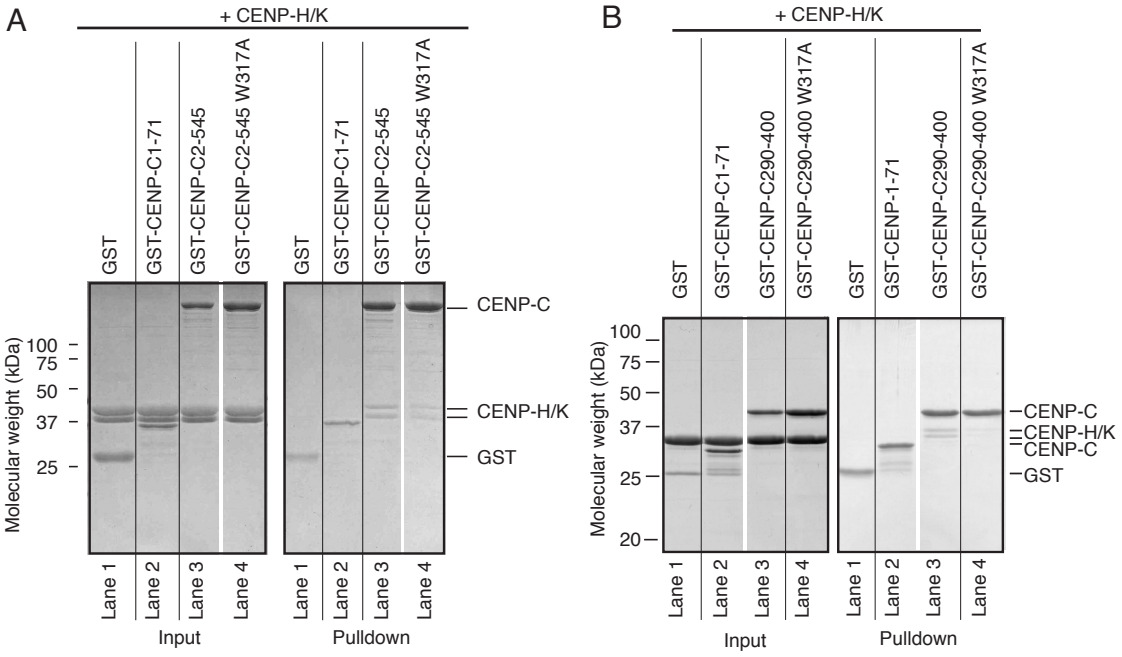

FIGURE 2.34: **GST-CENP-CW317A CENP-H/K pulldown experiment.** GST-CENP-CW317A or wild type constructs have been used as bait (1 μM) and CENP-H/K as prey (3 μM) to investigate the involvement of Trp 317 in the CENP-C:CENP-H/K interaction. CENP-C$^{2-545}$W317A is able to bind CENP-H/K to a less extent compared to wild type CENP-C$^{2-545}$, whereas the binding to CENP-C$^{290-400}$ is completely abolished.

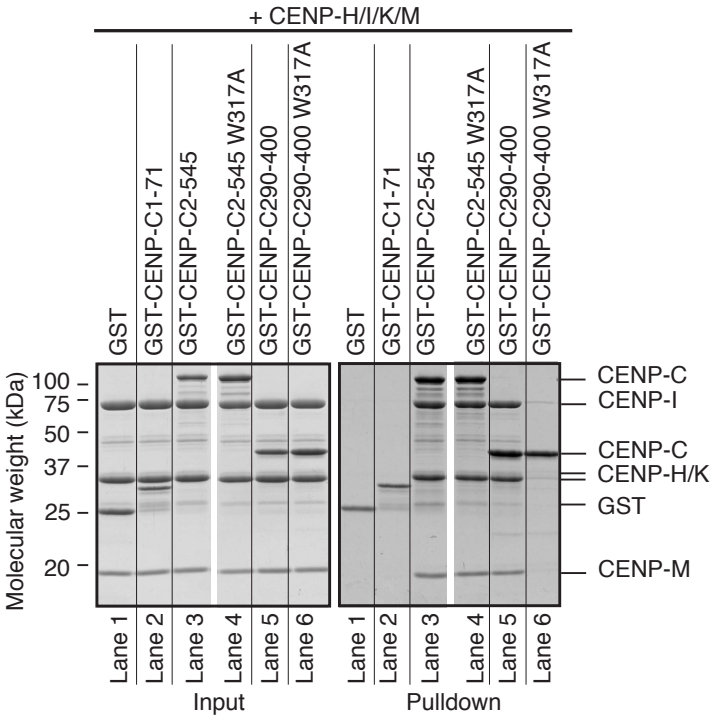

FIGURE 2.35: **GST-CENP-CW317A CENP-H/I/K/M pulldown**. GST-CENP-CW317A or wild type constructs have been used as bait (1 μM) and CENP-H/I/K/M as prey (3 μM) to investigate the involvement of Trp317 in the CENP-C:CENP-H/I/K/M interaction. Whereas, CENP-C$^{2-545}$W317A was not significantly diminished in its capability to bind CENP-H/I/K/M, the interaction was abolished in CENP-C$^{290-400}$W317A, demonstrating that this residue is the interaction site for CENP-H/I/K/M within that construct.

The effect of W317A mutation on CENP-N/L binding was also tested in a GST-CENP-C$^{2-545}$ pulldown. In agreement with the hypothesis that CENP-N/L binds to different sites on CENP-C than CENP-H/I/K/M, no difference in CENP-N/L binding to CENP-C$^{2-545}$W317A compared to wildtype CENP-C$^{2-545}$ was observed (**Figure** 5.3, lane 2 and 3). In summary, the residue Trp317 of CENP-C is involved in binding to CENP-H/I/K/M, but not CENP-N/L.

To confirm the involvement of Trp317 in CENP-C's interaction with CENP-H/I/K/M, binding of CENP-C$^{2-545}$W317A to CENP-H/I/K/M was analyzed in analytical SEC experiment (**Figure** 2.40 compare **A** and **B**). Although the shift in elution volume of the CENP-C$^{2-545}$W317A: CENP-H/I/K/M complex in the chromatogram is smaller compared to CENP-C$^{2-545}$:CENP-H/I/K/M, complex formation is evident. This supports the hypothesis that several residues of CENP-C contribute to the CENP-H/I/K/M interaction and Trp317 is one of them.

2.22 CENP-C L265A/F266A/L267A binding to CENP-H/K, -H/I/K/M and -N/L

A conserved leucine at position 265, phenylalanine at 266 and leucine at 267 of CENP-C were tested for their involvement in CENP-C interactions with other CCAN coponents. Mutating these residues to alanine (this Leu265A Phe266A Leu267A triple mutant is subsequently called 3A) did not affect the binding of CENP-C^{2-545} to CENP-H/K (**Figure** 2.36). Combining this 3A mutation with the previously discussed W317A mutation (this Leu265A Phe266A Leu267A Trp317A quaternary mutant is subsequently called 4A) did not further decrease the binding of CENP-C^{2-545} to CENP-H/K compard to CENP-C^{2-545}W317A (**Figure** 2.37). This indicates no involvement of Leu265, Phe266 and Leu267 of CENP-C in the CENP-H/K interaction.

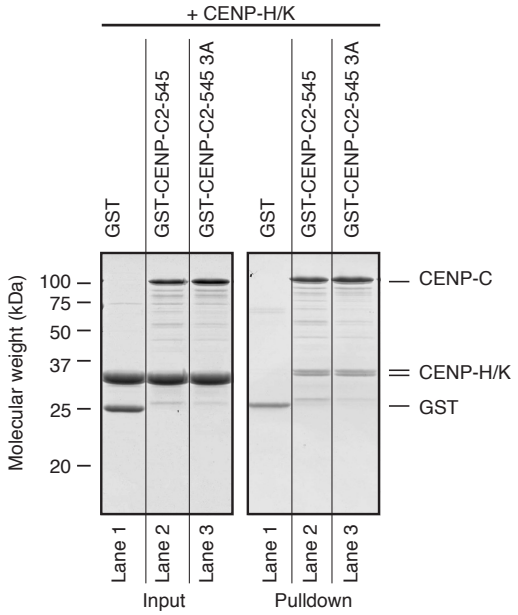

FIGURE 2.36: **GST-CENP-C^{2-545}3A CENP-H/K pulldown**. GST-CENP-C^{2-545}3A or wild type constructs have been used as bait (1 μM) and CENP-H/K as prey (3 μM) to investigate the involvement of Leu265, Phe266 and Leu267 in the CENP-C:CENP-H/K interaction. CENP-C^{2-545}3A binds CENP-H/K as efficiently as wild type CENP-C^{2-545} in this pulldown assay, speaking against a contribution from Leu265, Phe266 and Leu267 to CENP-C:CENP-H/K interaction.

Interestingly, the 3A mutation abolishes the binding of CENP-H/I/K/M to CENP-$C^{189-290}$ (**Figure** 2.38 lane 2 and 3), suggesting that within CENP-$C^{189-290}$ Leu265, Phe266 and Leu267 are responsible for the CENP-C:CENP-H/I/K/M interaction. To distinguish whether this impaired interaction can only be observed with CENP-$C^{189-290}$, because this construct is lacking other CENP-H/I/K/M binding interfaces or if this is a CENP-H/I/K/M specific effect, CENP-C^{2-545}3A was tested for its binding to CENP-H/I/K/M. Indeed, a remarkable decrease in CENP-H/I/K/M binding to CENP-C^{2-545}3A compared to wild type CENP-C^{2-545}, but also CENP-C^{2-545}W317A was observed (**Figure** 2.39 Lane 2, 3 and 4). Combining these two mutants shown to decrease the binding of CENP-H/I/K/M to CENP-C (4A mutant) causesd complete loss of the CENP-H/I/K/M:CENP-C interaction in the context of CENP-C^{2-545} in a GST-pulldown experiment (**Figure** 2.39 Lane 2 and 5). This indicates a complete disruption of the CENP-C:CENP-H/I/K/M binding interface.

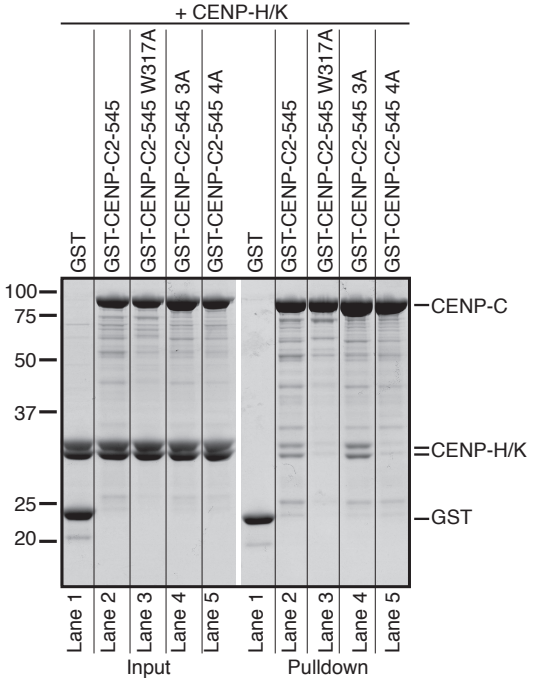

FIGURE 2.37: **GST-CENP-C^{2-545}4A CENP-H/K pulldown**. GST-CENP-C^{2-545}4A or wild type constructs have been used as bait (1 μM) and CENP-H/K as prey (3 μM) to investigate the involvement of Leu265, Phe266 and Leu267 in combination with Trp317 in the CENP-C:CENP-H/K interaction. CENP-C^{2-545}3A is able to bind CENP-H/K comparable to wild type CENP-C^{2-545} and CENP-C^{2-545}4A is binding to CENP-H/K comparable to CENP-C^{2-545}W317A in this pulldown assay, speaking against a contribution from Leu265, Phe266 and Leu267 to the CENP-C:CENP-H/K interaction.

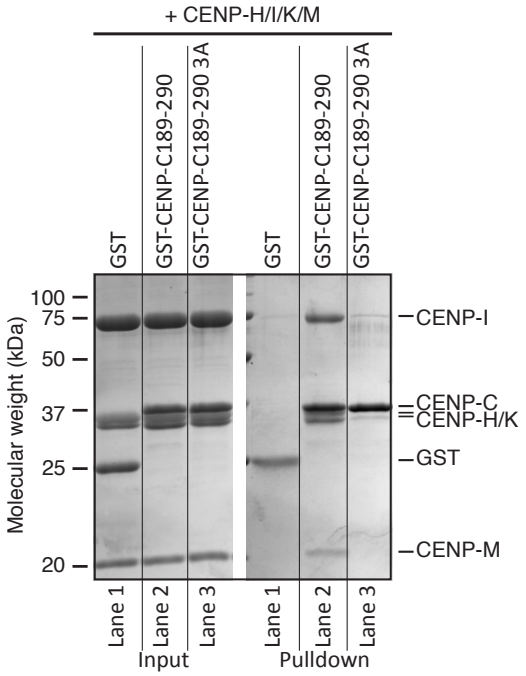

FIGURE 2.38: **GST-CENP-C$^{189-290}$3A CENP-H/I/K/M pulldown**. GST-CENP-C$^{189-290}$3A or wild type constructs have been used as bait (1 μM) and CENP-H/I/K/M as prey (3 μM) to investigate the involvement of Leu265, Phe266 and Leu267 in the CENP-C:CENP-H/I/K/M interaction. CENP-C$^{189-290}$3A does not bind to CENP-H/I/K/M, demonstrating a contribution from these residues to CENP-C:CENP-H/I/K/M interaction.

To confirm the disruption of the CENP-C:CENP-H/I/K/M binding interface, wild type CENP-C$^{2-545}$, CENP-C$^{2-545}$W317A, CENP-C$^{2-545}$3A and CENP-C$^{2-545}$4A binding to CENP-H/I/K/M was tested in a SEC experiment (**Figure** 2.40). CENP-C$^{2-545}$W317A only slightly effected CENP-H/I/K/M binding to CENP-C in solution. In contrast, the shift of the elution volume of CENP-C$^{2-545}$3A was much smaller compared to wild type CENP-C$^{2-545}$. In the Coomassie stained SDS-PAGE gel, a shift of all proteins can still be observed, but the peaks of CENP-H/I/K/M and CENP-C$^{2-545}$ are not comigrating, indicative of a partial, but significant disruption of the binding interface.

In agreement with the pulldown experiments, CENP-C$^{2-545}$4A completely hinders the formation of the CENP-C:CENP-H/I/K/M complex, since no shift to an earlier elution volume of any component in the chromatogram or in the Coomassie stained SDS-PAGE gel can be observed. Therefore, the CENP-C:CENP-H/I/K/M interface was completely disrupted *in vitro* by introducing four point mutations into evolutionary conserved residues of CENP-C.

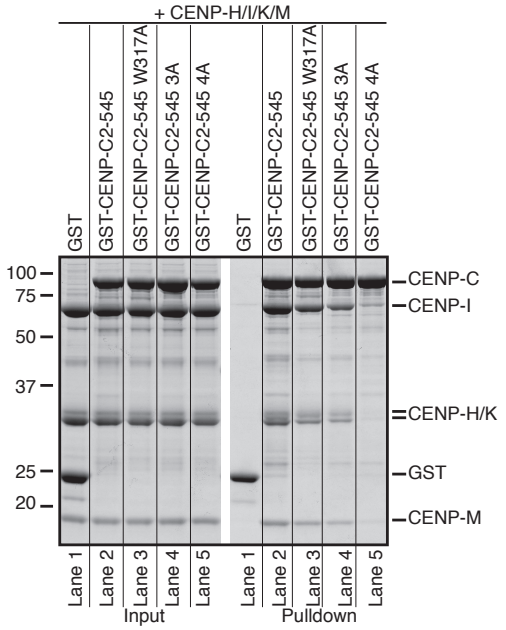

FIGURE 2.39: **GST-CENP-C$^{2-545}$W317A 3A and 4A CENP-H/I/K/M pulldown**. GST-CENP-C$^{2-545}$, GST-CENP-C$^{2-545}$W317A, GST-CENP-C$^{2-545}$3A and GST-CENP-C$^{2-545}$4A have been used as bait (1 μM) and CENP-H/I/K/M as prey (3 μM) to investigate the involvement of Leu265 Phe266 and Leu267 in combination with Trp317 in the CENP-C:CENP-H/I/K/M interaction. CENP-C$^{2-545}$3A binds much less CENP-H/I/K/M compared to wild type CENP-C$^{2-545}$. CENP-C$^{2-545}$4A abolishes the binding of CENP-H/I/K/M to CENP-C$^{2-545}$. Therefore, these two patches of CENP-C are the main interaction sites for CENP-H/I/K/M.

To support the hypothesis that different residues of CENP-C are involved in its interaction with CENP-H/I/K/M and CENP-N/L, GST-CENP-C$^{2-545}$4A was tested for its capability to interact with CENP-N/L in a GST pulldown assay. Indeed, no difference in CENP-N/L binding to the mutant or wild type GST-CENP-C$^{2-545}$ was observed (**Supplementary Figure** 5.4). Unfortunately, the residues of CENP-C relevant for CENP-N/L interaction were not found. This might be a consequence of contributions from several CENP-C residues to its interaction with CENP-N/L.

In summary the minimal binding interface of CENP-C for CENP-H/I/K/M interaction was defined as a region of about 200 residues within the N-terminal half of CENP-C (amino acids 189-400), although contributions from regions N- and C-terminal of CENP-C$^{189-400}$ to the interaction with CENP-H/I/K/M were suggested. Within CENP-C$^{189-400}$ two conserved patches are necessary for the interaction. All CENP-C constructs tested in a GST pulldown assay or in a SEC

experiment with either CENP-H/K, CENP-H/I/K/M or CENP-N/L and the results of such tests are summarized in **Tables** 2.4, 2.5, 2.6 and 2.7.
During our investigations, other conserved residues of CENP-C were tested for their involvement in CENP-C's interaction with CENP-H/K, CENP-H/I/K/M and CENP-N/L. Since mutating these residues did not affect the interaction of CENP-H/K, CENP-H/I/K/M or CENP-N/L to CENP-C, a different role of these residues is likely. The results of GST-pulldowns with additional point mutations on CENP-C investigated in this work are summaryzed in **Section** 2.23 and 2.24.

2.23 CENP-C$^{2-545}$E302A/F303A or I305A/D306A binding to CENP-H/K and -N/L

Residues Glu302, Phe303, Ile305 and Asp306 of CENP-C were found to be conserved and were therefore tested for the involvement in CENP-C's interaction with CENP-H/K and CENP-N/L. Neither GST-CENP-C$^{2-545}$E302A/F303A nor GST-CENP-C$^{2-545}$I305A/D306A was affected in its capability to bind to CENP-H/K compared to wild type GST-CENP-C$^{2-545}$ (**Supplementary Figure** 5.5, lane 4). GST-CENP-C$^{2-545}$E302R/F303S, which reverses the charges of these residues, also showed no effect in interacting with CENP-H/K (**Supplementary Figure** 5.5, lane 5).
Furthermore, GST-CENP-C$^{2-545}$E302R/F303S as well as GST-CENP-C$^{2-545}$I305A/D306A seems not to majorly influence the binding of CENP-N/L to CENP-C, although there might be a slight reduction in the binding (**Supplementary Figure** 5.6, lane 3).
Taken together, residues Glu302, Phe303, Ile305 and Asp306 of CENP-C do not play a major role in its interaction with CENP-H/K.

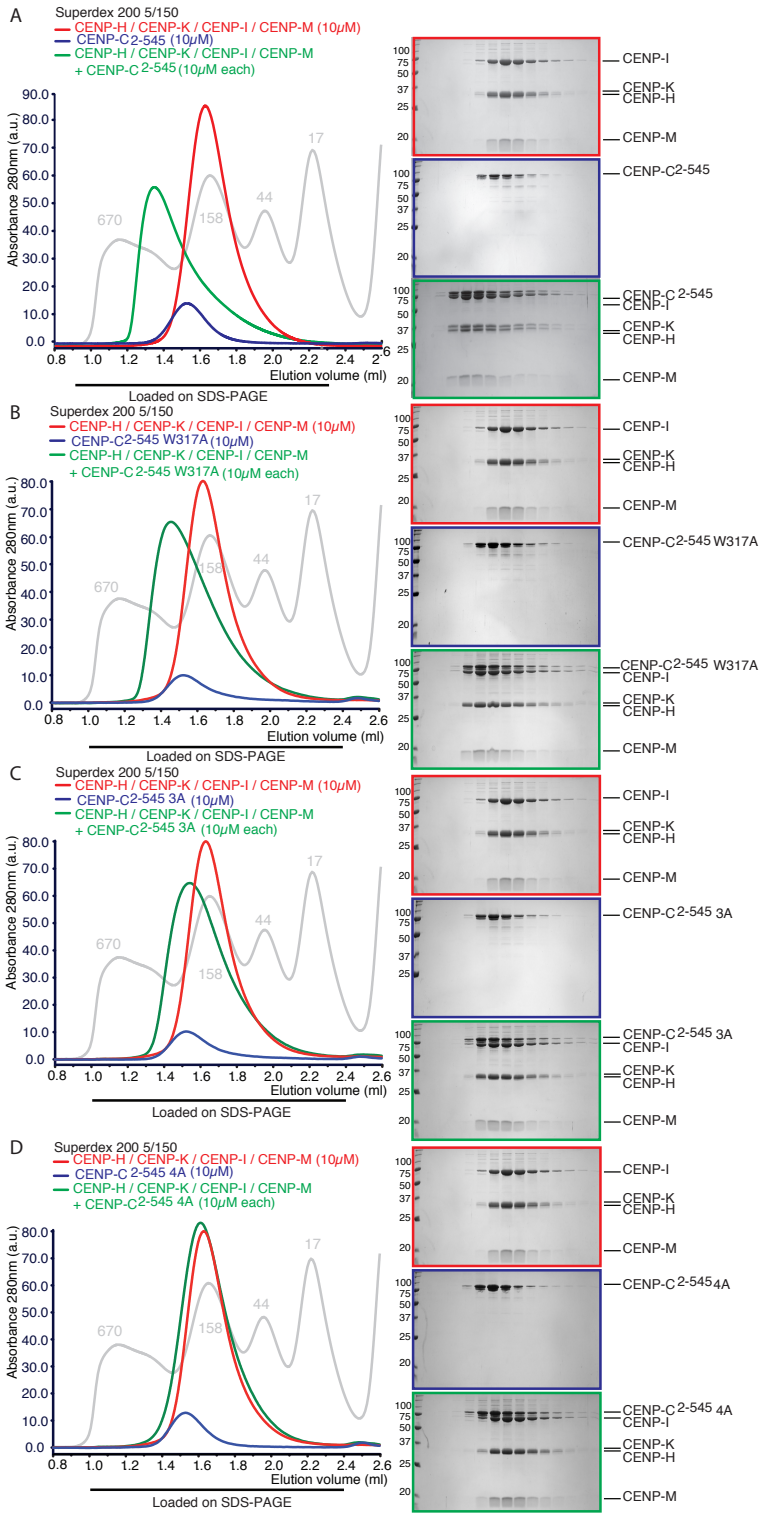

FIGURE 2.40: **CENP-C$^{2-545}$4A CENP-H/I/K/M interaction on SEC**. SEC elution profiles and SDS-PAGE analyses of CENP-H/I/K/M complex (red), CENP-C$^{2-545}$ wild type and mutants (blue) and their combination (green) is shown. 10 μM of CENP-C$^{2-545}$ and CENP-H/I/K/M were mixed, incubated for 1 h at 4°C and run on a Superdex 200 5/150. CENP-C$^{2-545}$W317A and CENP-C$^{2-545}$3A do not bind to CENP-H/I/K/M as efficiently as wild type CENP-C$^{2-545}$, whereas CENP-C$^{2-545}$4A disrupts complex formation with CENP-H/I/K/M demonstrating an involvement of both CENP-C patches in the CENP-C:CENP-H/I/K/M interaction.

2.24 CENP-C L207A/F209A binding to CENP-H/K, -H/I/K/M and -N/L

Leu207 and Phe209 of CENP-C were shown to be conserved. Therefore, GST-CENP-C^{2-545}L207A/F209A was tested for its interaction with CENP-H/K, CENP-H/I/K/M and CENP-N/L. Mutating these residues to alanines did not show any effect on GST-CENP-C^{2-545} binding to CENP-H/K (**Supplementary Figure** 5.8 **A**) or GST-CENP-$C^{189-290}$ binding to CENP-/H/I/K/M (**Supplementary Figure** 5.8 **B**) compared to wild type CENP-C.
GST-CENP-$C^{189-290}$L207A/F209A was also tested for its binding to CENP-N/L. However, the result was difficult to interpret, since the band of GST-CENP-C runs between the bands of CENP-N and CENP-L in a Coomassie stained SDS-PAGE gel (**Supplementary Figure** 5.7). Nevertheless, a decrease on the lowest running band was observed. An involvement of residues Glu302 and Phe303 of CENP-C in the interaction with CENP-N/L also remained uncertain from previous experiments, since there was only a very minor impact on the binding of CENP-N/L to GST-CENP-C^{2-545}E302R/F303S. Therefore, L207A/F209A and E302R/F303S mutations were combined in GST-CENP-C^{2-545} and the binding of CENP-N/L was monitored.

Even the mutation of these four residues did not significantly decrease CENP-N/L binding to CENP-C in a GST-pulldown experiment (**Supplementary Figure** 5.9). This does not rule out an involvement of these residues in the CENP-C:CENP-N/L interaction, but if involved their contribution is not major.

Table 2.4: Summary of CENP-C binding to CENP-H/K on solid surface

CENP-C construct (a.a.)	**CENP-H/K binding**	**Figure**
2-545	Yes	2.14
1-400	Yes	2.14
104-504	Yes	2.14
189-544	Yes	2.14
189-447	Yes	2.14

CENP-C construct (a.a.)	**CENP-H/K binding**	**Figure**
189-420	Yes	2.14
189-400	Yes	2.14
225-400	Reduced	2.14
263-400	Reduced	2.15
290-400	Reduced	2.15
189-364	Yes	2.16
189-311	No	2.16
189-290	No	2.16
402-544	No	2.27
2-545^{E302AF303A}	Yes	5.5
2-545^{I305AD306A}	Yes	5.5
2-545^{L207AF209A}	Yes	5.8
2-545^{W317A}	Reduced	2.34
290-400^{W317A}	No	**??**
2-545^{3A}	Yes	2.36
2-545 ^{4A}	No	2.37

TABLE 2.5: Summary of CENP-C binding to CENP-H/I/K/M on solid surface

CENP-C construct (a.a.)	**CENP-H/I/K/M binding**	**Figure**
2-545	Yes	2.24
290-400	Yes	2.35
189-290	Yes	2.24
189-290^{L207AF209A}	Yes	5.8
2-545^{W317A}	Yes	2.35
290-400^{W317A}	No	2.35
2-545^{3A}	Reduced	2.39
189-290^{3A}	No	2.38
2-545^{4A}	No	2.39

TABLE 2.6: Summary of CENP-C binding to CENP-N/L on solid surface

CENP-C construct (a.a.)	**CENP-N/L binding**	**Figure**
2-545	Yes	2.30
1-400	Yes	2.30
104-544	Yes	2.30
189-544	Yes	2.30
189-400	Yes	2.30
189-290	Yes	2.31
290-400	Yes	2.31
2-545^{W317A}	Yes	5.3
189-290^{L207AF209A}	Yes	5.7
2-545^{W317A}	Yes	5.3
2-545^{4A}	Yes	5.4
2-545^{E302AF303A}	Yes	5.6
2-545^{I305RD306S}	Yes	5.6
2-545^{L207AF209AE302RF303S}	Yes	5.9

TABLE 2.7: Summary of CENP-C binding to CENP-H/K and CENP-H/I/K/M in solution

CENP-C construct (a.a.)	**CENP-H/K binding**	**CENP-H/I/K/M binding**
2-545	Yes	Yes
1-400	Yes	
189-544	Reduced	Yes
189-400	No	Yes
402-544	No	
2-545^{W317A}		Reduced
2-545^{3A}		Reduced
2-545^{4A}		No

2.25 CENP-C4A is a separation of function mutant *in vitro*

Since we clearly demonstrated that CENP-C$^{2-545}$4A loses the capability to bind CENP-H/I/K/M *in vitro*, we asked whether it is able to fulfill its outer kinetochore binding function through direct interaction with the Mis12 complex.
Mis12c binding to CENP-C$^{2-545}$4A was investigated in a GST-pulldown assay and in a SEC experiment. CENP-H/I/K/M was included in both assays to confirm the specific effect of the CENP-C4A mutation on CENP-H/I/K/M.

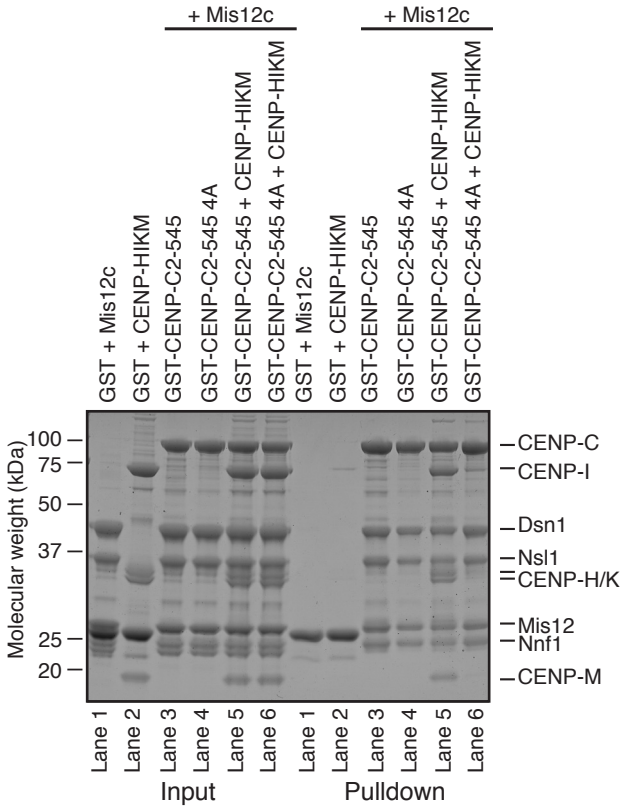

FIGURE 2.41: **GST-CENP-C$^{2-545}$4A Mis12c pulldown**. GST-CENP-C$^{2-545}$4A or wild type constructs have been used as bait (1 μM) and Mis12 complex with and without CENP-H/I/K/M as prey (3 μM) to investigate whether CENP-C$^{2-545}$4A can fulfill its function of Mis12c binding *in vitro*. GST-CENP-C$^{2-545}$4A and wildtype are able to bind Mis12c, whereas CENP-H/I/K/M is not interacting with GST-CENP-C$^{2-545}$4A, demonstrating a specific disruption of CENP-C's function to bind CENP-H/I/K/M *in vitro*.

GST-CENP-C$^{2-545}$ efficiently interacts with Mis12c and CENP-H/I/K/M in a GST-pulldown assay. As expected, CENP-H/I/K/M is lost in the GST-CENP-C$^{2-545}$4A pulldown, whereas Mis12 complex is binding as efficient as to the wild type form of CENP-C$^{2-545}$ (**Figure** 2.41). In agreement, Mis12c interacts with both CENP-C$^{2-545}$ and CENP-C$^{2-545}$4A in solution, whereas CENP-H/I/K/M only binds to CENP-C$^{2-545}$ (**Figure** 2.42).

These two experiments clearly demonstrate that the CENP-C4A mutant specifically disrupts the CENP-H/I/K/M binding interface on CENP-C, but does not impair other function of CENP-C including interaction with CENP-N/L (**Supplementary Figure** 5.4) and Mis12 complex *in vitro*.

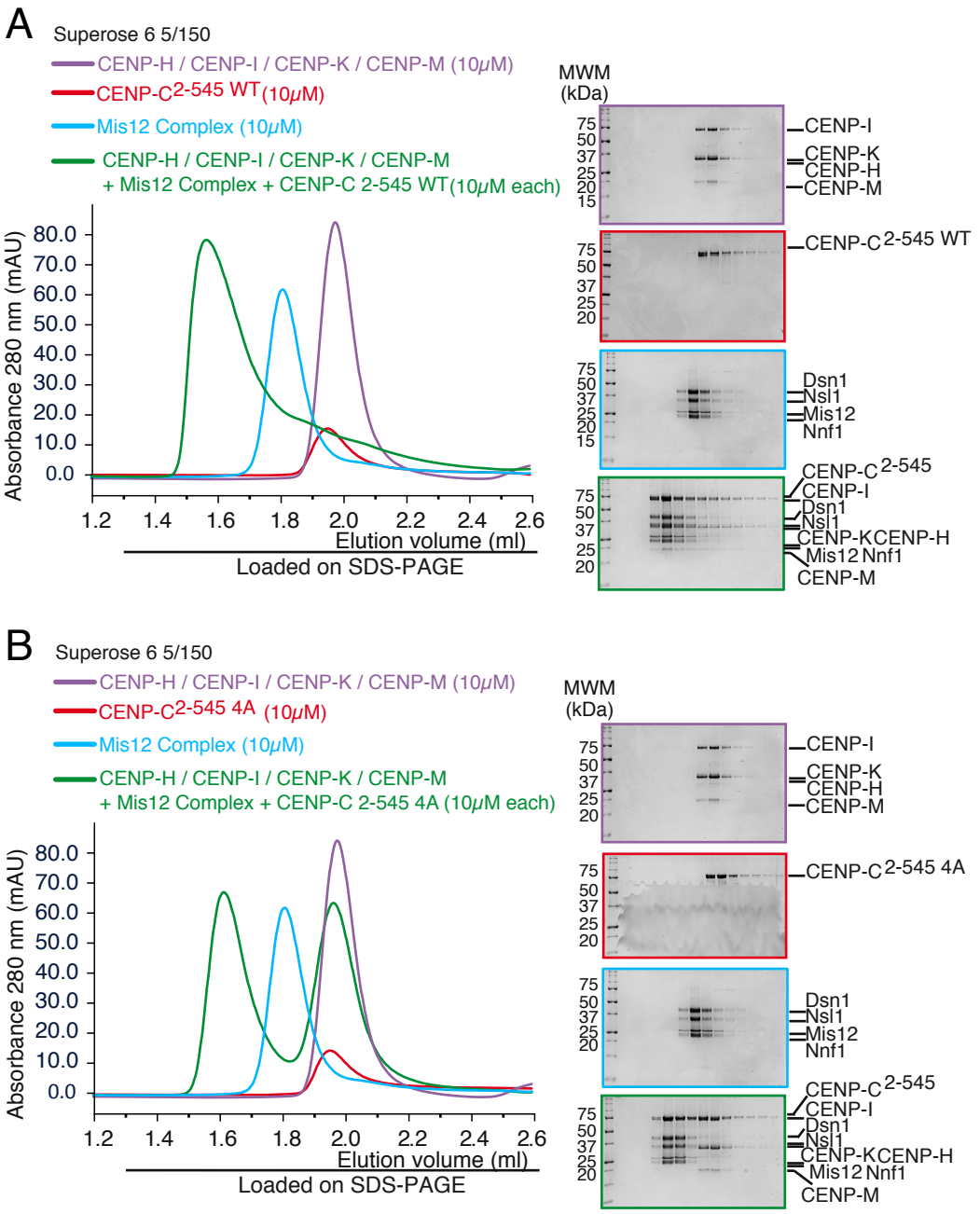

FIGURE 2.42: **CENP-C$^{2-545}$4A Mis12c interaction in SEC**. SEC elution profiles and SDS-PAGE analyses of CENP-H/I/K/M complex (purple), CENP-C$^{2-545}$ wild type and mutants (red), Mis12c (blue) and their combination (green) is shown. 10 μM of CENP-C$^{2-545}$, Mis12c and CENP-H/I/K/M were mixed in a 1:1:1 ratio, incubated for 1 h at 4°C and run on a Superose 6 5/150. CENP-C$^{2-545}$ forms a complex with CENP-H/I/K/M and Mis12c as seen by a shift of the peak in the chromatogram to an earlier elution volume and a complex formation in Coomassie stained SDS-PAGE gels. In contrast, CENP-C$^{2-545}$4A only shifts to an earlier elution volume with Mis12c in both the chromatogram and the Coomassie stained SDS-PAGE gels, whereas the peak of CENP-H/I/K/M in the chromatogram does not shift, which is confirmed in the Coomassie stained SDS-PAGE gel.

2.26 *In vivo* role of CENP-C in CCAN assembly

To understand the role of CENP-C in the CCAN assembly within human cells and confirm the physiological relevance of the results obtained *in vitro*, a protocol for RNAi based CENP-C depletion was established. Since CENP-C is a crucial, constitutively bound component of kinetochores its depletion raises two potential problems. First, an efficient depletion might only be observed after a long treatment with CENP-C RNAi. CENP-C RNAi does only effect translation of new CENP-C, but the portion of CENP-C already localized to kinetochores will stay at the centromeric region dependent on its half life. Therefore, the cells might need to undergo several cell cycles, until an efficient CENP-C depletion is achieved. To overcome this problem, cells had to be RNAi treated for 96 h to obtain very low CENP-C levels (see **Figure** 2.43). Second, cells that are completely depleted of CENP-C will not be able to assemble a functional kinetochore, not proceed through mitosis and eventually enter apoptosis. Speaking for this, a high number of dying cells was observed in the CENP-C RNAi treated population (data not shown). Therefore, cells obtained in this study might have a residual level of CENP-C. RNAi efficiency was confirmed by western blotting of total cell lysate against CENP-C (see **Figure** 2.43) and indeed RNAi treated cells display clearly reduced CENP-C total protein levels, but a residual level of CENP-C is observed. In contrast, protein levels of other CCAN components were not affected, demonstrating that depletion of CENP-C does not decrease the overall stability of other CCAN components.

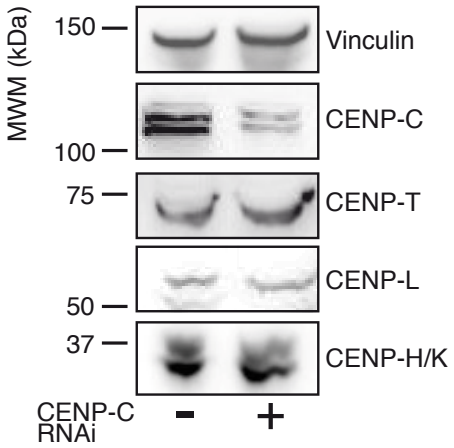

FIGURE 2.43: **CENP-C RNAi depletion in total cell lysates by RNAi**. Cells were treated with CENP-C RNAi for 96 h, during which cells were transfected 3 times with 60 nM RNAi in 24 h intervals. Proteins levels of total cell lysate of CENP-C and several other CCAN proteins in RNAi treated (+) and mock treated (-) cells were observed in SDS PAGE followed by western blotting against the indicated proteins. MWM indicates the molecular weight marker in kDa. Vinculin served as loading control. CENP-C showed a clear reduction in total protein levels, whereas other protein expression was not influenced by the treatment. The double band observed for CENP-C might be a posttranslationally modified version of the protein.

2.26.1 Establishment of doxycycline inducible mCherry-CCAN cell lines

CENP-C RNAi depletion was applied to investigate the role of CENP-C in the recruitment of the CCAN to human kinetochores using immunoflourescence. This describes a technique that makes use of the possibility to visualize proteins within fixed biological samples by treatment with specific primary antibodies and flourochrome conjugated secondary antibodies. Since several antibodies can be combined and therefore different proteins can be stained simultaneously, it is possible to observe correlations in the expression or localization patterns between these proteins. As a limitation, only a limited number of antibodies against CCAN components were available that were applicable for immunofluorescence (IF). Antibodies used in this study that were initially available in the lab included a commercial antibody isolated from CREST syndrome patients that has been extensively reported to stain mammalian centromeres. It was used in the experiments as centromere marker and reference to normalize levels of kinetochore proteins.

Additionally, a CENP-C antibody raised against CENP-C$^{23-410}$, a CENP-I antibody raised against CENP-I$^{57-281}$ and a CENP-T/W antibody raised against the full length proteins, generated in house were used. As alternative for CCAN proteins lacking functional antibodies, we used Flp-In T-REx HeLa cells to generate stable cell lines inducible for CCAN protein expressing. These included stable Flp-In T-REx HeLa cell lines inducible for mCherry-CENP-N, -CENP-L and -CENP-K full length protein expression (for a detailed protocol of cell line generation see **Section** 4.20). In Flp-In T-REx HeLa cells Cre-recombinase inserts a single copy of the gene of interest into a specific locus of the DNA under an doxycycline inducible promoter. Since the gene is always inserted into the same DNA locus, cell line generation is reproducible and different cell lines are comparable. Moreover this approach reduces the potentially harmful effects of random integration into the host's DNA. Inducible gene expression bears the advantage that target gene expression can be induced at specific time points of the experiment and it is possible to alter protein expression levels through titration of doxycycline.

Here, cell lines inducible for mCherry-CENP-K, -N and -L were generated and all fusion proteins were efficiently recruited to the centromeric region throughout the cell cycle, as indicated by colocalization of the protein with the centromeric marker CREST (see **Figure** 2.44). This suggests that the tag does not interphere with the localization of these proteins. Therefore, these cell lines were used to test the dependency of CENP-K, CENP-N and CENP-L centromeric targeting from CENP-C. Since CCAN proteins are always bound to the centromeric region and the signal of the mCherry-CCAN proteins as well as the antibodies recognizing CENP-T/W, CENP-I and CENP-C gave the cleanest signal in interphasic cells (data not shown), in all experiments cells in interphase were used for quantification and image preparation.

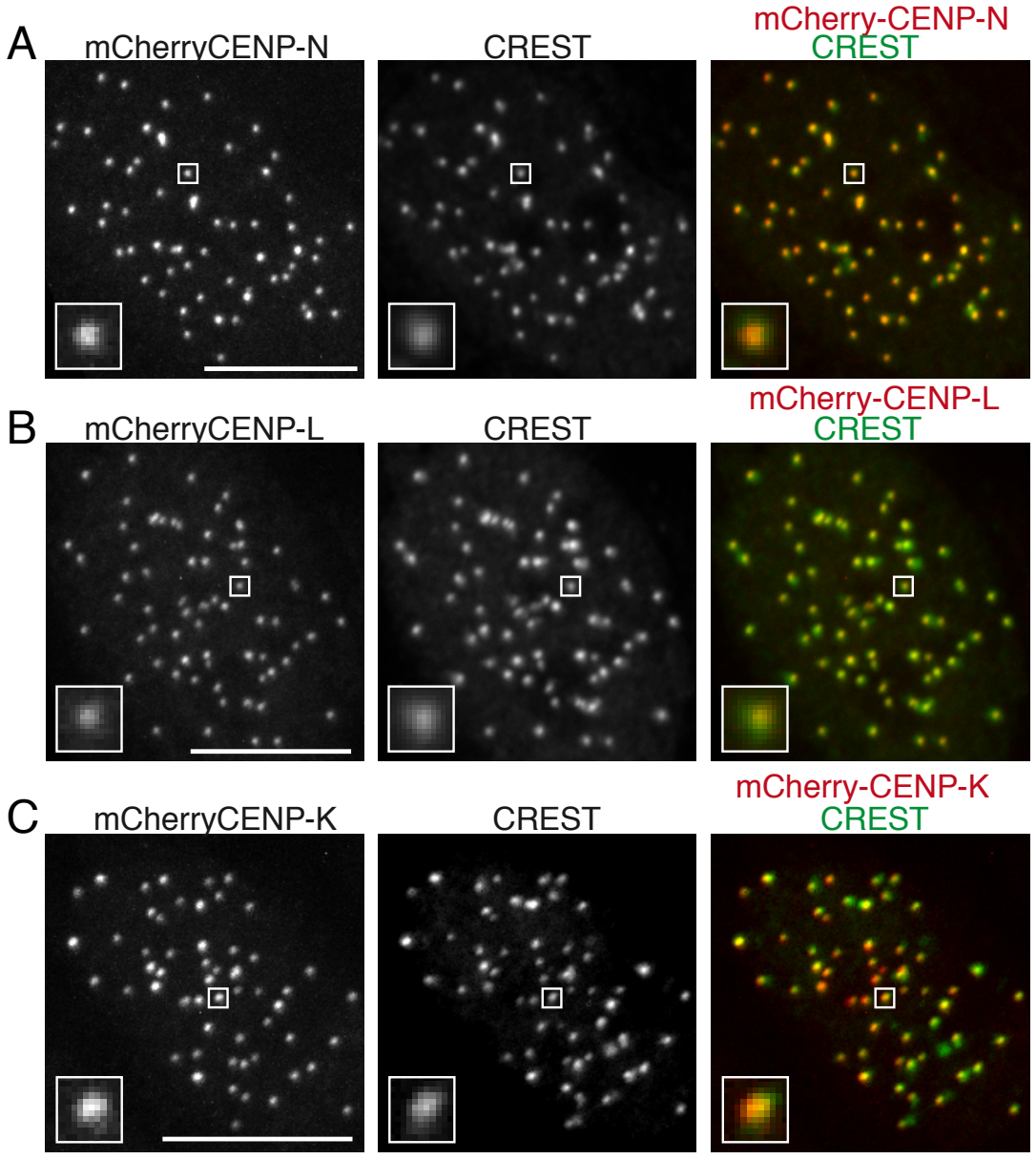

FIGURE 2.44: **Generation of mCherry-CCAN cell lines**. Expression and centromere localization of mCherry-CENP-N (**A**), mCherry-CENP-L (**B**) and mCherry-CENP-K (**C**) was observed on fixed material by costaining with the kinetochore marker CREST. All of these mCherry fused proteins efficiently localize to kinetochores. Scale bar = 10 μm.

2.26.2 Depletion of CENP-C abolishes localization of CCAN proteins to kinetochores

We have shown that CENP-H/K and CENP-N/L directly interact with CENP-C *in vitro* (see **Section** 2.13 and 2.17). To validate this interaction within human cells, mCherry-CENP-K, -CENP-N and -CENP-L expressing Flp-In T-REx HeLa cell lines described in **Section** 2.26.1 were RNAi depleted for CENP-C (for detailed protocol see **Section** 4.21) to investigate the dependency of these CCAN proteins on CENP-C for their kinetochore localization. Cells were analysed by immunoflourescence with CREST antibody as centromere marker and CENP-C antibody to judge its depletion efficiency in individual cells. Levels of CENP-C and all mCherry-CCAN proteins were quantified at individual kinetochores with use of the software Imaris7.6 (Bitplane) and normalized against the CREST signal. As mentioned before, CENP-C RNAi treatment only reduced total protein levels of CENP-C, excluding any off target effects on the other CCAN proteins investigated here, as shown by western blotting (see **Figure** 2.43).
Cells efficiently depleted for CENP-C reduced mCherry-CENP-N to 17 %, CENP-L to 22 % total levels and completely abolished CENP-K recruitment to kinetochores (**Figure** 2.45 **A** and 2.46). This result clearly demonstrates a physiological relevance of the CENP-C:CENP-H/I/K/M interaction and the CENP-C:CENP-N/L interaction observed *in vitro*.
The different residual levels of mCherry-CENP-K compared to mCherry-CENP-N and mCherry-CENP-L could be a consequence of different expression levels of these mCherry-CCAN proteins. As a functional possibility, mCherry-CENP-N and mCherry-CENP-L centromeric localization could depend on other proteins besides CENP-C. Destruction of one of their interaction sites at kinetochores by depleting CENP-C would then effectively reduce, but not completely abolish, their recruitment to kinetochores.
To further confirm the dependency of the CENP-H/I/K/M on CENP-C for its kinetochore localization, CENP-I levels at kinetochores were observed in CENP-C RNAi treated cells. Parental Flp-In T-REx HeLa cells were depleted for CENP-C by RNAi and stained against CREST, CENP-C and CENP-I. CENP-I levels were quantified as described for the mCherry-CCAN expressing cell lines, normalized against CREST and compared to mock treated cells. CENP-I was reduced to 3% of total levels compared to mock treated cells (see **Figure** 2.45 **B**, red bars and **Figure** 2.47 **A**).

CENP-T/W was demonstrated previously to depend on CENP-H/I/K/M for its centromere localization [264]. Therefore, we also stained for CENP-T/W in CENP-C RNAi treated cells and quantified normalized kinetochore levels as for the CENP-I antibody. CENP-T/W levels were reduced to 12 % compared to mock treated cells (see **Figure** 2.45 **B**, blue bars and **Figure** 2.47 **B**). Since we already observed a dependency of CENP-H/I/K/M on CENP-C, we propose an indirect dependency of CENP-T/W on CENP-C mediated by CENP-H/I/K/M as further discussed in **Section** 3.1.8.

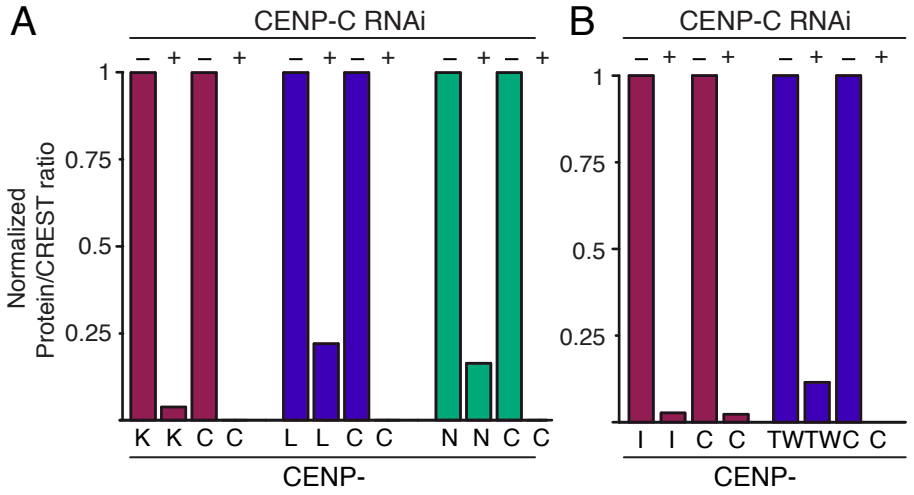

FIGURE 2.45: **Quantification of CENP-N, CENP-L, CENP-K CENP-I and CENP-T/W dependency on CENP-C for their kinetochore localization**. Cells expression mCherry-CENP-K, -CENP-N and CENP-L or parental Flp-In T-REx HeLa were treated with CENP-C RNAi to obtain dependencies of these proteins on CENP-C for their centromere targeting in individual experiments. 10 cells were quantified for CENP-C RNAi (+) and mock (-) treated cells. Levels of CENP-C, all mCherry-CCAN proteins, CENP-I and CENP-T/W were quantified at individual kinetochores with use of the software Imaris7.6 and normalized against CREST at the same kinetochore. The average numbers of kinetochore levels of a single experiment are represented here, values of mock treated cells were set to 1. mCherry-CENP-K expressing cells are depicted in red, CENP-L in blue and CENP-N in green (**A**). Cells stained for CENP-I depicted in red, CENP-T/W in blue (**B**).

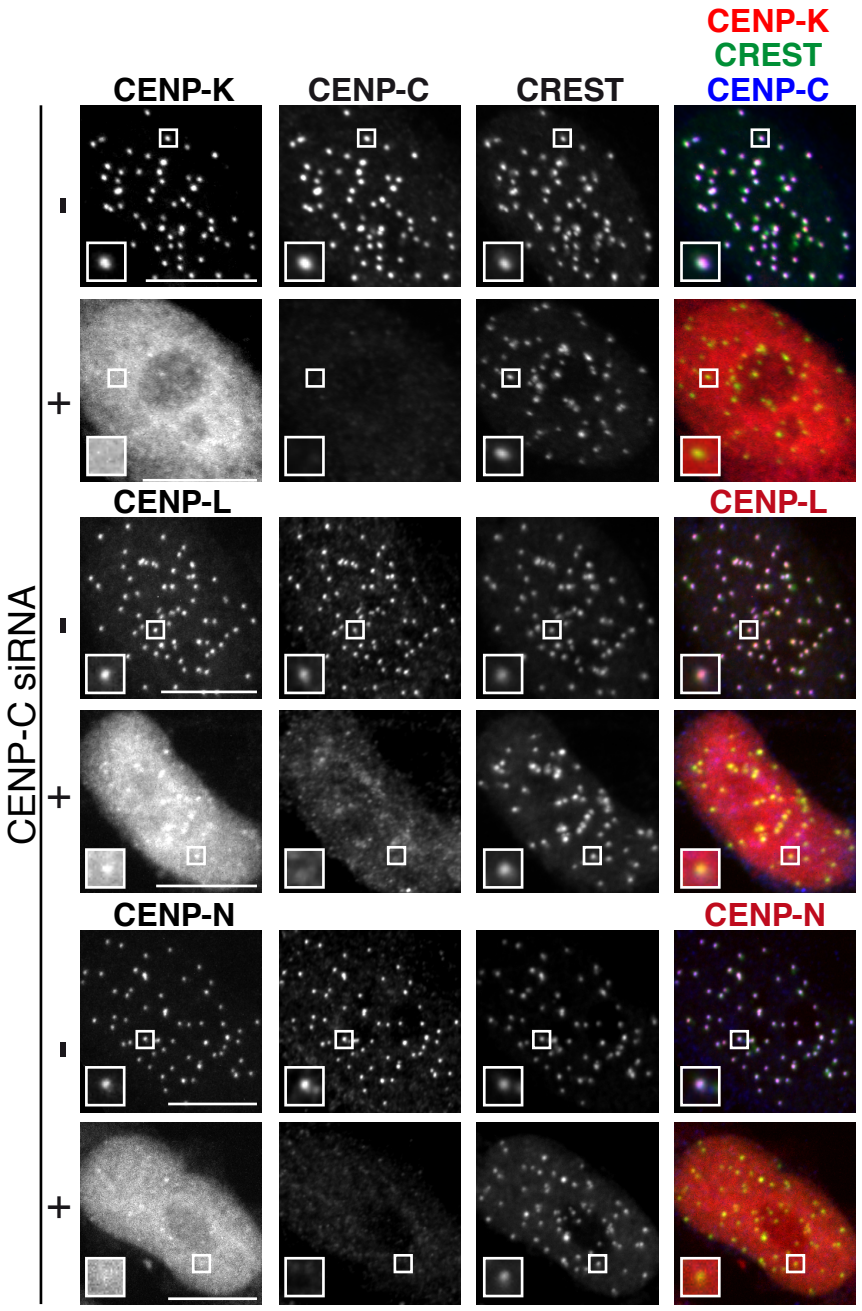

FIGURE 2.46: **CENP-N, CENP-L and CENP-K dependency on CENP-C**. Cells expression mCherry-CENP-K, -CENP-N and CENP-L were treated with CENP-C RNAi or mock treated to obtain potential dependencies of these proteins on CENP-C for their centromere targeting. Cells were fixed and stained for CENP-C and CREST. Kinetochore levels of mCherry-CCAN proteins was quantified at single kinetochores and normalized against CREST at the same kinetochore. In cells depleted for CENP-C a clear reduction of all of these proteins was observed. Representative images are shown here, scale bar indicates 10 μm.

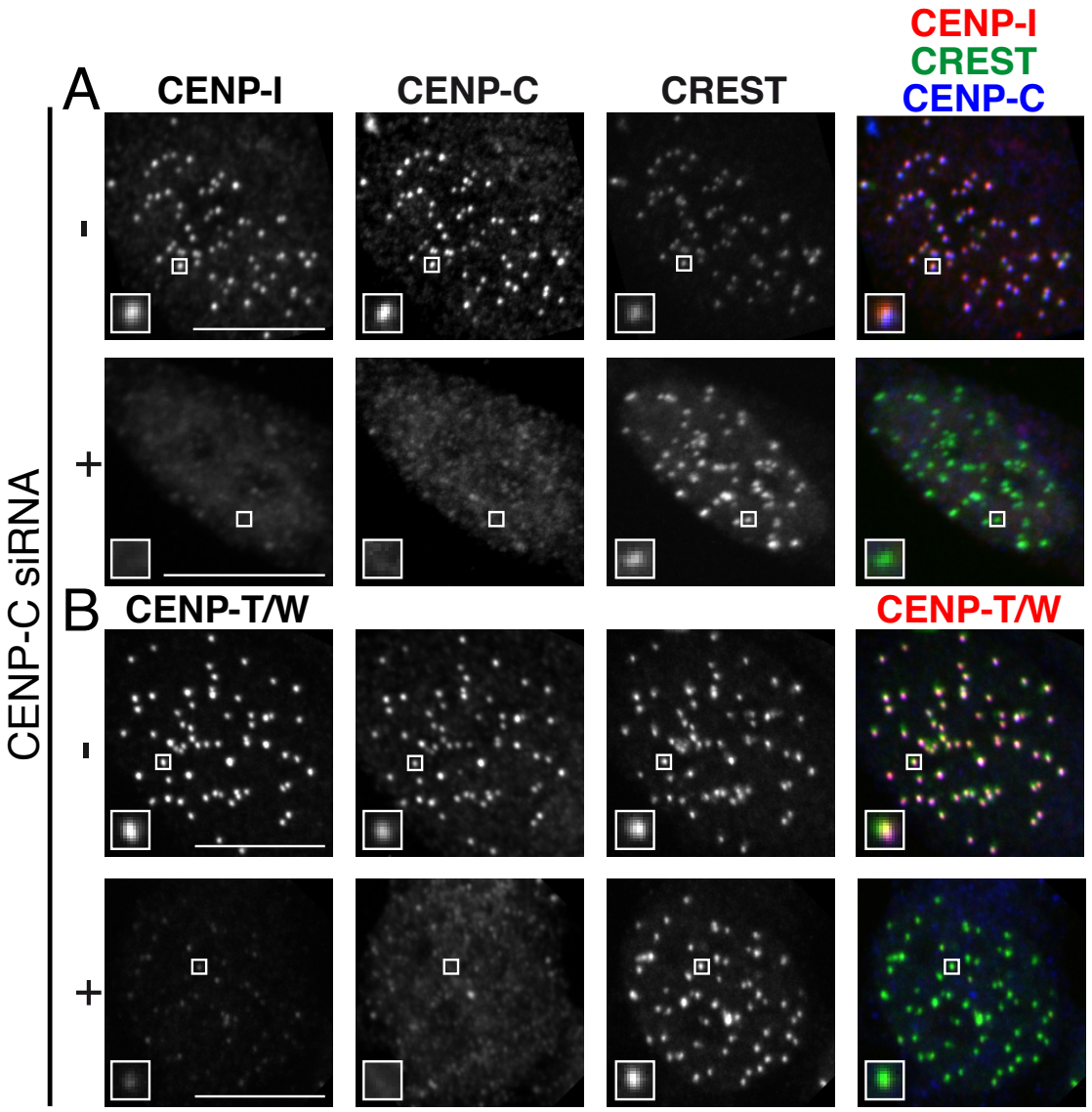

FIGURE 2.47: **CENP-I and CENP-T/W dependency on CENP-C**. Cells were treated with CENP-C RNAi or mock treated to obtain potential dependencies of CENP-I and CENP-T/W on CENP-C for their centromere targeting. Cells were fixed and stained for CENP-I or CENP-T/W, CENP-C and CREST. Kinetochore levels of CENP-I and CENP-T/W were quantified at single kinetochores and normalized against CREST at the same kinetochore. In cells depleted for CENP-C a clear reduction of CENP-C, CENP-I and CENP-T/W was observed. Representative images are shown here, scale bar indicates 10 μm.

2.26.3 Production of CCAN antibodies and generation of GFP-CENP-C cell lines

Next, we wanted to understand the role of CENP-C residues responsible for CENP-H/I/K/M interaction identified *in vitro* (see **Figure** 2.40) in the context of human cells. Trials to transiently transfect GFP-CENP-C wild type and 4A mutant constructs in CENP-C RNAi depleted cells failed, since the cells did not survive this treatment. Therefore, we decided to generate stable cell lines inducible for GFP-CENP-C expression as explained in **Section** 2.26.1 for the mCherry-CCAN expressing cell lines.

To further evaluate CENP-C's *in vivo* role in CCAN assembly, cell lines expressing GFP-CENP-C$^{1-544}$ or GFP-CENP-C full length wild type and W317A, 3A as well as 4A mutant were produced. Expression of fusion proteins was tested by immunofluorescence of fixed material. Kinetochore localization of the GFP-CENP-C proteins was judged by the colocalization with the centromere marker CREST. All GFP-CENP-C full length proteins (wild type and mutants) and GFP-CENP-C$^{1-544}$ wild type efficiently localize to kinetochores. In contrast, GFP-CENP-C$^{1-544}$ mutants are impaired in their kinetochore localization, as seen by a weaker signal at centromeres and a diffuse signal in the whole nucleus. We assume that the 4A mutant mildly impairs kinetochore localization and therefore GFP-CENP-C$^{1-544}$ 4A is not able to displace the endogenous CENP-C from kinetochores as good as the wild type form in the context of GFP-CENP-C$^{1-544}$ that does only provide one CENP-A binding motif. The CENP-C full length 4A mutant contains two CENP-A interaction sites and is therefore able to efficiently target kinetochores, even in the presence of endogenous CENP-C. For representative images of GFP-CENP-C full length and GFP-CENP-C$^{1-544}$ wild type and 4A mutant see **Figure** 2.48.

We tested the ability of GFP-CENP-C$^{1-544}$ or GFP-CENP-C full length wild type and mutant constructs to rescue CCAN protein localization in a CENP-C RNAi depleted background. As explained before, only a CENP-T/W and CENP-I antibody was available in the lab. Therefore, antibodies against CENP-H/K, CENP-N/L and CENP-N$^{1-212}$ were produced in rabbits. In addition, an antibody against CENP-C$^{732-849}$ was raised to detect endogenous CENP-C depletion in GFP-CENP-C$^{1-544}$ expressing cell lines.

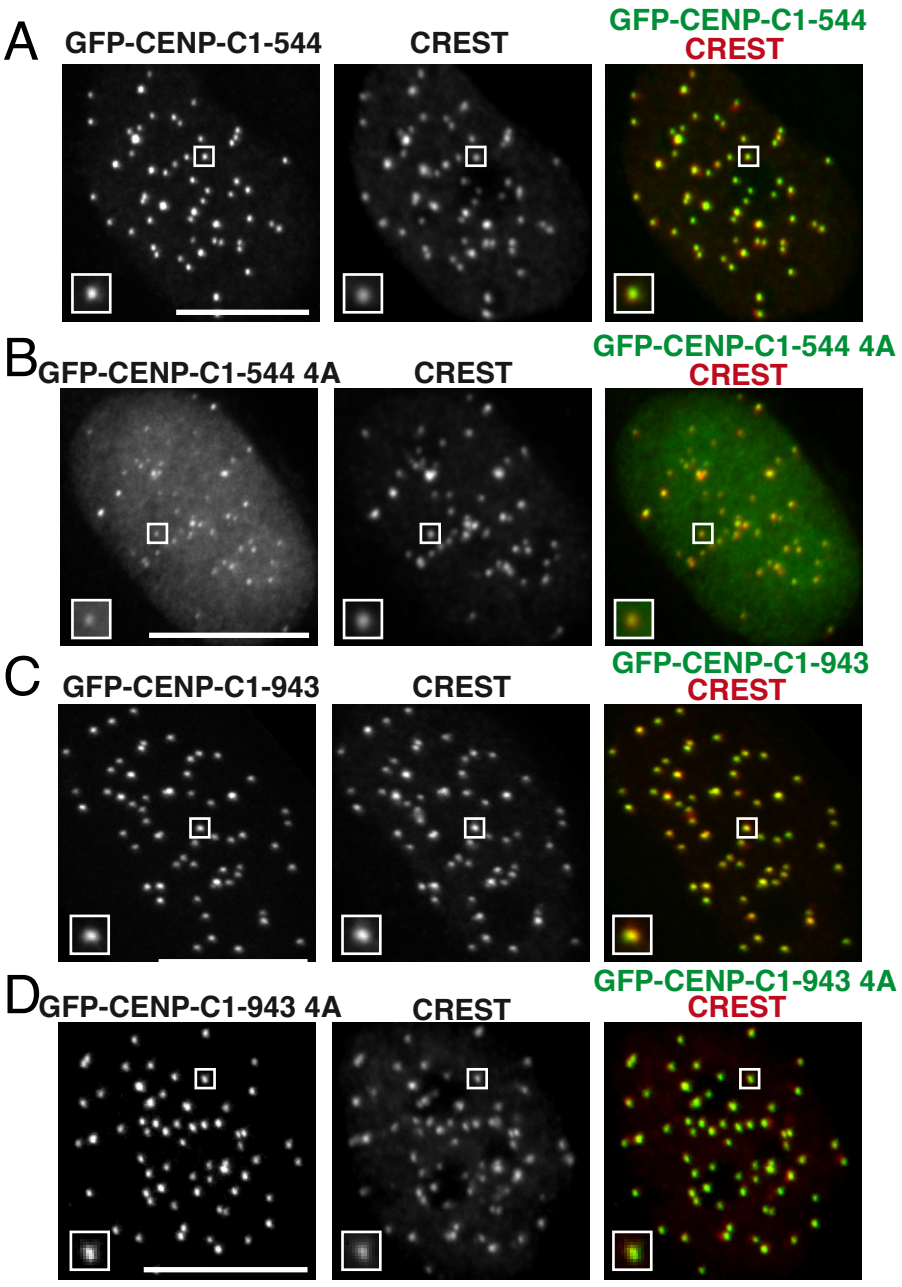

FIGURE 2.48: **Generation of GFP-CENP-C cell lines**. CENP-C protein expression and localization to kinetochores was observed on fixed material by staining with the kinetochore marker CREST. The GFP fused CENP-C full length wild type and mutant proteins efficiently localize to kinetochores throughout the cell cycle as indicated by colocalization with the centromere marker CREST (**C** and **D**). In contrast, GFP-CENP-C^{1-544} was impaired in its localization to kinetochores, when the 4A mutant was introduced, whereas the wild type efficiently localized (**A** and **B**). This might display a slightly impaired kinetochore localization through the mutated CENP-H/I/K/M interface in the presence of only one CENP-A binding motif of CENP-C.

The induction of an immune response, the applicability of the produced antibodies in western blotting and immunofluorescence and whether the antibodies were conjugated with fluorochromes is summarized in **Table** 2.8. Respresentative images of immunofluorescence with the working antibodies are shown in **Figure** 2.50.

TABLE 2.8: Summary of antibody production against CCAN proteins

CCAN protein	**Immune response**	**Application**	**Conjugation**
CENP-H/K	Yes	IF, western blotting	Alexa488/568
CENP-$C^{732-849}$	Yes	IF, western blotting	Alexa568
CENP-N^{1-212}	Yes	Western blotting	No
CENP-N/L	No	None	No

In summary, injections of CENP-N/L did not lead to any specific immune response in the rabbits, checked both in immunoflourescence and western blotting against the recombinant proteins. CENP-N^{1-212} antibody was successfully produced, as shown in western blotting against the recombinant protein, but did not stain kinetochores in human cells in different conditions by immunoflourescence. CENP-$C^{732-849}$ also induced an immune response and let to an antibody that is working in western blotting and immunofluorescence. However, the quality of the antibody in immunofluorescence is poor and affinity purification against GST-CENP-$C^{732-849}$ did not majorly improve the sample. Therefore, it can only be used for western blotting and immunoflourescence of initial experiments, but not for statistical quantifications of CENP-C levels at single kinetochores (see **Figure** 2.49). Here, the CENP-C C-terminal antibody was used in an initial experiment to asses whether CENP-C protein was depleted within a single cell that simultaneously expressed GFP-CENP-C^{1-544}.

The CENP-H/K antibody showed a clean specific signal both by western blotting and immunoflourescence (see **Figure** 2.50). In order to use it simultaneously with the CENP-C C-terminal antibody introduced above, CENP-H/K antibody was directly conjugated with Alexa568 and Alexa488 (see **Figure** 2.50). The signal of these antibodies was weak, therefore quantifications on experiments using these antibodies were not sufficiently robust. For this reason, we used the directly conjugated anibody only for initial experiments, whereas the unconjugated was applied in the final analysis.

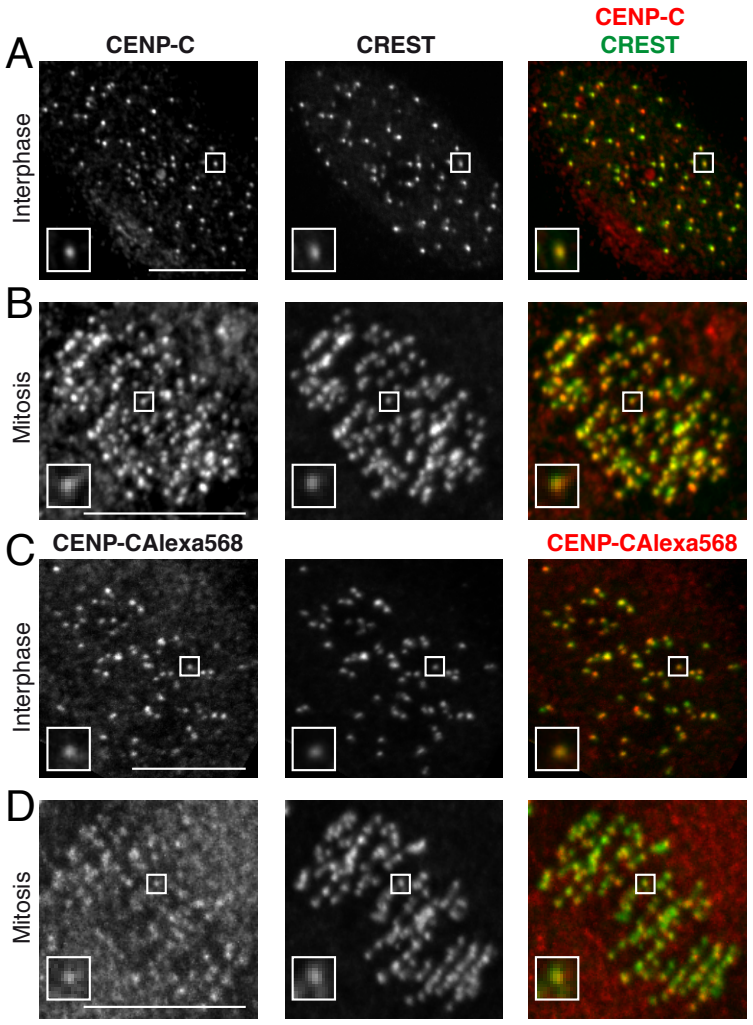

FIGURE 2.49: **CENP-C$^{732-849}$ rabbit polyclonal antibody production**. CENP-C$^{732-849}$ protein was used to raise polyclonal antibodies in rabbits. Initial bleeds were affinity purified and antibody quality was checked in immunofluorescence. A representative cell in interphase (**A**) and mitosis (**B**) is shown. The antibody specifically stains centromeres as shown by its colocalization with CREST. A directly conjugated CENP-C with Alexa568 showed a similar quality. Respresentative cells in interphase (**C**) and mitosis (**D**) are depicted here. The antibody was used only for initial experiments, but not for publication quality data.

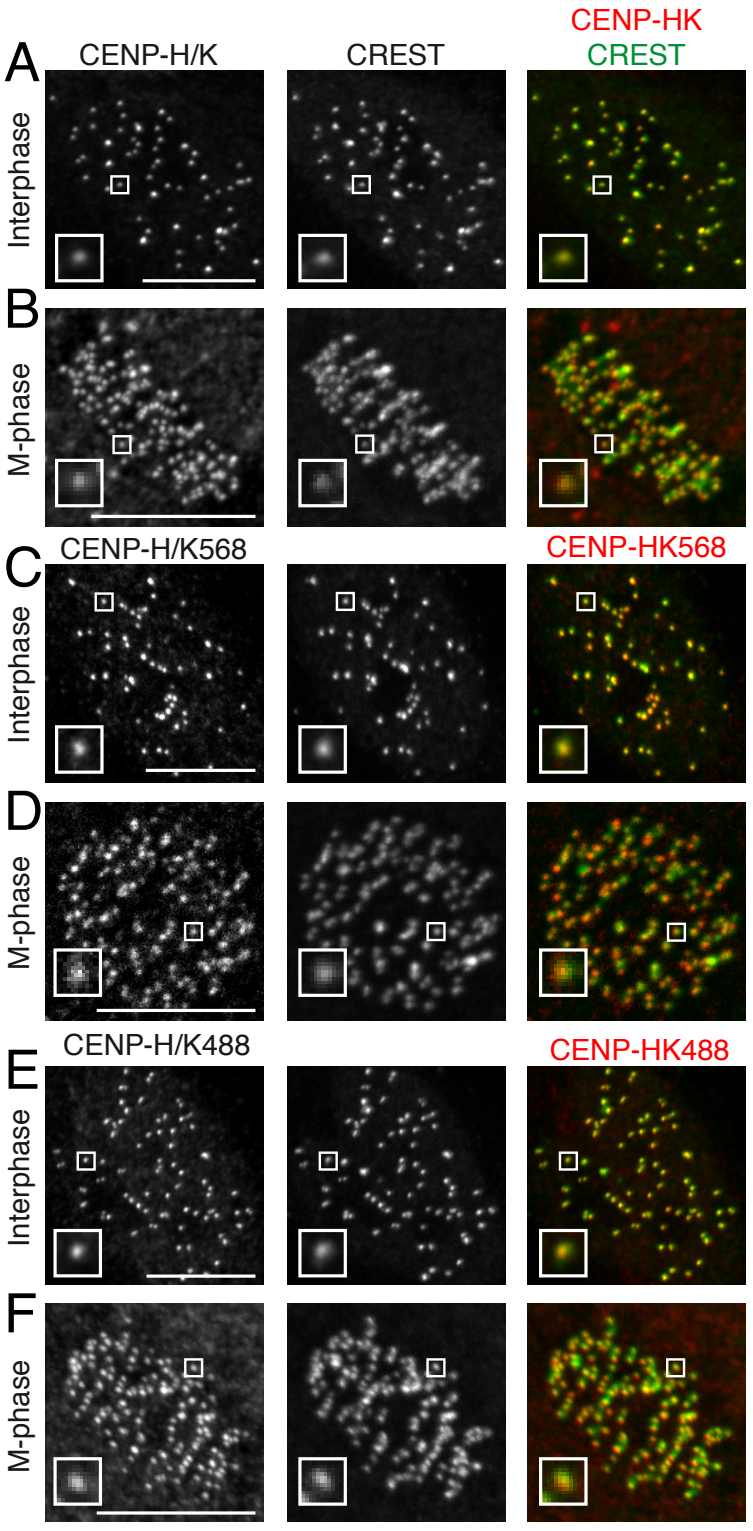

FIGURE 2.50: **CENP-H/K rabbit polyclonal antibody production**. CENP-H/K protein was used to raise polyclonal antibodies in rabbits. Initial bleeds were affinity purified and antibody quality was checked in immunofluorescence. A representative cell in interphase (**A**) and mitosis (**B**) is shown. The antibody specifically stains centromeres as shown by its colocalization with CREST. A directly conjugated CENP-C with Alexa568 and Alexa488 showed a similar quality. Respresentative cells in interphase (**C,E**) and mitosis (**D,F**) are depicted here.

2.26.4 GFP-CENP-C$^{1-544}$ rescue of CENP-H/K localization to kinetochores

The GFP-CENP-C expressing cell lines and the antibody against CENP-H/K were used to test whether the CENP-C N-terminal half, identified *in vitro* to bind CENP-H/I/K/M (see **Figure** 2.40), is sufficient to rescue CENP-H/K recruitment to kinetochores in cells RNAi depleted for endogenous CENP-C. CENP-C$^{732-849}$ antibody was used to detect endogenous CENP-C levels within cells expressing GFP-CENP-C$^{1-544}$. Only cells clearly depleted for endogenous CENP-C were taken into account.

In agreement with the *in vitro* data, GFP-CENP-C$^{1-544}$ rescues CENP-H/K localization to kinetochores as shown by colocalization with the kinetochore marker CREST (see **Figure** 2.51 and 2.52) to levels higher than in mock treated cells. This might be explained by a higher expression level of CENP-C$^{1-544}$ compared to endogenous CENP-C, as observed in western blotting of total cell lysate against CENP-C (data not shown).

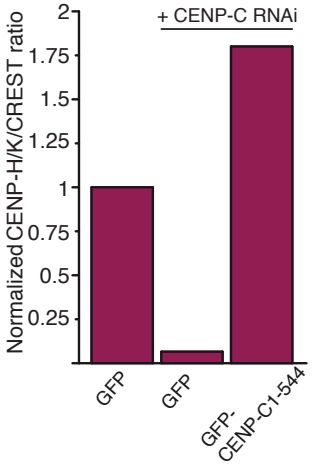

FIGURE 2.51: **Quantification of CENP-H/K kinetochore localization rescue by GFP-CENP-C$^{1-544}$.** In cells expressing GFP or GFP-CENP-C$^{1-544}$, endogenous CENP-C was depleted by RNAi. Cells were fixed and stained for CREST, CENP-H/K and CENP-C$^{732-849}$. Only cells clearly depleted for endogenous CENP-C were taken into account. Here, 10 cells of a single experiment were quantified for their kinetochore levels of CENP-H/K and normalized against CREST at the same kinetochore. CENP-H/K levels in mock treated cells were set to 1.

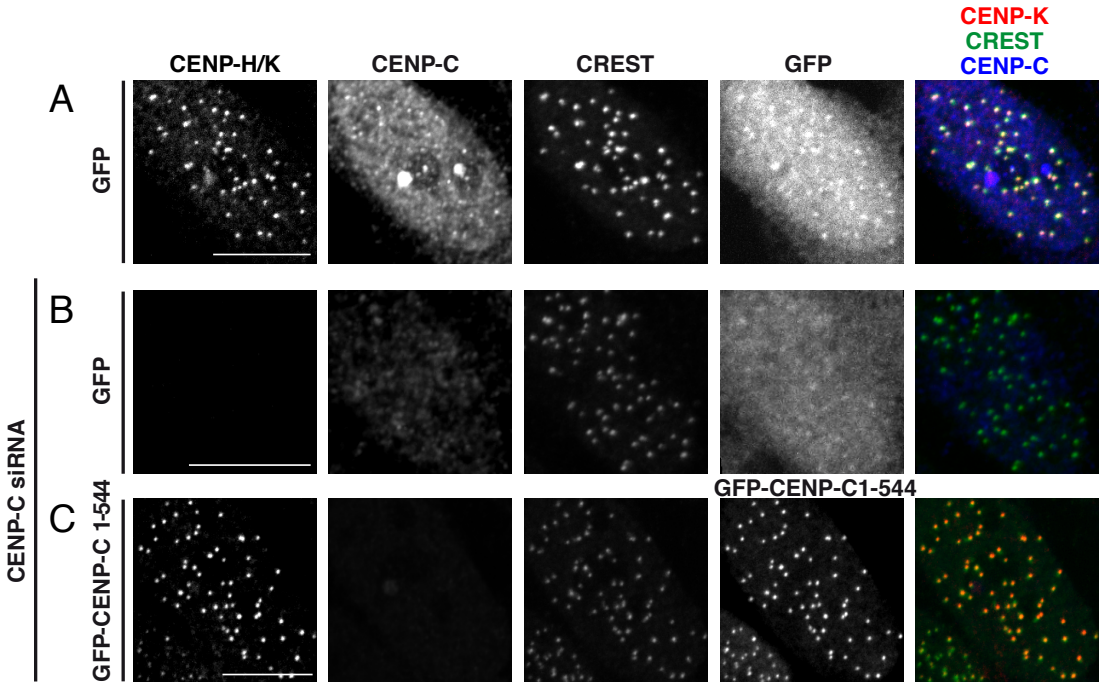

FIGURE 2.52: **Rescue of CENP-H/K kinetochore localization by GFP-CENP-C$^{1-544}$.** In cells expressing GFP or GFP-CENP-C$^{1-544}$, endogenous CENP-C was depleted by RNAi. Cells were fixed and stained for CREST, CENP-H/K and CENP-C with the C-terminal antibody that does only recognize the endogenous CENP-C, but not GFP-CENP-C$^{1-544}$. Only cells clearly depleted for endogenous CENP-C were taken into account. Here, representative images of single cells are shown, scale bars indicate 10 μm. Unspecific dots in the GFP channel of the control cells is a consequence of false image aquisition at the microscope and subsequent crosstalk with CREST.

2.26.5 CENP-H/I/K/M dependency on CENP-C for its kinetochore localization

To confirm the relevance of the CENP-C residues identified *in vitro* to interact with CENP-H/I/K/M (see **Figure** 2.40), we expressed GFP-CENP-C full length wild type or W317A, 3A and 4A mutants in cells RNAi depleted for CENP-C. CENP-H/K levels at kinetochores (co-localizing with CREST) were quantified. CENP-H/K is dependent on CENP-C for its kinetochore localization, since CENP-C RNAi reduces CENP-H/K levels at kinetochores to only 17 % versus to control cells. In this condition, induction of full length GFP-CENP-C wild type expression rescued 90 % of CENP-H/K localization to kinetochores. The 3A mutation or the W317A mutation on full-length GFP-CENP-C showed 43 % and 67 % of CENP-H/K rescue to kinetochores, respectively.

In line with our expectations, CENP-H/K levels were reduced to 17 % in a full-length GFP-CENP-C carrying the 4A mutation (**Figure** 2.53 and 2.54). This clearly shows that the two patches on CENP-C responsible for CENP-H/I/K/M interaction *in vitro* are also required for CENP-H/I/K/M recruitment to kinetochores *in vivo*.

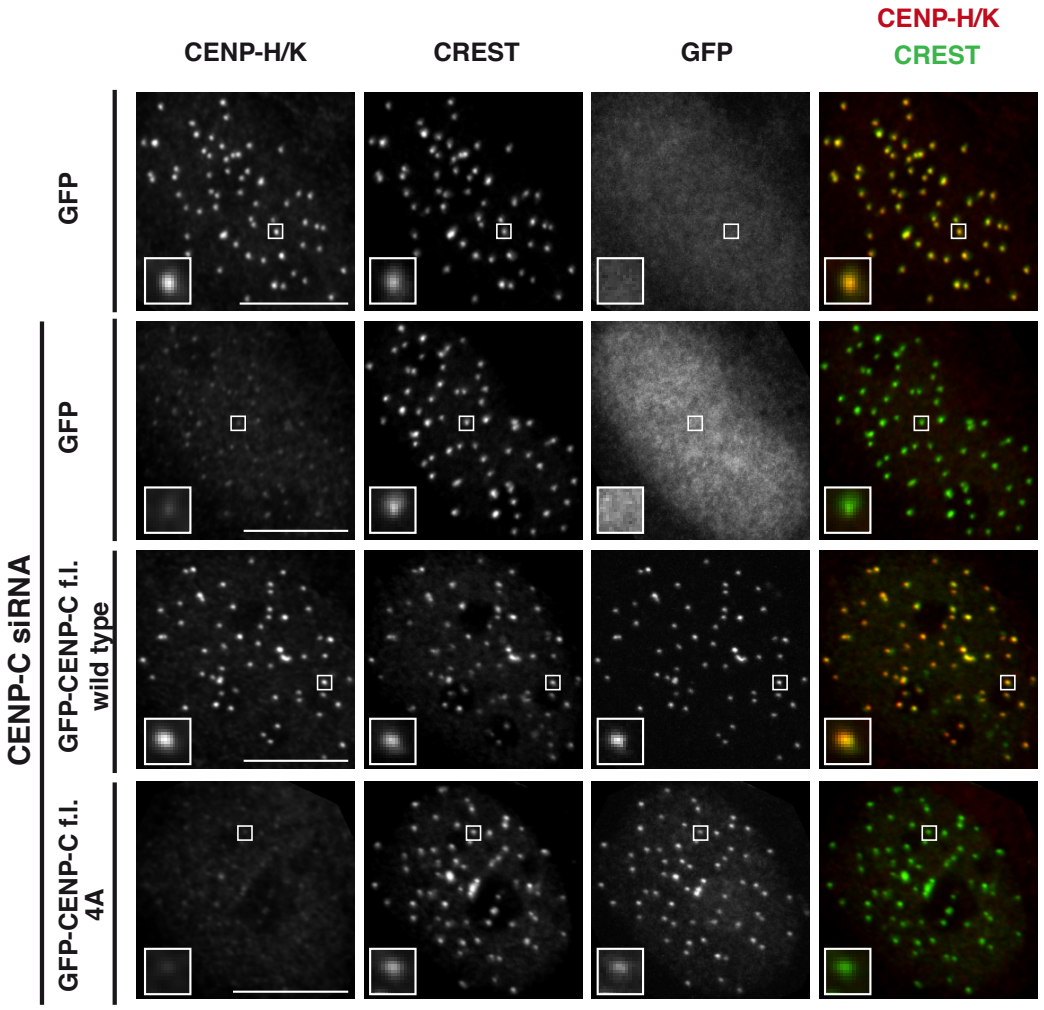

FIGURE 2.53: **CENP-H/K kinetochore localization rescue by GFP-CENP-C full length wild type and 4A**. Cells expressing GFP-CENP-C full length wild type or 4A mutant were depleted for endogenous CENP-C by RNAi and levels of CENP-H/K quantified at kinetochores (normalized against CREST). Representative images of the dataset are depicted here. Scale bar = 10 μM.

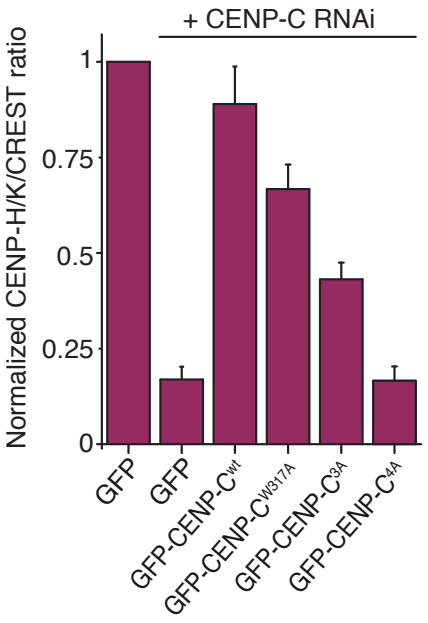

FIGURE 2.54: **Quantification of CENP-H/K kinetochore localization rescue by GFP-CENP-C full length wild type and mutants**. Quantification of immunofluorescence experiment in fixed Flp-In T-REx HeLa cells depleted of endogenous CENP-C (where indicated) and expressing the indicated GFP constructs. The kinetochore levels of CENP-H/K were measured and normalized to CREST. Graphs and bars indicate mean ± SEM of three independent experiments.

2.26.6 CENP-T/W dependency on CENP-H/I/K/M for its kinetochore localization

CENP-T/W has been shown to depend on CENP-H/I/K/M for its kinetochore localization through a direct interaction between these complexes [264]. Therefore, the ability of GFP-CENP-C full length wild type and mutants to rescue CENP-T/W recruitment to kinetochores in CENP-C RNAi depleted cells was explored. CENP-T/W is dependent on CENP-C for its kinetochore localization (see **Figure** 2.47), but no direct interaction to GST-CENP-C^{2-545} was found in a GST pulldown assay. In the same assay, CENP-T/W was pulled down by GST-CENP-C^{2-545} when CENP-H/I/K/M was included in the reaction. As CENP-I and CENP-T comigrate, the result was confirmed in SDS-PAGE followeg by western blotting of 10 % of the pulldown fractions against CENP-I or CENP-T/W (**Figure** 2.55).

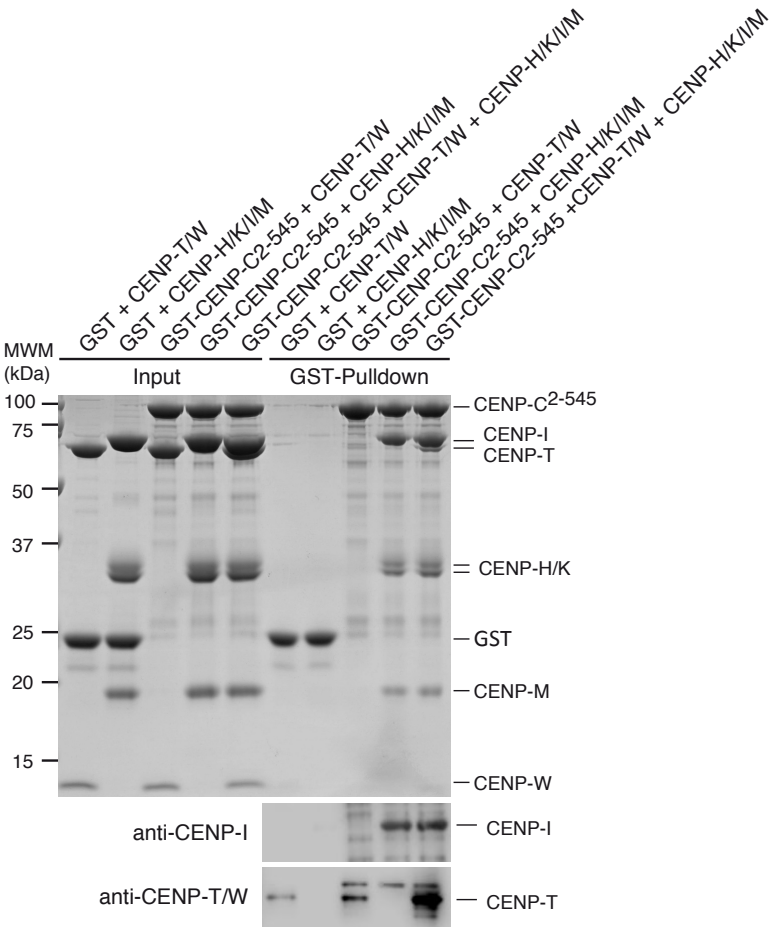

FIGURE 2.55: **GST-CENP-C$^{2-545}$ CENP-H/I/K/M CENP-T/W pull-down.** GST-CENP-C$^{2-545}$ does not bind directly to CENP-T/W in a GST pulldown assay. Only when CENP-H/I/K/M is included in the assay, CENP-T/W is incorporated into the complex. Since CENP-I and CENP-T co-migrate on the comassie stained SDS-PAGE gel, 10 % of the pulldown samples were separated on a new SDS-PAGE and subjected to western blotting with either a CENP-T or CENP-I antibody.

To confirm the dependeny of CENP-T/W on CENP-H/I/K/M for its kinetochore recruitment, we asked whether GFP-CENP-C wild type and mutants rescue CENP-C RNAi induced loss of CENP-T/W from kinetochores. CENP-T/W levels were reduced in CENP-C RNAi treated cell lines to 30 % of the control cells. After expression of GFP-CENP-C full-length wild type in CENP-C RNAi depleted cells, CENP-T/W kinetochore levels were rescued to levels comparable to mock treated cells. In cells expressing the full-length GFP-CENP-C 3A or W317A, CENP-T/W levels were rescued by 78 % and 66 % compared to mock treated cells, respectively.

GFP-CENP-C full-length 4A mutant recruited comparable CENP-T/W levels to CENP-C RNAi treated cells (see **Figure** 2.56 and 2.57). This strongly indicates that CENP-T/W is dependent on CENP-H/I/K/M and indirectly on CENP-C for its centromere localization and therefore CENP-C is the platform for all these proteins to be recruited to kinetochores.

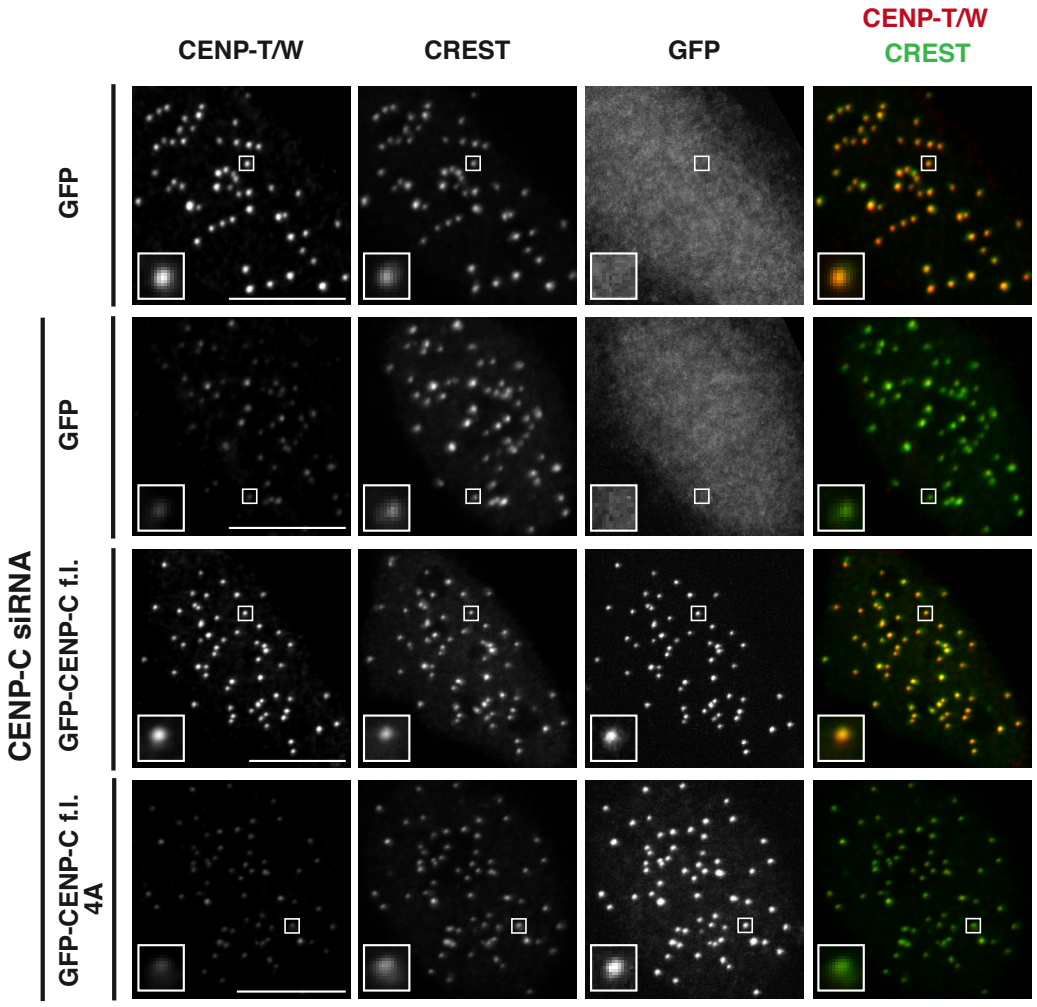

FIGURE 2.56: **CENP-T/W kinetochore localization rescue by GFP-CENP-C full length wild type and 4A**. Cells expressing GFP-CENP-C full length wild type or 4A mutant were depleted for endogenous CENP-C by RNAi and levels of CENP-T/W quantified at kinetochores (normalized against CREST). Representative images of the dataset are depicted here. Scale bar = 10 μM.

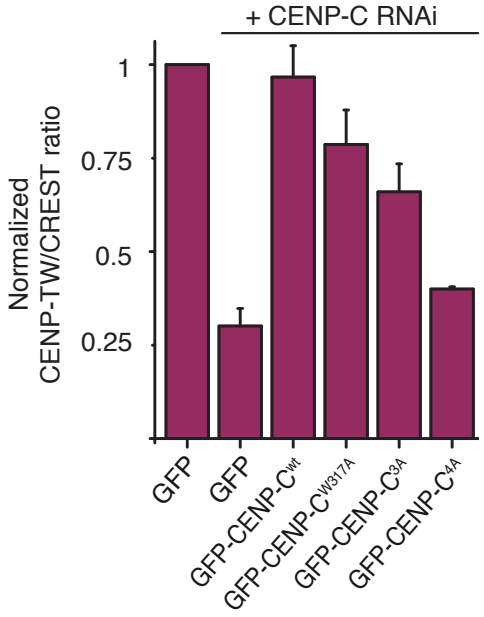

FIGURE 2.57: **Quantification of CENP-T/W kinetochore localization rescue by GFP-CENP-C full length wild type and mutants**. Quantification of immunofluorescence experiment in fixed Flp-In T-REx HeLa cells depleted of endogenous CENP-C (where indicated) and expressing the indicated GFP constructs. The kinetochore levels of CENP-T/W were quantified and normalized to CREST. Graphs and bars indicate mean ± SEM of three independent experiments. CENP-T/W levels in mock treated cells were set to 1.

2.26.7 GFP-CENP-C immunoprecipitation

The inability of CENP-C 4A mutant to rescue CENP-H/I/K/M and CENP-T/W localization to kinetochores was confirmed in an immunoprecipitation experiment against GFP-CENP-C^{1-544} wild type or 4A mutant. We used the GFP-CENP-C^{1-544}, since the full length did not give a clear result, presumably because it is capable of binding to endogenous CENP-C through the C-terminal dimerization domain. Wildtype GFP-CENP-C^{1-544} efficiently pulls down CENP-H/K, CENP-I, CENP-M and CENP-T, whereas in the 4A mutant does not (see **Figure** 2.58). This strongly indicates a binding of CENP-H/I/K/M to the two conserved patches of CENP-C identified previously. We assume that the inability of CENP-T/W to bind to the 4A mutant is mediated indirectly through the loss of CENP-H/I/K/M. Interestingly, the 4A mutant did also not pull down CENP-L from cell lysate. This suggests a dependency of CENP-N/L not only on CENP-C, but also other CCAN components that are lost in the 4A mutant, presumably CENP-H/I/K/M. This will be further addressed in **Section** 3.1.8.

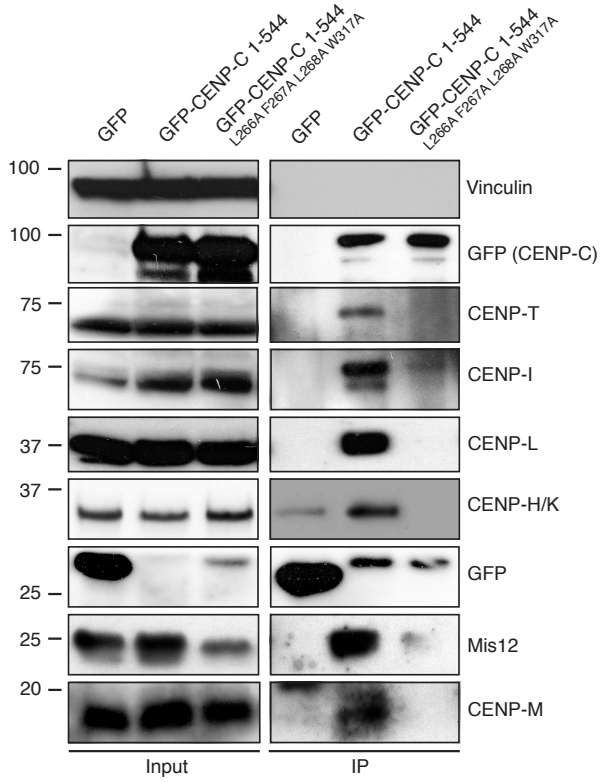

FIGURE 2.58: **Kinetochore assembly dependency on the CENP-C:CENP-H/I/K/M interaction**. Cells expressing GFP-CENP-C$^{1-544}$ wild type or 4A mutant were harvested and immunoprecipitated against the GFP-tag. Proteins bound to GFP-CENP-C$^{1-544}$ were detected by SDS-PAGE analysis followed by western blotting against the indicated proteins. Wild type CENP-C$^{1-544}$ is able to pull down other CCAN and outer kinetochore components, whereas the 4A mutant is impaired in assembly of the whole kinetochore structure.

Our results demonstrate a remarkably clear consistency between the *in vitro* and *in vivo* data, confirming that CENP-H/I/K/M binds directly to CENP-C, and that four highly conserved residues on CENP-C are mainly responsible for this interaction. Disrupting the interaction of CENP-H/K/I/M to CENP-C is followed by a loss of CENP-T/W and CENP-N/L complex. Therefore, we hypothesize that CENP-N/L is directly binding to CENP-C, but also to CENP-H/I/K/M and therefore relying on both for its kinetochore recruitment. In contrast, CENP-T/W is no direct CENP-C interactor, therefore the effect seen here is probably due to its dependency on CENP-H/I/K/M for its kinetochore localization.

Suprisingly, pulling down of the Mis12 complex was inconsistent. It always pulled down with the wild type GFP-CENP-C, but only in two of four cases in the 4A mutant. This indicates that the assumption that CENP-C is the only interaction hub for Mis12c kinetochore localization, might not be the complete truth. Instead, other CCAN components might be involved in the Mis12 complex recruitment to centromeres. As an initial experiment to clarify this further we tested the binding of Mis12c to CENP-C^{2-545} and to CENP-$C^{189-400}$ in the absence and presence of CENP-H/I/K/M and CENP-N/L in a GST-pulldown assay. However, we did not observe any increase in binding of Mis12 complex to CENP-C^{2-545} in the presence of CENP-H/I/K/M and no binding to CENP-$C^{189-400}$ in the presence of other CCAN components (see **Figure** 2.59 and 2.60). This speaks against but does not rule out contribution to the Mis12complex:CENP-C interaction through other proteins. To come to a conclusion, additional experiments are required.

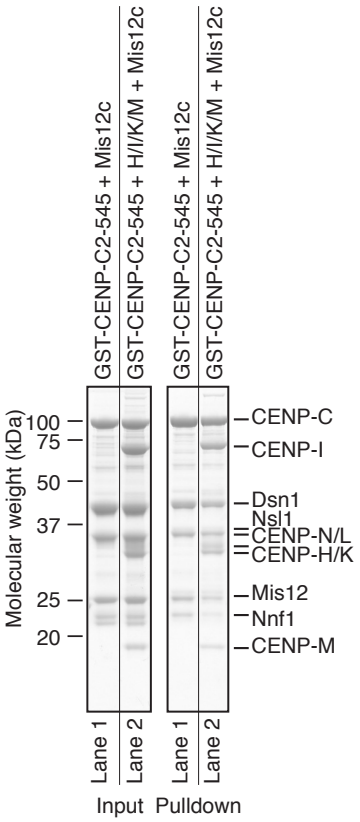

FIGURE 2.59: **GST-CENP-C^{2-545} CENP-H/I/K/M Mis12 complex pulldown**. GST-CENP-C^{2-545} has been used as bait (1 μM) and Mis12 complex with and without CENP-H/I/K/M as prey (3 μM) to investigate the involvement of CENP-H/I/K/M in the interaction of Mis12 complex to CENP-C. Mis12 complex binds to CENP-C^{2-545} equally good in the absence and presence of CENP-H/I/K/M, speaking against a contribution from CENP-H/I/K/M to Mis12c binding to CENP-C.

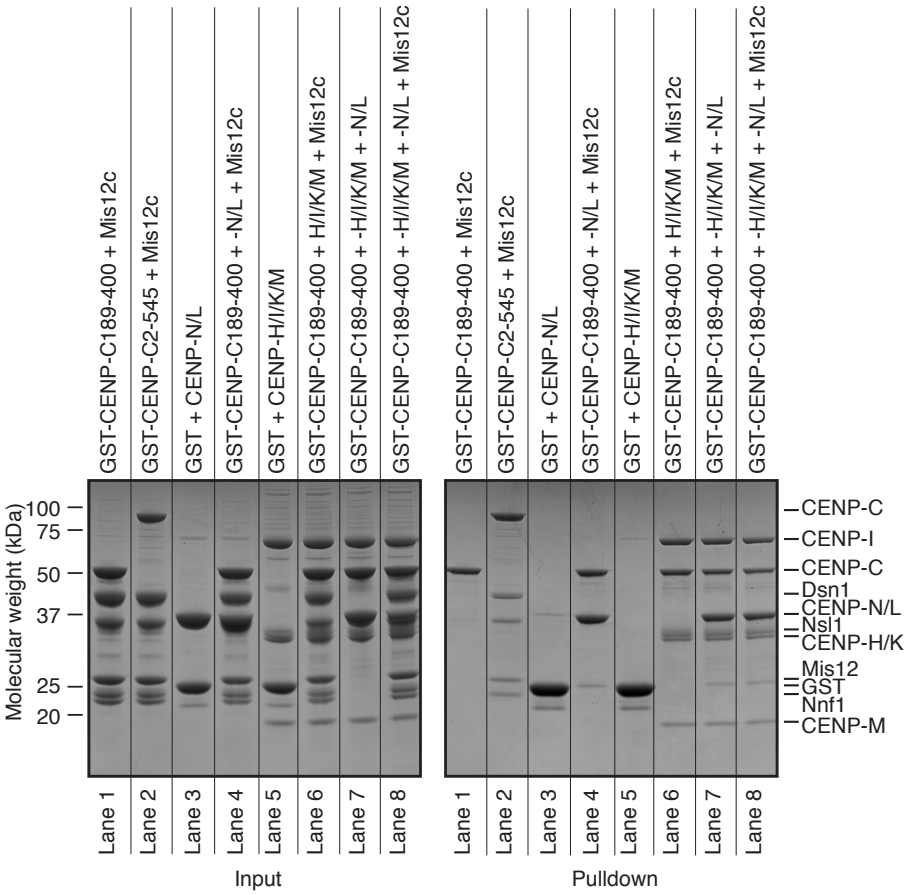

FIGURE 2.60: **GST-CENP-C$^{189-400}$ CCAN Mis12c pulldown**. GST-CENP-C$^{189-400}$ has been used as bait (1 μM) and Mis12 complex with and without CENP-H/I/K/M and/or CENP-N/L as prey (3 μM) to investigate whether Mis12 complex binding to CENP-C can be mediated by the CCAN. CENP-C$^{189-400}$ is not able to bind Mis12 complex in the presence of several CCAN components, speaking against a strong contribution from the CCAN components investigated here.

In summary, we have shown that CENP-C recruits the CENP-H/I/K/M complex via four highly conserved residues. Mutation of these residues of CENP-C leads to a complete loss of CENP-H/I/K/M kinetochore localization. The same mutations on CENP-C also cause a nearly complete loss of CENP-T/W from kinetochores, consistent with the finding that CENP-T/W is bound directly via the CENP-H/I/K/M complex [264]. We have demonstrated that CENP-C is also required for CENP-N and CENP-L kinetochore localization *in vivo* through a direct interaction identified *in vitro*. In addition, Mis12 complex might be dependent on additional kinetochore components besides CENP-C, since it is lost in immunoprecipitations with GFP-CENP-C$^{1-544}$4A.

Chapter 3

Discussion

3.1 CENP-C's role in the CCAN assembly hierarchy

In this work we provide strong evidence that CENP-C plays a major role in kinetochore assembly. By using the powerful combination of biochemical assays and work in human cells, valuable information about the structural and functional organization of the CCAN has been revealed, with a few of the interactions being further investigated in great detail.

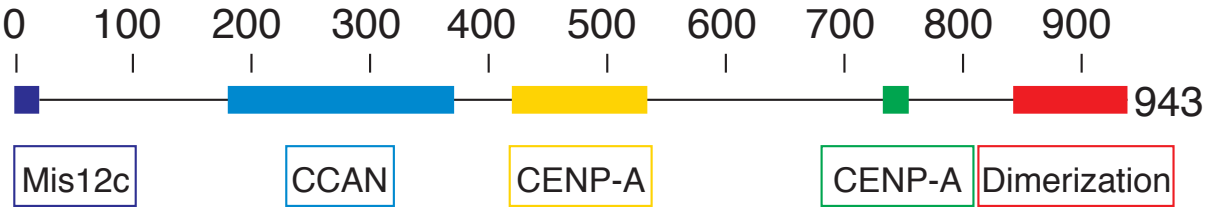

FIGURE 3.1: **CENP-C:kinetochore interaction interfaces**. The Mis12c binding domain is located in the very N-terminus of CENP-C (dark blue) and followed by the PEST rich region that has now been shown to be the interaction hub for other CCAN components (cyan). Two motifs located central (yellow) and C-terminal (green) within CENP-C are both responsible for interaction with CENP-A containing nucleosomes. The cupin domain that is located at the very C-terminus of CENP-C (red) is known to dimerize the protein.

Dissection of CENP-C demonstrated a linear organization of binding motifs within CENP-C, a largely disordered protein (see **Figure** 3.1). The N-terminal region of CENP-C interacts with the outer kinetochore, while the central domain binds to the centromere by interacting with CENP-A nucleosomes [89, 202, 260]. The C-terminus is responsible for CENP-C dimerization and has been shown to recruit proteins involved in new CENP-A deposition [109, 110, 277, 281]. Here, we have reported a new binding site for CCAN components, located between the outer kinetochore binding-site and the central CENP-A binding-site on CENP-C. We demonstrated that all CCAN components investigated in this thesis depend on this CENP-C motif for their centromere localization, either directly or indirectly (see **Section** 2.26.2 to 2.26.7). This linear organization of motifs justifies our interpretation that CENP-C may be a blueprint that determines the correct positioning of kinetochore subunits along the inner to outer kinetochore axis [300]. Interestingly, CENP-C$^{1-544}$ is sufficient to build the kinetochore structure, since it contains a CENP-A interaction site and it was shown in this study that CENP-C$^{1-544}$ localizes to kinetochores in cells and is able to interact with recombinant CENP-A nucleosomes (see **Figure** 2.48 and 2.32). Furthermore, CENP-C$^{1-544}$ possesses the interaction site for the outer kinetochore component Mis12 complex. Here, CENP-N/L and CENP-H/I/K/M have been demonstrated to interact with CENP-C$^{1-544}$ construct directly (see **Figure** 2.30 and 2.24), and in turn CENP-T/W/S/X is recruited by CENP-H/I/K/M [264]. Thus all known kinetochore components can be theoretically build on CENP-C$^{1-544}$. As such a reconstitution of the whole human kinetochore structure is currently being performed as a collaborative effort within the lab.

Here, the focus was on the role of CENP-C in CCAN assembly. In more detail, it was shown that CCAN sub-complexes including CENP-H/I/K/M, CENP-N/L and CENP-T/W are displaced from kinetochores in cells depleted of CENP-C (**Figure** 2.46 and 2.47). This raises the fundamental question, which of these proteins directly depend on CENP-C for their kinetochore localization, which localizations are indirect or in more general terms, what is the recruitment hierarchy within the CCAN protein complex?

3.1.1 CENP-C interaction with CENP-H/I/K/M

It has been shown previously that CENP-H and CENP-K depend on CENP-C for their kinetochore localization [90, 270], however the interactions responsible for these dependencies had not been identified. By showing a direct interaction of the N-terminal half of CENP-C with CENP-H/K (see **Figure** 2.14), I have demonstrated that CENP-C is directly responsible for CENP-H/K localization to centromeres. We further extended this study to the newly identified CENP-H/I/K/M complex. CENP-H/I/K/M binding to CENP-C constructs that were not able to interact with CENP-H/K under the same condition (**Figure** 2.24) as well as the binding of CENP-H/I/K/M at a lower concentration *in vitro* (**Figure** 2.25), led to the conclusion, that the affinity of CENP-C to CENP-H/I/K/M is higher in comparison to CENP-H/K alone. Unfortunately, it was not possible to measure directly the binding affinity between CENP-C and CENP-H/I/K/M due to technical problems. Nevertheless, the CENP-C:CENP-H/K interaction has a low μM Kd, which is remarkably weak, given the very low cellular concentrations of these proteins. Inner kinetochore interactions would be expected to be quite strong, since they likely have to resist forces of the mitotic spindle. The improved CENP-H/I/K/M binding compared to CENP-H/K is therefore a logical expectation. Knowing CENP-H/I/K/M bound more strongly to CENP-C raised the question whether this improved binding is a consequence of a direct interaction through CENP-I and/or CENP-M within the CENP-H/I/K/M complex with CENP-C or the induction of a conformational change of CENP-H/K within the CENP-H/I/K/M complex that leads to a stronger binding of these components to CENP-C. These possibilities are not mutually exclusive and we support a model that combines both possibilities.

Some of our findings support the idea of a structural change in CENP-H/K within the CENP-H/I/K/M complex. First, more residues cross-linked to CENP-C were found in CENP-H/K within the CENP-H/I/K/M complex (**Figure** 2.32) than in CENP-H/K alone (**Figure** 2.13). In further agreement with this idea, CENP-H/K complex runs as an elongated dimer on a SEC column (see **Figure** 2.9). This behaviour is not due to oligomerization, as SLS analysis revealed a dimeric structure of the complex (data not shown). In contrast, CENP-H/I/K/M eluted as expected for a globular molecule with its actual molecular weight (see **Figure** 2.25), and 3D negative-stain EM reconstitutions also shows a more globular structure

[264], which clearly speaks in favor of a compaction of CENP-H/K when incorporated into the complex. Further strengthening the hypothesis that CENP-H/K undergoes a conformational change when incorporated into the CENP-H/I/K/M complex, no binding of CENP-H/K to CENP-C^{2-545}W317A in a GST-pulldown assay was observed, whereas the 3A mutant within CENP-C^{2-545} did not have any effect on CENP-H/K binding (**Figure** 2.37). In contrast, the W317A mutant only mildly negatively influences CENP-H/I/K/M binding to CENP-C^{2-545}, whereas the 3A mutant had an apparently greater effect (**Figure** 2.39). Although showing only a minor effect in CENP-C^{2-545}, W317A is involved in the CENP-C:CENP-H/I/K/M interaction, as seen in a pulldown of CENP-$C^{290-400}$, where the binding was lost upon introduction of the W317A mutation (**Figure** 2.35). Therefore, we hypothesize a binding model of CENP-H/I/K/M to CENP-C that involves Trp317 as well as Leu265, Phe266 and Leu267. In contrast CENP-H/K only requires Trp317 of CENP-C, and this would explain the overall lower binding affinity of CENP-C to CENP-H/K compared to CENP-H/I/K/M. In favor of that, CENP-H/K does not bind to CENP-$C^{189-290}$ (**Figure** 2.16), whereas CENP-H/I/K/M does (**Figure** 2.24). In addition, the affinity of CENP-$C^{290-400}$ to CENP-H/K, as revealed by ITC, is similar to the binding affinity of CENP-$C^{189-400}$ (**Figure** 2.23 and 2.22). A change in the structural features of CENP-H/K may be introduced by CENP-I, since it was observed that the addition of CENP-I^{57-281} increases the amount of CENP-H/K bound to CENP-C in a GST-pulldown assay (**Figure** 2.27).

As a second possibility, CENP-I or CENP-M might directly contribute to the interaction of CENP-H/I/K/M with CENP-C. Speaking against a direct binding of CENP-C to CENP-I^{57-281} or CENP-M is the absence of any interaction of these components in GST-pulldown assays (**Figure** 2.28). However, the inability to detect binding in a GST-pulldown assay does not rule out a limited contribution from CENP-I^{57-281} or CENP-M within the CENP-H/I/K/M complex to the CENP-C interaction. In addition, only CENP-I^{57-281} could be produced recombinantly. Therefore, the missing parts of CENP-I might well be involved in the interaction, although from the knowledge that CENP-I^{57-281} is directly interacting with CENP-H/K [264], the assumption that CENP-I^{57-281} is in closer proximity to CENP-C and therefore more likely to interact, seems reasonable. Cross-linking coupled with mass spectrometry revealed cross-links between CENP-M and CENP-C within the CENP-C/H/I/K/M/N/L/CENP-$A^{nucleosome}$complex (**Figure** 2.32). Nevertheless,

one should consider that absence of crosslinks does not necessarily rule out an interaction of proteins. Furthermore, a crosslink between two proteins in this assay reports two lysins that are in close enough proximity for a crosslinker of defined length (7.7 Å) to bind to both lysine residues. Therefore, a crosslink does not prove direct interaction, but close proximity of two lysins within the complex, which is indeed often but not always a hint for a direct interaction. Nevertheless, the crosslinks of CENP-M with CENP-C might point towards a direct contribution from CENP-M to the CENP-C:CENP-H/I/K/M interaction. In addition, since CENP-M does not bind to CENP-C in a pulldown assay on its own, but shows some cross-linking to CENP-C, it is also possible that CENP-M undergoes a conformational change within the CENP-H/I/K/M complex, which than allows it to bind to CENP-C and support the CENP-C:CENP-H/I/K/M interaction. Indeed, cross-links of CENP-M with CENP-C flank the residues Leu265 Phe266 and Leu267. Interestingly, cross-links between CENP-M and CENP-I that are found in the isolated CENP-H/I/K/M complex [264] are lost in the CENP-C/H/I/K/M/N/K/CENP-$A^{nucleosome}$complex, suggesting a distict structural conformation of CENP-H/I/K/M and its separate components.

To gain an even deeper understanding of the human CENP-C:CENP-H/I/K/M interaction, structural information on the complex would be particularly useful. Efforts in this direction are already underway in our lab. In addition, improved complexes are being produced that lack predicted structurally unfolded regions, like the N-termini of CENP-H and CENP-K and the C-terminus of CENP-I. It may be easier to reveal the structure of these truncated complexes.

We assume that CENP-H/I/K/M forms a constitutive complex within cells, but this has not been fully proven. It is possible that CENP-H/K are always bound to CENP-C, whereas CENP-M and CENP-I only form a complex with CENP-H and CENP-K in certain cell cycle phases, e.g. mitosis, where kinetochores have to resist the strongest forces. However, this would raise the question of where CENP-I and CENP-M bind in the other cell cycle phases, since they both localize constitutively to kinetochores. CENP-M has been shown to be a pseudo GTPase. It is conceivable that CENP-M has lost its GTPase activity through evolution to the point where its function in humans is merely in CCAN stabilization. In contrast, in lower organisms like yeast CENP-M might exist as a functional homolog

that fulfills an additional role involving promoting disassembly from kinetochores in parts of the cell cycle, for example during DNA replication. This might explain why no CENP-M ortholog has been identified in yeast so far. All experimental evidence for this theory has used pulldowns of known kinetochore components to identify proteins associated with them. If CENP-M has a high turnover rate it would be difficult to find its ortholog in yeast, and would likely require the use of nucleotide analogues to inhibit GTPase activity. Indeed, kinetochores fulfill their function during mitosis and disassembly of the whole kinetochore would make sense, since the presence of the kinetochore is a challenge during DNA replication and it is not understood yet, how the centromeric DNA is replicated and at the same time kinetochores are maintained; a question that goes far beyond the focus of this study, but is interesting and challenging.

3.1.2 CENP-C interaction with CENP-N/L

CENP-N/L complex was revealed in this study to depend on CENP-C for its kinetochore recruitment (**Figure** 2.45) and make a direct interaction with CENP-C^{1-544} *in vitro* (**Figure** 2.30). It has to be taken into account here that a reconstituted heterodimeric complex of CENP-N and CENP-L has been used, although the formation of constitutive complex within cells has not been clearly demonstrated. Nevertheless, a direct interaction of these proteins and binding of the dimeric complex to CENP-C has already been identified in yeast [258]. As with its yeast homologs, CENP-N seems to bind to CENP-C via its N-terminal region, as revealed by cross-linking analysis (**Figure** 2.32), indicating a conserved binding mode across species. However, the exact mode of interaction could not be revealed here, since no mutation on CENP-C influenced CENP-N/L binding in a pulldown assay (**Table** 2.6). As with CENP-H/I/K/M, CENP-N/L binds to a very elongated interface of CENP-C, mainly spanning CENP-$C^{189-400}$. It is clear that different residues of CENP-C are involved in the CENP-H/I/K/M and the CENP-N/L interaction, although they both interact with the same region of CENP-C. The mutants that disrupt CENP-H/I/K/M interaction with CENP-C clearly have no effect on CENP-N/L interaction (**Supplementary Figure** 5.4) and in addition both complexes can bind to CENP-C simultaneously, as shown by CENP-C/H/I/K/M/N/L/CENP-$A^{nucleosome}$ complex formation. Also in this case, structural analysis of the CENP-C/N/L complex would answer a lot of remaining

questions about the interaction mode of CENP-C and CENP-N/L.
Previously, the CENP-H, CENP-K, CENP-I and CENP-M group of proteins was found to be associated with CENP-N/L proteins by immunoprecipitation experiments, but a direct interaction was never shown [76, 250]. The results presented here give a possible explanation for this observation: CENP-N/L could be immunoprecipitated by CENP-H/K/I or -M via CENP-C. However, we also find cross-links between CENP-N/L and the CENP-H/I/K/M complex. In addition, the interaction of CENP-N/L to CENP-C does not seem very strong in solution. Unfortunately, trials to detect the binding affinity of CENP-N/L to CENP-C failed, but from the SEC experiments a rather weak binding was proposed. Therefore, CENP-N/L could bind to CENP-C as well as CENP-H/I/K/M, which would lead to the formation of a very stable complex. Strongly supporting this hypothesis, CENP-L is lost in immunoprecipitations against GFP-CENP-C$^{1-544}$4A, although these mutations do only affect the CENP-C:CENP-H/I/K/M interaction *in vitro*. Therefore, *in vivo*, CENP-C alone is not sufficient to recruit CENP-N/L to kinetochores and a likely explanation is the lack of the CENP-H/I/K/M binding interface. As an alternative explanation, again a structural change in one of the components is possible. For example, CENP-H/I/K/M could undergo a structural rearrangement upon binding to CENP-C that allows binding to CENP-N/L, or CENP-H/I/K/M exposes a binding site within CENP-C that allows it to bind to CENP-N/L more tightly. Whether there is a direct contribution to CENP-N/L recruitment to kinetochores from CENP-H/I/K/M or a structural rearrangement of one of the components involved, would be difficult to distinguish experimentally. Again, structural insights into the single and the larger complexes would answer these questions. Confirming the idea that CENP-N/L is dependent on both CENP-C and CENP-H/I/K/M for its kinetochore localization was considered more appropriate. Measuring the binding affinity of CENP-N/L to CENP-C, to CENP-H/I/K/M and to CENP-C/H/I/K/M was performed. However, these experiments prooved to be too challenging and therefore have not led to a clear picture yet. In addition, monitoring CENP-N/L levels in cells depleted of endogenous CENP-C and induced for expression of CENP-C 4A would further reveal the role of CENP-H/I/K/M in the CENP-N/L complex recruitment. At the moment these experiments are challenging, as there is no CENP-N or CENP-L antibody available that is effective in immunofluorescence experiments. Alternatively, RNAi against one of the CENP-H/I/K/M complex components and quantification of mCherry-CENP-N or mCherry-CENP-L, as done in this work for CENP-C RNAi, would

answer the same question. All of these experiments are currently in progress. So far, we have identified a clear dependency of mCherry-CENP-L on CENP-H/I/K/M for its kinetochore localization as revealed by CENP-H RNAi, whereas levels of CENP-C remain unaltered (data not shown). This strongly points towards our model that places CENP-N/L into the CCAN recruitment hierarchy downstream of CENP-C and CENP-H/I/K/M, in contrast to being downstream of CENP-C only (see **Figure** 3.2).

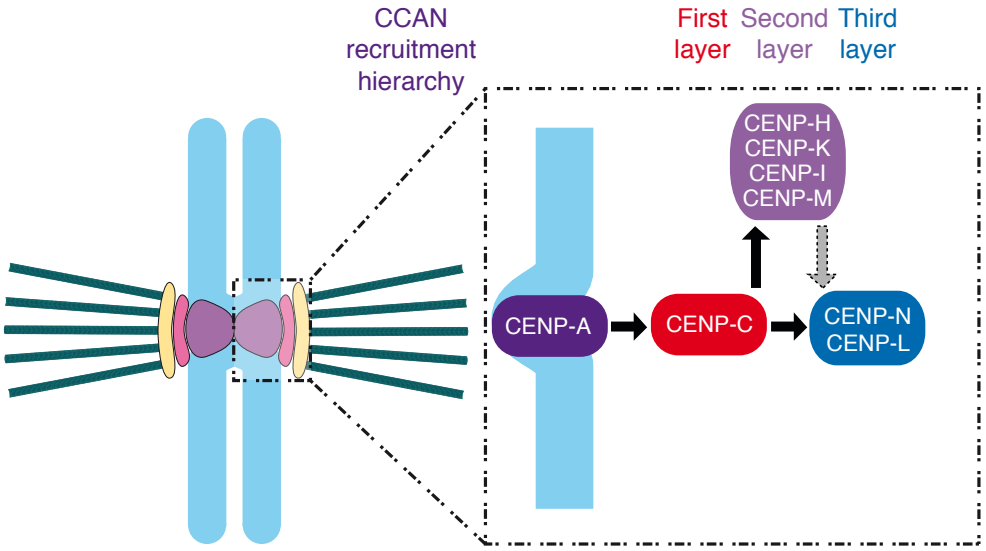

FIGURE 3.2: **CCAN recruitment by direct CENP-C binding**. Black arrows indicate recruitment dependencies through direct interactions. CENP-C directly binds to CENP-A containing nucleosomes and is the first layer in the CCAN recruitment hierarchy. The second layer consists of the CENP-H/I/K/M that directly interacts with CENP-C. CENP-N/L is the second direct interactor of CENP-C and might also depend on CENP-H/I/K/M for its centromere localization and therefore belongs to the third layer in the CCAN recruitment hierarchy. However, a direct interaction between CENP-N/L and CENP-H/I/K/M has not been observed so far and is only hypothesised from experiments within human cells.

CENP-N was shown to bind to the CATD of histone CENP-A within CENP-A nucleosomes [76, 91], thus providing another interaction site at the kinetochore that is probably needed for CENP-N/L localization. Indeed, this interaction could explain the residual levels of CENP-N and CENP-L found at kinetochores in cells efficiently depleted for CENP-C. The physical proximity of CENP-N to CENP-A was shown in cross-linking analysis, suggesting there is indeed a physical interaction (**Figure** 2.32). However, the fact that CENP-N is found at kinetochore like foci that were introduced by targeting CENP-C and CENP-T to ectopic sites in the absence of CENP-A speaks against a requirement of CENP-A in CENP-N/L recruitment [153]. Interestingly, a role for CENP-N in CENP-A deposition has been suggested, since CENP-A levels decrease upon CENP-N depletion [91, 250]. CENP-C has been shown to directly interact with CENP-A and play a role in its loading, [89, 90, 279] thus CENP-C and CENP-N/L might therefore function together in this yet undefined pathway of CENP-A deposition, as discussed further below.

3.1.3 The stoichiometry of the CENP-C/H/I/K/M/N/L complex

CENP-N/L and CENP-H/I/K/M bind to the same region of CENP-C (**Figure** 2.32), but the interaction involves different CENP-C residues, since mutations disrupting the CENP-H/I/K/M binding to CENP-C do not affect the CENP-N/L:CENP-C interaction (**Supplementary Figure** 5.4).
CENP-A nucleosomes possess a two-fold symmetry. Therefore, two CENP-C molecules can in theory bind to one CENP-A containing nucleosome [89], placing two CENP-C molecules in immediate physical proximity. This suggests a model in which two CENP-C molecules bind two CENP-H/I/K/M and two CENP-N/L complexes, leading to a 1:2:2:2 stoichiometry of CENP-A nucleosomes: CENP-C: CENP-H/I/K/M: CENP-N/L (**Figure** 3.3 Model 1). However, the compatibility of CENP-H/I/K/M and CENP-N/L to the same CENP-C molecule was not proven. Simultaneous binding of these complexes to the same CENP-C molecule might be prevented by steric hindrance. This suggests two additional theoretical models of CCAN assembly onto CENP-A nucleosomes.

In model 2 (**Figure** 3.3), CENP-H/I/K/M complex binds to one CENP-C protein and CENP-N/L complex binds to a second, both on the same CENP-A nucleosome, leading to a 1:2:1:1 stoichiometry of CENP-A nucleosomes: CENP-C: CENP-H/I/K/M: CENP-N/L. There is no discrepancy between this model and the suggested interaction of CENP-N/L and CENP-H/I/K/M. These complexes could form a bridge like structure between the two CENP-C molecules.
As a third theoretical model, CENP-H/I/K/M and CENP-N/L could interact with two CENP-C molecules bound to neighboring CENP-A nucleosomes (**Figure** 3.3, Model 3), leading to a 2:2:1:1 stoichiometry of CENP-A nucleosomes: CENP-C: CENP-H/I/K/M: CENP-N/L. In all these models CENP-T/W could bind to this bridge from the site, which is also not inconsistent with its proposed binding to H3 nucleosomes.
All three models (**Figure** 3.3) do not take into account that CENP-C possesses two CENP-A interaction sites. Nevertheless, none of the models is inconsistent with this fact. In model 1 and 2, the second CENP-A interaction site of CENP-C can bind to a neighboring CENP-A nucleosome. In model 3, the second CENP-A binding site of CENP-C can interact with the second CENP-A histone within the same nucleosome. However, preliminary data shows that CENP-$C^{545-943}$ does not properly localize to kinetochores throughout the cell cycle, but seems to be increased at centromeres in mitosis (data not shown). To confirm this observation and understand a possible physiological function of this behavior, additional experiments are required.
It is possible that the C-terminal CENP-A binding domain of CENP-C interacts with an H3 nucleosome. It has been shown that CENP-A levels are reduced by half during DNA replication and that CENP-A deposition occurs after mitosis. Since part of the CENP-A reloading machinery has been shown to assemble directly onto CENP-C's C-terminus [109] we suggest a model where CENP-C C-terminal half bound to H3 nucleosomes during G_2-phase and mitosis and assembles the CENP-A replenishment machinery after mitosis. This machinery would then exchange the H3 nucleosome bound to CENP-Cs C-terminus with a new CENP-A nucleosome. The mechanism of CENP-A deposition will be further discussed in **Section** 3.1.7.

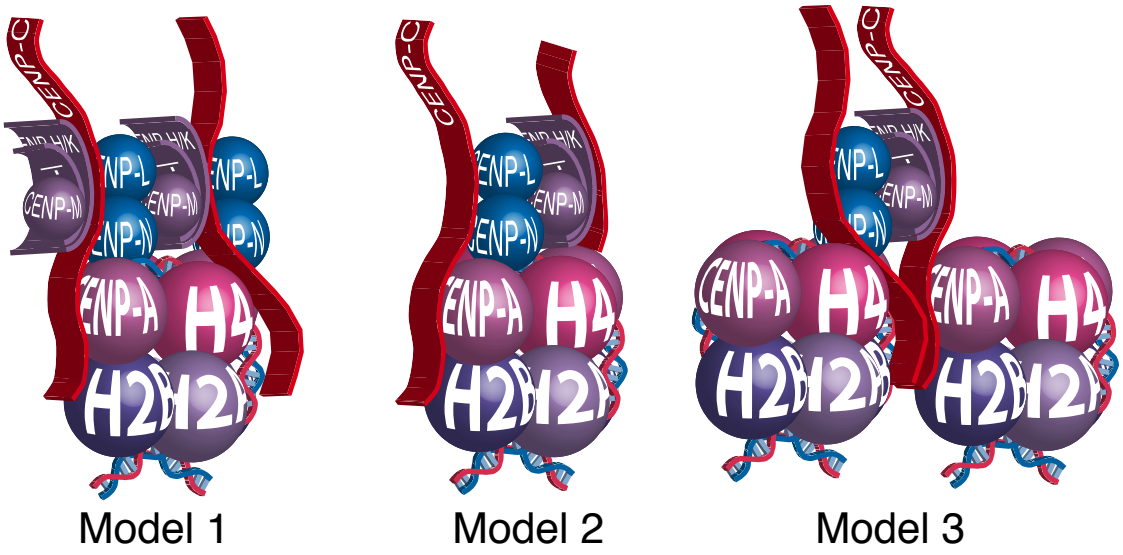

FIGURE 3.3: **CCAN assembly models**. CENP-A nucleosomes possess a two fold symmetry. Therefore, two CENP-C molecules can bind to one nucleosome. CENP-N/L and CENP-H/I/K/M bind to the same region, but not the same residues of CENP-C. Therefore, it is easy to hypothesize the simultaneous binding of CENP-N/L and CENP-H/I/K/M to the same CENP-C molecule (Model 1). However, the simultaneous binding of CENP-H/I/K/M and CENP-N/L to CENP-C was not proven. Therefore, only one copy of CENP-N/L and CENP-H/I/K/M could bind to different CENP-C molecules on the same nucleosome (Model 2) or CENP-N/L and CENP-H/I/K/M could bind to different CENP-C molecules on neighboring nucleosomes (Model 3).

3.1.4 CENP-C interaction with CENP-T/W

The third complex that was shown in this thesis to depend on CENP-C for its kinetochore localization is CENP-T/W (**Figure** 2.47). A direct interaction was not observed (**Figure** 2.55), but the inability of CENP-C full length 4A mutant to rescue CENP-T/W localization to kinetochores (**Figure** 2.56) together with previous observations that show a direct interaction of CENP-T/W with CENP-H/I/K/M [264] strongly supports the hypothesis that CENP-T/W is directly recruited by CENP-H/I/K/M. Therefore, CENP-C occupies the first position downstream of CENP-A in a single pathway of kinetochore assembly, followed by CENP-H/I/K/M that then recruits CENP-T/W and (together with CENP-C and possibly CENP-A) CENP-N/L. CENP-T/W is therefore located downstream of CENP-C and parallel to CENP-N/L in the CCAN recruitment hierarchy (see **Figure** 3.4).

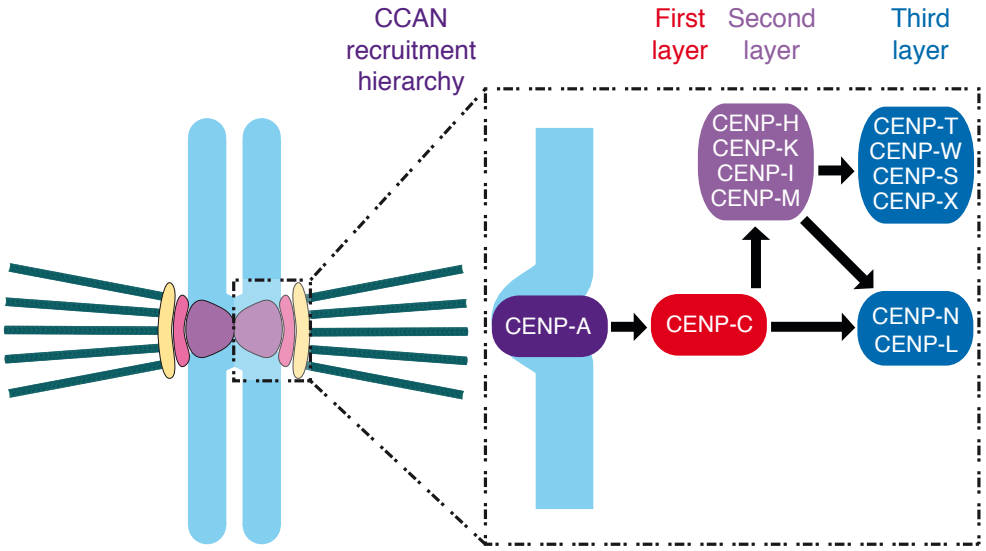

FIGURE 3.4: **CCAN recruitment hierarchy**. Black arrows indicate recruitment dependencies through direct interactions. As shown before CENP-C directly binds to CENP-A containing nucleosomes, CENP-H/I/K/M and CENP-N/L. Since CENP-N/L is dependent on both CENP-C and CENP-H/I/K/M it belongs to the third layer in the CCAN recruitment hierarchy. CENP-T/W is directly interacting with CENP-H/I/K/M and depends on this complex for its kinetochore recruitment, thus placing it into the same layer as CENP-N/L in the recruitment hierarchy.

An independent pathway of CENP-T/W localization via its direct binding to H3 nucleosomes [78] or even the formation of a nucleosome like structure by the CENP-T/W/S/X has been proposed in the past [242]. CENP-T/W was placed parallel to, rather than dependent on, CENP-C in kinetochore localization by knockout studies in chicken cells [78]. In contrast, CENP-T was placed downstream of CENP-C based on RNAi experiments in human cells [90]. Therefore, the interdependence of CENP-C and CENP-T/W are still a matter of debate. Overall, we have strong evidence to propose a model where CENP-T/W is highly dependent on CENP-H/I/K/M and therefore CENP-C for its centromere recruitment. Binding to H3 nucleosomes or centromeric DNA contribute to CENP-T/W stability at kinetochores and might keep a portion of CENP-T/W bound to centromeres after CENP-C depletion. Indeed, we see a high residual level of CENP-T/W at kinetochores in the absence of CENP-C (**Figure** 2.57). In addition, it has been shown that CENP-T/W/S/X binds to inter-nucleosomal DNA and was suggested to form a nucleosome like structure at centromeres [301]. The model placing CENP-T/W downstream of CENP-C in the CCAN recruitment hierarchy is not inconsistent with the identified role of CENP-T in regulating outer kinetochore

assembly through an interaction with the Ndc80 complex and possibly other outer kinetochore components [153, 242, 261, 262, 302]. The conclusion, however, implies that such role of CENP-T/W in kinetochore assembly occurs downstream of CENP-C. In addition, our model answers how CENP-T/W localization is restricted to centromeric regions, which would be challenging for a protein recruited by H3 nucleosomes or DNA without sequence specificity. The results presented here therefore strongly support our suggestion that CENP-C is at the top of the recruitment hierarchy of human kinetochores. An updated view of the kinetochore scheme shown in the Introduction (**Figure** 1.5) considering the results obtained here can be found in **Figure** 3.6.

3.1.5 Role of CENP-C in outer kinetochore recruitment

It has been shown in the literature that the very N-terminus of CENP-C directly binds to the Mis12 complex *in vitro* and that strong overexpression of GFP-CENP-C^{1-71} displaces Mis12c from kinetochores in human cells [202]. These experiments clearly show an interaction between CENP-C and the Mis12 complex. However, the involvement of other factors in this interaction cannot be excluded from these observations. Here, indirect evidence is provided that demonstrate the involvement of other factors, besides CENP-C, in Mis12c recruitment to kinetochores. GFP-CENP-C^{1-544} immunoprecipitates the Mis12 complex, as expected. In contrast, GFP-CENP-C^{1-544}4A, which does not bind to CENP-H/I/K/M also does not pull down Mis12 complex from human cell lysate (**Figure** 2.58). The idea that other factors are involved in the recruitment of the Mis12 complex to the kinetochores cannot be limited to the CENP-H/I/K/M from this experiment, since it was shown that CENP-N/L, CENP-T/W and possibly other factors do not bind to CENP-C in the absence of CENP-H/I/K/M (**Figure** 2.58). Interestingly, the CENP-C interaction site for CENP-H/I/K/M was revealed through multiple sequence alignments to be located very close to the Mis12 complex binding site within the yeast ortholog of CENP-C, Mif2 (see **Figure** 3.5). In addition, the CENP-H/K/I group of proteins has been shown to contribute to the localization of outer kinetochore components [188, 250, 268, 288], further strengthening this hypothesis.

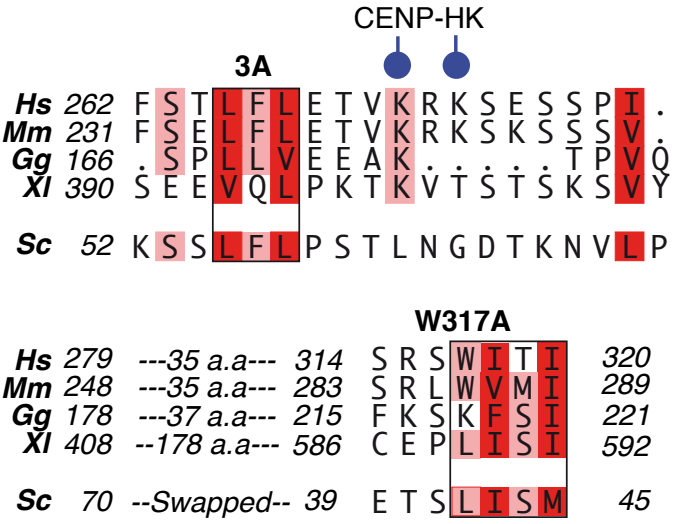

FIGURE 3.5: **MSA of CENP-H/K/I/M binding sites on CENP-C.** A Multiple Sequence Alignment (MSA) is a sequence alignment of three or more biological sequences e.g. of proteins. Here, a MSA of CENP-C's conserved patches shown to interact with CENP-H/I/K/M was performed. Within the boxed regions the two conserved hydrophobic motifs in CENP-C shown to interact with CENP-H/I/K/M can be found. Two lysine residues found to cross-link with CENP-H/K are shown with blue circles. Budding yeast Mif2 is shown for comparison. Curiously, the regions conserved in Mif2 seem to be swapped, close to each other and to the binding site of Mis12 complex to Mif2.

Thus far, we were not able to confirm the results observed in IP experiments showing involvement of CCAN proteins besides CENP-C in Mis12c recruitment *in vitro*. Mis12c was pulled down equally good by GST-CENP-C$^{2-545}$ in the absence and presence of CENP-H/I/K/M (**Figure** 2.59), suggestion no contribution from CENP-H/I/K/M to the CENP-C:Mis12c interaction. In addition, it was not possible to bind the Mis12c to GST-CENP-C$^{189-400}$ by including CENP-H/I/K/M and CENP-N/L in the pulldown (**Figure** 2.60). Therefore, CENP-H/I/K/M and CENP-N/L are not sufficient for binding the Mis12c to CENP-C lacking the N-terminal Mis12c interaction site *in vitro*. However, this does not rule out a contribution from the CCAN to Mis12c assembly onto kinetochores. It might well be that the effect observed in immunoprecipitations is achieved by other factors that were not included in the pulldown. Alternatively, the very N-terminus of CENP-I, which is not present in the recombinant CENP-H/I/K/M complex, could be the mediating component. Experiments including other recombinant kinetochore proteins might lead to a conclusion. Cross-linking and mass spectrometry experiments as shown for the CCAN complex in this work (**Figure** 2.32) including the Mis12 complex would provide valuable information.

The inability of Mis12 complex to bind to GFP-CENP-C$^{1-544}$4A seen in immunoprecipitation experiments (**Figure** 2.58) might also be a consequence of the incapability of GFP-CENP-C$^{1-544}$4A to bind CENP-T/W. Therefore, no Ndc80 complex, which has been shown to interact with Mis12 complex [158], is involved in the interaction and subsequently less Mis12 complex is pulled down. In agreement, it has been shown recently that levels of Mis12c are reduced to 50 % by Ndc80c depletion [303]. The same study also suggests an involvement of CENP-H/I/K in Ndc80c recruitment to kinetochores, therefore absence of both CENP-T/W and CENP-H/I/K/M in IPs against GFP-CENP-C$^{1-544}$4A might indirectly contribute to a loss of Mis12c in these experiments by decreasing the amounts of Ndc80c bound to the kinetochore.

It has to be taken into account here that all GFP-CENP-C cell lines produced in this study carry an N-terminal eGFP tag, which might impair the binding of Mis12c to the N-terminus of CENP-C. Mis12c localization to kinetochores is remarkably reduced in cells depleted for CENP-C by RNAi, as seen by immunofluorescence against the Dsn1 component of the Mis12c. Unfortunately, wild type GFP-CENP-C full length expression did not rescue Mis12c recruitment (data not shown), supporting the idea of the N-terminal tag to cause problems in Mis12c localization. However, the N-terminal GFP tag does not explain why Mis12c binding is reduced in the IP against GFP-CENP-C$^{1-544}$4A compared to GFP-CENP-C$^{1-544}$. To get a better understanding of the dependencies of the Mis12c on other CCAN components besides CENP-C, cell lines inducible for the expression of CENP-C-GFP full length wild type or 4A mutant carrying a C-terminal eGFP tag are currently produced in the lab.
To rule out the possibility that CENP-C4A is impaired in Mis12c binding itself, we performed *in vitro* GST-pulldown assays and analytical SEC. Mis12c binds to CENP-C$^{2-545}$4A or GST-CENP-C$^{2-545}$4A as efficient as to the wild type form of these constructs (**Figure** 2.41 and 2.42), whereas CENP-H/I/K/M is not incorporated into the CENP-C$^{2-545}$4A/Mis12c complex in solution and on solid surface. Therefore, CENP-C$^{2-545}$4A is a separation of function mutant *in vitro*, whereas the situation *in vivo* turns out to be more complicated. Therefore, additional experiments within human cells need to be performed to understand whether Mis12 complex recruitment is dependent on CENP-C alone or if other proteins are involved in this. As a starting point, recruitment of the Mis12c to kinetochores can

be monitored in cells depleted of CENP-C and induced for CENP-C-GFP constructs that are lacking the very N-terminus of CENP-C. These constructs have already been designed. If Mis12 complex recruitment depends solely on CENP-C, these constructs should not rescue Mis12 complex localization. The possible involvement of CCAN proteins in the Mis12 complex recruitment is included in the updated kinetochore scheme (**Figure** 3.6).

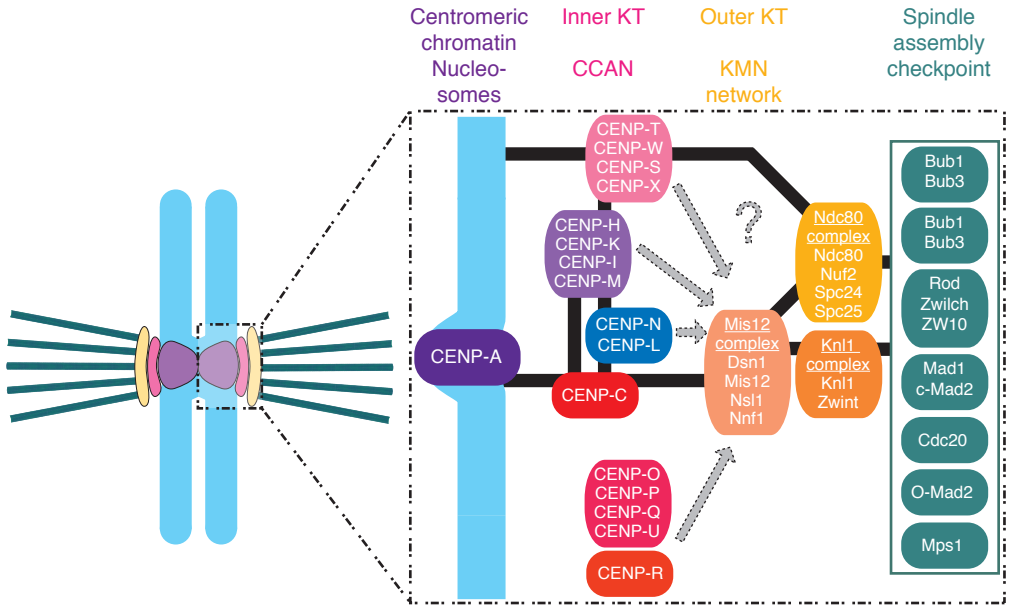

FIGURE 3.6: **Updated schematic kinetochore organization**. Black lines indicate direct interactions. CENP-C makes direct contact to centromeric DNA via its interaction with CENP-A. CENP-C is responsible for the recruitment of all CCAN components investigated here, either directly or indirectly. CENP-C further assembles the outer kinetochore by directly binding to Mis12 complex and also indirectly by recruitment of CENP-T/W that interacts with the Ndc80 complex. As a consequence, CENP-C is required for the whole kinetochore to be build, which explains its crucial role throughout evolution.

3.1.6 The stoichiometry of the kinetochore

In the updated CCAN assembly scheme (**Figure** 3.6), one copy of each protein or complex is depicted. This depiction should however not imply the assumption of a 1:1 stoichiometry of all proteins and complexes. To understand the actual stoichiometry of the CCAN bound to CENP-A nucleosomes, analytical ultra centrifugation (AUC) could be performed on samples of increasing complexity. As

an example, AUC could be performed on CENP-C$^{1-544}$/H/I/K/M. Here, binding of one molecule of CENP-H/I/K/M to one molecule of CENP-C$^{1-544}$ is expected. In addition CENP-N/L could be added to the CENP-C$^{1-544}$/H/I/K/M to understand whether CENP-N/L binds to the same molecule of CENP-C that CENP-H/I/K/M does or if it binds to a different molecule of CENP-C, which would lead to a 2:1:1 stoichiometry of CENP-C: CENP-H/I/K/M : CENP-N/L. These complexes should also be measured in the presence of CENP-A containing nucleosomes, because they might provoke a change in the stoichiometry of the complexes, due to their two-fold symmetry. By using more complex structures, the stoichiometry of the kinetochore could be determined, however the possibility that the stoichiometry of the complex might further change through the addition of more components has to be taken into account. Since this would be an *in vitro* determination of the kinetochore stoichiometry, the question would remain whether this reflects the kinetochore setup within cells. In addition, CENP-C full length so far could not be produced recombinantly in sufficient amounts. Therefore, for the aforementioned experiments the second CENP-A binding motif on CENP-C would be missing and this might lead to a different setup of the whole kinetochore structure. An alternative to CENP-C full length, currently produced in the lab, is a CENP-C molecule that consists of two parts, CENP-C$^{1-544}$ and CENP-C$^{545-943}$. The amino acids LPETGG and GG are added at the C- and N-terminus of the two constructs, respectively. As has been reported, the bacterial enzyme Sortase possesses transpeptidase activity, which enables it to specifically break and reform peptide bonds [304, 305]. Sortase was used in this thesis for protein engineering of the full length CENP-C. So far, CENP-C$^{1-544}$-LPETGG and GG-CENP-C$^{545-943}$ have been produced in sufficient amounts and it has been shown that they can be covalently linked by a peptide bond through sortase treatment (data not shown). CENP-C$^{1-544}$ was used for all experiments explained in this thesis, because it is sufficient to assemble the whole kinetochore onto CENP-A containing nucleosomes. The engineered CENP-C full length will be used for additional questions regarding the stoichiometry of the kinetochore and the role of the C-terminus of CENP-C that includes the second CENP-A binding motif, a dimerizing domain and a supposed platform for the assembly of the CENP-A replenishment machinery. These additional roles of CENP-C have not been examined in this study, but do provide another interesting field for investigations.

3.1.7 CENP-A deposition

This study provides important knowledge for potential further studies regarding CENP-A deposition, since the CCAN has been implicated in this mechanism [306]. CENP-C is probably directly involved in this fascinating mechanism by recruiting factors essential for CENP-A deposition like Mis18BP1 [109]. To be in a good position to investigate CENP-A deposition in great detail both *in vitro* and *in vivo*, tools are currently established in the lab. These include the introduction of a SNAP-tag to the endogenous CENP-A histone gene using the CAS9-CRISPR system [307]. The CENP-A-SNAP protein is a tool that has already been reported to allow the monitoring of the incorporation of newly synthesized CENP-A into chromatin [92]. The SNAP-tagged CENP-A cell line will allow us to investigate the role of different CCAN proteins in CENP-A deposition by depletion of selected proteins via RNAi. In addition, proteins shown to be part of the CENP-A reloading machinery are currently produced in the lab, mainly by Dr. Dongqing Pan. These include HJURP, Mis18 complex and FACT complex.

To investigate the role of CENP-C in this mechanism, the CENP-C N- and C-terminal halves would be bound to reconstituted CENP-A and H3 nucleosomes and lysate from either mitotic or interphasic cells would be applied. After washing off the unbound proteins, western blots would be performed against HJURP, Mis18 complex and CCAN proteins. If, as we expect, CCAN proteins bind to the N-terminal halves of CENP-C, whereas the other factors assemble on its C-terminus, the experiment would be expanded to Stable Isotope Labeling by Amino acids in Cell culture (SILAC). This might identify additional factors involved in the CENP-A deposition. These factors would be potential candidates to be tested for their role in CENP-A deposition by RNAi in the CENP-A-SNAP cell line.

3.1.8 Posttranslational modifications of CENP-C

Another interesting aspect that should be mentioned here is the fact that CENP-C^{1-544} (**Figure** 2.5), and also CENP-$C^{545-943}$ (data not shown) produced from insect cells, have been shown to be phosphorylated by mass-spectrometry. In addition CENP-C^{1-544}His from insect cells binds CENP-H/K more efficiently in solution compared to the same construct produced from bacteria. Phosphorylations or other protein modifications could be partly responsible for an improved interaction with CENP-H/K. We show that the amino acid mainly involved in CENP-H/K interaction is a conserved Trp and therefore cannot be a potential phosphorylation site that is citical for this interaction. In addition, CENP-C/H/I/K/M complex formation does not protect any phosphates on either CENP-C or CENP-H/I/K/M from phosphatase treatment, as revealed by mass-spectrometry (data not shown). However, CENP-C^{1-544} produced from insect cells elutes at a later volume in a SEC compared to the bacterial protein, which might suggest the introduction of some structural elements within CENP-C that is predicted to be mainly unstructured. A phosphate at serine 225 might be responsible for folding, since this site has been shown to resist phosphatase treatment on CENP-C^{1-544}. An altered conformation of CENP-C^{1-544} could lead to improved binding of some of its binding partners. Again, the role of posttranslational modifications on CENP-C is elusive and needs a more systematic investigation to be understood.

Taken together, we propose a model for kinetochore assembly with CENP-C at its base. The direct interaction of CENP-C with CENP-H/I/K/M was shown and the residues involved in the interaction were revealed. In addition, we have strong evidence to indicate a dependency of CENP-T/W on CENP-H/I/K/M, placing CENP-T/W downstream of CENP-C, as well as recruitment of CENP-N/L that involves CENP-C and CENP-H/I/K/M. The possibility of the Mis12 complex being recruited by other factors besides CENP-C was raised here as well. Overall, this work provides major knowledge about the structural and functional organization of the CCAN protein complex. Moreover, this work provides essential knowledge for further scientific investigations, including the role of CENP-C in CENP-A deposition and the function of CENP-C posttranslational modifications.

Chapter 4

Materials and Methods

4.1 Instrumentation and software

Table 4.1: Instrumentation

Instrument	Type	Provider
Aekta purifier	ÄKTA purifier	GE Healthcare, Freiburg, Germany
Aekta micro	ÄKTA micro liquid chromatography system	GE Healthcare, Freiburg, Germany
Aekta prime	ÄKTA prime	GE Healthcare, Freiburg, Germany
Agarose gel electrophoresis system	Nucleic acid Elctrophoresis system	Carl Roth, Karlsruhe, Germany
Balances		
	CP225D	Sartorius, Göttingen, Germany
	BA3100P	Sartorius, Göttingen, Germany
	PM480 Delta range	Mettler Toledo, Gießen, Germany

Instrument	Type	Provider
Bioprint DS Videodocumentation system		LTT Labortechnik Tasler GmbH, Würzburg, Germany
Centrifuges		
	5418R	Eppendorf, Hamburg, Germany
	5424R	Eppendorf, Hamburg, Germany
	Universal 320R	Hettich Lab technology, Tuttlingen, Germany
	Sorvall RC3PB+	Thermo Scientific, Hennigsdorf, Germany
	Avanti 30 centrifuge	Beckman Coulter, Krefeld, Germany
	Avanti J-30I	Beckman Coulter, Krefeld, Germany
	Allegra X-15R	Beckman Coulter, Krefeld, Germany
	Biofuge 13	Heraeus Holding GmbH, Hanau, Germany
Cell counters		
	Countess automated cell counter	Invitrogen, California, USA
	Scepter Handheld Automated Cell Counter	Merck Millipore, Darmstadt, Germany
	Neubauer counting chamber	Marienfeld-Superior, Lauda Knigshofen, Germany
Chemibis	Chemibis3.2	Dnr Bio-Imaging Systems,Jerusalem, Israel
Columns		
Heparin	Hitrap 5ml HeparinHP	GE Healthcare, Freiburg, Germany

Instrument	Type	Provider
Anion-Exchange	Resource Q 5ml	GE Healthcare, Freiburg, Germany
Affinity	GSH-Sepharose fast flow column	GE Healthcare, Freiburg, Germany
Kation-Exchange	Resource S 5ml	GE Healthcare, Freiburg, Germany
SEC	Superdex200 10/300	GE Healthcare, Freiburg, Germany
SEC	Superdex200 16/600	GE Healthcare, Freiburg, Germany
SEC	Superdex200 5/150	GE Healthcare, Freiburg, Germany
SEC	Superdex75 10/300	GE Healthcare, Freiburg, Germany
SEC	Superdex75 16/600	GE Healthcare, Freiburg, Germany
SEC	Superose 6 16/70 GE Healthcare, Freiburg, Germany	
SEC	Superdex200 5/150	GE Healthcare, Freiburg, Germany
Affinity	TALON^{TM} column	GE Healthcare, Freiburg, Germany
Concentrators	Amicon Ultra	Merck Millipore, Darmstadt, Germany
Heating Block	Dri-Block DB 2A	Techne, Staffordshire, UK
	Thermomixer comfort	Eppendorf, Hamburg, Germany
Homogenizer	Sonifier cell disrupter	G. Heinemann, Schwäbisch Gmünd, Germany

Instrument	Type	Provider
Incubators		
	CO_2 Water Jacketed Incubator	Nuaire, Plymouth, USA
	Kelvitron K	Heraeus Holding GmbH, Hanau, Germany
	WTC binder BD53	Biotron Healthcare, Mumbai, India
ITC machine	ITC200	Malvern Instruments Ltd, Herrenberg, Germany
Microscopes		
Optical	Axiovert25	Carl Zeiss Microscopy GmbH, Cologne, Germany
	DFC290	Leica, Wetzlar, German
Fluoresence	3i Marianas	Intelligent Imaging Innovations, Denver, CO
	Axio Observer Z1 microscope	Zeiss, Carl Zeiss Microscopy GmbH, Cologne, Germany
	Evos Fluorescence Microscope	Life technologies, Darmstadt, Germany
	CSU-X1 confocal scanner unit	Yokogawa Electric Corporation, Tokyo, Japan
	Plan-Apochromat 63x or 100x/1.4NA objectives	Carl Zeiss Microscopy GmbH, Cologne, Germany
	Orca Flash 4.0 sCMOS Camera	Hamamatsu, Hamamatsu City, Japan
Multi Rotator	Multi-Bio PS-24	Kisker Biotech, Steinfurt, Germany
Nucleic acid vizualization system	Safe imager 2.0	Invitrogen, California, USA
	Bioprint DS videoducumentation system	LTF Labortechnik, Wasserburg, Germany

Instrument	Type	Provider
PCR machines		
	T3000Thermocycler	Biometra, Göttingen, Germany
	Profesional TRIO Thermocycler	Biometra, Göttingen, Germany
pH meter	PB-11	Sartorius, Göttingen, Germany
Photometer	BioPhotometer	Eppendorf, Hamburg, Germany
Peristaltic pump	Vacuum-Absaugsystem	HLC-Haep Labor Consult, Bovenden, Germany
Power supply unit	Power Pac 300	Bio-Rad, München, Germany
Protein gel system	Mini-Protan Tetra System	Bio-Rad, München, Germany
Rotating wheels		
	Rotator SB3	Stuart, Staffordshire, UK
	Bio-RS-24 Mini-Rotator	Biosan, Riga, Latvia
Shaker	Polymax1040	Heidolph, Schwabach, Germany
Shaking Incubator	Multitron standard	Infors HT, Einsbach, Germany
Sodium dodecyl sulfate (SDS) gel running system	2-D Protein electrophoresis system	Bio-Rad, München, Germany
Sterile work bench	Class II biological safety cabinet	LAUDA, Lauda-Knigshofen, Germany
Spectrometer-Nanodrop	Nanodrop1000 Spectrophotometer	PEQLAB Biotechnologie GmbH, Erlangen, Germany
Thermomixer	Thermomixer comfort	Eppendorf, Hamburg, Germany
Water bath	Aqualine A225	LAUDA, Lauda-Knigshofen, Germany

Instrument	Type	Provider
Water purification system	Synergy UV water purification system	Merck Millipore, Darmstadt, Germany
Western blot transfer unit	Mini-Protean tetra system	Bio-Rad, München, Germany

Table 4.2: Software

Software	Version	Provider
InDesign CS4	6.0.6	Adobe
Photoshop CS4	11.0.2	Adobe
Illustrator CS4	14.0.0	Adobe
Jalview	14.0	Jalview
ImageJ	1.46r	National Institutes of Health
A plasmid Editor	2.0.38	by Wayne Davis
Excel	14.3.6	Microsoft
LaTeX	LaTeX2$_\varepsilon$	by Leslie Lamport
TexMaker	4.0.3	by Pascal Brachet
Unicorn Control software	Unicorn5.0	GE Healthcare, Freiburg, Germany
Origin	9.1	OriginLab
PSIPRED	v3.3	Bloomsbury Centre for Bioinformatics
Imaris	7.3.4	Bitplane, Zurich, Switzerland

4.2 Chemicals

Table 4.3: Chemicals & Solutions

Chemical	Ingredients	Provider
Acetic Acid (AcOH)		Sigma Aldrich, Hamburg, Germany
Acrylamide		AppliChem GmbH, Darmstadt, Germany
Agarose		Sigma Aldrich, Hamburg, Germany
Albumin from Bovine Serum		Sigma Aldrich, Hamburg, Germany
Albumin standard		Pierce, Rockford, USA
Ammonium persulfate		Serva Electrophoresis GmbH, Heidelberg, Germany
Ampicillin		Serva Electrophoresis GmbH, Heidelberg, Germany
Benzonaise Nuclease		Sigma Aldrich, Hamburg, Germany
Blasticidin		Invitrogen, California, USA
Bradford protein assay (5x)		Bio-Rad, München, Germany
Bovine Serum Albumin (BSA) Powder		Carl Roth, Karlsruhe, Germany
Bovine Serum Albumin		Gibco, Life Technologies^{TM}
CENP-C siRNA	5'-GGAUCAUCUCAGAA UAGAA-3'	Sigma Aldrich, Hamburg, Germany
Coomassie staining solution		
	10 % Acetic acid (AcOH)	Sigma Aldrich, Hamburg, Germany
	2.5 % Coomassie G250	Serva Electrophoresis GmbH, Heidelberg, Germany

Chemical	Ingredients	Provider
	2.5 % Coomassie R250	Serva Electrophoresis GmbH, Heidelberg, Germany
	50 % Ethanol (EtOH)	Fisher Scientific, Schwerte, Germany
Dimethyl sulfoxyde (DMSO) research grade		Serva Electrophoresis GmbH, Heidelberg, Germany
Dithiothreitol		Serva Electrophoresis GmbH, Heidelberg, Germany
DNA loading buffer (6x)		
	0.4 % Orange G	Sigma Aldrich, Hamburg, Germany
	30 % Glycerol	GERBU Biotechnik GmbH, Heidelberg, Germany
	10 mM Tris-HCl	Carl Roth, Karlsruhe, Germany
	25 mM Ethylenediaminetetraacetic acid (EDTA)	GERBU Biotechnik GmbH, Heidelberg, Germany
Doxycyclin		Sigma Aldrich, Hamburg, Germany
Dulbecco's Modified Eagle's Medium (DMEM)		PAN Biotech, Aidenbach, Germany
Dyalisis membrane		Thermo Scientific, Hennigsdorf, Germany
ECL Prime Western Blotting Detection Reagent		GE Healthcare, Freiburg, Germany
E.coli		
	Rosetta2 (DE3)	DPF
	C41 (DE3)	DPF
	OmniMax (DE3)	DPF
Ethanol (EtOH)		Fisher Scientific, Schwerte, Germany

Chemical	Ingredients	Provider
Ethylendiamintetraacetic acid (EDTA)		Merck Millipore, Darmstadt, Germany
Ethylenglycol-bis(aminoethylether) (EGTA)		Serva Electrophoresis GmbH, Heidelberg, Germany
Fetal Bovine Serum (heat inactivated)		Gibco Life Technologies, Darmstadt, Germany
FuGENE transfection reagent		Promega, Mannheim, Germany
GeneRuler 1kbPlus DNA ladder		Fermentas, Hennigsdorf, Germany
Gentamycin		Serva Electrophoresis GmbH, Heidelberg, Germany
GFP-Traps		ChromoTek, Martinsried, Germany
Glutathione Sepharose 4 Fast Flow beads		GE Healthcare, Freiburg, Germany
Glycerol		GERBU Biotechnik GmbH, Heidelberg, Germany
GSH Amintra Glutathion Resin		Amintra, Cambridge, UK
HEPES Ultrapure		GERBU Biotechnik GmbH, Heidelberg, Germany
Hygromycin		Invitrogen, California, USA
HiPerFect Transfection Reagent		Quiagen, Hilden, Germany
Isopropyl$-\beta$-D-thiogalactopyranosid (IPTG)		Carl Roth, Karlsruhe, Germany
Imidazol		Merck Millipore, Darmstadt, Germany
Immun-Blot PVDF Membrane		Bio-Rad, München, Germany

Chemical	Ingredients	Provider
Isopropanol		J.T.Baker Chemicals, Center Valley, USA
Kaliumchlorid (KCl)		J.T.Baker Chemicals, Center Valley, USA
Kanamycin		GERBU Biotechnik GmbH, Heidelberg, Germany
Lennox Broth (LB) medium		
	1.0 % peptone	Sigma Aldrich, Hamburg, Germany
	0.5 % yeast extract	GERBU Biotechnik GmbH, Heidelberg, Germany
	0.5 % NaCl	VWR Chemicals, Darmstadt, Germany
L-Glutamine		PAN Biotech, Aidenbach, Germany
L-Glutathion reduced		Biochemica, Darmstadt, Germany
Magnesium chloride ($MgCl_2$)		J.T.Baker Chemicals, Center Valley, USA
Magnesium sulfoxide ($MgSO_4$)		
Methanol (MeOH)		Sigma Aldrich, Hamburg, Germany
2-(N-morpholino) ethanesulfonic acid (MES)		Sigma Aldrich, Hamburg, Germany
Midori Green Advanced DNA stain		Nippon Genetics, Düren, Germany
Milk powder blocking grade		Carl Roth, Karlsruhe, Germany
MOPS SDS running buffer NUPAGE		Invitrogen, California, USA

Chemical	Ingredients	Provider
Mowiol mounting medium		Calbiochem, San Diego, USA
Nickel His60 Ni Superflow Resin		Clontech, California, USA
Nickel-NTA-Superose Beads		GE Healthcare, Freiburg, Germany
Nitrocellulose		GE Healthcare, Freiburg, Germany
Nonidet P40 (NP-40)		Sigma Aldrich, Hamburg, Germany
Nucleoside triphosphate (NTP)		Sigma Aldrich, Hamburg, Germany
OPTIMEM		Life technologies, Darmstadt, Germany
Paraformaldehyde (PFA, 16 %)		Alfa Aesar GmbH, Karlsruhe, Germany
PHEM buffer (pH 7)		
	60 mM PIPES Buffer grade	AppliChem GmbH, Darmstadt, Germany
	25 mM HEPES ultrapure	GERBU Biotechnik GmbH, Heidelberg, Germany
	5 mM Ethylenglycol-bis (aminoethylether) (EGTA)	Serva Electrophoresis GmbH, Heidelberg, Germany
	4 mM Magnesium Sulfate ($MgSO_4$)	Fisher Scientific, Schwerte, Germany
Phenylmethylsulfonylfluorid (PMSF)		Serva Electrophoresis GmbH, Heidelberg, Germany
Phosphate buffered saline (PBS)		
	Sodium Chloride (8g/l)	VWR Chemicals, Darmstadt, Germany

Chemical	Ingredients	Provider
	Potassim chloride (0.2 g/l)	J.T.Baker Chemicals, Center Valley, USA
	Di-Sodium hydrogen phosphate dihydrate (Na_2HPO_4) (1.15 g/l)	Merck Millipore, Darmstadt, Germany
	Potassium dihydrogenphophate (K_2HPO_4) (0.2 g/l)	AppliChem GmbH, Darmstadt, Germany
DPBS		PAN Biotech, Aidenbach, Germany
Poly-L-Lysin		Sigma Aldrich, Hamburg, Germany
Potassium chloride (KCl)		J.T.Baker Chemicals, Center Valley, USA
Precision Plus Protein Unstained Standards		Bio-Rad, München, Germany
Precision Plus Protein Prestained Standards		Bio-Rad, München, Germany
Protease Inhibitor Mix HP Plus		Serva Electrophoresis GmbH, Heidelberg, Germany
Protein A-Sepharose (CL-4B)		GE Healthcare, GE Healthcare, Freiburg, Germany
Protein G-Sepharose (rec-Protein G-Sepharose 4B)		Invitrogen, California, USA
Protein sample loading buffer		
	50 mM Tris-HCl	Carl Roth, Karlsruhe, Germany
	4 % SDS	Carl Roth, Karlsruhe, Germany
	10 % Glycerol	GERBU Biotechnik GmbH, Heidelberg, Germany

Chemical	Ingredients	Provider
	0.02 % Bromophenol blue	Sigma Aldrich, Hamburg, Germany
	1% β-mercaptoethanol	erva Electrophoresis GmbH, Heidelberg, Germany
Rnase free water		Thermo Scientific, Hennigsdorf, Germany
SDS PAGE electrophoresis buffer		
	25 mM Tris-HCl	Carl Roth, Karlsruhe, Germany
	200 mM Glycin	Sigma Aldrich, Hamburg, Germany
	3.5 mM SDS	Carl Roth, Karlsruhe, Germany
SDS gel runnung buffer	1.5 M Tris-HCl pH 8.8	Carl Roth, Karlsruhe, Germany
SDS gel stacking buffer	0.5 M Tris-HCl pH 6.8	Carl Roth, Karlsruhe, Germany
SDS pellets		Carl Roth, Karlsruhe, Germany
Sodium Chloride (NaCl)		VWR Chemicals, Darmstadt, Germany
Terrific Broth (TB) medium		
	1.2 % peptone	Sigma Aldrich, Hamburg, Germany
	2.4 % yeast extract	GERBU Biotechnik GmbH, Heidelberg, Germany
	72 mM Dikaliumhydrogenphosphat (K_2HPO_4)	Sigma Aldrich, Hamburg, Germany
	17 mM Kaliumdihydrogenphosphat (KH_2PO_4)	Sigma Aldrich, Hamburg, Germany

Chemical	Ingredients	Provider
	0.4 % glycerol	GERBU Biotechnik GmbH, Heidelberg, Germany
Tetramethyl-ethylenediamine		Serva Electrophoresis GmbH, Heidelberg, Germany
Tris-Acetate-EDTA (TAE) buffer (50x)		
	50 mM Tris-Base	Carl Roth, Karlsruhe, Germany
	57.1 ml Glacial acetic acid	Sigma Aldrich, Hamburg, Germany
	0.5 M EDTA (pH 8)	GERBU Biotechnik GmbH, Heidelberg, Germany
Tris(2-carboxyethyl) phosphine (TCEP)		Serva Electrophoresis GmbH, Heidelberg, Germany
Tet free Fetal Bovine Serum (FBS)		Clontech, Mountainview, USA
Tetracyclin-Hcl		Serva Electrophoresis GmbH, Heidelberg, Germany
Tris		Carl Roth, Karlsruhe, Germany
Tris-EDTA buffer		Thermo Scientific, Hennigsdorf, Germany
Tris/HCl		Carl Roth, Karlsruhe, Germany
Triton X-100		Serva Electrophoresis GmbH, Heidelberg, Germany
Trypsin		PAN Biotech, Aidenbach, Germany
Twwen-20		Serva Electrophoresis GmbH, Heidelberg, Germany
Ultra pure Agarose		Invitrogen, California, USA

Chemical	**Ingredients**	**Provider**
Western Blot transfer buffer		
	25 mM Tris	Carl Roth, Karlsruhe, Germany
	190 mM Glycin	Carl Roth, Karlsruhe, Germany
	10 % MeOH	Sigma Aldrich, Hamburg, Germany
X-Gal		Thermo Scientific, Hennigsdorf, Germany
X-tremeGENE 9 DNA Transfection Reagent		Roche, Basel, Switzerland
Zeocin		Invitrogen, California, USA
4-(2-Aminoethyl) benzenesulfonyl fluoride (AEBSF)		Sigma Aldrich, Hamburg, Germany
4,6-Diamidin-2-phenylindoldihydrochlorid (DAPI)		Serva Electrophoresis GmbH, Heidelberg, Germany
β-Mercaptoethanol		Serva Electrophoresis GmbH, Heidelberg, Germany

4.3 Enzymes

Table 4.4: Enzymes

Enzyme class	Name	Provider
Restriction Enzyme	BamHI	New England Biolabs
Restriction Enzyme	BglII	New England Biolabs
Restriction Enzyme	BstZ17I	New England Biolabs
Restriction Enzyme	DpnI	New England Biolabs
Restriction Enzyme	EcoRI	New England Biolabs
Restriction Enzyme	NdeI	New England Biolabs
Restriction Enzyme	NgoMIV	New England Biolabs
Restriction Enzyme	NodI	New England Biolabs
Restriction Enzyme	SalI	New England Biolabs
Restriction Enzyme	XhoI	New England Biolabs
Restriction Enzyme	XmaI	New England Biolabs
Polymerase	Flash Phusion	Thermo Scientific
	Benzonase	Merck MiIlipore, Darmstadt
Ligase	T4 DNA Ligase	Thermo Scientific
Protease	Trypsin	Promega, Mannheim, Germany
Protease	Elastase	Promega, Mannheim, Germany
Protease	Chymotrypsin	Promega, Mannheim, Germany
Protease	Glu C	Promega, Mannheim, Germany
Protease	Subtilisin	Promega, Mannheim, Germany
Protease	3C Prescicion	DPF (in house)
Protease	Tobacco Etch Virus protease (TEV)	DPF (in house)

4.4 Kits

Table 4.5: Kits

Kit	Provider
NucleoSpin Plasmid (NoLid)	Macherey-Nagel, Düren, Germany
Nucleobond PC10000	Macherey-Nagel, Düren, Germany
QIAprep Miniprep Kit	Quiagen, Hilden, Germany
Wizard SV Gel and PCR cleanup System	Promega, Mannheim, Germany

4.5 Antibodies

Table 4.6: Antibodies

Target	Type	Provider
CENP-C$^{23-410}$ (rabbit 410)	rabbit polyclonal anti human	created by Stefania Trazzi
CENP-C$^{731-849}$ (rabbit SI0934)	rabbit polyclonal anti human	created in collaboration with IFOM, Milan, italy
CENP-C$^{731-849}$-Alexa568 (rabbit SI0934)	rabbit polyclonal anti human	created in collaboration with IFOM, Milan, italy
CENP-H (FL-247)	rabbit polyclonal anti human IgG	Santa Cruz Biotechnology, Inc., Heidelberg, Germany
CENP-H/K (rabbit SI0930/SI0931)	rabbit polyclonal anti human	created in collaboration with IFOM, Milan, italy
CENP-H/K-Alexa488 (rabbit SI0930/SI0931)	rabbit polyclonal anti human	created in collaboration with IFOM, Milan, italy

Target	Type	Provider
CENP-H/K-Alexa568 (rabbit SI0930/SI0931)	rabbit polyclonal anti human	created in collaboration with IFOM, Milan, italy
CENP-I	rabbit polyclonal anti human	a kind gift from Song-Tao Liu, University of Toledo, USA
CENP-I (rabbit 887)	rabbit anti human polyclonal	generated in house [264]
CENP-L (17007-1-AP)	rabbit polyclonal anti human	Proteintech, Chicago, USA
CENP-M	rabbit anti human polyclonal	generated in house [264]
CENP-N (sc-69153)	goat polyclonal anti human IgG	Santa Cruz Biotechnology, Inc., Heidelberg, Germany
CENP-T/W (rabbit SI0822)	rabbit polyclonal anti human	created in house
CREST/anti-centromere	human anti human polyclonal	Antibodies Inc., Davis, CA
Mis 12 (QO15-1)(32)	mouse monoclonal anti-human	generated in house
GFP	rabbit anti human polyclonal	generated in house
Vinculin (V9131)	mouse anti human monoclonal	Sigma Aldrich, Hamburg, Germany
RhodamineRed-X-conjugated secondary	donkey anti rabbit polyclonal	Jackson ImmunoResearch, Pennsylvania, USA
DyLigth649-conjugated secondary	donkey anti rabbit polyclonal	Jackson ImmunoResearch, Pennsylvania, USA
Alexa 488-labeled secondary	goat anti rabbit polyclonal	Life technologies, Darmstadt, Germany
Alexa 405-labeled secondary	mouse anti human polyclonal	VWR Chemicals, Darmstadt, Germany
HRP-conjugated secondary (NXA931-1ML)	sheep anti mouse polyclonal	Amersham Biosciences, New Jersey, USA
HRP-conjugated secondary (NXA934-1ML)	donkey anti rabbit polyclonal	Amersham Biosciences, New Jersey, USA

4.6 Recombinant proteins

Table 4.7: Recombinant CENP-C proteins

Protein	Construct	Mutation
CENP-C	2-545	Wildtype
GST-CENP-C	2-545	Wildtype
GST-CENP-C	2-545	E302A F303A
GST-CENP-C	2-545	E302R F303S
GST-CENP-C	2-545	I305A D306A
GST-CENP-C	2-545	I305A D306A W317A
GST-CENP-C	2-545	L207A F209A
GST-CENP-C	2-545	L207A F209A E302R F303S
CENP-C	2-545	L266A F267A L268A (3A)
GST-CENP-C	2-545	L266A F267A L268A (3A)
CENP-C	2-545	L266A F267A L268A W317A (4A)
GST-CENP-C	2-545	L266A F267A L268A W317A (4A)
CENP-C	2-545	W317A
GST-CENP-C	2-545	W317A
GST-CENP-C	1-71	Wildtype
GST-CENP-C	1-400	Wildtype
CENP-C	402-544	Wildtype
GST-CENP-C	402-544	Wildtype
GST-CENP-C	104-544	Wildtype
CENP-C	189-544	Wildtype
GST-CENP-C	189-544	Wildtype
CENP-C	189-447	Wildtype
GST-CENP-C	189-447	Wildtype
GST-CENP-C	189-420	Wildtype
CENP-C	189-400	Wildtype
GST-CENP-C	189-400	Wildtype
GST-CENP-C	225-400	Wildtype
GST-CENP-C	263-400	Wildtype

Protein	**Construct**	**Mutation**
GST-CENP-C	290-400	Wildtype
GST-CENP-C	290-400	W317A
GST-CENP-C	189-364	Wildtype
GST-CENP-C	189-311	Wildtype
GST-CENP-C	189-290	Wildtype
GST-CENP-C	189-290	L207A F209A
GST-CENP-C	189-290	3A
CENP-C	1-400-His	Wildtype
CENP-C	1-544-His	Wildtype
CENP-H/K	Full length	Wildtype
CENP-H/K	CENP-H^{29-C}, CENP-K^{50-C}	Wildtype
CENP-H/I/K/M	CENP-H/K/M Full length CENP-I^{57-C}	Wildtype
CENP-N/L	Full length	Wildtype
CENP-N	1-212	Wildtype
CENP-M	Full length	Wildtype
CENP-I	57-281	Wildtype
CENP-T/W	Full length	Wildtype
GST	Full length	Wildtype
CENP-A nucleosomes	CENP-A, H4, H2A, H2B full length	Wildtype

4.7 Cell lines

Table 4.8: Cell lines

Cell line	Origin	Inducable protein
Flp-In T-REx HeLa	Human	-
Flp-In T-REx HeLa	Human	eGFP
Flp-In T-REx HeLa	Human	eGFP-CENP-C $^{1-544}$
Flp-In T-REx HeLa	Human	eGFP-CENP-C $^{1-544L265AF266AL267A}$
Flp-In T-REx HeLa	Human	eGFP-CENP-C $^{1-544W317A}$
Flp-In T-REx HeLa	Human	eGFP-CENP-C $^{1-544L265AF266AL267AW317A}$
Flp-In T-REx HeLa	Human	eGFP-CENP-C $^{189-544}$
Flp-In T-REx HeLa	Human	eGFP-CENP-C $^{189-544W317A}$
Flp-In T-REx HeLa	Human	eGFP-CENP-C $^{189-544L265AF266AL267A}$
Flp-In T-REx HeLa	Human	eGFP-CENP-C $^{189-544L265AF266AL267AW317A}$
Flp-In T-REx HeLa	Human	eGFP-CENP-C $^{1-943}$
Flp-In T-REx HeLa	Human	eGFP-CENP-C $^{1-943W317A}$
Flp-In T-REx HeLa	Human	eGFP-CENP-C $^{1-943L265AF266AL267A}$
Flp-In T-REx HeLa	Human	eGFP-CENP-C $^{1-943L265AF266AL267AW317A}$
Flp-In T-REx HeLa	Human	mCherry-CENP-N
Flp-In T-REx HeLa	Human	mCherry-CENP-L
Flp-In T-REx HeLa	Human	mCherry-CENP-I
Flp-In T-REx HeLa	Human	mCherry-CENP-H
Flp-In T-REx HeLa	Human	mCherry-CENP-K

4.8 Plasmids for bacterial expression

All plasmids for bacterial expression of proteins were generated by restriction enzyme based cloning methods.
The gene of interest was amplified in a Polymerase chain reaction (PCR) using the Phusion Flash High-Fidelity PCR Master Mix. PCR primers were designed to introduce restriction sites 5' and 3' of the amplified gene. The generated insert and the target vector were both cut with compatible restriction enzymes following the respective protocols for single and double digestions from New England Biolabs (NEB). Restriction enzymes and buffers were removed with the Wizard SV Gel and PCR Clean-Up System. Digested vector and insert were ligated following the protocol for rapid ligation with T4 DNA ligase from Thermo Scientific. 5 μl of ligated plasmid were transfected into 50 μl chemically competent OmniMax E.coli cells (kindly provided by the Dortmund Protein Facility (DPF), in house), using the standard protocol for transforming chemically competent cells. Plasmids were extracted from single clones with a QIAprep Miniprep Kit or NucleoSpin Plasmid (NoLid) Kit and send to Beckman Coulter Genomics, UK, for sequence verification.

4.8.1 CENP-C

cDNA encoding the human CENP-C sequence (codon optimized from GeneArt, Life Technologies^{TM}) has been subcloned into a pGEX6p-2rbs vector, a modified pGEX-6P vector (GE Healthcare, New Jersey, USA), as a 3' fusion to the sequence encoding GST using the restriction endonucleases BamHI and SalI. The vector encodes for a GST N-terminal of the protein, with an intervening 3C protease site. All CENP-C constructs and mutants purified and used in this work are summarised in **Table** 2.1. All plasmids were sequence verified before usage.

4.8.2 CENP-T/W

A cDNA sequence encoding the human CENP-T isoform was subcloned into the 1st cassette of the vector pGEX-6P-2rbs, as a 3' fusion to the sequence encoding GST by using the restriction endonucleases EcoRI and SalI. In addition a cDNA sequence encoding human CENP W was subcloned into the 2nd cassette of said

vector by using the restriction endonucleases BglII and NotI. Plasmid preparation was performed by Dr. Siva Jeganathan. The plasmid was sequence varified before usage.

4.8.3 CENP-I$^{57-281}$

A synthetic and codon-optimized DNA sequence encoding the human CENP-I$^{57-281}$ was subcloned into a pGEX6p-2rbs vector using the restriction endonucleases BamHI and SalI. Plasmid preparation was performed by Dr. John Weir. The vector was sequence verified before usage.

4.8.4 CENP-N$1-212$

A cDNA sequence encoding the human CENP-N isoform two was subcloned into the vector pST50Tr-DHFRHIS with the restriction enzymes NdeI and NgoMIV, what leads to the formation of an C-terminal cleavable His-tag.

4.8.5 CENP-M

A cDNA segment encoding human CENP-M isoform 1 was subcloned into a pGEX6p-2rbs vector using the restriction endonucleases BamHI and SalI. Plasmid preparation was performed by Dr. Federica Basilico. The vector was sequence verified before usage.

4.9 Site specific mutagenesis

Site-directed mutagenesis methods can be used to generate DNA sequences with mutated codons. Here, site specific mutations were introduced following the Stratagene Quikchange protocol. Concisely, in a Quickchange protocol, mutations are generated by a PCR using a pair of complementary oligonucleotide primers designed with mismatching nucleotides at the center of the primers that encode for the mutation to be introduced. After PCR, the reaction is digested for 1 h with the restriction enzyme DpnI, which only cleaves at methylated sites, so it

cuts within the template plasmid but not within the PCR product. The remaining DNA is transformed into chemically competent OmniMax E.Coli cells (kindly provided by the DPF) from which single clones are picked to extract the plasmid of interest with a MiniPrepKit and send to Beckman Coulter Genomics, UK, for sequence verification. All plasmids were sequence varified before usage.

4.10 Protein expression and purification from E. coli

In order to isolate the overexpressed recombinant protein from the complex mixture of E.coli proteins, all recombinant proteins used for this study expressed in bacteria were processed in a three step purification. Since all proteins purified here were tagged with either a GST- or Histidine-tag, the first purification step comprised an affinity chromatography. In a second step, the protein was either bound to a 5 ml HiTrap Heparin HP column or to a Kat- or Anionexchange column. In the last step, the protein was passed over a size-exclusion chromatography (SEC) column that was appropriate for the proteins size. In these last two steps, elution of proteins was always measured by absorbance measurements at 280 nm using an Äkta Prime system connected to a Windows based laptop running the UNICORN control software. All proteins were flash frozen in liquid nitrogen and stored at -80°C until usage. None of the proteins was reused after thawing.

4.10.1 (GST-)CENP-C constructs

The expression procedure was the same for all CENP-C constructs that were produced in bacterial cells. E. coli C41 (DE3) cells (kindly provided by the DPF) harboring vectors expressing the protein of interest were grown in Terrific Broth (TB) supplemented with 100 μg/ml Ampicillin at 37°C to an OD_{600} of 0.8 - 1.0, then the temperature was reduced to 20°C, when 0.2 mM IPTG was added and the culture was grown at 20°C overnight. Cells were harvested at 4600 g for 15 minutes. Bacterial pellets were resuspended in lysis buffer (20mM HEPES pH 7.5, 500 mM NaCl, 10 % Glycerol, 2 mM β-mercaptoethanol) and directly processed for the protein purification or stored at -20°C. E.coli cells were lysed by sonication and cleared by centrifugation at 100000 g at 4°C for 30 minutes. The cleared lysate

was applied to Glutathione Sepharose 4 Fast Flow beads pre-equilibrated in lysis buffer, incubated at 4°C for 2 h while rotating, washed with 70 volumes of lysis buffer and either eluted with lysis buffer complemented with 20 mM Glutathion or subjected to an overnight cleavage reaction with GST-tagged 3C protease (1 μg 3C protease per 100 μg protein sample, kindly provided by the Dortmund protein facility (DPF), in house). A 5 ml HiTrap Heparin HP column was pre-equilibrated in a mixture of 90 % buffer A (20 mM HEPES pH 7.5, 5 % Glycerol, 2 mM β mercaptoethanol) and 10 % buffer B (20 mM HEPES pH 7.5, 2 M NaCl, 5 % Glycerol, 2 mM β marcaptoethanol). The eluate from Glutathione beads was diluted with buffer A to reach a final concentration of 200 mM NaCl, loaded onto the Heparin column and eluted with a linear gradient of buffer B from 200 to 1200 mM NaCl in 20 bed column volumes. Fractions containing GST-CENP-C constructs or untagged CENP-C constructs were concentrated, depending on the proteins size, in 3-50 kDa molecular weight cut-off Vivaspin concentrators and loaded onto a Superdex 200 size-exclusion chromatography (SEC) column, pre-equilibrated in SEC buffer (10 mM HEPES pH 7.5, 2.5 % Glycerol, 300 mM NaCl, 1 mM TCEP). SEC was performed under isocratic conditions. To obtain fractions containing GST-CENP-C or CENP-C constructs, they were run on a 10 - 14 % SDS PAGE gel and visualized with coomassie brilliant blue staining solution (2.5 % coomassie brilliant blue R250, 2.5 % coomassie brilliant blue R250, 50 % Ethanol, 10 % Acetic acid). Appropriate fractions were concentrated, flashfrozen in liquid nitrogen and stored at -80°C.

The expression and purification procedure was the same for all CENP-C constructs, except for the gradient in the Heparin column step. Since some constructs were highly sensitive to NaCl concentrations lower than 300 mM, they were only diluted to that concentration and loaded to a Heparin column at 15 % buffer B. The gradient was adjusted accordingly.

Coomassie stained gels and chromatograms for the purification procedure of GST-CENP-C$^{2-545}$ with and without cleavage of the tag is shown as a representative example in **Section** 2.2.

4.10.2 CENP-T/W

Escherichia coli Rosetta2 (DE3) cells were transformed with the produced CENP-T/W vector according to standard protocols and grown in LB Medium supplemented with 100 μg/ml Ampicillin at 37°C to an OD_{600} of ∼0.8-1 before being

cooled to 20°C. 0.3 mM IPTG was added and the bacterial cell culture was grown at 20°C for ∼20 hours. Subsequently the cells were pelleted via centrifugation for 15 min at about 4600 g. Cell pellets were resuspended in lysis buffer containing 50 mM Tris/HCl pH 6.8, 300 mM NaCl, 10% glycerol, 1mM EDTA, 2 mM DTT and Protease Inhibitor Mix HP Plus and stored at -20°C.
Cell pellets were thawed, lysed by sonication and cleared by centrifugation at 48,000 g at 4°C for 1h. The cleared lysate was applied to Glutathione Sepharose 4 Fast Flow beads, pre-equilibrated in working buffer (50 mM Tris/HCl pH 6.8, 300 mM NaCl, 10% glycerol, 1mM EDTA, 2mM DTT), incubated at 4°C for 2h, washed with 10 column volumes of working buffer and subjected to an overnight cleavage reaction with GST-tagged 3C protease (1 μg 3C protease per 100 μg protein sample) to cleave off the GST-tag from CENP-T within the CENP-T/W complex. Untagged CENP-T/W complex was separated from the beads via centrifugation. The sample was concentrated to 5 ml using an Amicon Ultra Centrifugal Filter having a 30kDa cut-off and then diluted 10 fold with buffer A (50mM Tris/HCl pH 6.8, 5% glycerol, 1mM EDTA, 2mM DTT) in order to obtain a final NaCl concentration of 30 mM and loaded onto a Resource S anion exchange column, pre-equilibrated in buffer A. The sample was eluted from the column with a linear gradient of 3 - 100% of buffer B (50mM Tris/HCl pH 6.8, 1M NaCl, 5% glycerol, 1mM EDTA, 2mM DTT) in 20 column bed volumes. Fractions containing the CENP-T/W complex were concentrated and loaded onto a Superdex 200 10/300 column or onto a Superdex 200 16/600 column pre-equilibrated in gelfiltration buffer (20mM HEPES pH 7.5, 300 mM NaCl, 5% glycerol, 1 mM TCEP). Fractions containing the CENP-T/W complex were concentrated, flash-frozen in liquid nitrogen and stored at -80°C. Protein purification was performed by Doro Vogt.

4.10.3 CENP-I$^{57-281}$

E. coli C41 (DE3) cells harboring vectors expressing CENP-I$^{57-281}$ were grown in TB supplemented with 100 μg/ml Ampicillin at 37°C to an OD_{600} of ∼0.6, then the temperature was reduced to 18°C and 0.2 mM IPTG was added when the culture reached OD_{600} of ∼1.0 - 1.5. The culture was grown at 18°C overnight. Cells were harvested at 4600 g for 15 minutes. Bacterial pellets were resuspended in lysis buffer (50mM HEPES pH 7.5, 500 mM NaCl, 5 mM $MgCl_2$, 10 % Glycerol, 5 mM β mercaptoethanol) and directly processed for the protein purification or

stored at -20°C.

E.coli cell pellets were lysed by sonication and cleared by centrifugation at 100000 g at 4°C for 30 minutes. The cleared lysate was applied to Glutathione Sepharose 4 Fast Flow beads pre-equilibrated in lysis buffer, incubated at 4°C for 2 h while rotating, washed with 70 volumes of lysis buffer supplemented with 1M NaCl and eluted in 50mM HEPES pH 7.5, 500 mM NaCl, 5 mM $MgCl_2$, 10 % Glycerol, 5 mM β mercaptoethanol, 30 mM reduced glutathione. The eluted protein was subjected to an overnight cleavage reaction with GST-tagged 3C protease (1 μg 3C protease per 100 μg protein sample) while it was dialized against Resource S buffer A (20 mM MES pH 6.5, 100 mM NaCl, 5 % Glycerol, 5 mM β mercaptoethanol) at 4°C over night. A 6 ml Resource S cation exchange column was pre-equilibrated in Resource S buffer A. The cleaved and dialyzed protein was loaded onto the Resource S column and eluted with a linear gradient of buffer B from 100 to 1000 mM NaCl in 20 bed column volumes. The cleaved GST appears in the flow through of the column. CENP-I^{57-281} containing fractions that were not nucleic acid contaminated were concentrated in 10 kDa molecular weight cut-off Vivaspin concentrators and loaded onto a Superdex 75 10/300 column or onto a Superdex 75 16/600 column pre-equilibrated in gelfiltration buffer (20mM HEPES pH 7.5, 300 mM NaCl, 5% glycerol, 1 mM TCEP). Fractions containing the CENP-I^{57-281} complex were concentrated, flash-frozen in liquid nitrogen and stored at -80°C.

4.10.4 CENP-N^{1-212}His

E. coli C41 (DE3) cells harboring vectors expressing CENP-N^{1-212}His were grown in TB supplemented with 100 μg/ml Ampicillin at 37°C to an OD_{600} of 0.8 - 1.0, then the temperature was reduced to 20°C, when 0.2 mM IPTG was added and the culture was grown at 20°C overnight. Cells were harvested at 4600 g for 15 minutes. Bacterial pellets were resuspended in lysis buffer (50 mM HEPES pH 7.5, 500 mM NaCl, 10 mM $MgCl_2$, 10 % Glycerol, 20 mM Imidazol, 1 mM TCEP, 1 mM PMSF) and directly processed for the protein purification or stored at -20°C. E.coli cell pellets were lysed by sonication and cleared by centrifugation at 100000 g at 4°C for 30 minutes. The cleared lysate was applied to Ni-NTA Agarose beads and incubated at 4°C for 2 h while rotating, washed with 70 volumes of lysis buffer (without PMSF) and eluted with lysis buffer complemented with 300 mM Imidazol. A 6 ml Resource S cation exchange column was pre-equilibrated in 15 % Resource S buffer B (20 mM HEPES pH 7.5, 1 M NaCl, 10 mM $MgCl_2$, 10 %

Glycerol, 1 mM TCEP) and 85 % Resourse S buffer A (20 mM HEPES pH 7.5, 10 mM $MgCl_2$, 10 % Glycerol, 1 mM TCEP). CENP-N^{1-212}His was diluted with buffer A to reach a final concentration of 150 mM NaCl, loaded onto the Resource S cation exchange column and eluted with a linear gradient of buffer B from 150 to 1000 mM NaCl in 15 bed column volumes. Fractions containing CENP-N^{1-212}His were concentrated in 10 kDa molecular weight cut-off Vivaspin concentrators and loaded onto a Superdex 75 SEC column, pre-equilibrated in SEC buffer (10 mM HEPES pH 7.5, 2.5 % Glycerol, 300 mM NaCl, 1 mM TCEP). SEC was performed under isocratic conditions. To obtain fractions containing CENP-N^{1-212}His, they were run on a 14 % SDS PAGE gel and visualized with coomassie brilliant blue staining solution. Appropriate fractions were concentrated, flashfrozen in liquid nitrogen and stored at -80°C.

4.10.5 CENP-M

Escherichia coli C41 (DE3) cells harboring vectors expressing CENP-M were grown in TB at 37°C to an OD_{600} of 0.6 - 0.8, when 0.2 mM IPTG was added and the culture was grown at 18°C for ∼15 hours. Cell pellets were resuspended in lysis buffer (50 mM Tris/HCl pH 7.4, 300 mM NaCl, 5 % glycerol, 1 mM DTT) supplemented with protease inhibitor cocktail, lysed by sonication and cleared by centrifugation at 48,000 g at 4°C for 1 hour. The cleared lysate was applied to Glutathione Sepharose 4 Fast Flow beads pre-equilibrated in lysis buffer, was incubated at 4°C for 2 hours, washed with 70 volumes of lysis buffer and subjected to an overnight cleavage reaction with GST-tagged 3C protease to separate CENP-M from GST. A Resource S cation exchange column was pre-equilibrated in 20 mM MES pH 6.0, 50 mM NaCl, 5 % glycerol, 1 mM DTT. The eluate from Glutathione beads was adjusted to a final salt concentration of 50 mM, loaded onto the Resource S column and eluted with a linear gradient of 50 - 500 mM NaCl in 10 column bed volumes. Fractions containing CENP-M were concentrated and loaded onto a Superdex75 SEC column pre-equilibrated in SEC buffer (10 mM MES pH 6.0, 150 mM NaCl, 1 mM TCEP). Fractions containing CENP-M were concentrated, flash-frozen in liquid nitrogen and stored at -80°C. Protein purification was performed by Dr. Federica Basilico.

4.10.6 CENP-A nucleosomes

The reconstitution and purification of CENP-A nucleosomes, which consist of CENP-A, H4, H2A, H2B and a short sequence of centromeric DNA, was accomplished with slight modifications in accordance with a protocol from the prior art [308].

In summary: A cDNA encoding for CENP-A and a cDNA encoding for H4 were cloned into a polycistronic expression vector, co-expressed in E. coli and purified as CENPA/H4 as tetramers. A cDNA encoding for H2A was cloned into pET3, expressed in E. coli and purified. A cDNA encoding for H2B was cloned into pET3, expressed in E. coli and purified. Then purified H2A and H2B were mixed in equal amounts to reconstitute H2A/H2B dimers. A cDNA fragment of centromeric DNA with eight repeats of the 601-145 bp sequence was cloned into pUC57 and transformed into E. coli, amplified, purified and isolated from its host vector via restriction endonucleases digestion. Finally, CENPA/H4 tetramers, H2A/H2B dimers and centromeric DNA were mixed to reconstitute CENP-A nucleosomes. Protein purification of the histones and DNA amplification was performed by Doro Vogt. Nucleosome assembly was done by Doro Vogt and Dr. Federica Basilico.

4.11 Protein production with the MultiBac expression system

Some of the proteins and protein complexes used in this study, failed to be expressed and purified in good yields from E.coli cells. Since some recombinant proteins depend on a eukaryotic host cell machinery for expression, proper folding, post-translational modification etc. we decided to express and purify these proteins with help of a Baculovirus expression vector system, the MultiBac expression system. This system is based on the introduction of a gene of interest into a baculo-viral genome by homologous recombination. In the resulting recombinant Baculovirus one nonessential gene is replaced with the gene encoding the protein of interest which can be expressed in cultured insect cells.

4.12 Plasmids for insect cell expression

All genes for insect cell expression were subcloned into either a PFL, PFG or PFH vector [309], [310]. As for bacterial expression plasmids, all plasmids for insect cell expression of proteins were generated by a restriction enzyme based cloning method as explained in **Section** 4.8. All plasmids were sequence verified before usage.

4.12.1 CENP-C$^{1-544}$-His

cDNA encoding the human CENP-C sequence (codon optimized from geneart) has been subcloned into a PFL vector. The gene encoding for amino acids 1-544 of CENP-C was amplified in a Polymerase chain reaction as described above. The 3' primer was designed in such way that a non-cleavable histidine-tag comprised of 6 histidines was introduced C-terminal of the protein. The construct was introduced into the vector by restriction digestion through the enzymes BamHI and SalI.

4.12.2 CENP-C$^{1-400}$-His

cDNA encoding the human CENP-C sequence (codon optimized from geneart) has been subcloned into a PFL vector. The gene encoding for amino acids 1-400 of CENP-C was amplified in a Polymerase chain reaction as described above. The 3' primer was designed in such way that a non-cleavable histidine-tag comprised of 6 histidines was introduced C-terminal of the protein. The construct was introduced into the vector by restriction digestion through the enzymes BamHI and SalI.

4.12.3 CENP-C$^{189-400}$

cDNA encoding the human CENP-C sequence (codon optimized from geneart) has been subcloned into a PFG vector. The gene encoding for amino acids 189-400 of CENP-C was amplified in a Polymerase chain reaction as described above. The construct was introduced into the vector by restriction digestion through the enzymes BamHI and SalI.

4.12.4 CENP-H/CENP-K-His

A cDNA segment encoding human CENP-K was subcloned in pFH vector as a C-terminal fusion to His-tag, with an intervening TEV protease site, while a cDNA segment encoding human CENP-H was subcloned in pUCDM vector, without any tag. Constructs were sequence verified. The two vectors were then fused via *in vitro* Cre-loxP recombination as described in **Section** 4.13. Construct design was performed by Lucia Massimiliano.

4.12.5 CENP-H^{29-C}/His-CENP-K^{50-C}

The vector encoding for CENP-H/His-CENP-K was produced as described in **subsection ??**, but the forward primers were designed in such a way that they start at residue 29 of CENP-H and 50 of CENP-K.

4.12.6 CENP-H/I^{57-C}/K/M

A synthetic and codon-optimized DNA sequence coding for human CENP-I$^{57-756}$ (also referred to as CENP-I^{57-C}) was amplified via PCR from the full length DNA coding for human CENP-I$^{1-756}$ and was then subcloned into the 1st multiple cloning site (MCS) of a MultiBac pFL-derived vector [309], [310] also referred to as pFH with an N-terminal 6xHis tag cleavable by TEV-protease (tobacco etch virus protease), under the control of the polh promoter using the restriction sites for the restriction endonucleases BamHI and SalI. Subsequently, a cDNA segment encoding human CENP-M isoform 1 was subcloned into the 2nd MCS of the same vector using the restriction endonucleases XmaI and NheI, under the control of the p10 promoter. Simultaneously, a second MultiBac pFL vector [309], [310] was created with an untagged and codon-optimized cDNA sequence coding for human CENP-H and an untagged and codon-optimized cDNA sequence coding for CENP-K under the control of the polh and p10 promoters, respectively, and cloned by using the same restriction endonuclease combinations as above for CENP-I and CENP-M. The vector containing CENP-I^{57-C} and CENP-M was then linearized by use of the restriction endonuclease BstZ17I. Then, the expression region of the vector containing CENP-H and CENP-K was amplified via polymerase chain reaction by use of a forward primer and a reverse primer designed for sequence and

ligation independent cloning (SLIC) of the PCR fragment into the linearized vector containing CENP-I^{57-C} and CENP-M. The SLIC reaction was then carried out to produce a single pFL-based vector with four expression cassettes, thus resulting in a pFL-based vector harboring CENP-H, CENP-K, CENP-I^{57-C} and CENP-M (also referred to as CENP-H/I^{57-C}/K/M). Construct design was performed by Dr. John Weir. The constructs were sequence verified.

4.12.7 CENP-N/L

A cDNA sequence coding for human CENP-L was cloned into the first MCS of a Multi-Bac pFL-derived vector, which we refer to as pFG, containing an N-terminal GST fusion followed by a 3C protease cleavage site. Cloning was done using the restriction endonucleases BamHI and SalI and GST-tagged CENP-L was placed under control of the polh promotor. After successful generation of the GST-tagged CENP-L construct, a cDNA sequence coding for human full-length CENP-N was cloned into the 2nd MCS using the restriction endonucleases XmaI and XhoI and placed under control of the p10 promotor. Construct design was performed by Dr. John Weir. The constructs were sequence verified.

4.12.8 Mis12 complex

The complete cDNA sequences coding for individual Mis12 complex subunits were cloned in pFL vector. Briefly, a cDNA sequence coding for Nnf1 and a cDNA sequence coding for Mis12 were subcloned into the 1st and 2nd multiple cloning site of a MultiBac pFL vector respectively. In parallel, a cDNA sequence coding for DSN1 (carrying a non-cleavable C-terminal 6xHis tag) and a cDNA sequence coding for Nsl1 subunit were subcloned into the 1st and 2nd multiple cloning site of a MultiBac pFL vector respectively. pFL vectors coding for individual Mis12 subcomplexes (Nnf1/Mis12 or Dns1-6xHis/Nsl1) were recombined with bacmid DNA via transformation of DH10EMBacY cells and selected via blue-white screening. Construct design was performed by Sabine Wohlgemuth. The constructs were sequence verified.

4.13 Virus production and protein expression in insect cells

Bacoluviruses for all vectors described above were produced according to [310]. In summary, plasmids encoding for the proteins of interested were transformed into DH10EMBacY cells with the standard protocol for plasmid transformation, except that the recovery time at 37°C was extended to 6 h. These cells contain the baculovirus genome as a bacterial artificial chromosome in which they are able to integrate the chosen multigene fusion plasmid. Transformed cells were plated on LB plates competed with 10 μg/ml Gentamycin, 7 μg/ml Tetracyclin, 50 μg/ml Kanamycin, 40 μg/ml IPTG and 100 μg/ml X-Gal. The E.coli cells contain a helper plasmid that expresses the Tn7 transposon complex upon induction with IPTG. Selection of positive integrands occurs via blue-white screening, positive clones are white. Single white clones were used for plasmid amplification in LB complemented with 10 μg/ml Gentamycin, 7 μg/ml Tetracyclin, 50 μg/ml Kanamycin 37 °C, shaking over night. The plasmid was extracted with the QIAprep Miniprep Kit, but instead of loading the DNA onto the QuIAPrep column that is contained in the Kit, it is precipitated with 50 % Isopropanol at -20°C over night. The DNA was washed twice with 70 % Ethanol and resuspended in Tris-EDTA buffer. The DNA was transfected with FuGENE into Sf-9 cells, an immortalized cell line isolated from *Spodoptera frugiperda*, at a density of $1 \cdot 10^6$/ml in a 6 well plate. Cells were incubated for 48 h at 27°C to allow cells integrate the target DNA into their genome and virus production to occur. Then 1 ml of the supernatant was transferred to a 10 cm dish with 10 ml fresh Sf-9 cells at $1 \cdot 10^6$/ml final volume. Virus amplification was allowed for 72 h at 27°C. The supernatant from the dish was safed as Virus_0 and stored at 4°C complemented with 5 % BSA (bovine serum albumin). Cells of the 10 cm dish were collected and tested in a small scale affinity chromatography to obtain efficiency of protein production. For this small scale test chromatography, cells were resuspended in 2 ml lysis buffer (20mM HEPES pH 7.5, 500 mM NaCl, 10 % Glycerol, 1 mM TCEP) and lysed by sonycation. Lysated were cleared at 17000 g for 30 minutes and loaded (dependent on the tag of the protein) to 25 μl of either Glutathione Sepharose 4 Fast Flow beads or NickelNTA-Superose Beads pre-equilibrated in lysis buffer. After incubation at 4°C for 2 h while rotating, beads were washed five times with 1 ml lysis buffer and proteins eluted in 25 μl lysis buffer complemented with either 20 mM Glutathion or 200 mM Imidazol. Samples for the full fraction,

cleared lysates and the elution from the beads were loaded on an SDS-PAGE. If the protein production was found to be efficient, virus V_1 and V_2 was produced by infecting Sf-9 cells at $1 \cdot 10^6$/ml with 1:100 V_0 or V_1, respectively and incubated at 27°C shaking. The V_2 was used to set up a test expression to find the optimal conditions for protein expression in Tnao38 insect cells, an immortalized cell line derived from *Trichoplusia ni*. For each protein V_2 dilutions of 1:10, 1:40 and 1:80 were tested for 48 h and 72 h. 10 ml of each condition was tested in a small scale affinity chromatography, as described for the V_0 protein production test. The coomassie stained gel of the small scale affinity chromatography from CENP-C^{1-544}-His expression test in Tnao38 cells is shown in the **Supplementary Figure** 5.11.
Based on the coomassie stained gel, the optimal viral dilution and expression time were chosen. For preparative scale purification of recombinant proteins, large scale expressions with at least 500 ml were set up. Cells were harvested at 1500 g for 15 minutes. Pellets were resuspended in PBS and spun again, before the supernatant was removed and pellets were flash frozen in liquid nitrogen and stored at -80° or processed directly.

4.13.1 Protein purification from insect cells

The general protocol for the purification of proteins from insect cells did not differ significantly from the purification from E.coli cells. The lysates were cleared by centrifugation at 100000 g at 4°C for 1 hour instead of 30 minutes. The detailed purification protocols for the recombinant proteins expressed in insect cells used in this study are specified below.

4.13.2 CENP-C^{1-544}-His

Tnao38 cells expressing CENP-C^{1-544}-His were resuspended in lysis buffer (20 mM HEPES pH 7.5, 500 mM NaCl, 10 % Glycerol, 2 mM β-mercaptoethanol) and lysed by sonycation before centrifugation at 100000 g at 4°C for 1 h and incubation of the cleared lysates with Ni-NTA Agarose beads 4°C for 2 h. After washing with 70 column volumes of lysis buffer, CENP-C^{1-544}-His was diluted to 300 mM NaCl with buffer A (20 mM HEPES pH 7.5, 5 % Glycerol, 1mM TCEP) and loaded to a pre-equlibrated HiTrap Heparin HP column and eluted with a linear gradient of

buffer B (20 mM HEPES pH 7.5, 2 M NaCl, 5 % Glycerol, 1 mM TCEP) from 300 to 1200 mM NaCl. Fractions containing CENP-C^{1-544}-His were loaded to a Superdex 200 16/60 SEC column pre-equilibrated in SEC buffer (10 mM HEPES pH 7.5, 200 mM NaCl, 2.5 % Glycerol, 1 mM TCEP). Fractions containing CENP-C^{1-544}-His were concentrated, flash-frozen in liquid nitrogen and stored at -80°C. Coomassie stained gels and chromatograms for the purification procedure of CENP-C^{1-544}-His is shown in the **Figure** 2.4.

4.13.3 CENP-H/His-CENP-K

Cell pellets were resuspended in lysis buffer (50 mM Tris/HCl pH 8.0, 300 mM NaCl, 20 mM Imidazole, 5 % Glycerol, 2 mM β-mercaptoethanol) supplemented with protease inhibitor cocktail, lysed by sonication and cleared by centrifugation at 100000 g at 4°C for 1 h. The cleared lysate was applied to Ni-NTA Agarose beads pre-equilibrated in lysis buffer, incubated at 4°C for 2 h and washed with 70 volumes of lysis buffer. Tag cleavage was performed in an over night incubation with TEV protease (kindly provided by the DPF, in house). The complex was diluted to a final concentration of 75 mM NaCl with buffer A (50 mM Tris/HCl pH 8.0, 5 % Glycerol, 1 mM TCEP). A 6ml Resource Q anion exchange chromatography column was pre-equilibrated in a mixture of 92.5 % buffer A and 7.5 % buffer B (50 mM Tris/HCl pH 8.0, 1 M NaCl, 5 % Glycerol, 1 mM TCEP). CENP-H/K was loaded onto the Resource Q column and eluted with a linear gradient of buffer B from 75 to 500 mM NaCl in 10 bed column volumes. Fractions containing CENP-H/K complex were concentrated in 10 kDa molecular weight cut-off Vivaspin concentrators and loaded onto a Superdex 200 SEC column pre-equilibrated in SEC buffer (10 mM HEPES pH 7.5, 150 mM NaCl, 1 mM TCEP). SEC was performed under isocratic conditions at a flow rate of 0.5 ml/min. Fractions containing CENP-H/K complex were concentrated up to 10 mg/ml, flash-frozen in liquid nitrogen and stored at -80°C. Purification was performed in collaboration with Dr. Federica Basilico.

4.13.4 CENP-H^{29-C}/His-CENP-K^{50-C}

CENP-H^{29-C}/His-CENP-K^{50-C} was purified with the same protocol as CENP-H/CENP-K-His full length complex.

4.13.5 CENP-N/L

Tnao38 cells were infected at a density between $1.5 - 2 \cdot 10^6$/ml using a viral titer of 1:40. Infected Tnao38 cells were cultured at 27°C for 72 hours before being harvested. Careful testing revealed that it was not possible to freeze these cells, as doing so would result in insoluble CENP-N/L complexes. Therefore, purification was done immediately after harvesting the cells. Pellets equivalent to 2.5 L of Tnao38 cell culture containing GST-tagged CENP-N/L were resuspended in buffer (50 mM HEPES pH 7.5, 300 mM NaCl, 10 % glycerol, 1 mM $MgCl_2$, 10 mM β-mercaptoethanol, 0.1 mM 4-(2-Aminoethyl) benzenesulfonyl fluoride (AEBSF), and 2.5 units/mL Benzonase). Cells were lysed by sonication and cleared by centrifugation at 100,000 g for 1 hour at 4°C. The cleared lysate was incubated for 30 minutes with GSH-Sepharose 4 Fast Flow resin that was pre-equilibrated in buffer (50 mM HEPES pH 7.5, 300 mM NaCl, 10 % glycerol, 10 mM β-mercaptoethanol). After incubation the lysate-resin slurry was transferred to gravity flow chromatography columns, and the lysate was allowed to flow through said column. The resin was extensively washed in buffer (50 mM HEPES pH 7.5, 300 mM NaCl, 10 % glycerol, 10 mM β-mercaptoethanol) and then washed with 2 column volumes of buffer (50 mM HEPES pH 7.5, 1 M NaCl, 10 % glycerol, 10 mM β-mercaptoethanol). The resin was then returned to the 300 mM NaCl containing buffer (50 mM HEPES pH 7.5, 300 mM NaCl, 10 % glycerol, 10 mM β-mercaptoethanol), before the bound GST-tagged CENP-N/L complex was eluted in buffer (50 mM HEPES pH 7.5, 300 mM NaCl, 10 % glycerol, 10 mM β-mercaptoethanol, 30 mM reduced glutathione). The eluted GST-tagged CENP-N/L complex was then incubated at 4°C for several hours with a sufficient quantity GST-tagged 3C protease (usually 1 μg 3C protease per 100 μg protein sample to be cleaved) to remove the GST tag from CENP-L to obtain an untagged CENP-L in complex with untagged CENP-N.

A 5 mL GSH-Sepharose fast flow column was connected to the outlet of a SuperdexTM 200 16/600 column, so that the columns were connected in series, and both columns were equilibrated with a buffer containing 20 mM HEPES pH 7.5, 300 mM NaCl, 2.5 % Glycerol and 4 mM TCEP. The eluted and untagged CENP-N/L complex was concentrated in a 30 kDa centrifugal concentrator, and then loaded onto said S200 16/60 column connected to said GSH-Sepharose FF column. Both free GST (cleaved off), GST-tagged 3C protease and any residual, uncleaved GST-tagged CENP-N/L complex was captured on the GSH-sepharose FF column.

Fractions containing CENP-N/L complex were confirmed by SDS-PAGE, concentrated, and flash frozen in liquid nitrogen and stored at -80°C. Purification was performed by Dr. John Weir with kind help of Nina Ludwigs and Ingrid Hoffmann.

4.13.6 CENP-H/I^{57-C}/K/M

Expression of CENP-H/I^{57C}/K/M complex was carried out in TnAo38 cells, using a virus:culture ratio of 1:40. Infected cells were incubated for 72 hr at 27°C. For one round of purification of the CENP-H/I^{57-C}/K/M complex, pellets equivalent to 2.5 L of cell culture were thawed and resuspended in buffer containing 50 mM HEPES pH 7.5, 300 mM NaCl, 1 mM MgCl2, 10 % glycerol, 5 mM imidazole, 5 mM β-mercaptoethanol, 0.1 mM AEBSF and 2.5 units/mL Benzonase. Following resuspension, cells were lysed by sonication and the crude cell lysate was then cleared by centrifugation for 1h at 100000 g at 4°C. The cleared cell lysate was then loaded onto a 5 mL TALON^{TM} column, and then washed extensively with buffer (50 mM HEPES pH 7.5, 300 mM NaCl, 1 mM MgCl2, 10 % glycerol, 5 mM imidazole, 5 mM β-mercaptoethanol), followed by a short wash step with buffer (50 mM HEPES pH 7.5, 1000 mM NaCl, 1 mM MgCl2, 10 % glycerol, 5 mM imidazole, 5 mM 2-mercaptoethanol). Intact CENP-H/I^{57-C}/K/M complex was eluted using a gradient of 5-400 mM imidazole, over 20 column volumes. The fractions containing the complex were confirmed by SDS-PAGE, which were then pooled, and the 6xHis tag on CENP-I^{57-C} was cleaved overnight using TEV protease resulting in a CENP-H/I^{57-C}/K/M complex with untagged CENP-I^{57-C}. On the following day the obtained CENP-H/I^{57-C}/K/M complex was mixed with sufficient water and 1M 2-(N-morpholino)ethanesulfonic acid (MES, pH 5.5) to dilute the 300 mM NaCl to 150 mM and to change the pH to 6.5. The sample was then loaded onto a 6 mL Resource S column, equilibrated in 20 mM MES (pH 6.5), 150 mM NaCl, 5 % glycerol, 5 mM β-mercaptoethanol. After loading the column was washed with 4 column volumes of equilibration buffer and then CENP-H/I^{57-C}/K/M complex was eluted from the column using a gradient of 150-1000 mM NaCl over 20 column volumes and elution was measured by absorbance measurements at 280 nm using an Äkta Prime system connected to a Windows based laptop running the UNICORN control software. Fractions were collected, and subsequently run on a 14 % SDS-PAGE gel stained with coomassie brilliant blue. The peak corresponding to the elution was pooled, concentrated, and then run over a Superdex^{TM} 200 16/600 column equilibrated in 20 mM HEPES pH 7.5,

300 mM NaCl, 5 % glycerol, 2 mM TCEP. The peak corresponding to CENP-H/I^{57-C}/K/M was again pooled, concentrated in a 100 kDa MWCO concentrator and then flash frozen in liquid nitrogen and stored at -80 °C. Purification was performed by Dr. John Weir with kind help of Nina Ludwigs and Ingrid Hoffmann.

4.13.7 CENP-C$^{1-544}$/H/I^{57-C}/K/L/M/N/CENP-A^{nucleosome}

CENP-C$^{1-544}$, CENP-N/L complex and CENP-H/I^{57-C}/K/M complex were pre-purified as described in **Section** 4.13.2, 4.13.5 and 4.13.6. CENP-C$^{1-544}$ was subsequently incubated with a 1.2 fold molar excess of both pre-purified CENP-H/I^{57-C}/K/M complex and pre-purified CENP-N/L complex for 1-2 h on ice in equilibration buffer (20 mM HEPES pH 7.5, 300 mM NaCl, 2.5 % glycerol, 4 mM TCEP). The sample containing the resulting CENP-C$^{1-544}$/H/I^{57-C}/K/L/M/N complex was then loaded onto a Superose 6 16/70 column (custom made by GE Healthcare and having column bed dimension of 16 mm in diameter and 700 mm in height and containing preparative grade Superose 6) equilibrated in equilibration buffer. Fractions containing the complete CENP-C$^{1-544}$/H/I^{57-C}/K/L/M/N complex were confirmed by SDS-PAGE and then pooled.
The resulting CENP-C$^{1-544}$/H/I^{57-C}/K/L/M/N complex was bound to CENP-A nucleosomes by incubating them at 4°C in a 2.5 fold molar excess of the purified CENP-C1-544/H/I57-C/K/L/M/N complex in buffer (20 mM HEPES pH 7.5, 300 mM NaCl, 2.5 % glycerol, 2 mM TCEP) on ice for at least 2h. Herein, it has proven to be important to carry out this reaction in 300 mM NaCl, as at lower concentrations significant precipitations occur. The complex of CENP-C$^{1-544}$/H/I^{57-C}/K/L/M/N together with CENP-A nucleosomes was further purified on a Superose 6 10/300 column. Using centrifugal concentrators on this sample is problematic here, so a PEG6000 precipitation method as recently described for protein:nucleosome complexes [311] was used to pellet the complex. Pellets containing the complex were resuspended in buffer containing 20 mM HEPES pH 7.5, 300 mM NaCl, 2.5 % glycerol and 4 mM TCEP. However, attention has to be paid not to subject the sample to freeze and thaw cycles, since this will disrupt the nucleosomes. As such samples were either used immediately, or stored at 4°C. This complex was prepared in collaboration with Dr. John Weir and Dr. Federica Basilico.

4.13.8 Mis12 complex

Individual baculoviruses containing either full-length Nnf1/Mis12 or Dsn1-6xHis/Nsl1 were produced separately, as described previously [310]. High-titer V_2 virus was produced in the manner already described in **Section** 4.13. For the expression of Mis12 complex, V_2 viral stocks (generated in parallel for Nnf1/Mis12 and Dsn1-6xHis/Nsl1 sub-complexes) were used for co-infection (at a 1:20 dilution) of Tnao38 38 cells (at a cell density of $1 \cdot 10^6$ cells/mL) following which the cells were cultured for additional 96 hours at 27°C, before being harvested, washed in 1xPBS and stored at -80°C. Transfected Tnao38 cells were lysed in buffer A1 (20 mM Tris pH 8.0, 300 mM NaCl, 5 % glycerol and 2 mM β-mercaptoethanol) supplemented with protease inhibitor cocktail mix. Cells were sonicated, spun down (100.000g for 60 min) and loaded onto a 2x5 ml crude Ni-NTA columns equilibrated in buffer A1. The sample was additionally filtered through 0.8 μm filter paper before loading onto a Ni-NTA column. Following sample loading the column was washed with 500 ml buffer A1 (supplemeted with 20 mM imidazole), followed by step elution in buffer A1 (supplemented with 300 mM imidazole). Relevant fractions were pooled, and diluted (or dialyzed) into a buffer A2 (20 mM Tris pH 8.0, 30 mM NaCl, 1 mM EDTA and 1 mM TCEP). The Sample was loaded onto a Resource Q column (GE Healthcare) and eluted using a linear gradient (buffer A2 with 300 mM NaCl) over 20 column volumes. Relevant fractions were pooled, concentrated and loaded onto a Superdex 200 16/600 column (previously equilibrated in SEC buffer 20 mM Tris pH 8.0, 150 mM NaCl and 1 mM TCEP). Relevant fractions were pooled, concentrated and snap-frozen in liquid nitrogen and stored at -80°C. Protein purification as performed by Sabine Wohlgemuth.

4.14 GST pulldown assays

All GST pulldown experiments shown here were performed using preblocked GSH Sepharose beads (for detailed protocol see **Section** 4.14.1). Furthermore, they were all performed in the same buffer conditions (10mM HEPES pH 7.5, 200 mM NaCl, 0.05 % Triton, 2.5 % Glycerol, 1 mM TCEP). GST-CENP-C various constructs always served as bait at a 1 μM concentration, whereas potential binding partners served as prey at a 3 μM concentration. The bait was loaded to 6 μl preblocked beads first, before the prey was added. At the same time, 1 μg of

each protein was added into Laemmli sample loading buffer for the input gel. The reaction volume was added up to 40 μl with buffer and incubated at 4°C for 1 h, shaking. Subsequently, beads were spun down at 500 *g* for 3 minutes. The supernatant was removed and beads washed twice with 250 μl buffer (500 *g*, 1 minute). After the last washing step, supernatant was removed completely, samples boiled in 15 μl Laemmli sample loading buffer and run on a 14 % SDS-PAGE gel. Bands were visualized with coomassie brilliant blue staining.

4.14.1 Preblocking of GSH sepharose beads

750 μl of GSH Sepharose beads (which consist of 2/3 beads and 1/3 storage buffer) were washed twice with 1 ml washing buffer (20 mM HEPES pH 7.5, 150 mM NaCl) and incubated in 1 ml blocking buffer (20mM HEPES pH 7.5, 500 mM NaCl, 500 μg/ml BSA) over night at 4°C rotating. After incubation, beads were washed 5 times with 1 ml washing buffer and resuspended in 500 μl washing buffer to have a 50/50 slurry of beads and buffer.

4.15 Analytical Size exclusion chromatography (SEC) migration shift assays

For analytical SEC experiments, proteins were mixed in 50 μl final volume (usually in a 1:1 stoichiometry, unless a different stochimetry of the binding partners was assumed), incubated for at least 1 h on ice and subjected to a calibrated Superdex 200 5/150 column. All samples were eluted under isocratic conditions at 4°C in SEC buffer (10 mM HEPES pH 7.5, 300 mM NaCl, 2.5 % Glycerol, 2 mM TCEP) at a flow rate of 0.2 ml/min. Elution of proteins was monitored at 280 nm. 100 μl fractions were collected and analyzed by SDS-PAGE and Coomassie blue staining. Complex formation was judged from the elution profile in the chromatogram and the coomassie stained gels.

4.16 Limited proteolysis

For limited proteolysis on CENP-C^{2-545}, CENP-H/K, CENP-H/I/K/M and the complexes, the proteins were subjected to cleavage by five proteases with different cleavage sites: Trypsin (cuts at Arg and Lys), Elastase (cuts at Ala and Val), Chymotrypsin (cuts large hydrophobics), Glu C (cuts at Glu) and Subtilisin (cuts large uncharged residues). Protease stocks at 1 mg/ml were diluted 1:10, 1:100 and 1:1000 in protease dilution buffer (20 mM HEPES pH 7.5, 50 mM NaCl, 10 mM $MgSO_4$). 3 μg of protein or protein complex was incubated with 3 μl of diluted protease, in 13 μl final reaction volume for 30 minutes at 4°C. Untreated protein and a tube with the highest protease concentration served as controls. 5 μl 3x Laemmli sample buffer was added to stop the reaction, boiled at 95°C for 5 minutes and visualized on a coomassie stained gel.
In order to obtain reproducible results, aliquots of the same protease in all mentioned dilutions was flash frozen in liquid nitrogen and stored at -80°C.

4.17 Cross linking coupled with mass spectrometry

Experiments of cross-linking coupled with mass spectrometry were carried out in a collaboration with Dr. Franz Herzogs laboratory at the Ludwig Maximilian University in Munich. Experimental setup was essentially as in [312]. In brief: CENP-C^{2-545}/CENP-H/CENP-K or CENP-C^{2-545}/CENP-H/CENP-I/CENP K/CENP-N/CENP-M/CENP-L/CENP-$A^{nucleosome}$ complex was cross-linked with isotope-labeled disuccinimidyl suberate and digested with Lys-C and trypsin after quenching with ammonium bicarbonate. Cross-linked peptides were enriched using size-exclusion chromatography, analyzed by liquid chromatography coupled to tandem mass spectrometry and identified by the search algorithm, xQuest. Cross-linking, MS analysis and database searching were performed as described [313].
Visualization of the crosslinks was done by converting the raw data (in form of Excel spreadsheets) to the GEXF data format (Graph Exchange XML Format) using custom shell scripts. The data were then imported into the Gephi software (http://gephi.org) that was modified to allow simultaneous calculation and display of curved and straight connectors (i.e., intra- and intermolecular crosslinks). This

was achieved in collaboration with Dr. Ingrid Vetter at the MPI Dortmund. The Gephi graph was exported as an Adobe Illustrator file for final processing.

4.18 Isothermal Calorimetry (ITC)

Binding of CENP-C$^{2-545}$, CENP-C$^{189-400}$, CENP-C$^{290-400}$ or CENP-C$^{189-290}$ to CENP-H/K was measured using a ITC200 microcalorimeter with a reaction cell volume of 0.5 ml. All proteins were extensively dialyzed into fresh buffer (20 mM HEPES 7.5, 300 mM NaCl, 2.5 % Glycerol, 2 mM TCEP). ITC measurements were performed at 25°C on a ITC200 microcalorimeter (MicroCal). The cell contained 30 μM CENP-C$^{2-545}$ stirred at 1000 rev min^{-1} and the syringe contained 300 μM CENP-H/K. In each titration, the protein in the cell was titrated with 20-2ul injections (at 5 minutes intervals) of protein ligand with the chamber maintained at 298 K. Data were fitted by least-square procedures to a single-site binding model using ORIGIN 5.0 software package (MicroCal).

4.19 Plasmids for mammalian expression

DNA encoding the human CENP-C sequence (codon optimized for insect cell expression from GeneArt, Life Technogolies^{TM}) has been subcloned into a the pcDNA5/FRT/TO-eGFP-ires vector, a derivative of pcDNA5/FRT/TO vector (Invitrogen, Carlsbad, CA) generated in house [158], encoding an N-terminal eGFP. Mutant CENP-C constructs were created as described in **Section** 4.9. A cDNA sequence coding for human CENP-L, CENP-N, CENP-I, CENP-H or CENP-K has been subcloned into a the pcDNA5/FRT/TO-mCherry-ires vector, a derivative of pcDNA5/FRT/TO vector generated in house, encoding an N-terminal mCherry. In both cases BamHI and XhoI have been used as restriction enzymes to cleave the PCR product and the vector for subsequent ligation.

4.20 Generation of stable cell lines

Parental Flp-In T-REx HeLa cell lines (a kind gift of Prof. Stephen S. Taylor, University of Manchester) are adherent cell lines. They were grown in Dulbecco's

Modified Eagle's Medium supplemented with 10 % Tetracylin-free Fetal Bovine Serum, 2 mM L-Glutamine. To keep the cells growing exponentially, they need to be sub-cultured before they reach a confluent stage. For passaging, the medium was removed and cells were washed with 1x phosphate buffered saline (PBS). Cells were detached by 5 minutes incubation at 37°C with the protease Trypsin (0.05 % in PBS). To stop the trypsination, fresh medium containing serum was added. 1/10 of the cells was seeded for every new passage. Cells were cultured as a monolayer in 10 cm dishes at 37°C and 5 % CO_2 and were subcultured at a confluence of 70 - 80 %.

Parental Flp-In T-REx HeLa cell lines were used to generate stable Doxycycline-inducible cell lines. Flp-In T-REx HeLa cells expressing CENP-C fusions to GFP or other CCAN protein fusions to mCherry were generated as previously described [314] and maintained in DMEM supplemented with 10% tetracycline-free FBS, 2mM L-Glutamine, 250 μg/ml Hygromycin and 4 μg/ml Blasticidin.

In summary, cell lines were generated by co-transfection of the Flp-recombinase expression vector (pOG44) and a pcDNA5/FRT/TO expression plasmid in a 9:1 ratio. Co-transfections were performed following the manufacturers guidelines of X-tremeGENE 9 DNA Transfection Reagent. 48 h after transfection, cells were selected in DMEM supplemented with 10 % TET-free Fetal Bovine Serum, 2 mM L-Glutamine, 250 μg/ml Hygromycin and 5 μg/ml Blasticidin. Selection medium was exchanged every second day. After 2 weeks of selection, single cell clones were transferred to separate dishes and grown to be frozen and optimized for protein expression by adjusting Doxycycline concentrations and treatment time. For each cell line, 3 clones plus a pooled cell line was checked for protein expression in immunofluorescence and the best cell line used for experiments. Protein expression was induced with 5 - 25 ng/ml Doxycycline for 48 h.

4.21 Small interfering RNA depletion of CENP-C

Endogenous CENP-C was depleted by transient transfection of a single small interfering RNA (5'-GGAUCAUCUCAGAAUAGAA-3'), targeting the coding region of endogenous CENP-C mRNA. Transfection was performed with HiPerFect Transfection Reagent according to the manufacturer's instructions. To obtain an efficient depletion of CENP-C, 60 nM siRNA was transfected 3 times within 72

hours. In the last 48 h 5-25 ng/ml Doxycycline was added to the medium to induce GFP-CENP-C construct or mCherry-CCAN protein expression. Since we used a codon optimized DNA sequence for all CENP-C constructs, the siRNA did not effect expression of these proteins. Phenotypes were analyzed 96 hr after the first siRNA addition and protein depletion was monitored by western blotting or immunofluorescence.

4.22 Generation of an rabbit anti-CENP-H/K and anti-CENP-C$^{731-849}$ antibody

CENP-H/K and CENP-C$^{731-849}$ antibodies were generated in rabbit in colaboration with Eurogentech, Belgium and affinity purified and conjugated with fluorochromes by Cogentech s.c.a.r.l at the IFOM in Milan, italy, with kind support by Giuseppe Ossolengo. Antibody quality was checked in western blot against the recombinant proteins or cell lysate and by immunofluorescence in HeLa cells. To obtain a good quality antibody, initial bleeds were affinity purified against CENP-H/His-CENP-K or GST-CENP-C$^{731-849}$.

4.23 Immunofluorescence (IF) and image generation

Flp-In T-REx HeLa cells were grown on coverslips pre-treated with 15 μg/ml poly(L)lysin. Cells were fixed with 4 % paraformaldehyde in PHEM or PBS buffer for 10 minutes. Before incubation with antibodies, cells were permeabilized using 0.1 % Triton X-100 in PHEM or PBS buffer for 10 min and blocked with 5 % BSA in PHEM or PBS buffer. The following antibodies were used for immunostaining: anti-CENP-T/W (1:800), CREST/anti-centromere antibodies (1:100), anti-CENP-C$^{23-410}$ (1:1000), anti-CENP-H/K (1:800). Rodamine Red-conjugated, DyLight649-conjugated, Alexa Fluor 405- and 488-labeled served as secondary antibodies. After 1.5 h of incubation, unbound primary antibody is removed by washing 3 times with PBS 0.1 % Triton X-100 or PHEM 0.1 % Triton X-100. Secondary antibody were subsequently added for 45 min and removed in three washing steps. Primary and secondary antibodies used in this study are

summarized in **Table** 4.6. Before mounting, coverslips were washed in destilled water to remove salt residues. Coverslips were mounted with Mowiol mounting media.

All experiments were imaged at room temperature using the spinning disk confocal microscopy of a 3i Marianas system equipped with an Axio Observer Z1 microscope, a CSU-X1 confocal scanner unit, Plan-Apochromat 63x or 100x/1.4NA objectives and Orca Flash 4.0 sCMOS Camera and converted into maximal intensity projections Tiff files for illustrative purposes. Quantification of kinetochore signals was performed on unmodified Z-series images using Imaris 7.3.4 software. After background subtraction, all signals were normalized to CREST and values obtained for control cells were set to 1. Quantifications are based on a 5 - 10 representative cell analyses. Error bars indicate mean ± SEM.

For representation of microscope images, single cells were cropped and the same channel was adjusted to the same level in each cell to be comparable. Maximum image projections were generated. Images were exported as 16-bit Tiff files for all channels separately. Additionally, a 16-bit Tiff file including all channels and a scale bar of 10 μm was exported. Contrast and brightness was adjusted in ImageJ to the same value. Additionally, images were converted into 8-bit Tiff files and finally merged in Photoshop.

4.24 Immunoprecipitation and immunoblotting

Cycling cells were harvested by trypsinization, incubated in lysis buffer (75 mM HEPES pH 7.5, 150 mM KCl, 1.5 mM EGTA, 1.5 mM $MgCl_2$, 10 % glycerol, 0.075 % Nonidet P40 (NP-40), 90 U/ml benzonase, protease inhibitor cocktail) at 4°C for 15 min and finally lysed by sonication and centrifugation at 15000 g for 30 minutes at 4 °C. Extracts were pre-cleared with a mixture of protein A-Sepharose and protein G-Sepharose beads at 4°C for 1 h. Subsequently, extracts were incubated with GFP-Traps at 4°C for 3 - 4 hr. Immunoprecipitates were washed with lysis buffer, resuspended in Laemmli sample buffer, boiled and analyzed by SDS-PAGE followed western blotting using 12 % SDS gels. To check protein size, molecular weight marker was loaded. Nitrocellulose or PVDF membrane were blocked after protein transfer with 5 % non-fat milk in Phosphate-Buffered Saline Tween-20 (PBST) for 60 minutes at RT. The following antibodies were used:

anti-GFP (1:4000), anti-Vinculin (1:15000), anti-CENP-T/W (1:800), anti-CENP-C (1:1200), anti-CENP-H/K (1:1000), anti-Mis12 (1:1000), anti-CENP-M (1:500), anti-CENP-I (1:500). Secondary antibodies were affinity purified anti-mouse, anti-rabbit conjugated to horseradish peroxidase (1:10000). After incubation with ECL western blotting system, images were acquired with ChemiBIS 3.2. Levels were adjusted with ImageJ and Photoshop and images were cropped accordingly.
Western blotting was also used in this work to check for efficient depletion of CENP-C. Cells from a 10 cm dish were trypsinized and resuspended in lysis buffer. The samples were lysed sonicated and cleared by centrifugation. The protein concentration in the cleared lysate was measured in a Bradford assay with 1 μg BSA as reference. 30 - 50 μg of lysate was analysed in SDS-PAGE followed by western blotting as described above.

Chapter 5

Supplemetary Figures

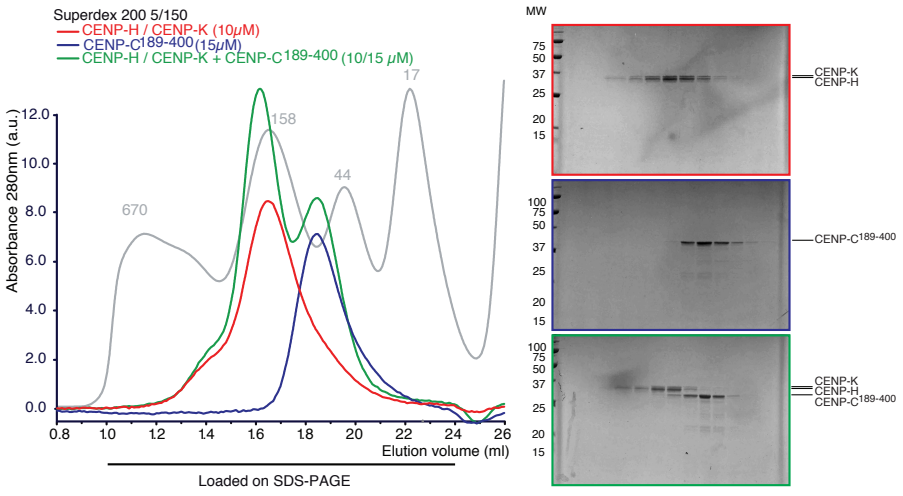

FIGURE 5.1: **CENP-C$^{189-400}$ binding to CENP-H/K in SEC**. SEC elution profiles and SDS-PAGE analyses of CENP-H/K complex (red), CENP-C$^{189-400}$ (blue) and their combination (green) is shown. 15 μM of CENP-C and 10 μM CENP-H/K were mixed, incubated for 1 h at 4°C and run on a Superdex 200 5/150. No complex formation is observed.

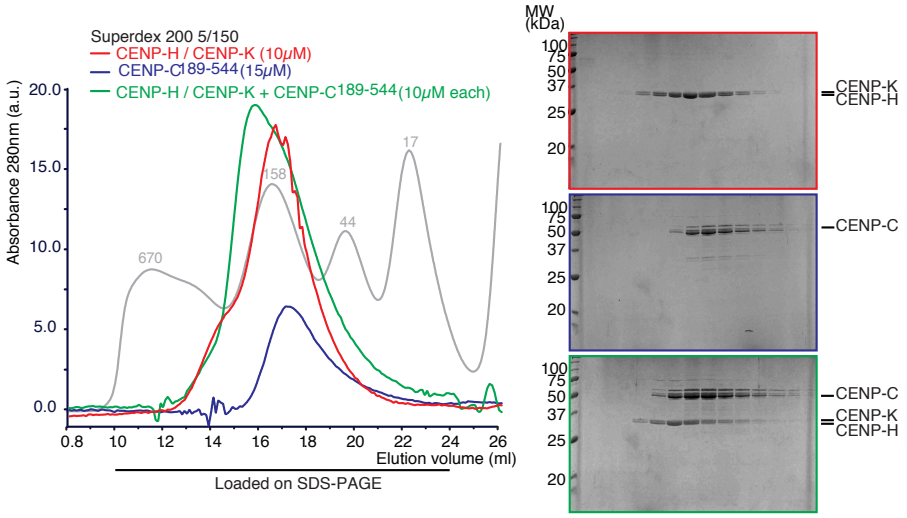

FIGURE 5.2: **CENP-C$^{189-544}$ binding to CENP-H/K in SEC**. SEC elution profiles and SDS-PAGE analyses of CENP-H/K complex (red), CENP-C$^{189-544}$ (blue) and their combination (green) is shown. 10 μM of CENP-C and 10 μM of CENP-H/K, incubated for 1 h at 4 C and run on a Superdex 200 5/150. A shift of both components to an earlier elution volume in the chromatogramm and on the coomassie stained gel is observed although a stoichiometric complex is not formed.

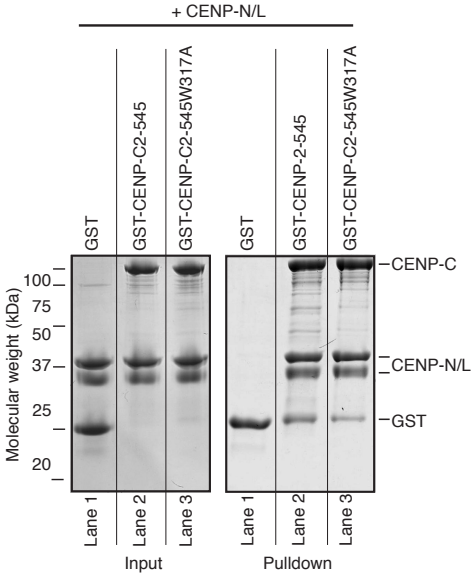

FIGURE 5.3: **GST-CENP-C$^{2-545}$W317A CENP-N/L pulldown**. GST-CENP-C$^{2-545}$W317A or wild type have been used as bait (1 μM) and CENP-N/L as prey (3 μM) to investigate the involvement of Trp317 in the CENP-C:CENP-N/L interaction. As hypothesized, the residue Trp317, that is important in CENP-H/I/K/M binding to CENP-C, was found not to be involved in CENP-N/L interaction, since CENP-C$^{2-545}$W317A pulled down CENP-N/L as efficiently as the wild type construct.

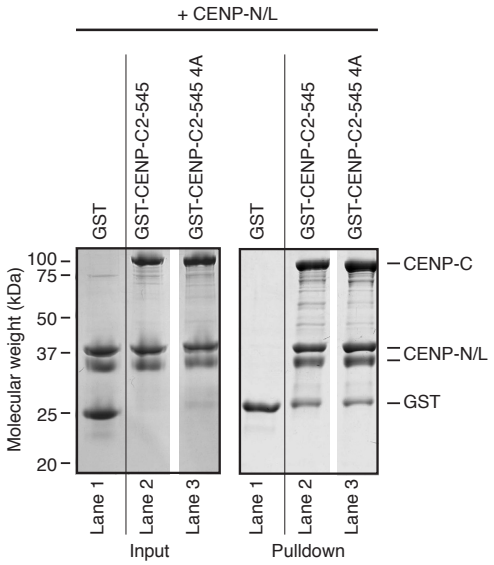

FIGURE 5.4: **GST-CENP-C$^{2-545}$4A CENP-N/L pulldown**. GST-CENP-C$^{2-545}$4A or wild type constructs have been used as bait (1 μM) and CENP-N/L as prey (3 μM) to investigate the involvement of Leu265, Phe266, Leu267 and Trp317 in the CENP-C:CENP-N/L interaction. GST-CENP-C$^{2-545}$4A is able to bind CENP-N/L as efficiently as wild type CENP-C$^{2-545}$ in this pulldown assay, speaking against a contribution of these residues in CENP-C:CENP-N/L interaction.

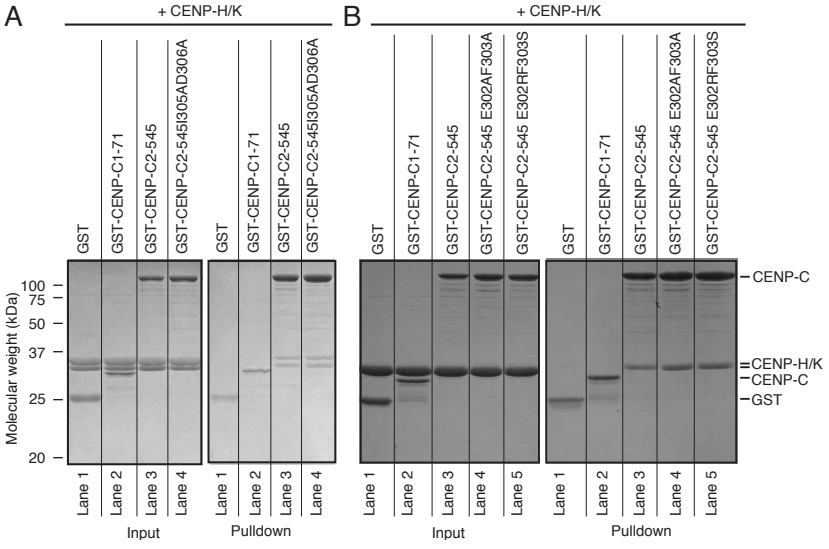

FIGURE 5.5: **GST-CENP-C$^{2-545}$E302/F303 and GST-CENP-C$^{2-545}$I305A/D306A CENP-H/K pulldown**. GST-CENP-C$^{2-545}$ mutants and wild type have been used as bait (1 μM) and CENP-H/K as prey (3 μM) to test the involvement of residues E302/F303 and I305/D306 of CENP-C in the CENP-H/K interaction. GST-CENP-C$^{2-545}$ E302/F303 and I305/D306 mutants pull down CENP-H/K as efficiently as wild type GST-CENP-C$^{2-545}$, indicating no involvement of these residues in the CENP-C:CENP-H/K interaction.

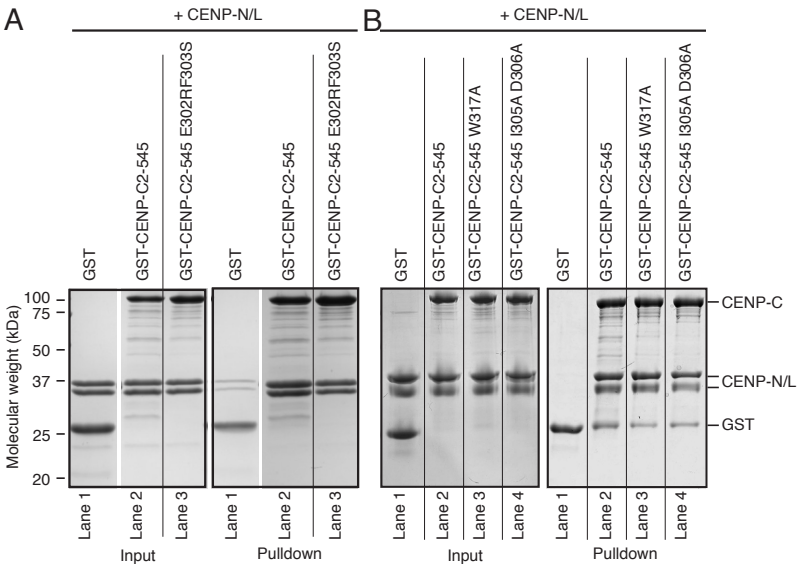

FIGURE 5.6: **GST-CENP-C$^{2-545}$E302/F303 and GST-CENP-C$^{2-545}$I305/D306 CENP-N/L pulldown experiment.** GST-CENP-C$^{2-545}$ mutants and wild type have been used as bait (1 μM) and CENP-N/L as prey (3 μM) to test the involvement of residues E302/F303 and I305/D306 in the CENP-N/L interaction. GST-CENP-C$^{2-545}$ E302/F303 (**A**) and I305/D306 (**B**) mutants pull down CENP-N/L almost as well as the wild type GST-CENP-C$^{2-545}$, indicating no major involvement of these residues in the CENP-C:CENP-N/L interaction.

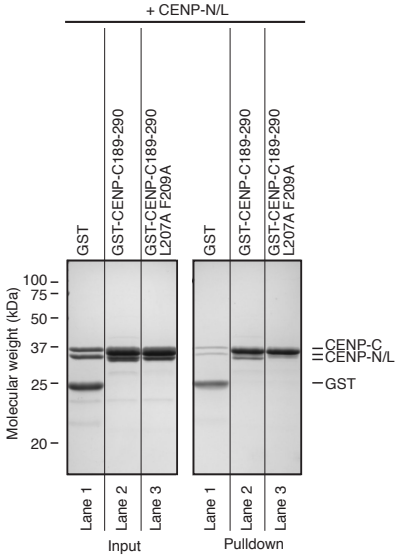

FIGURE 5.7: **GST-CENP-C$^{189-290}$L207A/F209A CENP-N/L pulldown.** GST-CENP-C$^{189-290}$L207A/F209A or wild type constructs have been used as bait (1 μM) and CENP-N/L as prey (3 μM) to investigate the involvement of L207A/F209A in the CENP-C:CENP-N/L interaction. CENP-C$^{189-290}$L207A/F209A seems to be able to bind CENP-N/L as efficiently as wild type CENP-C$^{189-290}$ in this pulldown assay. However, the close proximity of all bands in the gel complicates the interpretation of the result.

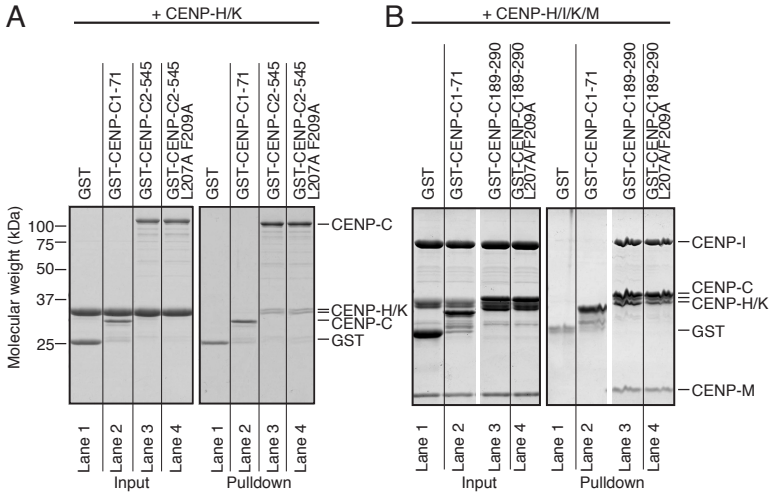

FIGURE 5.8: **GST-CENP-CL207A/F209A CENP-H/K and CENP-H/I/K/M pulldown**. GST-CENP-C$^{2-545}$L207A/F209A, GST-CENP-C$^{189-290}$L207A/F209A or wild type constructs have been used as bait (1 μM) and CENP-H/K or CENP-H/I/K/M as prey (3 μM) to investigate the involvement of Leu207 and Phe209 in the CENP-C:CENP-H/I/K/M interaction. CENP-C$^{2-545}$L207A/F209A is able to bind CENP-H/K as efficiently as wild type CENP-C$^{2-545}$ and CENP-C$^{189-290}$L207A/F209A is able to bind CENP-H/I/K/M as efficiently as wild type CENP-C$^{189-290}$ in this pulldown assay, speaking against a contribution of these residues in the interaction.

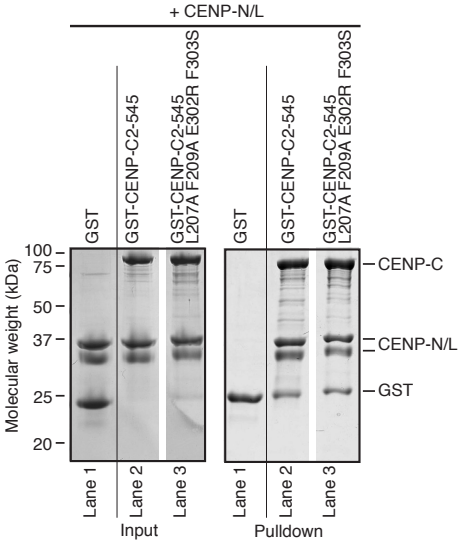

FIGURE 5.9: **GST-CENP-C$^{2-545}$L207A/F209A/E302R/F303S CENP-N/L pulldown**. GST-CENP-C$^{2-545}$L207A/F209A/E302R/F303S or wild type construct have been used as bait (1 μM) and CENP-N/L as prey (3 μM) to investigate the involvement of L207A/F209A in combination with E302R/F303S in the CENP-C:CENP-N/L interaction. CENP-C$^{2-545}$L207A/F209A/E302R/F303S is able to bind CENP-N/L comparable to wild type CENP-C in this pulldown assay, speaking against a contribution of these residues in CENP-C:CENP-N/L interaction.

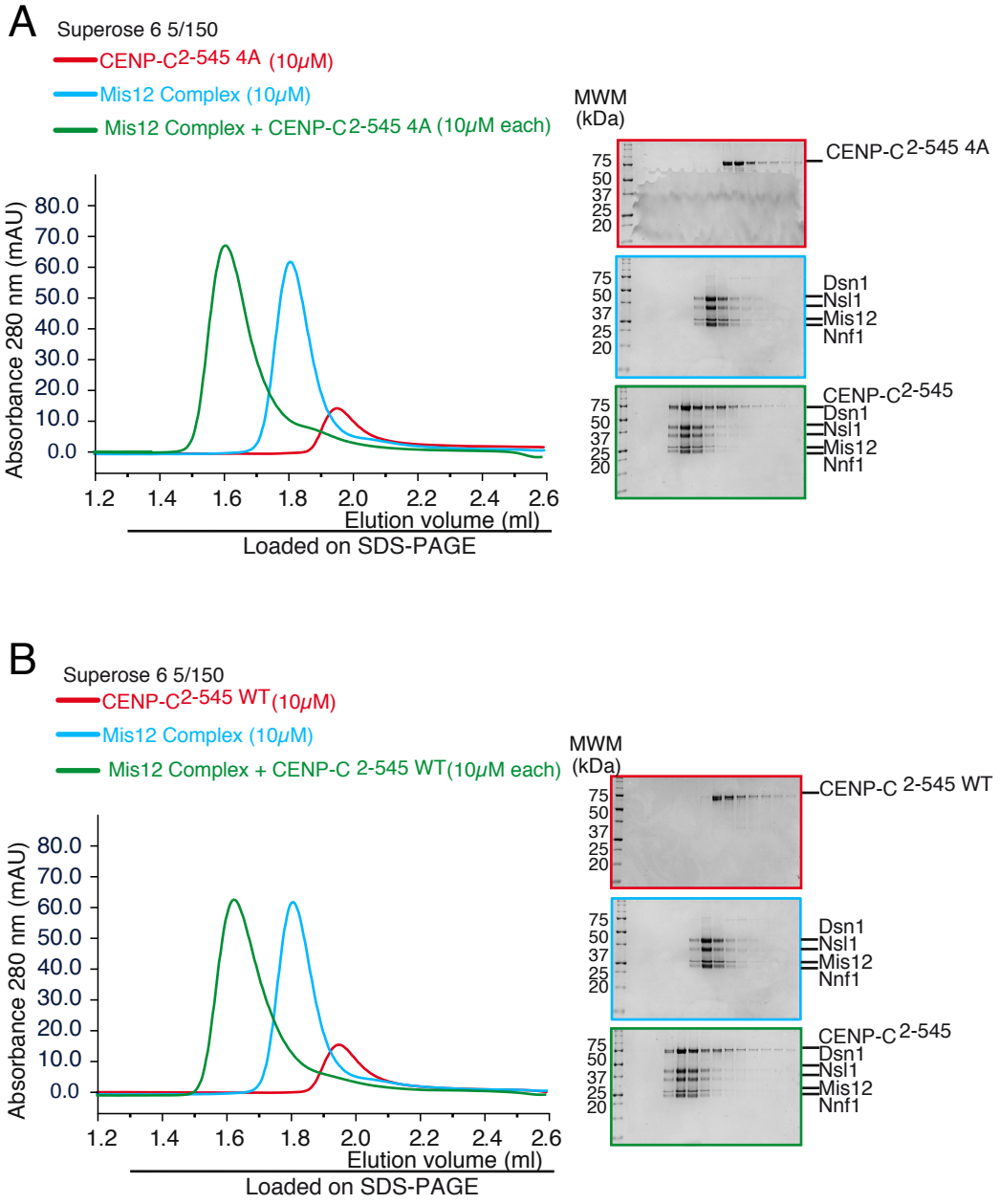

FIGURE 5.10: **CENP-C$^{2-545}$4A Mis12c interaction on SEC**. SEC elution profiles and SDS-PAGE analyses of CENP-C$^{2-545}$4A and wild type (red), Mis12c (blue) and their combination (green) is shown. 10 μM of CENP-C$^{2-545}$ and Mis12c were mixed in a 1:1 ratio, incubated for 1 h at 4 C and run on a Superdex 200 5/150. The shift of the chromatograms and the proteins in the Coomassie stained SDS-PAGE gel to an earlier elution volume show a complex formation of CENP-C$^{2-545}$4A and wild type with the Mis12c, demonstrating that the 4A mutant does not effect the CENP-C:Mis12 interaction.

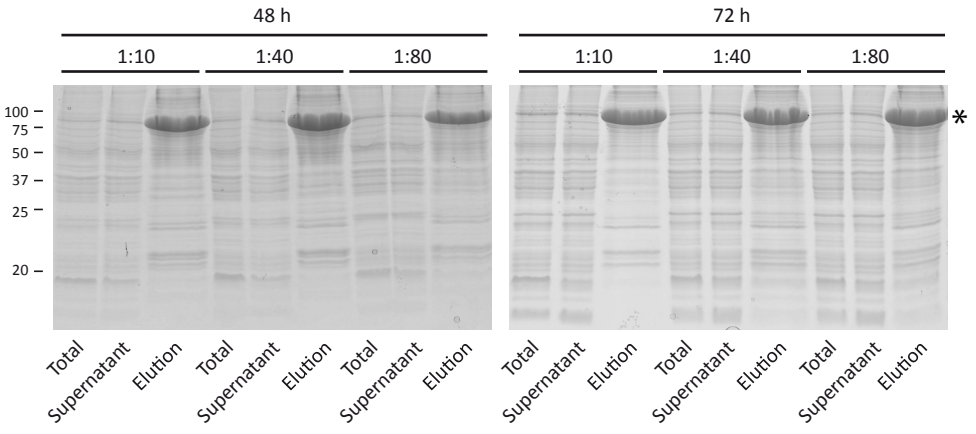

FIGURE 5.11: **CENP-C$^{1-544}$-His test expression in Tnao38 cells**. After three rounds of virus amplification, obtained V_2 was tested for its ability to induce expression of CENP-C$^{1-544}$-His in Tnao38 cells. Viral titer of 1:10, 1:40 and 1:80 was used and expression was performed for 48 and 72 h. Total lysate, supernatant and elution from Nickel beads were visualized on a Coomassie stained SDS-PAGE gel. The asterisk indicates the band of CENP-C$^{1-544}$-His.

Bibliography

[1] D. M. Olson, E. Dinerstein, E. D. Wikramanayake, N. D. Burgess, G. V. N. Powell, E. C. Underwood, J. A. Damico, I. Itoua, H. E. Strand, J.C. Morrison, C. J. Loucks, T. F. Allnutt, T. H. Rickets, Y. Kura, J. F. Lamoreux, W. W. Wettengel, P. Hedao, and K. R. Kassem. *Terrestrial Ecoregions of the World: A New Map of Life on Earth A new global map of terrestrial ecoregions provides an innovative tool for conserving biodiversity. BioScience*, 51 (11):933–938, 2001.

[2] Knoll A. H. *Life on a young planet: the first three billion years of evolution on earth.* Princeton University Press, 2003.

[3] G.M. Cooper. *The Cell: A Molecular Approach. 2nd edition. Chapter: The Origin and Evolution of Cells.* Sinauer Associates, 2000.

[4] Wright and Sewall. The roles of mutation, inbreeding, crossbreeding and selection in evolution. In *Proceedings of the sixth international congress on genetics*, volume 1, pages 356–366, 1932.

[5] D. Prescott. *Reproduction of eukaryotic cells.* Elsevier, 2012.

[6] Loeb and Lawrence. Mutator phenotype may be required for multistage carcinogenesis. *Cancer Res*, 51(12), 1991.

[7] B. A. A. Weaver and D. W. Cleveland. Does aneuploidy cause cancer? *Current opinion in cell biology*, 18(6):658–667, 2006.

[8] Hartwell and Leland. Defects in a cell cycle checkpoint may be responsible for the genomic instability of cancer cells. *Cell*, 71(4):543–546, 1992.

[9] R. D. Kolodner, D. W. Cleveland, and C. D. Putnam. Aneuploidy drives a mutator phenotype in cancer. *Science (New York, NY)*, 333(6045):942, 2011.

[10] S. Santaguida and A. Musacchio. The life and miracles of kinetochores. *The EMBO journal*, 28(17):2511–2531, 2009.

[11] E. Frisoni and H. von Mohl. *Resp. Ueber die Verbindung der Pflanzen-Zellen unter einander. eine Inaugural-Dissertation... Präs. H. Mohl, etc.* 1835.

[12] W. Flemming. *Zellsubstanz, Kern und Zelltheilung.* FCW Vogel, Leipzig, 1882.

[13] T.J. Mitchison and E.D. Salmon. Mitosis: a history of division. *Nature cell biology*, 3(1):E17–E21, 2001.

[14] B. Alberts, A. Johnson, J. Lewis, M. Raff, and P.W. Roberts. *Molecular Biology of the Cell, 5th Edition, Chapter 17.* Garland Science, 2008.

[15] I. C. Waizenegger, S. Hauf, A. Meinke, and J.-M. Peters. Two distinct pathways remove mammalian cohesin from chromosome arms in prophase and from centromeres in anaphase. *Cell*, 103(3):399–410, 2000.

[16] T. Hirano. Chromosome cohesion, condensation, and separation. *Annual review of biochemistry*, 69(1):115–144, 2000.

[17] C. Lengauer, K. W. Kinzler, and B. Vogelstein. Genetic instabilities in human cancers. *Nature*, 396(6712):643–649, 1998.

[18] D. Coudreuse and P. Nurse. Driving the cell cycle with a minimal cdk control network. *Nature*, 468(7327):1074–1079, 2010.

[19] A. Musacchio and E. D. Salmon. The spindle-assembly checkpoint in space and time. *Nature reviews Molecular cell biology*, 8(5):379–393, 2007.

[20] T. Wittmann, A. Hyman, and A. Desai. The spindle: a dynamic assembly of microtubules and motors. *Nature cell biology*, 3(1):E28–E34, 2001.

[21] C. E. Walczak and R. Heald. Mechanisms of mitotic spindle assembly and function. *International review of cytology*, 265:111–158, 2008.

[22] S. Inoué and H. Sato. Cell motility by labile association of molecules the nature of mitotic spindle fibers and their role in chromosome movement. *The Journal of general physiology*, 50(6):259–292, 1967.

[23] A. S. Bajer and J. Molè-Bajer. Spindle dynamics and chromosome movements. *International review of cytology*, (Suppl. 3), 1972.

[24] G. G. Borisy and E. W. Taylor. The mechanism of action of colchicine binding of colchincine-3h to cellular protein. *The Journal of cell biology*, 34 (2):525–533, 1967.

[25] H. Mohri. Amino-acid composition of"tubulin"constituting microtubules of sperm flagella. *Nature*, 217:1053–1054, 1968.

[26] B. Kiefer, H. Sakai, A. J. Solari, and D. Mazia. The molecular unit of the microtubules of the mitotic apparatus. *Journal of molecular biology*, 20(1): 75–79, 1966.

[27] E. Karsenti and I. Vernos. The mitotic spindle: a self-made machine. *Science*, 294(5542):543–547, 2001.

[28] T. S. Hays, D. Wise, and E. D. Salmon. Traction force on a kinetochore at metaphase acts as a linear function of kinetochore fiber length. *The Journal of cell biology*, 93(2):374–382, 1982.

[29] T. Mitchison, L. Evans, E. Schulze, and M. Kirschner. Sites of microtubule assembly and disassembly in the mitotic spindle. *Cell*, 45(4):515–527, 1986.

[30] C. L. Rieder and E. D. Salmon. The vertebrate cell kinetochore and its roles during mitosis. *Trends in cell biology*, 8(8):310–318, 1998.

[31] K. E. Sawin, K. LeGuellec, M. Philippe, and T. J. Mitchison. Mitotic spindle organization by a plus-end-directed microtubule motor. *Nature*, 359(6395): 540–543, 1992.

[32] E. R. Steuer, L. Wordeman, T. A. Schroer, and M. P. Sheetz. Localization of cytoplasmic dynein to mitotic spindles and kinetochores. *Nature*, 345(6272): 266–268, 1990.

[33] R. B. Nicklas. Measurements of the force produced by the mitotic spindle in anaphase. *The Journal of cell biology*, 97(2):542–548, 1983.

[34] A. D. McAinsh, J. D. Tytell, and P. K. Sorger. Structure, function, and regulation of budding yeast kinetochores. *Annual review of cell and developmental biology*, 19(1):519–539, 2003.

[35] S. Westermann, D. G. Drubin, and G. Barnes. Structures and functions of yeast kinetochore complexes. *Annu. Rev. Biochem.*, 76:563–591, 2007.

[36] I. M. Cheeseman and A. Desai. Molecular architecture of the kinetochore–microtubule interface. *Nature Reviews Molecular Cell Biology*, 9(1):33–46, 2008.

[37] J. P. I. Welburn and I. M. Cheeseman. Toward a molecular structure of the eukaryotic kinetochore. *Developmental cell*, 15(5):645–655, 2008.

[38] R. P. Zinkowski, J. Meyne, and B. R. Brinkley. The centromere-kinetochore complex: a repeat subunit model. *The Journal of cell biology*, 113(5):1091–1110, 1991.

[39] M. D. Blower, B. A. Sullivan, and G. H. Karpen. Conserved organization of centromeric chromatin in flies and humans. *Developmental cell*, 2(3): 319–330, 2002.

[40] A. P. Joglekar, D. Bouck, K. Finley, X. Liu, Y. Wan, J. Berman, X. He, E. D. Salmon, and K. S. Bloom. Molecular architecture of the kinetochore-microtubule attachment site is conserved between point and regional centromeres. *The Journal of cell biology*, 181(4):587–594, 2008.

[41] A. P. Joglekar, K. Bloom, and E. D. Salmon. In vivo protein architecture of the eukaryotic kinetochore with nanometer scale accuracy. *Current Biology*, 19(8):694–699, 2009.

[42] R. B. Schittenhelm, S. Heeger, F. Althoff, A. Walter, S. Heidmann, K. Mechtler, and C. F. Lehner. Spatial organization of a ubiquitous eukaryotic kinetochore protein network in drosophila chromosomes. *Chromosoma*, 116(4):385–402, 2007.

[43] X. Wan, R. P. O'Quinn, H. L. Pierce, A. P. Joglekar, W. E. Gall, J. G. DeLuca, C. W. Carroll, S. Liu, T. J. Yen, B. F. McEwen, P. T. Stukenberg, A. Desai, and E. D. Salmon. Protein architecture of the human kinetochore microtubule attachment site. *Cell*, 137(4):672–684, 2009.

[44] B. F. McEwen, Y. Dong, and K. J. VandenBeldt. Using electron microscopy to understand functional mechanisms of chromosome alignment on the mitotic spindle. *Cellular Electron Microscopy*, 79:259–293, 2007.

[45] B. F. McEwen, C.-E. Hsieh, A. L. Mattheyses, and C. L. Rieder. A new look at kinetochore structure in vertebrate somatic cells using high-pressure freezing and freeze substitution. *Chromosoma*, 107(6-7):366–375, 1998.

[46] Y. Dong, K. J. V. Beldt, X. Meng, A. Khodjakov, and B. F. McEwen. The outer plate in vertebrate kinetochores is a flexible network with multiple microtubule interactions. *Nature cell biology*, 9(5):516–522, 2007.

[47] B. A. Pinsky and S. Biggins. The spindle checkpoint: tension versus attachment. *Trends in cell biology*, 15(9):486–493, 2005.

[48] A. E. Kelly and H. Funabiki. Correcting aberrant kinetochore microtubule attachments: an aurora b-centric view. *Current opinion in cell biology*, 21 (1):51–58, 2009.

[49] R. B. Nicklas and C. A. Koch. Chromosome micromanipulation iii. spindle fiber tension and the reorientation of mal-oriented chromosomes. *The Journal of cell biology*, 43(1):40–50, 1969.

[50] X. Li and R. B. Nicklas. Mitotic forces control a cell-cycle checkpoint. *Nature*, 373(6515):630–632, 1995.

[51] J.-M. Peters. The anaphase promoting complex/cyclosome: a machine designed to destroy. *Nature Reviews Molecular Cell Biology*, 7(9):644–656, 2006.

[52] D. W. Cleveland, Y. Mao, and K. F. Sullivan. Centromeres and kinetochores: from epigenetics to mitotic checkpoint signaling. *Cell*, 112(4):407–421, 2003.

[53] S. Henikoff, K. Ahmad, and H. S. Malik. The centromere paradox: stable inheritance with rapidly evolving dna. *Science*, 293(5532):1098–1102, 2001.

[54] L. J. Vos, J. K. Famulski, and G. K. T. Chan. How to build a centromere: from centromeric and pericentromeric chromatin to kinetochore assembly this paper is one of a selection of papers published in this special issue, entitled 27th international west coast chromatin and chromosome conference, and has undergone the journal's usual peer review process. *Biochemistry and cell biology*, 84(4):619–639, 2006.

[55] F. G. Westhorpe and A. F. Straight. Functions of the centromere and kinetochore in chromosome segregation. *Current opinion in cell biology*, 25(3): 334–340, 2013.

[56] R. C. Allshire and G. H. Karpen. Epigenetic regulation of centromeric chromatin: old dogs, new tricks? *Nature Reviews Genetics*, 9(12):923–937, 2008.

[57] O. Marshall, A.T. Marshall, and K. H. A. Choo. Three-dimensional localization of cenp-a suggests a complex higher order structure of centromeric chromatin. *The Journal of cell biology*, 183(7):1193–1202, 2008.

[58] W. C. Earnshaw and R. L. Bernat. Chromosomal passengers: toward an integrated view of mitosis. *Chromosoma*, 100(3):139–146, 1991.

[59] H. Masumoto, H. Masukata, Y. Muro, N. Nozaki, and T. Okazaki. A human centromere antigen (cenp-b) interacts with a short specific sequence in alphoid dna, a human centromeric satellite. *The Journal of cell biology*, 109 (5):1963–1973, 1989.

[60] L. E. Voullaire, H. R. Slater, V. Petrovic, and K. H. Choo. A functional marker centromere with no detectable alpha-satellite, satellite iii, or cenp-b protein: activation of a latent centromere? *American journal of human genetics*, 52(6):1153, 1993.

[61] T. Okada, J. Ohzeki, M. Nakano, K. Yoda, W. R. Brinkley, V. Larionov, and H. Masumoto. Cenp-b controls centromere formation depending on the chromatin context. *Cell*, 131(7):1287–1300, 2007.

[62] O. J. Marshall, A. C. Chueh, L. H. Wong, and K. H. Choo. Neocentromeres: new insights into centromere structure, disease development, and karyotype evolution. *The American Journal of Human Genetics*, 82(2):261–282, 2008.

[63] B. A. Sullivan and G. H. Karpen. Centromeric chromatin exhibits a histone modification pattern that is distinct from both euchromatin and heterochromatin. *Nature structural & molecular biology*, 11(11):1076–1083, 2004.

[64] C. W. Carroll and A. F. Straight. Centromere formation: from epigenetics to self-assembly. *Trends in cell biology*, 16(2):70–78, 2006.

[65] B. E. Black and E. A. Bassett. The histone variant cenp-a and centromere specification. *Current opinion in cell biology*, 20(1):91–100, 2008.

[66] V. De Rop, A. Padeganeh, and P. S. Maddox. Cenp-a: the key player behind centromere identity, propagation, and kinetochore assembly. *Chromosoma*, 121(6):527–538, 2012.

[67] K. F. Sullivan, M. Hechenberger, and K. Masri. Human cenp-a contains a histone h3 related histone fold domain that is required for targeting to the centromere. *The Journal of cell biology*, 127(3):581–592, 1994.

[68] D. K. Palmer, K. O'Day, M. H. Wener, B. S. Andrews, and R. L. Margolis. A 17-kd centromere protein (cenp-a) copurifies with nucleosome core particles and with histones. *The Journal of cell biology*, 104(4):805–815, 1987.

[69] D. K. Palmer, K. O'Day, H. L. Trong, H. Charbonneau, and R. L. Margolis. Purification of the centromere-specific protein cenp-a and demonstration that it is a distinctive histone. *Proceedings of the National Academy of Sciences*, 88(9):3734–3738, 1991.

[70] P. B. Meluh, P. Yang, L. Glowczewski, D. Koshland, and M. M. Smith. Cse4p is a component of the core centromere of¡ i¿ saccharomyces cerevisiae¡/i¿. *Cell*, 94(5):607–613, 1998.

[71] S. Furuyama and S. Biggins. Centromere identity is specified by a single centromeric nucleosome in budding yeast. *Proceedings of the National Academy of Sciences*, 104(37):14706–14711, 2007.

[72] W. C. Earnshaw and N. Rothfield. Identification of a family of human centromere proteins using autoimmune sera from patients with scleroderma. *Chromosoma*, 91(3-4):313–321, 1985.

[73] W.C. Earnshaw, B. Bordwell, C. Marino, and N. Rothfield. Three human chromosomal autoantigens are recognized by sera from patients with anti-centromere antibodies. *Journal of Clinical Investigation*, 77(2):426, 1986.

[74] M. M. Valdivia and B. R. Brinkley. Fractionation and initial characterization of the kinetochore from mammalian metaphase chromosomes. *The Journal of cell biology*, 101(3):1124–1134, 1985.

[75] P. E. Warburton, C. A. Cooke, S. Bourassa, O. Vafa, B. A. Sullivan, G. Stetten, G. Gimelli, D. Warburton, C. Tyler-Smith, K. F. Sullivan, G.G Poirier, and W. C. Earnshaw. Immunolocalization of cenp-a suggests a distinct nucleosome structure at the inner kinetochore plate of active centromeres. *Current Biology*, 7(11):901–904, 1997.

[76] D. R. Foltz, L. E. T. Jansen, B. E. Black, A. O. Bailey, J. R. Yates, and D. W. Cleveland. The human cenp-a centromeric nucleosome-associated complex. *Nature cell biology*, 8(5):458–469, 2006.

[77] S.-T. Liu, J. B. Rattner, S. A. Jablonski, and T. J. Yen. Mapping the assembly pathways that specify formation of the trilaminar kinetochore plates in human cells. *The Journal of cell biology*, 175(1):41–53, 2006.

[78] T. Hori, M. Okada, K. Maenaka, and T. Fukagawa. Cenp-o class proteins form a stable complex and are required for proper kinetochore function. *Molecular biology of the cell*, 19(3):843–854, 2008.

[79] V. Régnier, P. Vagnarelli, T. Fukagawa, T. Zerjal, E. Burns, D. Trouche, W.C. Earnshaw, and W. Brown. Cenp-a is required for accurate chromosome segregation and sustained kinetochore association of bubr1. *Molecular and cellular biology*, 25(10):3967–3981, 2005.

[80] S. Stoler, K. C. Keith, K. E. Curnick, and M. Fitzgerald-Hayes. A mutation in cse4, an essential gene encoding a novel chromatin-associated protein in yeast, causes chromosome nondisjunction and cell cycle arrest at mitosis. *Genes & Development*, 9(5):573–586, 1995.

[81] E. V. Howman, K. J. Fowler, A. J. Newson, S. Redward, A. C. MacDonald, P/ Kalitsis, and K. H. A. Choo. Early disruption of centromeric chromatin organization in centromere protein a (cenpa) null mice. *Proceedings of the National Academy of Sciences*, 97(3):1148–1153, 2000.

[82] K. Oegema, A. Desai, S. Rybina, M. Kirkham, and A. A. Hyman. Functional analysis of kinetochore assembly in caenorhabditis elegans. *The Journal of cell biology*, 153(6):1209–1226, 2001.

[83] A. O. Bailey, T. Panchenko, K. M. Sathyan, J. J. Petkowski, P.-J. Pai, D. L. Bai, D. H. Russell, I. G. Macara, J. Shabanowitz, D. F. Hunt, B. E. Black, and D. R. Foltz. Posttranslational modification of cenp-a influences the conformation of centromeric chromatin. *Proceedings of the National Academy of Sciences*, 110(29):11827–11832, 2013.

[84] D. Fachinetti, H. D. Folco, Y. Nechemia-Arbely, L. P. Valente, K. Nguyen, A. J. Wong, Q. Zhu, A. J. Holland, A. Desai, L. E. T. Jansen, and D. W. Cleveland. A two-step mechanism for epigenetic specification of centromere identity and function. *Nature cell biology*, 2013.

[85] M. Torras-Llort, O. Moreno-Moreno, and F. Azorín. Focus on the centre: the role of chromatin on the regulation of centromere identity and function. *The EMBO journal*, 28(16):2337–2348, 2009.

[86] K. C. Keith, R. E. Baker, Y. Chen, K. Harris, S. Stoler, and M. Fitzgerald-Hayes. Analysis of primary structural determinants that distinguish the centromere-specific function of histone variant cse4p from histone h3. *Molecular and cellular biology*, 19(9):6130–6139, 1999.

[87] D. Vermaak, H. S. Hayden, and S. Henikoff. Centromere targeting element within the histone fold domain of cid. *Molecular and cellular biology*, 22(21): 7553–7561, 2002.

[88] B. E. Black, D. R. Foltz, S. Chakravarthy, K. Luger, V. L. Woods, and D. W. Cleveland. Structural determinants for generating centromeric chromatin. *Nature*, 430(6999):578–582, 2004.

[89] H. Kato, J. Jiang, B.R. Zhou, M. Rozendaal, H. Feng, R. Ghirlando, T.S. Xiao, A. F. Straight, and Y. Bai. A conserved mechanism for centromeric nucleosome recognition by centromere protein cenp-c. *Science*, 340:1110–1113, 2013.

[90] C. W. Carroll, K. J. Milks, and A. F. Straight. Dual recognition of cenp-a nucleosomes is required for centromere assembly. *The Journal of cell biology*, 189(7):1143–1155, 2010.

[91] C. W. Carroll, M. C. C. Silva, K. M. Godek, L. E. T. Jansen, and A. F. Straight. Centromere assembly requires the direct recognition of cenp-a nucleosomes by cenp-n. *nature cell biology*, 11(7):896–902, 2009.

[92] L. E. T. Jansen, B. E. Black, D. R. Foltz, and D. W. Cleveland. Propagation of centromeric chromatin requires exit from mitosis. *The Journal of cell biology*, 176(6):795–805, 2007.

[93] L. M. Hereford, M. A. Osley, J. R. Ludwig II, and C. S. McLaughlin. Cell-cycle regulation of yeast histone mrna. *Cell*, 24(2):367–375, 1981.

[94] N. Heintz, H. L. Sive, and R. G. Roeder. Regulation of human histone gene expression: kinetics of accumulation and changes in the rate of synthesis and in the half-lives of individual histone mrnas during the hela cell cycle. *Molecular and cellular biology*, 3(4):539–550, 1983.

[95] P. S. Maddox, F. Hyndman, J. Monen, K. Oegema, and A. Desai. Functional genomics identifies a myb domain–containing protein family required for

assembly of cenp-a chromatin. *The Journal of cell biology*, 176(6):757–763, 2007.

[96] M. Schuh, C. F. Lehner, and S. Heidmann. Incorporation of¡ i¿ drosophila¡/i¿ cid/cenp-a and cenp-c into centromeres during early embryonic anaphase. *Current biology*, 17(3):237–243, 2007.

[97] P. Hemmerich, S. Weidtkamp-Peters, C. Hoischen, L. Schmiedeberg, I. Erliandri, and S. Diekmann. Dynamics of inner kinetochore assembly and maintenance in living cells. *The Journal of cell biology*, 180(6):1101–1114, 2008.

[98] M. Xu, C. Long, X. Chen, C. Huang, S. Chen, and B. Zhu. Partitioning of histone h3-h4 tetramers during dna replication–dependent chromatin assembly. *Science*, 328(5974):94–98, 2010.

[99] D. R. Foltz, L. E. T. Jansen, A. O. Bailey, J. R. Yates III, E. A. Bassett, S. Wood, B. E. Black, and D. W. Cleveland. Centromere-specific assembly of cenp-a nucleosomes is mediated by hjurp. *Cell*, 137(3):472–484, 2009.

[100] E. M. Dunleavy, D. Roche, H. Tagami, N. Lacoste, D. Ray-Gallet, Y. Nakamura, Y. Daigo, Y. Nakatani, and G. Almouzni-Pettinotti. Hjurp is a cell-cycle-dependent maintenance and deposition factor of cenp-a at centromeres. *Cell*, 137(3):485–497, 2009.

[101] H. Hu, Y. Liu, M. Wang, J. Fang, H. Huang, N. Yang, Y. Li, J. Wang, X. Yao, Y. Shi, G. Li, and R.-M. Xu. Structure of a cenp-a–histone h4 heterodimer in complex with chaperone hjurp. *Genes & development*, 25(9): 901–906, 2011.

[102] M. Shuaib, K. Ouararhni, S. Dimitrov, and A. Hamiche. Hjurp binds cenp-a via a highly conserved n-terminal domain and mediates its deposition at centromeres. *Proceedings of the National Academy of Sciences*, 107(4):1349–1354, 2010.

[103] U.-S. Cho and S. C. Harrison. Recognition of the centromere-specific histone cse4 by the chaperone scm3. *Proceedings of the National Academy of Sciences*, 108(23):9367–9371, 2011.

[104] T. Hayashi, Y. Fujita, O. Iwasaki, Y. Adachi, K. Takahashi, and M. Yanagida. Mis16 and mis18 are required for cenp-a loading and histone deacetylation at centromeres. *Cell*, 118(6):715–729, 2004.

[105] Y. Fujita, T. Hayashi, T. Kiyomitsu, Y. Toyoda, A. Kokubu, C. Obuse, and M. Yanagida. Priming of centromere for cenp-a recruitment by human hmis18α, hmis18β, and m18bp1. *Developmental cell*, 12(1):17–30, 2007.

[106] A. L. Pidoux, E. S. Choi, J. K. R. Abbott, X. Liu, A. Kagansky, A. G. Castillo, G. L. Hamilton, W. Richardson, J. Rappsilber, X. He, and R. C. Allshire. Fission yeast scm3: A cenp-a receptor required for integrity of subkinetochore chromatin. *Molecular cell*, 33(3):299–311, 2009.

[107] J. S. Williams, T. Hayashi, M. Yanagida, and P. Russell. Fission yeast scm3 mediates stable assembly of cnp1/cenp-a into centromeric chromatin. *Molecular cell*, 33(3):287–298, 2009.

[108] M. C. Barnhart, P. H. J. L. Kuich, M. E. Stellfox, J. A. Ward, E. A. Bassett, B. E. Black, and D. R. Foltz. Hjurp is a cenp-a chromatin assembly factor sufficient to form a functional de novo kinetochore. *The Journal of cell biology*, 194(2):229–243, 2011.

[109] B. Moree, C. B. Meyer, C. J. Fuller, and A. F. Straight. Cenp-c recruits m18bp1 to centromeres to promote cenp-a chromatin assembly. *The Journal of cell biology*, 194(6):855–871, 2011.

[110] S. Dambacher, W. Deng, M. Hahn, D. Sadic, J. Fröhlich, A. Nuber, C. Hoischen, S. Diekmann, H. Leonhardt, and G. Schotta. Cenp-c facilitates the recruitment of m18bp1 to centromeric chromatin. *Nucleus*, 3(1):101–110, 2012.

[111] P. De Wulf, A. D. McAinsh, and P. K. Sorger. Hierarchical assembly of the budding yeast kinetochore from multiple subcomplexes. *Genes & development*, 17(23):2902–2921, 2003.

[112] A. Desai, S Rybina, T. Müller-Reichert, A. Shevchenko, A. Shevchenko, A. Hyman, and K. Oegema. Knl-1 directs assembly of the microtubule-binding interface of the kinetochore in c. elegans. *Genes & development*, 17 (19):2421–2435, 2003.

[113] B. A. Pinsky, S. Y. Tatsutani, K. A. Collins, and S. Biggins. An mtw1 complex promotes kinetochore biorientation that is monitored by the ipl1/aurora protein kinase. *Developmental cell*, 5(5):735–745, 2003.

[114] S. Westermann, I. M. Cheeseman, S. Anderson, J. R. Yates, D. G. Drubin, and G. Barnes. Architecture of the budding yeast kinetochore reveals a conserved molecular core. *The Journal of cell biology*, 163(2):215–222, 2003.

[115] I. M. Cheeseman, S. Niessen, S. Anderson, F. Hyndman, J. R. Yates, K. Oegema, and A. Desai. A conserved protein network controls assembly of the outer kinetochore and its ability to sustain tension. *Genes & development*, 18(18):2255–2268, 2004.

[116] C. Obuse, O. Iwasaki, T. Kiyomitsu, G. Goshima, Y. Toyoda, and M. Yanagida. A conserved mis12 centromere complex is linked to heterochromatic hp1 and outer kinetochore protein zwint-1. *Nature cell biology*, 6(11):1135–1141, 2004.

[117] X. Liu, I. McLeod, S. Anderson, J. R. Yates, and X. He. Molecular analysis of kinetochore architecture in fission yeast. *The EMBO journal*, 24(16): 2919–2930, 2005.

[118] M. R. Przewloka, W. Zhang, P. Costa, V. Archambault, P. P. D'Avino, K. S. Lilley, E. D. Laue, A. D. McAinsh, and D. M. Glover. Molecular analysis of core kinetochore composition and assembly in drosophila melanogaster. *PLoS One*, 2(5):e478, 2007.

[119] D. Varma and E. D. Salmon. The kmn protein network–chief conductors of the kinetochore orchestra. *Journal of cell science*, 125(24):5927–5936, 2012.

[120] K. .E Gascoigne and I. M. Cheeseman. Cdk-dependent phosphorylation and nuclear exclusion coordinately control kinetochore assembly state. *The Journal of cell biology*, 201(1):23–32, 2013.

[121] H. Maiato, J. DeLuca, E. D. Salmon, and W. C. Earnshaw. The dynamic kinetochore-microtubule interface. *Journal of cell science*, 117(23):5461–5477, 2004.

[122] T. N. Davis and L. Wordeman. Rings, bracelets, sleeves, and chevrons: new structures of kinetochore proteins. *Trends in cell biology*, 17(8):377–382, 2007.

[123] D. E. Koshland, T. J. Mitchison, and M. W. Kirschner. Polewards chromosome movement driven by microtubule depolymerization in vitro. 1988.

[124] M. Coue, V. A. Lombillo, and J. R. McIntosh. Microtubule depolymerization promotes particle and chromosome movement in vitro. *The Journal of cell biology*, 112(6):1165–1175, 1991.

[125] P. A. Wigge and J. V. Kilmartin. The ndc80p complex from saccharomyces cerevisiae contains conserved centromere components and has a function in chromosome segregation. *The Journal of cell biology*, 152(2):349–360, 2001.

[126] M. L. McCleland, R. D. Gardner, M. J. Kallio, J. R. Daum, G. J. Gorbsky, D. J. Burke, and P. T. Stukenberg. The highly conserved ndc80 complex is required for kinetochore assembly, chromosome congression, and spindle checkpoint activity. *Genes & development*, 17(1):101–114, 2003.

[127] I. M. Cheeseman, J. S. Chappie, E. M. Wilson-Kubalek, and A. Desai. The conserved kmn network constitutes the core microtubule-binding site of the kinetochore. *Cell*, 127(5):983–997, 2006.

[128] A. Kerres, C. Vietmeier-Decker, J. Ortiz, I. Karig, C. Beuter, J. Hegemann, J. Lechner, and U. Fleig. The fission yeast kinetochore component spc7 associates with the eb1 family member mal3 and is required for kinetochore–spindle association. *Molecular biology of the cell*, 15(12):5255–5267, 2004.

[129] J. G. DeLuca, Y. Dong, P. Hergert, J. Strauss, J. M. Hickey, E. D. Salmon, and B. F. McEwen. Hec1 and nuf2 are core components of the kinetochore outer plate essential for organizing microtubule attachment sites. *Molecular biology of the cell*, 16(2):519–531, 2005.

[130] J. G. DeLuca, W. E. Gall, C. Ciferri, D. Cimini, A. Musacchio, and E. D. Salmon. Kinetochore microtubule dynamics and attachment stability are regulated by hec1. *Cell*, 127(5):969–982, 2006.

[131] M. J. Emanuele, M. L. McCleland, D. L. Satinover, and P. T. Stukenberg. Measuring the stoichiometry and physical interactions between components elucidates the architecture of the vertebrate kinetochore. *Molecular biology of the cell*, 16(10):4882–4892, 2005.

[132] S. L. Kline, I. M. Cheeseman, T. Hori, T. Fukagawa, and A. Desai. The human mis12 complex is required for kinetochore assembly and proper chromosome segregation. *The Journal of cell biology*, 173(1):9–17, 2006.

[133] V. V. Vorozhko, M. J. Emanuele, M. J. Kallio, P. T. Stukenberg, and G. J. Gorbsky. Multiple mechanisms of chromosome movement in vertebrate cells mediated through the ndc80 complex and dynein/dynactin. *Chromosoma*, 117(2):169–179, 2008.

[134] L. L. Fava, M. Kaulich, E. A. Nigg, and A. Santamaria. Probing the in vivo function of mad1: C-mad2 in the spindle assembly checkpoint. *The EMBO journal*, 30(16):3322–3336, 2011.

[135] T. Kiyomitsu, H. Murakami, and M. Yanagida. Protein interaction domain mapping of human kinetochore protein blinkin reveals a consensus motif for binding of spindle assembly checkpoint proteins bub1 and bubr1. *Molecular and cellular biology*, 31(5):998–1011, 2011.

[136] T. Kiyomitsu, C. Obuse, and M. Yanagida. Human blinkin/af15q14 is required for chromosome alignment and the mitotic checkpoint through direct interaction with bub1 and bubr1. *Developmental cell*, 13(5):663–676, 2007.

[137] S. Martin-Lluesma, V. M. Stucke, and E. A. Nigg. Role of hec1 in spindle checkpoint signaling and kinetochore recruitment of mad1/mad2. *Science*, 297(5590):2267–2270, 2002.

[138] A. D. McAinsh, P. Meraldi, V. M. Draviam, A. Toso, and P. K. Sorger. The human kinetochore proteins nnf1r and mcm21r are required for accurate chromosome segregation. *The EMBO journal*, 25(17):4033–4049, 2006.

[139] S. A. Miller, M. L. Johnson, and P. T. Stukenberg. Kinetochore attachments require an interaction between unstructured tails on microtubules and ndc80¡ sup¿ hec1¡/sup¿. *Current biology*, 18(22):1785–1791, 2008.

[140] W. Nijenhuis, E. von Castelmur, D. Littler, V. De Marco, E. Tromer, M. Vleugel, M. H. J. van Osch, B. Snel, A. Perrakis, and G. J. P. L Kops. A tpr domain–containing n-terminal module of mps1 is required for its kinetochore localization by aurora b. *The Journal of cell biology*, 201(2):217–231, 2013.

[141] C. Pagliuca, V. M. Draviam, E. Marco, P. K. Sorger, and P. De Wulf. Roles for the conserved spc105p/kre28p complex in kinetochore-microtubule binding and the spindle assembly checkpoint. *PLoS One*, 4(10):e7640, 2009.

[142] R. B. Schittenhelm, R. Chaleckis, and C. F. Lehner. Intrakinetochore localization and essential functional domains of drosophila spc105. *The EMBO journal*, 28(16):2374–2386, 2009.

[143] L. A. Shepperd, J. C. Meadows, A. M. Sochaj, T. C. Lancaster, J. Zou, G. J. Buttrick, J. Rappsilber, K. G. Hardwick, and J. Millar. Phosphodependent recruitment of bub1 and bub3 to spc7/knl1 by mph1 kinase maintains the spindle checkpoint. *Current Biology*, 22(10):891–899, 2012.

[144] Y. Yamagishi, C.-H. Yang, Y. Tanno, and Y. Watanabe. Mps1/mph1 phosphorylates the kinetochore protein knl1/spc7 to recruit sac components. *Nature cell biology*, 14(7):746–752, 2012.

[145] G. J. P. L. Kops, Y. Kim, B. A. A. Weaver, Y. Mao, I. McLeod, J. R. Yates, M. Tagaya, and D. W. Cleveland. Zw10 links mitotic checkpoint signaling to the structural kinetochore. *The Journal of cell biology*, 169(1):49–60, 2005.

[146] J. G. DeLuca, B. Moree, J. M. Hickey, J. V. Kilmartin, and E. D. Salmon. hnuf2 inhibition blocks stable kinetochore–microtubule attachment and induces mitotic cell death in hela cells. *The Journal of cell biology*, 159(4): 549–555, 2002.

[147] R. R. Wei, P. K. Sorger, and S. C. Harrison. Molecular organization of the ndc80 complex, an essential kinetochore component. *Proceedings of the National Academy of Sciences of the United States of America*, 102(15): 5363–5367, 2005.

[148] C. Ciferri, J. De Luca, S. Monzani, K. J. Ferrari, D. Ristic, C. Wyman, H. Stark, J. Kilmartin, E. D. Salmon, and A. Musacchio. Architecture of the human ndc80-hec1 complex, a critical constituent of the outer kinetochore. *Journal of Biological Chemistry*, 280(32):29088–29095, 2005.

[149] E. M. Wilson-Kubalek, I. M. Cheeseman, C. Yoshioka, A. Desai, and R. A. Milligan. Orientation and structure of the ndc80 complex on the microtubule lattice. *The Journal of cell biology*, 182(6):1055–1061, 2008.

[150] G. M. Alushin, V. H. Ramey, S. Pasqualato, D. A. Ball, N. Grigorieff, A. Musacchio, and E. Nogales. The ndc80 kinetochore complex forms oligomeric arrays along microtubules. *Nature*, 467(7317):805–810, 2010.

[151] C. Ciferri, S. Pasqualato, E. Screpanti, G. Varetti, S. Santaguida, G. Dos Reis, A. Maiolica, J. Polka, J. G. De Luca, P. De Wulf, M. Salek, J. Rappsilber, C.A. Moores, E.D. Salmon, and A. Musacchio. Implications for kinetochore-microtubule attachment from the structure of an engineered ndc80 complex. *Cell*, 133(3):427–439, 2008.

[152] J. G. DeLuca and A. Musacchio. Structural organization of the kinetochore–microtubule interface. *Current opinion in cell biology*, 24(1):48–56, 2012.

[153] K. E. Gascoigne and I. M. Cheeseman. Kinetochore assembly: if you build it, they will come. *Current opinion in cell biology*, 23(1):102–108, 2011.

[154] A. P. Joglekar, K. S. Bloom, and E. D. Salmon. Mechanisms of force generation by end-on kinetochore-microtubule attachments. *Current opinion in cell biology*, 22(1):57–67, 2010.

[155] J. Tooley and P. T. Stukenberg. The ndc80 complex: integrating the kinetochore's many movements. *Chromosome Research*, 19(3):377–391, 2011.

[156] L. J. R. Sundin, G. J. Guimaraes, and J. G. DeLuca. The ndc80 complex proteins nuf2 and hec1 make distinct contributions to kinetochore–microtubule attachment in mitosis. *Molecular biology of the cell*, 22(6):759–768, 2011.

[157] T. Hori and T. Fukagawa. Establishment of the vertebrate kinetochores. *Chromosome Research*, 20(5):547–561, 2012.

[158] A. Petrovic, S. Pasqualato, P. Dube, V. Krenn, S. Santaguida, D. Cittaro, S. Monzani, L. Massimiliano, J. Keller, A. Tarricone, Maiolica A., H. Stark, and Musacchio A. The mis12 complex is a protein interaction hub for outer kinetochore assembly. *The Journal of cell biology*, 190(5):835–852, 2010.

[159] J. C. Schmidt, H. Arthanari, A. Boeszoermenyi, N. M. Dashkevich, E. M. Wilson-Kubalek, N. Monnier, M. Markus, M. Oberer, R. A. Milligan, M. Bathe, G. Wagner, E. L. Grishchuk, and Cheeseman I. M. The kinetochore-bound ska1 complex tracks depolymerizing microtubules and binds to curved protofilaments. *Developmental cell*, 23(5):968–980, 2012.

[160] A. P. Joglekar, D. C. Bouck, J. N. Molk, K. S. Bloom, and E. D. Salmon. Molecular architecture of a kinetochore–microtubule attachment site. *Nature cell biology*, 8(6):581–585, 2006.

[161] A. F. Powers, A. D. Franck, D. R. Gestaut, J. Cooper, B. Gracyzk, R. R. Wei, L. Wordeman, T. N. Davis, and C. L. Asbury. The ndc80 kinetochore complex forms load-bearing attachments to dynamic microtubule tips via biased diffusion. *Cell*, 136(5):865–875, 2009.

[162] G. Alushin and E. Nogales. Visualizing kinetochore architecture. *Current opinion in structural biology*, 21(5):661–669, 2011.

[163] J. J. L. Miranda, P. De Wulf, P. K. Sorger, and S. C. Harrison. The yeast dash complex forms closed rings on microtubules. *Nature structural & molecular biology*, 12(2):138–143, 2005.

[164] S. Westermann, A. Avila-Sakar, H.-W. Wang, H. Niederstrasser, J. Wong, D. G. Drubin, E. Nogales, and G. Barnes. Formation of a dynamic kinetochore-microtubule interface through assembly of the dam1 ring complex. *Molecular cell*, 17(2):277–290, 2005.

[165] E. L. Grishchuk, A. K. Efremov, V. A. Volkov, I. S. Spiridonov, N. Gudimchuk, S. Westermann, D. Drubin, G. Barnes, J. R. McIntosh, and F. I. Ataullakhanov. The dam1 ring binds microtubules strongly enough to be a processive as well as energy-efficient coupler for chromosome motion. *Proceedings of the National Academy of Sciences*, 105(40):15423–15428, 2008.

[166] C. L. Asbury, D. R. Gestaut, A. F. Powers, A. D. Franck, and T. N. Davis. The dam1 kinetochore complex harnesses microtubule dynamics to produce force and movement. *Proceedings of the National Academy of Sciences*, 103 (26):9873–9878, 2006.

[167] S. Westermann, H.-W. Wang, A. Avila-Sakar, D. G. Drubin, E. Nogales, and G. Barnes. The dam1 kinetochore ring complex moves processively on depolymerizing microtubule ends. *Nature*, 440(7083):565–569, 2006.

[168] A. Hanisch, H. H. W. Sillje, and E. A. Nigg. Timely anaphase onset requires a novel spindle and kinetochore complex comprising ska1 and ska2. *The EMBO Journal*, 25(23):5504–5515, 2006.

[169] J. R. Daum, J. D. Wren, J. J. Daniel, S. Sivakumar, J. N. McAvoy, T. A. Potapova, and G. J. Gorbsky. Ska3 is required for spindle checkpoint silencing and the maintenance of chromosome cohesion in mitosis. *Current Biology*, 19(17):1467–1472, 2009.

[170] T. N. Gaitanos, A. Santamaria, A. A. Jeyaprakash, B. Wang, E. Conti, and E. A. Nigg. Stable kinetochore–microtubule interactions depend on the ska complex and its new component ska3/c13orf3. *The EMBO journal*, 28(10): 1442–1452, 2009.

[171] M. Theis, M. Slabicki, M. Junqueira, M. Paszkowski-Rogacz, J. Sontheimer, R. Kittler, A.-K. Heninger, T. Glatter, K. Kruusmaa, I. Poser, A. A. Hyman, M. T. Pisabarro, M. Gstaiger, R. Aebersold, A. Shevchenko, and F. Buchholz. Comparative profiling identifies c13orf3 as a component of the ska complex required for mammalian cell division. *The EMBO journal*, 28(10): 1453–1465, 2009.

[172] J. P. I. Welburn, E. L. Grishchuk, C. B. Backer, E. M. Wilson-Kubalek, J. R. Yates III, and I. M. Cheeseman. The human kinetochore ska1 complex facilitates microtubule depolymerization-coupled motility. *Developmental cell*, 16(3):374–385, 2009.

[173] A. A. Jeyaprakash, A. Santamaria, U. Jayachandran, Y. W. Chan, C. Benda, E. A. Nigg, and E. Conti. Structural and functional organization of the ska complex, a key component of the kinetochore-microtubule interface. *Molecular cell*, 46(3):274–286, 2012.

[174] Y. W. Chan, A. A. Jeyaprakash, E. A. Nigg, and A. Santamaria. Aurora b controls kinetochore–microtubule attachments by inhibiting ska complex–kmn network interaction. *The Journal of cell biology*, 196(5):563–571, 2012.

[175] J. P. I. Welburn, M. Vleugel, D. Liu, J. R. Yates III, M. A. Lampson, T. Fukagawa, and I. M. Cheeseman. Aurora b phosphorylates spatially distinct targets to differentially regulate the kinetochore-microtubule interface. *Molecular cell*, 38(3):383–392, 2010.

[176] M. Carmena, M. Wheelock, H. Funabiki, and W. C. Earnshaw. The chromosomal passenger complex (cpc): from easy rider to the godfather of mitosis. *Nature reviews Molecular cell biology*, 13(12):789–803, 2012.

[177] D. Cimini, X. Wan, C. B. Hirel, and E. D. Salmon. Aurora kinase promotes turnover of kinetochore microtubules to reduce chromosome segregation errors. *Current biology*, 16(17):1711–1718, 2006.

[178] S. Sandall, F. Severin, I. X. McLeod, J. R. Yates III, K. Oegema, A. Hyman, and A. Desai. A bir1-sli15 complex connects centromeres to microtubules and is required to sense kinetochore tension. *Cell*, 127(6):1179–1191, 2006.

[179] N. T. Umbreit, D. R. Gestaut, J. F. Tien, B. S. Vollmar, T. Gonen, C. L. Asbury, and T. N. Davis. The ndc80 kinetochore complex directly modulates microtubule dynamics. *Proceedings of the National Academy of Sciences*, 109 (40):16113–16118, 2012.

[180] S. Vigneron, S. Prieto, C. Bernis, J.-C. Labbé, A. Castro, and T. Lorca. Kinetochore localization of spindle checkpoint proteins: who controls whom? *Molecular biology of the cell*, 15(10):4584–4596, 2004.

[181] L. Hewitt, A. Tighe, S. Santaguida, A. M. White, C. D. Jones, A. Musacchio, S. Green, and S. S. Taylor. Sustained mps1 activity is required in mitosis to recruit o-mad2 to the mad1–c-mad2 core complex. *The Journal of cell biology*, 190(1):25–34, 2010.

[182] S. Santaguida, A. Tighe, A. M. D'Alise, St. S. Taylor, and A. Musacchio. Dissecting the role of mps1 in chromosome biorientation and the spindle checkpoint through the small molecule inhibitor reversine. *The Journal of cell biology*, 190(1):73–87, 2010.

[183] J. Maciejowski, K. A. George, M.-E. Terret, C. Zhang, K. M. Shokat, and P. V. Jallepalli. Mps1 directs the assembly of cdc20 inhibitory complexes during interphase and mitosis to control m phase timing and spindle checkpoint signaling. *The Journal of cell biology*, 190(1):89–100, 2010.

[184] G. J. Guimaraes, Y. Dong, B. F. McEwen, and J. G. DeLuca. Kinetochore-microtubule attachment relies on the disordered n-terminal tail domain of hec1. *Current biology*, 18(22):1778–1784, 2008.

[185] V. S. Nekrasov, M. A. Smith, S. Peak-Chew, and J. V. Kilmartin. Interactions between centromere complexes in saccharomyces cerevisiae. *Molecular biology of the cell*, 14(12):4931–4946, 2003.

[186] A. Kerres, V. Jakopec, and U. Fleig. The conserved spc7 protein is required for spindle integrity and links kinetochore complexes in fission yeast. *Molecular biology of the cell*, 18(7):2441–2454, 2007.

[187] J. Espeut, D. K. Cheerambathur, L. Krenning, K. Oegema, and A. Desai. Microtubule binding by knl-1 contributes to spindle checkpoint silencing at the kinetochore. *The Journal of cell biology*, 196(4):469–482, 2012.

[188] I. M. Cheeseman, T. Hori, T. Fukagawa, and A. Desai. Knl1 and the cenp-h/i/k complex coordinately direct kinetochore assembly in vertebrates. *Molecular biology of the cell*, 19(2):587–594, 2008.

[189] D. Liu, M. Vleugel, C. B. Backer, T. Hori, T. Fukagawa, I. M. Cheeseman, and M. A. Lampson. Regulated targeting of protein phosphatase 1 to the outer kinetochore by knl1 opposes aurora b kinase. *The Journal of cell biology*, 188(6):809–820, 2010.

[190] J. C. Meadows, L. A. Shepperd, V. Vanoosthuyse, T. C. Lancaster, A. M. Sochaj, G. J. Buttrick, K. G. Hardwick, and J. Millar. Spindle checkpoint silencing requires association of pp1 to both spc7 and kinesin-8 motors. *Developmental cell*, 20(6):739–750, 2011.

[191] J. S. Rosenberg, F. R. Cross, and H. Funabiki. Knl1/spc105 recruits pp1 to silence the spindle assembly checkpoint. *Current Biology*, 21(11):942–947, 2011.

[192] V. M. Bolanos-Garcia, T. Lischetti, D. Matak-Vinković, E. Cota, P. J. Simpson, D. Y. Chirgadze, D. R. Spring, C. V. Robinson, J. Nilsson, and T. L. Blundell. Structure of a blinkin-bubr1 complex reveals an interaction crucial for kinetochore-mitotic checkpoint regulation via an unanticipated binding site. *Structure*, 19(11):1691–1700, 2011.

[193] V. Krenn, A. Wehenkel, X. Li, S. Santaguida, and A. Musacchio. Structural analysis reveals features of the spindle checkpoint kinase bub1–kinetochore subunit knl1 interaction. *The Journal of cell biology*, 196(4):451–467, 2012.

[194] D. A. Starr, R. Saffery, Z. Li, A. E. Simpson, K. H. Choo, T. J. Yen, and M. L. Goldberg. Hzwint-1, a novel human kinetochore component that interacts with hzw10. *Journal of cell science*, 113(11):1939–1950, 2000.

[195] Y. T. Lin, Y. Chen, G. Wu, and W. H. Lee. Hec1 sequentially recruits zwint-1 and zw10 to kinetochores for faithful chromosome segregation and spindle checkpoint control. *Oncogene*, 25(52):6901–6914, 2006.

[196] H. Wang, X. Hu, X. Ding, Z. Dou, Z. Yang, A. W. Shaw, M. Teng, D. W. Cleveland, M. L. Goldberg, L. Niu, and X. Yao. Human zwint-1 specifies localization of zeste white 10 to kinetochores and is essential for mitotic checkpoint signaling. *Journal of Biological Chemistry*, 279(52):54590–54598, 2004.

[197] R. Gassmann, A. Essex, J.-S. Hu, P. S. Maddox, F. Motegi, A. Sugimoto, S. M. ORourke, B. Bowerman, I. McLeod, J. R. Yates, K. Oegema, I. M. Cheeseman, and A. Desai. A new mechanism controlling kinetochore–microtubule interactions revealed by comparison of two dynein-targeting components: Spdl-1 and the rod/zwilch/zw10 complex. *Genes & development*, 22(17):2385–2399, 2008.

[198] E. R. Griffis, N. Stuurman, and R. D. Vale. Spindly, a novel protein essential for silencing the spindle assembly checkpoint, recruits dynein to the kinetochore. *The Journal of cell biology*, 177(6):1005–1015, 2007.

[199] J. K. Famulski and G. K. Chan. Aurora b kinase-dependent recruitment of hzw10 and hrod to tensionless kinetochores. *Current Biology*, 17(24): 2143–2149, 2007.

[200] J. M. Kasuboski, J. R. Bader, P. S. Vaughan, S. B. F. Tauhata, M. Winding, M. A. Morrissey, M. V. Joyce, W. Boggess, L. Vos, G. K. Chan, E. H. Hinchcliffee, and K. T. Vaughan. Zwint-1 is a novel aurora b substrate required for the assembly of a dynein-binding platform on kinetochores. *Molecular biology of the cell*, 22(18):3318–3330, 2011.

[201] D. P. Maskell, X.-W. Hu, and M. R. Singleton. Molecular architecture and assembly of the yeast kinetochore mind complex. *The Journal of cell biology*, 190(5):823–834, 2010.

[202] E. Screpanti, A. De Antoni, G. M. Alushin, A. Petrovic, T. Melis, E. Nogales, and A. Musacchio. Direct binding of cenp-c to the mis12 complex joins the inner and outer kinetochore. *Current Biology*, 21(5):391–398, 2011.

[203] G. Goshima, T. Kiyomitsu, K. Yoda, and M. Yanagida. Human centromere chromatin protein hmis12, essential for equal segregation, is independent of cenp-a loading pathway. *The Journal of cell biology*, 160(1):25–39, 2003.

[204] K. Nasmyth and C. H. Haering. Cohesin: its roles and mechanisms. *Annual review of genetics*, 43:525–558, 2009.

[205] D. Liu, O. Davydenko, and M. A. Lampson. Polo-like kinase-1 regulates kinetochore–microtubule dynamics and spindle checkpoint silencing. *The Journal of cell biology*, 198(4):491–499, 2012.

[206] X. Liu and M. Winey. The mps1 family of protein kinases. *Annual review of biochemistry*, 81:561, 2012.

[207] S. Elowe. Bub1 and bubr1: at the interface between chromosome attachment and the spindle checkpoint. *Molecular and cellular biology*, 31(15):3085–3093, 2011.

[208] Q. Chen, X. Zhang, Q. Jiang, P. R. Clarke, and C. Zhang. Cyclin b1 is localized to unattached kinetochores and contributes to efficient microtubule attachment and proper chromosome alignment during mitosis. *Cell research*, 18(2):268–280, 2008.

[209] R. Karess. Rod–zw10–zwilch: a key player in the spindle checkpoint. *Trends in cell biology*, 15(7):386–392, 2005.

[210] N. London, S. Ceto, J. A. Ranish, and S. Biggins. Phosphoregulation of spc105 by mps1 and pp1 regulates bub1 localization to kinetochores. *Current Biology*, 22(10):900–906, 2012.

[211] E. A. Foley, M. Maldonado, and T. M. Kapoor. Formation of stable attachments between kinetochores and microtubules depends on the b56-pp2a phosphatase. *Nature cell biology*, 13(10):1265–1271, 2011.

[212] M. S. van der Waal, A. T. Saurin, M. J. M. Vromans, M. Vleugel, C. Wurzenberger, D. W. Gerlich, R. H. Medema, G. J. P. L Kops, and S. Lens. Mps1 promotes rapid centromere accumulation of aurora b. *EMBO reports*, 13(9): 847–854, 2012.

[213] Y. Yamagishi, T. Honda, Y. Tanno, and Y. Watanabe. Two histone marks establish the inner centromere and chromosome bi-orientation. *Science*, 330 (6001):239–243, 2010.

[214] A. E. Kelly, C. Ghenoiu, J. Z. Xue, C. Zierhut, H. Kimura, and H. Funabiki. Survivin reads phosphorylated histone h3 threonine 3 to activate the mitotic kinase aurora b. *Science*, 330(6001):235–239, 2010.

[215] F. Wang, J. Dai, J. R. Daum, E. Niedzialkowska, B. Banerjee, P. T. Stukenberg, G. J. Gorbsky, and J. M. G. Higgins. Histone h3 thr-3 phosphorylation by haspin positions aurora b at centromeres in mitosis. *Science*, 330(6001): 231–235, 2010.

[216] S. J. E. Suijkerbuijk, M. Vleugel, A. Teixeira, and G. J. P. L. Kops. Integration of kinase and phosphatase activities by bubr1 ensures formation of stable kinetochore-microtubule attachments. *Developmental cell*, 23(4): 745–755, 2012.

[217] P. Xu, E. A. Raetz, M. Kitagawa, D. M. Virshup, and S. H. Lee. Bubr1 recruits pp2a via the b56 family of targeting subunits to promote chromosome congression. *Biology open*, 2(5):479–486, 2013.

[218] L. Trinkle-Mulcahy, P. D. Andrews, S. Wickramasinghe, J. Sleeman, A. Prescott, Y. W. Lam, C. Lyon, J. R. Swedlow, and A. I. Lamond. Time-lapse imaging reveals dynamic relocalization of pp1γ throughout the mammalian cell cycle. *Molecular biology of the cell*, 14(1):107–117, 2003.

[219] A. Espert, P. Uluocak, R. N. Bastos, D. Mangat, P. Graab, and U. Gruneberg. Pp2a-b56 opposes mps1 phosphorylation of knl1 and thereby promotes spindle assembly checkpoint silencing. *The Journal of cell biology*, 206(7):833–842, 2014.

[220] L. Francisco, W. Wang, and C.S. Chan. Type 1 protein phosphatase acts in opposition to ipl1 protein kinase in regulating yeast chromosome segregation. *Molecular and cellular biology*, 14(7):4731–4740, 1994.

[221] J.-Y. Hsu, Z.-W. Sun, X. Li, M. Reuben, K. Tatchell, D. K. Bishop, J. M. Grushcow, C. J. Brame, J. A. Caldwell, D. F. Hunt, R. Lin, M.M Smith, and C. D. Allis. Mitotic phosphorylation of histone h3 is governed by ipl1/aurora kinase and glc7/pp1 phosphatase in budding yeast and nematodes. *Cell*, 102 (3):279–291, 2000.

[222] B. A. Pinsky, C. V. Kotwaliwale, S. Y. Tatsutani, C. A. Breed, and S. Biggins. Glc7/protein phosphatase 1 regulatory subunits can oppose the

ipl1/aurora protein kinase by redistributing glc7. *Molecular and cellular biology*, 26(7):2648–2660, 2006.

[223] B. A. Pinsky, C. R. Nelson, and S. Biggins. Protein phosphatase 1 regulates exit from the spindle checkpoint in budding yeast. *Current Biology*, 19(14): 1182–1187, 2009.

[224] V. Vanoosthuyse and K. G. Hardwick. A novel protein phosphatase 1-dependent spindle checkpoint silencing mechanism. *Current Biology*, 19(14): 1176–1181, 2009.

[225] N. London and S. Biggins. Mad1 kinetochore recruitment by mps1-mediated phosphorylation of bub1 signals the spindle checkpoint. *Genes & development*, 28(2):140–152, 2014.

[226] Y. Kim, A. J. Holland, W. Lan, and D. W. Cleveland. Aurora kinases and protein phosphatase 1 mediate chromosome congression through regulation of cenp-e. *Cell*, 142(3):444–455, 2010.

[227] T. Kruse, G. Zhang, M. S. Y. Larsen, T. Lischetti, W. Streicher, T. K. Nielsen, S. Petersen Bjørn, and J. Nilsson. Direct binding between bubr1 and b56–pp2a phosphatase complexes regulate mitotic progression. *Journal of cell science*, 126(5):1086–1092, 2013.

[228] R.-H. Chen, J. C. Waters, E. D. Salmon, and A. W. Murray. Association of spindle assembly checkpoint component xmad2 with unattached kinetochores. *Science*, 274(5285):242–246, 1996.

[229] J. C. Waters, R.-H. Chen, A. W. Murray, and E. D. Salmon. Localization of mad2 to kinetochores depends on microtubule attachment, not tension. *The Journal of cell biology*, 141(5):1181–1191, 1998.

[230] L. Sironi, M. Mapelli, S. Knapp, A. De Antoni, K.-T. Jeang, and A. Musacchio. Crystal structure of the tetrameric mad1–mad2 core complex: implications of a safety beltbinding mechanism for the spindle checkpoint. *The EMBO journal*, 21(10):2496–2506, 2002.

[231] A. De Antoni, C. G. Pearson, Da. Cimini, J. C. Canman, V. Sala, L. Nezi, M. Mapelli, L. Sironi, M. Faretta, E. D. Salmon, and A. Musacchio. The mad1/mad2 complex as a template for mad2 activation in the spindle assembly checkpoint. *Current biology*, 15(3):214–225, 2005.

[232] V. Sudakin, G. K. T. Chan, and T. J. Yen. Checkpoint inhibition of the apc/c in hela cells is mediated by a complex of bubr1, bub3, cdc20, and mad2. *The Journal of cell biology*, 154(5):925–936, 2001.

[233] H. Funabiki and D. J. Wynne. Making an effective switch at the kinetochore by phosphorylation and dephosphorylation. *Chromosoma*, 122(3):135–158, 2013.

[234] R. Gassmann, A. J. Holland, D. Varma, X. Wan, F. Çivril, D. W. Cleveland, K. Oegema, E. D. Salmon, and A. Desai. Removal of spindly from microtubule-attached kinetochores controls spindle checkpoint silencing in human cells. *Genes & development*, 24(9):957–971, 2010.

[235] B. J. Howell, B. F. McEwen, J. C. Canman, D. B. Hoffman, E. M. Farrar, C. L. Rieder, and E. D. Salmon. Cytoplasmic dynein/dynactin drives kinetochore protein transport to the spindle poles and has a role in mitotic spindle checkpoint inactivation. *The Journal of cell biology*, 155(7):1159–1172, 2001.

[236] F. Çivril and A. Musacchio. Spindly attachments. *Genes & development*, 22 (17):2302–2307, 2008.

[237] E. Choi, H. Choe, J. Min, J. Y. Choi, J. Kim, and H. Lee. Bubr1 acetylation at prometaphase is required for modulating apc/c activity and timing of mitosis. *The EMBO journal*, 28(14):2077–2089, 2009.

[238] E. A. Foley and T. M. Kapoor. Microtubule attachment and spindle assembly checkpoint signalling at the kinetochore. *Nature reviews Molecular cell biology*, 14(1):25–37, 2012.

[239] M. Mapelli, F. V. Filipp, G. Rancati, L. Massimiliano, L. Nezi, G. Stier, R. S. Hagan, S. Confalonieri, S. Piatti, M. Sattler, and A. Musacchio. Determinants of conformational dimerization of mad2 and its inhibition by p31comet. *The EMBO journal*, 25(6):1273–1284, 2006.

[240] R. S. Hagan, M. S. Manak, H. K. Buch, M. G. Meier, P. Meraldi, J. V. Shah, and P. K. Sorger. p31comet acts to ensure timely spindle checkpoint silencing subsequent to kinetochore attachment. *Molecular biology of the cell*, 22(22):4236–4246, 2011.

[241] M. Perpelescu and T. Fukagawa. The abcs of cenps. *Chromosoma*, 120(5): 425–446, 2011.

[242] T. Nishino, K. Takeuchi, K. E. Gascoigne, A. Suzuki, T. Hori, T. Oyama, K. Morikawa, I. M. Cheeseman, and T. Fukagawa. Cenp-twsx forms a unique centromeric chromatin structure with a histone-like fold. *Cell*, 148(3):487–501, 2012.

[243] H. Saitoh, J. Tomkiel, C. A. Cooke, H. Ratrie III, M. Maurer, N. F. Rothfield, and W. C. Earnshaw. Cenp-c, an autoantigen in scleroderma, is a component of the human inner kinetochore plate. *Cell*, 70(1):115–125, 1992.

[244] K. Takeuchi and T. Fukagawa. Molecular architecture of vertebrate kinetochores. *Experimental cell research*, 318(12):1367–1374, 2012.

[245] J. S. Verdaasdonk and K. Bloom. Centromeres: unique chromatin structures that drive chromosome segregation. *Nature Reviews Molecular Cell Biology*, 12(5):320–332, 2011.

[246] T. Hori, M. Amano, A. Suzuki, C. B. Backer, J. P. Welburn, Y. Dong, B. F. McEwen, W.-H. Shang, E. Suzuki, K. Okawa, I. M. Cheeseman, and T. Fukagawa. Ccan makes multiple contacts with centromeric dna to provide distinct pathways to the outer kinetochore. *Cell*, 135(6):1039–1052, 2008.

[247] T. Hori, W.-H. Shang, K. Takeuchi, and T. Fukagawa. The ccan recruits cenp-a to the centromere and forms the structural core for kinetochore assembly. *The Journal of cell biology*, 200(1):45–60, 2013.

[248] K. Takahashi, E. S. Chen, and M. Yanagida. Requirement of mis6 centromere connector for localizing a cenp-a-like protein in fission yeast. *Science*, 288 (5474):2215–2219, 2000.

[249] C. Obuse, H. Yang, N. Nozaki, S. Goto, T. Okazaki, and K. Yoda. Proteomics analysis of the centromere complex from hela interphase cells: Uv-damaged dna binding protein 1 (ddb-1) is a component of the cen-complex, while bmi-1 is transiently co-localized with the centromeric region in interphase. *Genes to Cells*, 9(2):105–120, 2004.

[250] M. Okada, I. M. Cheeseman, T. Hori, K. Okawa, I. X. McLeod, J. R. Yates, A. Desai, and T. Fukagawa. The cenp-hi complex is required for the efficient incorporation of newly synthesized cenp-a into centromeres. *Nature cell biology*, 8(5):446–457, 2006.

[251] H. Izuta, M. Ikeno, N. Suzuki, T. Tomonaga, N. Nozaki, C. Obuse, Y. Kisu, N. Goshima, F. Nomura, N. Nomura, and Y. Kinya. Comprehensive analysis of the icen (interphase centromere complex) components enriched in the cenp-a chromatin of human cells. *Genes to Cells*, 11(6):673–684, 2006.

[252] P. Meraldi, A. D. McAinsh, E.r Rheinbay, and P. K. Sorger. Phylogenetic and structural analysis of centromeric dna and kinetochore proteins. *Genome biology*, 7(3):R23, 2006.

[253] B. Akiyoshi, K. K. Sarangapani, A. F. Powers, C. R. Nelson, S. L. Reichow, H. Arellano-Santoyo, T. Gonen, J. A. Ranish, C. L. Asbury, and S. Biggins. Tension directly stabilizes reconstituted kinetochore-microtubule attachments. *Nature*, 468(7323):576–579, 2010.

[254] S. Westermann and A. Schleiffer. Family matters: structural and functional conservation of centromere-associated proteins from yeast to humans. *Trends in cell biology*, 23(6):260–269, 2013.

[255] S. E. McClelland, S. Borusu, A. C. Amaro, J. R. Winter, M. Belwal, A. D. McAinsh, and P. Meraldi. The cenp-a nac/cad kinetochore complex controls chromosome congression and spindle bipolarity. *The EMBO journal*, 26(24): 5033–5047, 2007.

[256] D. Hellwig, S. Emmerth, T. Ulbricht, V. Döring, C. Hoischen, R. Martin, C. P. Samora, A. D. McAinsh, C. W. Carroll, A. F. Straight, P. Meraldi, and S. Diekmann. Dynamics of cenp-n kinetochore binding during the cell cycle. *Journal of cell science*, 124(22):3871–3883, 2011.

[257] Y. H. Kang, J.-E. Park, L.-R. Yu, N.-K. Soung, S.-M. Yun, J. K. Bang, Y.-S. Seong, H. Yu, S. Garfield, T. D. Veenstra, and K.S. Lee. Self-regulated plk1 recruitment to kinetochores by the plk1-pbip1 interaction is critical for proper chromosome segregation. *Molecular cell*, 24(3):409–422, 2006.

[258] S. M. Hinshaw and S. C. Harrison. An iml3-chl4 heterodimer links the core centromere to factors required for accurate chromosome segregation. *Cell reports*, 5(1):29–36, 2013.

[259] Q. Guo, Y. Tao, H. Liu, M. Teng, and X. Li. Structural insights into the role of the chl4-iml3 complex in kinetochore assembly. *Acta Crystallographica Section D: Biological Crystallography*, 69(12):2412–2419, 2013.

[260] M. R. Przewloka, Z. Venkei, V. M. Bolanos-Garcia, J. Debski, M. Dadlez, and D. M. Glover. Cenp-c is a structural platform for kinetochore assembly. *Current Biology*, 21(5):399–405, 2011.

[261] A. Schleiffer, M. Maier, G. Litos, F. Lampert, P. Hornung, K. Mechtler, and S. Westermann. Cenp-t proteins are conserved centromere receptors of the ndc80 complex. *Nature Cell Biology*, 14(6):604–613, 2012.

[262] F. Malvezzi, G. Litos, A. Schleiffer, A. Heuck, K. Mechtler, T Clausen, and S. Westermann. A structural basis for kinetochore recruitment of the ndc80 complex via two distinct centromere receptors. *The EMBO journal*, 32(3): 409–423, 2013.

[263] S. A. Ribeiro, P. Vagnarelli, Y. Dong, T. Hori, B. F. McEwen, T. Fukagawa, C. Flors, and W. C. Earnshaw. A super-resolution map of the vertebrate kinetochore. *Proceedings of the National Academy of Sciences*, 107 (23):10484–10489, 2010.

[264] F. Basilico, S. Maffini, J. R. Weir, D. Prumbaum, A. M. Rojas, T. Zimniak, A. De Antoni, S. Jeganathan, B. Voss, S. van Gerwen, V. Krenn, L. Massimiliano, A. Valencia, I. R. Vetter, F. Herzog, S. Raunser, S. Pasqualato, and A. Musacchio. The pseudo gtpase cenp-m drives human kinetochore assembly. *eLife*, 3:e02978, 2014.

[265] J. Tomkiel, C. A. Cooke, H. Saitoh, R. L. Bernat, and W. C. Earnshaw. Cenp-c is required for maintaining proper kinetochore size and for a timely transition to anaphase. *The Journal of cell biology*, 125(3):531–545, 1994.

[266] T. Fukagawa and W. R. A. Brown. Efficient conditional mutation of the vertebrate cenp-c gene. *Human molecular genetics*, 6(13):2301–2308, 1997.

[267] T. Fukagawa, C. Pendon, J. Morris, and W. Brown. Cenp-c is necessary but not sufficient to induce formation of a functional centromere. *The EMBO journal*, 18(15):4196–4209, 1999.

[268] M.-S. Kwon, T. Hori, M. Okada, and T. Fukagawa. Cenp-c is involved in chromosome segregation, mitotic checkpoint function, and kinetochore assembly. *Molecular biology of the cell*, 18(6):2155–2168, 2007.

[269] P. Kalitsis, K. J. Fowler, E. Earle, J. Hill, and K. H. A. Choo. Targeted disruption of mouse centromere protein c gene leads to mitotic disarray and

early embryo death. *Proceedings of the National Academy of Sciences*, 95 (3):1136–1141, 1998.

[270] K. J. Milks, B. Moree, and A. F. Straight. Dissection of cenp-c–directed centromere and kinetochore assembly. *Molecular biology of the cell*, 20(19): 4246–4255, 2009.

[271] K. Tanaka, H. Li Chang, A. Kagami, and Y. Watanabe. Cenp-c functions as a scaffold for effectors with essential kinetochore functions in mitosis and meiosis. *Developmental cell*, 17(3):334–343, 2009.

[272] M. T. Brown, L. Goetsch, and L. H. Hartwell. Mif2 is required for mitotic spindle integrity during anaphase spindle elongation in saccharomyces cerevisiae. *The Journal of cell biology*, 123(2):387–403, 1993.

[273] L. L. Moore and M. B. Roth. Hcp-4, a cenp-c–like protein incaenorhabditis elegans, is required for resolution of sister centromeres. *The Journal of cell biology*, 153(6):1199–1208, 2001.

[274] S. Heeger, O. Leismann, R. Schittenhelm, O. Schraidt, S. Heidmann, and C. F. Lehner. Genetic interactions of separase regulatory subunits reveal the diverged drosophila cenp-c homolog. *Genes & development*, 19(17):2041–2053, 2005.

[275] S. Holland, D. Ioannou, S. Haines, and W. R. A. Brown. Comparison of dam tagging and chromatin immunoprecipitation as tools for the identification of the binding sites for s. pombe cenp-c. *Chromosome Research*, 13(1):73–83, 2005.

[276] K. Sugimoto, H. Yata, Y. Muro, and M. Himeno. Human centromere protein c (cenp-c) is a dna-binding protein which possesses a novel dna-binding motif. *Journal of biochemistry*, 116(4):877–881, 1994.

[277] K. Sugimoto, K. Kuriyama, A. Shibata, and M. Himeno. Characterization of internal dna-binding and c-terminal dimerization domains of human centromere/kinetochore autoantigen cenp-c in vitro: role of dna-binding and self-associating activities in kinetochore organization. *Chromosome Research*, 5(2):132–141, 1997.

[278] C. H. Yang, J. Tomkiel, H. Saitoh, D. H. Johnson, and W. C. Earnshaw. Identification of overlapping dna-binding and centromere-targeting domains

in the human kinetochore protein cenp-c. *Molecular and cellular biology*, 16 (7):3576–3586, 1996.

[279] S. Erhardt, B. G. Mellone, C. M. Betts, W. Zhang, G. H. Karpen, and A. F. Straight. Genome-wide analysis reveals a cell cycle–dependent mechanism controlling centromere propagation. *The Journal of cell biology*, 183(5):805–818, 2008.

[280] K. Song, B. Gronemeyer, W. Lu, E. Eugster, and J. E. Tomkiel. Mutational analysis of the central centromere targeting domain of human centromere protein c,(cenp-c). *Experimental cell research*, 275(1):81–91, 2002.

[281] R. L. Cohen, C. W. Espelin, P. De Wulf, P. K. Sorger, S. C. Harrison, and K.T. Simons. Structural and functional dissection of mif2p, a conserved dna-binding kinetochore protein. *Molecular biology of the cell*, 19(10):4480–4491, 2008.

[282] A. Nishihashi, T. Haraguchi, Y. Hiraoka, T. Ikemura, V. Regnier, H. Dodson, W. C. Earnshaw, and T. Fukagawa. Cenp-i is essential for centromere function in vertebrate cells. *Developmental cell*, 2(4):463–476, 2002.

[283] N. Sugata, E. Munekata, and K. Todokoro. Characterization of a novel kinetochore protein, cenp-h. *Journal of Biological Chemistry*, 274(39):27343–27346, 1999.

[284] N. Sugata, S. Li, W. C. Earnshaw, T. J. Yen, K. Yoda, H. Masumoto, E. Munekata, P. E. Warburton, and K. Todokoro. Human cenp-h multimers colocalize with cenp-a and cenp-c at active centromere–kinetochore complexes. *Human molecular genetics*, 9(19):2919–2926, 2000.

[285] S. Qiu, J. Wang, C. Yu, and D. He. Cenp-k and cenp-h may form coiled-coils in the kinetochores. *Science in China Series C: Life Sciences*, 52(4): 352–359, 2009.

[286] J.-P. Renou, B. Bierie, K. Miyoshi, Y. Cui, J. Djiane, M. Reichenstein, M. Shani, and L. Hennighausen. Identification of genes differentially expressed in mouse mammary epithelium transformed by an activated β-catenin. *Oncogene*, 22(29):4594–4610, 2003.

[287] B. Bierie, M. Edwin, J.J. Melenhorst, and L. Hennighausen. The proliferation associated nuclear element (pane1) is conserved between mammals and

fish and preferentially expressed in activated lymphoid cells. *Gene expression patterns*, 4(4):389–395, 2004.

[288] Y. Mikami, T. Hori, H. Kimura, and T. Fukagawa. The functional region of cenp-h interacts with the nuf2 complex that localizes to centromere during mitosis. *Molecular and cellular biology*, 25(5):1958–1970, 2005.

[289] A. Suzuki, T. Hori, T. Nishino, J. Usukura, A. Miyagi, K. Morikawa, and T. Fukagawa. Spindle microtubules generate tension-dependent changes in the distribution of inner kinetochore proteins. *The Journal of cell biology*, 193(1):125–140, 2011.

[290] M. Amano, A. Suzuki, T. Hori, C. Backer, K. Okawa, I. M. Cheeseman, and T. Fukagawa. The cenp-s complex is essential for the stable assembly of outer kinetochore structure. *The Journal of cell biology*, 186(2):173–182, 2009.

[291] Y. Minoshima, T. Hori, M. Okada, H. Kimura, T. Haraguchi, Y. Hiraoka, Y.-C. Bao, T. Kawashima, T. Kitamura, and T. Fukagawa. The constitutive centromere component cenp-50 is required for recovery from spindle damage. *Molecular and cellular biology*, 25(23):10315–10328, 2005.

[292] S. Hua, Z. Wang, K. Jiang, Y. Huang, T. Ward, L. Zhao, Z. Dou, and X. Yao. Cenp-u cooperates with hec1 to orchestrate kinetochore-microtubule attachment. *Journal of Biological Chemistry*, 286(2):1627–1638, 2011.

[293] N. Kagawa, T. Hori, Y. Hoki, O. Hosoya, K. Tsutsui, Y. Saga, T. Sado, and T. Fukagawa. The cenp-o complex requirement varies among different cell types. *Chromosome Research*, pages 1–11, 2014.

[294] A. C. Amaro, C. P. Samora, R. Holtackers, E. Wang, I. J. Kingston, M. Alonso, M. Lampson, A. D. McAinsh, and P. Meraldi. Molecular control of kinetochore-microtubule dynamics and chromosome oscillations. *Nature cell biology*, 12(4):319–329, 2010.

[295] Y. H. Kang, C. H. Park, T.-S. Kim, N.-K. Soung, J. K. Bang, B. Y. Kim, J.-E. Park, and K. S. Lee. Mammalian polo-like kinase 1-dependent regulation of the pbip1-cenp-q complex at kinetochores. *Journal of Biological Chemistry*, 286(22):19744–19757, 2011.

[296] F. Schmitzberger and S. C. Harrison. Rwd domain: a recurring module in kinetochore architecture shown by a ctf19–mcm21 complex structure. *EMBO reports*, 13(3):216–222, 2012.

[297] P. Hornung, P. Troc, F. Malvezzi, M. Maier, Z. Demianova, T. Zimniak, G. Litos, F. Lampert, A. Schleiffer, M. Brunner, K. Mechtler, F. Herzog, T.C. Marlovits, and S. Westermann. A cooperative mechanism drives budding yeast kinetochore assembly downstream of cenp-a. *The Journal of cell biology*, 206(4):509–524, 2014.

[298] H. W. Dirr, K. Mann, R. Huber, R. Ladenstain, and P. Reinemer. Class π glutathione s-transferase from pig lung. *European journal of biochemistry*, 196(3):693–698, 1991.

[299] P. Reinemer, H. W. Dirr, R. Ladenstein, J. Schäffer, O. Gallay, and R. Huber. The three-dimensional structure of class pi glutathione s-transferase in complex with glutathione sulfonate at 2.3 a resolution. *The EMBO journal*, 10(8):1997, 1991.

[300] A. Suzuki, B. L. Badger, X. Wan, J. G. DeLuca, and E. D. Salmon. The architecture of ccan proteins creates a structural integrity to resist spindle forces and achieve proper intrakinetochore stretch. *Developmental cell*, 30 (6):717–730, 2014.

[301] K. Takeuchi, T. Nishino, K. Mayanagi, N. Horikoshi, A. Osakabe, H. Tachiwana, T. Hori, H. Kurumizaka, and T. Fukagawa. The centromeric nucleosome-like cenp–t–w–s–x complex induces positive supercoils into dna. *Nucleic acids research*, 42(3):1644–1655, 2014.

[302] T. Nishino, F. Rago, T. Hori, K. Tomii, I. M. Cheeseman, and T. Fukagawa. Cenp-t provides a structural platform for outer kinetochore assembly. *The EMBO journal*, 32(3):424–436, 2013.

[303] S. Kim and H. Yu. Multiple assembly mechanisms anchor the kmn spindle checkpoint platform at human mitotic kinetochores. *The Journal of cell biology*, 208(2):181–196, 2015.

[304] M. W.-L. Popp, J. M. Antos, and H. L. Ploegh. Site-specific protein labeling via sortase-mediated transpeptidation. *Current Protocols in Protein Science*, pages 15–3, 2009.

[305] M. W.-L. Popp and H. L. Ploegh. Making and breaking peptide bonds: protein engineering using sortase. *Angewandte Chemie International Edition*, 50(22):5024–5032, 2011.

[306] T. Fukagawa and W. C. Earnshaw. The centromere: chromatin foundation for the kinetochore machinery. *Developmental Cell*, 30(5):496–508, 2014.

[307] F. Ran, P. D. Hsu, C.-Y. Lin, J. S. Gootenberg, S. Konermann, A. E. Trevino, D. A. Scott, A. Inoue, S. Matoba, Y. Zhang, and F. Zhang. Double nicking by rna-guided crispr cas9 for enhanced genome editing specificity. *Cell*, 154(6):1380–1389, 2013.

[308] Fuller C. J. Guse A. and Straight A. F. A cell free system for functional centromere and kinetochore assembly authors. *Nature protocols*, 10(7), 2012.

[309] D. J. Fitzgerald, P. Berger, C. Schaffitzel, K. Yamada, T. J. Richmond, and I. Berger. Protein complex expression by using multigene baculoviral vectors. *Nature methods*, 3(12):1021–1032, 2006.

[310] S. Trowitzsch, C. Bieniossek, Y. Nie, F. Garzoni, and I. Berger. New baculovirus expression tools for recombinant protein complex production. *Journal of structural biology*, 172(1):45–54, 2010.

[311] N. Arnaudo, I. S. Fernández, S. H. McLaughlin, S. Y. Peak-Chew, D. Rhodes, and F. Martino. The n-terminal acetylation of sir3 stabilizes its binding to the nucleosome core particle. *Nature structural & molecular biology*, 20(9):1119–1121, 2013.

[312] A. Maiolica, D. Cittaro, D. Borsotti, L. Sennels, C. Ciferri, C. Tarricone, A. Musacchio, and J. Rappsilber. Structural analysis of multiprotein complexes by cross-linking, mass spectrometry, and database searching. *Molecular & Cellular Proteomics*, 6(12):2200–2211, 2007.

[313] F. Herzog, A. Kahraman, D. Boehringer, R. Mak, A. Bracher, T. Walzthoeni, A. Leitner, M. Beck, F.-U. Hartl, N. Ban, L. Malmström, and R. Aebersold. Structural probing of a protein phosphatase 2a network by chemical cross-linking and mass spectrometry. *Science*, 337(6100):1348–1352, 2012.

[314] A. Tighe and S. S. Johnson, V. L .and Taylor. Truncating apc mutations have dominant effects on proliferation, spindle checkpoint control, survival and chromosome stability. *Journal of cell science*, 117(26):6339–6353, 2004.

Acknowledgements

First of all I want to thank Prof. Andrea Musacchio for giving me the opportunity to work as a PhD student in his laboratory at the MPI in Dortmund. He always supported me scientifically and personally and I cannot express how grateful I am. My internal advisor Dr. Ingrid Vetter and my external advisors Prof. Hemmo Meyer and Dr. Martin Singleton are highly acknowledged for scientific guidance, as well as Prof. Stefan Westermann for being the second evaluator of my PhD thesis.

I also want to express gratefulness to past and present members of the MPI Dortmund, for fruitful scientific discussions, sharing of reagents and scientific knowhow as well as the creation of a harmonic working atmosphere. In particular, I want to acknowledge Dr. John Weir, who was always a big help in the lab and answered all my questions in the most patient way I can imagine. I consider myself lucky, that I was working in close collaboration with him on the CENP-H/I/K/M:CENP-C interaction as well as current projects running in the lab. The CENP-H/I/K/M and CENP-N/L complexes were generated by John and produced with kind help of Nina Ludwigs and Ingrid Hoffmann, that I want to acknowledge here as well. Along these lines I want to thank Annika Take, who was a trainee at the MPI and working with me for some weeks, as well as Sabine Wohlgemuth for introducing me to protein production in insect cells as well as for establishing and purifying the Mis12 complex. My deepest thanks go to Dr. Federica Basilico who I started the CENP-H/K project and enjoyed working with and who developed from a great coworker to a close friend. In this context, I want to thank Lucia Massimiliano, who established the CENP-H/K production and purification. I greatly appreciate the collaboration with Dr. Franz Herzog, who managed to perform cross-linking experiments on our reconstituted complexes, which added a lot to my study. Again, I want to thank Dr. Ingrid Vetter for Data analysis and figure preparation of these cross-linking experiments. I feel also very grateful towards Dr. Stefano Maffini and Dr. Veronica Krenn, who were always willing to discuss scientific ideas and problems regarding tissue culture and share reagents and knowledge. I will definitely miss a clicking and singing noise behind my back. Warm thanks also go to Suzan van-Gerwen and Dr. Marta Mattiuzzo, who were always willing to give me a hand in the tissue culture and to Anna de Antoni, who supported me from the distance, when I was trying to fight CENP-C. I also want to thank Doro Vogt, who is providing high quality H3 and CENP-A nucleosomes

for the whole lab and I profited from that. Since Doro and me were working in the same room, I also want to express my thanks for creating a special and open working atmosphere, that made me feel like home. A part of this was also Claudia Breit and I simply thank her for being my friend, as I hope she knows what that means to me. I want to say thanks to Giuseppe Ossolengo, who helped providing high quality antibodies, that played a key role in my studies. Regarding antibodies, a big thanks goes to Dr. Siva Jeganathan for providing me with CENP-T/W antibody, as well as for CENP-C^{2-545} construct design and for scientific discussion and support. In addition, I also want to thank Katharina Overlack, who sometimes helped me find my way back home. In addition I want to thank Charlotte Smith, who is currently working with me on some evolving projects and has always been there for me. My warmest thanks also go to the remaining CCANers including Dr. Marion Pesenti, Dr. Julia Blümer, Dr. Alex Faesen and Dr. Dongqing Pan for fruitful scientific discussions and co-working that works. Dongqing is currently working with me on some new projects in the lab and he turns out to be a great co-worker. In addition, I also want to point out my gratefulness towards Dr. Arsen Petrovic, who introduced me to the ITC machine and helped me interpreting the data, while entertaining me. In addition, I am thankful for mass-spectrometry carried out by Dr. Tanja Bange. I also want to thank Dr. Maria Thanasoula, the only one that knows the trouble I have seen. Without her I would not be where I am now. For support around the lab, I want to thank Antje Peukert and the international Max Planck research school (IMPRS). The IMPRS supported me financially and scientifically by offering lectures and courses that were very useful for me and made the exchange with high profile scientists possible. Along these lines I want to thank Dr. Waltraud Hofmann-Goody and Christa Hornemann for taking care of all the IMPRS students. A very warm thanks goes especially to Christa, since she was always supportive and helped to resolve all bureaucratic barriers with an always friendly and dedicated personality. Last, but not least, I want to thank the whole Musacchio lab and Department 1. All of you created a great working atmosphere, that made me feel more like going to meet friends and talk science than going to work. I will always be grateful for the great time we spent together.

Natürlich möchte ich mich auch bei meiner Familie und bei meinen Freunden bedanken, die mich immer unterstützt und an mich geglaubt haben. Mein Dank geht an meinen Verlobten Kay, der immer alles dafür getan hat, damit es mir gut geht und welcher der Grund dafür ist, dass es das tut. An meine liebe und beste

Freundin Bianca, die immer für mich da ist und mich blind versteht. An meine Mutter, die ihr Leben für ihre Kinder geben würde ohne auch nur ein Wort der Beschwerde vernehmen zu lassen. An meine Schwestern, die so besonders sind, dass man sie lieben muss. An meinen Vater, der immer einen Platz in meinem Herzen haben wird. An Martin, dem ich bedingungslos vertraue. An Lutz, dessen Freundschaft mir mehr bedeutet als er es sich vorzustellen vermag. Zuletzt an Peter, dem ich diese Arbeit witme und der mich gelehrt hat niemals aufzugeben.

Kerstin Klare
Max-Planck-Institute of Molecular Physiology
44227 Dortmund
Germany
Kerstin.Klare@mpi-dortmund.mpg.de

Der Lebenslauf ist in der Online-Version aus Gründen des Datenschutzes nicht enthalten.

Declarations

Hiermit erkläre ich, Kerstin Klare, gem. §7 Abs. (2) d) + f) der Promotionsordnung der Fakultät fur Biologie zur Erlangung des Dr. rer. nat., dass ich die vorliegende Dissertation selbständig verfasst und mich keiner anderen als der angegebenen Quellen und Hilfsmittel bedient, sowie alle wörtlich oder inhaltlich übernommenen Stellen als solche gekennzeichnet habe.

Signed: _____

Date: _____

Hiermit erkläre ich, Kerstin Klare, gem. §6 Abs. (2) f) der Promotionsordnung der Fakultät fur Biologie zur Erlangung des Dr. rer. nat., dass mir das vorliegende Promotionsverfahren nicht kommerziell vermittelt worden ist. Insbesondere habe ich keine Organisation eingeschaltet, die gegen Entgelt Betreuerinnen und Betreuer fur die Anfertigung von Dissertatio- nen sucht oder die mir obliegenden Pflichten hinsichtlich der Prüfungsleistungen fur mich ganz oder teilweise erledigt. Hilfe Dritter wurde bis jetzt und wird auch künftig nur in wissenschaftlich vertretbarem und prüfungsrechtlich zulässigem Ausmaß in Anspruch genommen. Mir ist bekannt, dass Unwahrheiten hinsichtlich der vorstehenden Erklärung die Zulassung zur Promotion ausschlieen bzw. später zum Verfahrensabbruch oder zur Rücknahme des Titels führen können.

Signed: _____

Date: _____

Hiermit erkläre ich, Kerstin Klare, gem. §7 Abs. (2) e) + g) der Promotionsordnung der Fakultät für Biologie zur Erlangung des Dr. rer. nat., dass ich keine anderen Promotionen bzw. Promotionsversuche in der Vergangenheit durchgeführt habe und dass diese Arbeit bei keiner anderen Fakultät/Fachbereich eingereicht worden und von keiner anderen Fakultät/Fachbereich abgelehnt worden ist.

Signed:

Date:

Hiermit erkläre ich, Prof. Dr. Andrea Musacchio, gem. §6 Abs. (2) g) der Promotionsordnung der Fakultät für Biologie zur Erlangung der Dr. rer. nat., dass ich das Arbeitsgebiet, dem das Thema Functional organization of the CCAN protein complex zuzuordnen ist, in Forschung und Lehre vertrete und den Antrag von (Kerstin Klare) befürworte und die Betreuung auch im Falle eines Weggangs, wenn nicht wichtige Gründe dem entgegenstehen, weiterführen werde.

Signed:

Date: